Mathematical Methods for Managing Distributed Energy Resources

by

Hannah Moring

A dissertation submitted in partial fulfillment
of the requirements for the degree of
Doctor of Philosophy
(Electrical and Computer Engineering)
in the University of Michigan
2025

Doctoral Committee:

Associate Professor Johanna Mathieu, Chair
Assistant Professor Vladimir Dvorkin
Associate Professor Ruiwei Jiang
Assistant Professor Daniel Molzahn, Georgia Institute of Technology

Hannah Moring
hmoring@umich.edu
ORCID iD: 0000-0003-4163-2007

© Hannah Moring 2025

DEDICATION

To Duncan and Claude.

ACKNOWLEDGEMENTS

I would like to thank my advisor, Dr. Johanna Mathieu, for her guidance and support. It was truly a pleasure to learn from her and work with her. I would also like to thank the rest of my committee, Dr. Vladamir Dvorkin, Dr. Ruiwei Jiang, and Dr. Dan Molzahn, for your insightful feedback and encouragement.

I would like to thank Dr. Harsha Nagarajan from Los Alamos National Lab, as well as Dr. Bala Kameshwar Poolla and Dr. Andrey Bernstein from the National Renewable Energy Lab for being such wonderful collaborators and mentors. It was an honor to work with and learn from all of you. I would also like to thank the other students in my research group here at the University of Michigan, particularly Dr. Sunho Jang and Xavier Farrell for the work they contributed to our collaborations.

Next, I would like to thank the National Science Foundation (NSF) and the Office of Electricity of the U.S. Department of Energy (DOE), whose funding made this work possible.

Lastly, I would like to thank my friends and family for their love and support. To my parents, I am deeply grateful that you raised me to value education and to follow my passions. Dad, thank you for fostering within me a fascination with math and science. Mom, thank you for always being there for me and for providing advice when I needed it. To Duncan, thank you for always believing in me, even when I did not believe in myself. To all the other friends I made during my time in Ann Arbor, thank you for the joy that you added to my life.

TABLE OF CONTENTS

DEDICATION ii

ACKNOWLEDGEMENTS iii

LIST OF FIGURES viii

LIST OF TABLES xi

ABSTRACT xii

CHAPTER

1 Introduction 1

1.1 DERs: Opportunities and Challenges 2
1.1.1 Reliability 2
1.1.2 Resiliency 3
1.2 Electricity Market and Policy Implications 3
1.3 Considering Energy Justice 4
1.4 Contributions of Dissertation 5
1.5 Organization of Dissertation 6

2 A Comparison of Strategies for Managing Energy Constraints of Energy Storage Providing Frequency Regulation 10

2.1 Chapter Introduction 10
2.2 Regulation Controllers 12
2.2.1 PJM Conditional Neutrality Controller 13
2.2.2 CAISO Regulation Signals and REM 15
2.3 Simulation Approach and Metrics 17
2.3.1 Regulation signal-following performance 19
2.3.2 Additional system control effort 19
2.4 Case Study 20
2.4.1 Setup 21
2.4.2 Results 22
2.5 Chapter Conclusions 23

3 Robust Partitioning and Operation for Maximal Uncertain-Load Delivery in Distribution Networks 27

3.1 Chapter Introduction . . . 27
3.2 Problem Formulation . . . 29
3.2.1 Notation and Preliminaries . . . 29
3.2.2 Network Configuration Constraints . . . 30
3.2.3 Single-Stage Robust Partitioning and Operation Problem . . . 33
3.3 A Cutting-Plane Algorithm to solve the RPOP . . . 34
3.3.1 Two-stage Robust Partitioning and Operation Problem . . . 34
3.3.2 A Cutting-plane Algorithm . . . 37
3.4 Numerical Results . . . 37
3.4.1 Implementation details . . . 38
3.4.2 Test case: IEEE 37-bus test system . . . 38
3.4.3 RPOP's performance for varying levels of load uncertainty . . . 38
3.4.4 RPOP's performance against deterministic counterparts . . . 40
3.5 Chapter Conclusions . . . 42

4 Reconfiguration and Real-Time Operation of Networked Microgrids Under Load Uncertainty . . . 44

4.1 Chapter Introduction . . . 44
4.2 Robust Partitioning Problem Formulation . . . 46
4.2.1 Notation and Preliminaries . . . 46
4.2.2 Network Configuration Constraints . . . 47
4.2.3 Single-Stage Robust Partitioning and Operation Problem . . . 52
4.3 A Cutting-Plane Algorithm to solve the RPOP . . . 53
4.3.1 Two-stage Robust Partitioning and Operation Problem . . . 53
4.3.2 A Cutting-plane Algorithm . . . 56
4.4 Model-free Real-Time Optimal Power Flow . . . 56
4.5 Case Study: SMART-DS . . . 58
4.5.1 Network Details . . . 59
4.5.2 Implementation Details . . . 60
4.5.3 RPOP Results . . . 60
4.5.4 Real-time Control Results . . . 63
4.6 Chapter Conclusions . . . 66

5 Nodal Operating Envelopes vs. Network-wide Constraints: What is better for network-safe coordination of DERs? . . . 67

5.1 Chapter Introduction . . . 67
5.2 Discussion of Approaches . . . 70
5.2.1 General Discussion . . . 71
5.2.2 Considered Framework . . . 72
5.2.3 Discussion of Specific Approaches . . . 72
5.3 Constructing Nodal Constraints . . . 74
5.4 Constructing Network-wide Constraints . . . 76
5.5 Case Studies . . . 78
5.5.1 Setup . . . 78
5.5.2 Results . . . 80

5.6 Chapter Conclusions . . . 83

6 Inexactness of Second Order Cone Relaxations for Calculating Operating Envelopes . . . 85

6.1 Chapter Introduction . . . 85
6.2 Problem Formulations . . . 87
6.2.1 AC-OPF Branch Flow Formulation . . . 87
6.2.2 Second-Order Cone Relaxation . . . 89
6.2.3 Objective Function Modification . . . 90
6.3 Case Study . . . 91
6.3.1 Setup . . . 91
6.3.2 Results . . . 92
6.4 Chapter Conclusions . . . 97

7 Proof of the Inexactness of Second-Order Cone Relaxations for Operating Envelopes . . . 100

7.1 Chapter Introduction . . . 100
7.2 Problem Formulations . . . 102
7.2.1 Operating Envelope AC-OPF Branch Flow Formulation . . . 103
7.2.2 Second-Order Cone Relaxation . . . 104
7.3 SOC Inexactness . . . 105
7.3.1 Objective Function Modification . . . 105
7.3.2 Case Study Setup . . . 106
7.3.3 Case Study Results . . . 107
7.4 Conditions for Inexactness . . . 109
7.4.1 Conditions for an exact relaxation . . . 111
7.4.2 Purely Resistive Networks . . . 116
7.4.3 Purely Reactive Networks . . . 120
7.5 Conclusions . . . 121

8 Fair-Over-Time Distributed Energy Resource Coordination . . . 123

8.1 Chapter Introduction . . . 123
8.2 Fairness Concepts & Metrics . . . 125
8.2.1 Fairness in machine learning . . . 125
8.2.2 Fairness in DER coordination . . . 126
8.2.3 Comparing fairness landscapes . . . 128
8.3 Incorporating fairness . . . 128
8.4 Case study . . . 129
8.4.1 Incorporating fairness: the operating envelope problem . . . 129
8.4.2 Problem formulation . . . 130
8.4.3 Results . . . 133
8.5 Chapter Conclusions . . . 134

9 Conclusions and Directions of Future Work . . . 139

9.1 Summary of Key Results . . . 139
9.2 Future Work . . . 141

9.2.1 Managing the Energy Constraints of Energy Storage 141
9.2.2 Dynamic Networked Microgrids 142
9.2.3 Network-Safe DER Operation 142
9.3 Concluding Remarks 143

BIBLIOGRAPHY 145

LIST OF FIGURES

FIGURE

2.1 Block diagram for PJM conditional neutrality controller. 13
2.2 Block diagram of controller to generate CAISO regulation up and down signals. 15
2.3 One-line diagram of the PJM 5-bus system without battery. 20
2.4 Comparison of the PJM regulation signals with and without feedback. 2.4a shows a comparison between the RegA signal generated by the PJM controller and what the RegA signal would have been if there were no feedback. 2.4b shows the same comparison in terms of RegD. Both figures represents 1 hour of the signal taken from one of the simulated cases. 24
2.5 A plot of the fixed power transactions made by the battery in each 5-min real-time market period. A positive value represents power purchased from the market (charging) and a negative value represents power sold to the market (discharging). 25

3.1 Illustration of a dynamic partition of networked microgrids using switches. Here, load blocks are interconnected by switches to form connected components (CCs) that act as independent microgrids. Each CC contains uncertain loads and a set of DGs, with one acting as a Grid-Forming DG (GFM-DG) if that particular CC is energized. 30
3.2 Single-line diagram of the 37-bus network without loads shown. 39
3.3 Optimal robust partitioning of the 37-bus network with varying levels of uncertain loads. We assume the substation is out-of-service. Energized and de-energized CCs are colored in green and red, respectively. The GFM-DG and the closed switches are highlighted in blue. 41

4.1 Dynamic reconfiguration of networked microgrids via switches. Blocks are connected by switches to form connected components (CCs). Each energized CC, which functions as an independent microgrid, contains uncertain loads and DGs, with at least one DG serving as a voltage source. 48
4.2 Diagram illustrating the integration of the faster time scale MFRT-OPF algorithm with the RPOP. 59
4.3 Illustration of the load blocks and the switches that connect them. Load clusters A-G are indicated by the blue and orange backgrounds grouping blocks together. 60
4.4 Optimal partitioning of the SMART-DS network under varying uncertain loads. Black blocks indicate de-energized blocks, yellow blocks without outlines indicate the presence of a GFM-DG or substation voltage source, and black lines represent closed switches. Load clusters A-G are indicated by the blue and orange backgrounds grouping blocks together. 61

4.5 Optimal partitioning of the SMART-DS network assuming 20% load uncertainty. Black blocks indicate de-energized blocks, yellow blocks without outlines indicate the presence of a GFM-DG or substation voltage source, and black lines represent closed switches. Load clusters A-G are indicated by the blue and orange backgrounds grouping blocks together. 64
4.6 MFRT-OPF results. 65

5.1 Communications between the DSO, aggregator, network, and DERs. 72
5.2 Single-line diagram of 56-bus network presented in [1]. 79
5.3 Comparison of the real power limits based on nodal constraints found using the Maxsum OE approach, the Fair OE approach, and the Input Const approach at each node for Scenario 1. 81
5.4 Comparison of the real power limits found using the Maxsum OE approach, the Fair OE approach, and the Input Const approach at each node. 82
5.5 Comparison of the total network flexibility found using the Maxsum OE approach, the Fair OE approach, and the Input Const approach with respect to network loading increases for Scenario 2. 82
5.6 Comparison of the total network flexibility from nodal constraints (Fair OE and MaxSum OE) and network-wide constraints (Input Const) with respect to network loading increases for Scenario 3. 83

6.1 One line diagrams of the (a) 4-bus network, based on a network available from [2], and (b) 56-bus network presented in [1]. 92
6.2 The voltage at each bus in the 4-bus network resulting from solving AC power flow with power exports at each node equal to the operating envelope limits calculated using the nonlinear and SOC operating envelope formulations. 93
6.3 The inexactness of the SOC relaxation of the power flow equations for the 4-bus network. 95
6.4 The voltage at each bus in the 56-bus network resulting from solving AC power flow with power exports at each node equal to the operating envelope limits calculated using the nonlinear and SOC operating envelope formulations. 96
6.5 The inexactness of the SOC relaxation of the power flow equations for the 56-bus network. 96
6.6 The voltage at each bus in the 56-bus network resulting from solving AC power flow with power exports at each node equal to the operating envelope limits calculated using the nonlinear, original SOC, and modified SOC operating envelope formulations. 97
6.7 The inexactness of the modified SOC relaxation of the power flow equations for the 56-bus network. Note the different y-axis scale from Fig. 6.5. 98
6.8 The sum of the inexactness, i.e., $lv - (p^2 + q^2)$, at every bus, and the resulting operating envelope for each bus as the weighting parameter λ is increased. . . . 99

7.1 Results for the 141-bus network using nonlinear, SOC, and modified SOC formulations. 108

7.2 The impact of λ. Like in Fig. 7.1b, we plot the voltage at each bus in the 141-bus network resulting from solving AC power flow with power exports at each bus equal to the operating envelope limits calculated using the nonlinear and modified SOC formulations, but for three choices of λ. 110
7.3 The sum of the inexactness, i.e., $lv - (p^2 + q^2)$, at every bus, and the smallest resulting operating envelope as λ is increased. 111
7.4 Relationship between r, x and the feasibility (7.8). Black areas represent values for which (7.8) is infeasible, i.e., the SOC relaxation is exact. Yellow areas represent values for which (7.8) is feasible, i.e., the SOC relaxation is not exact. White areas represent values for which (7.1) was locally infeasible. 114
7.5 Deviations δ obtained by solving (7.8) for different r and x values in the 2-bus network. White space indicates values of r and x for which (7.8) is infeasible, i.e., the SOC relaxation is exact. 115
7.6 Relationship between r, x and the slack variables in (7.8). 117

8.1 Accumulated operating envelope allocation at each node in the network 135
8.2 Total percentage of forecasted capacity curtailed over the time horizon, $\frac{\sum_{t\in\mathcal{T}} p^f_{i,t} - p^{\mathrm{OE}}_{i,t}}{\sum_{t\in\mathcal{T}} p^f_{i,t}}$, at each node in the network 136
8.3 Comparison between the operating envelope allocation in the first time step, $H^{\mathrm{OE}}_{i,1}$, and the weighted average of historical unfairness at the end of the time horizon, $H^{\mathrm{OE}}_{i,25}$. 137

LIST OF TABLES

TABLE

2.1 Case Study Parameters 21
2.2 Average Performance Metrics (and Standard Deviations) 22

3.1 Sensitivity of Operating Costs and Algorithm Run Times to Load Uncertainty Percentage 39

4.1 RPOP run times and feasibility 62

5.1 Comparing the Assumptions for Nodal vs. Network-wide Constraint Approaches 73

6.1 Numerical Results for SOC Formulation 94
6.2 Numerical Results for AC Power Flow Using Operating Envelopes Generated from SOC Formulation 94
6.3 Numerical Results for Full Nonlinear Operating Envelope Formulation 94

7.1 Measures of Inexactness 109

8.1 Performance vs. Fairness 134
8.2 Performance vs. Fairness as DER Capacities Increase 137

ABSTRACT

Distributed energy resources (DERs) like roof-top solar, electric vehicles, and flexible loads, have emerged as promising solutions to both decarbonize and democratize the energy sector. Without the proper technical and socioeconomic tools, DERs will not only fail to achieve these goals, but they will also leave the grid less reliable and less resilient than it is today. This thesis explores methods for leveraging DERs to enhance grid reliability, resiliency, and equity. Grid reliability ensures the adequate and stable supply of electricity to meet demand while resilience defines the grid's ability to withstand and recover from disruptions such as faults or cyber-attacks. Energy equity is the concept that the benefits of energy should be distributed fairly and justly, regardless of race, socioeconomic status, or ability. This dissertation, containing 3 projects, uses optimization and control to tackle these critical issues in the context of DER integration.

Specifically, novel optimization algorithms and control strategies are proposed to reduce the extent of power outages using networked microgrids, to enable DERs and DER aggregations to participate in electricity markets while maintaining reliability, and to ensure DERs are treated equitably. Additionally, we present relevant sociotechnical analysis like how regulatory frameworks, market structures, and system operator decisions impact the benefits that DERs can provide society.

In the first project within this dissertation, the system impacts of two different market mechanisms currently implemented by two U.S. independent system operators for managing the energy constraints of battery energy storage providing frequency regulation are analyzed. A qualitative comparison in terms of the responsibilities of involved parties, impacts on resource requirements, and how market rules impact utilization is presented. Controller and market simulations are used to quantitatively compare the two strategies in terms of regulation-signal following performance and additional system control effort.

In the second project, we formulate a robust optimization problem for configuring a distribution network composed of networked microgrids to minimize load shedding and generator costs during contingencies, accounting for load uncertainty. After reformulation for tractability, we present a novel cutting-plane algorithm to solve the problem. In addition, we present a real-time optimal power flow algorithm to operate the DERs after reconfiguration

and present modifications to the cutting-plane algorithm to improve scalability. Detailed numerical studies highlight the benefits of networked microgrids on system resilience and the significance of considering load uncertainty in operational decision-making.

Without proper management DERs can cause reliability issues such as over- and under-voltages, over-current violations, and transformer overheating. In this three-part project, we investigate an existing method for managing DERs and DER aggregations, dynamic operating envelopes, to ensure network reliability. Dynamic operating envelopes, or simply operating envelopes, represent node-specific dynamic net export limits set by the system operator. In the first part of this project, we analyze market and social implications, comparing operating envelopes to another proposed DER aggregation management method. Next, we examine and address technical challenges in operating envelope implementation. Finally, we propose a more equitable implementation for determining operating envelopes. The novelty of our proposed fair-over-time implementation is that it allows the operating envelope allocations to be unfair at any time step but requires that the allocations be fair over the entire time horizon.

CHAPTER 1

Introduction

In response to climate change and technological innovation, the electricity sector is replacing many traditional energy generators, like coal power plants, with renewable sources like wind and solar photovoltaics (PV). According to the International Energy Agency (IEA), renewable generation made up almost 75% of all new electricity generation capacity added globally in 2024 [3]. While these renewable energy technologies provide environmental benefits, they simultaneously create new challenges for the energy industry. Specifically, renewable energy resources are intermittent and introduce greater uncertainty around resource availability compared to coal, natural gas, or nuclear power.

Not only are the types of generators changing, but the size and location of generation is also shifting. Generation capacity is being installed within distribution networks at an increasing rate. The IEA estimates that 167 GW of distributed PV were added globally from 2019 to 2021 [4]. Most distribution networks were not designed to contain generation, and because of this, are facing new challenges. For example, protection schemes were designed under the pretense that power flows in one direction from the substation to the load [5]. Reverse power flows caused by distributed generation are necessitating new protection schemes [6].

Also impacting distribution network operations is the introduction of new kinds of loads, like electric vehicles (EVs) and heat pumps. The number of EVs worldwide tripled between 2017 and 2020 [4], and it is forecasted that they could make up as much as 65% of cars sold worldwide by 2030 [7]. EVs have the potential to increase peak load demand, overload transformers and cables, increase voltage drop, increase system unbalance, increase power losses, and increase harmonic distortion [8, 9]. However, EVs and other loads also have the potential to provide grid services like load shifting, reactive power support, voltage stabilization, and frequency regulation [10–12].

The term 'distributed energy resource' or DER encompasses a wide variety of resources. Rooftop solar, battery energy storage, and flexible loads like EVs or smart thermostats can

all be considered DERs. What defines a resource as a DER is its location: "on the distribution system, any subsystem thereof or behind a customer meter" [13]. Due to their proximity to load centers and their operational flexibility, DERs offer many potential benefits. However, they increase the complexity of the design, control, and operation of both distribution networks and electricity markets.

Shifting to a greener and more decentralized energy system will require changing many aspects of how power systems and power markets are operated. The work presented in this dissertation explores the role of DERs in those changes, as well as the impacts that regulatory frameworks, market structures, and system operator decisions have on DERs.

1.1 DERs: Opportunities and Challenges

To ensure reliability and resiliency while increasing our reliance on uncertain and intermittent resources will require energy systems to become more flexible. DERs, like roof-top solar PV, batteries, and electric vehicles, can provide that flexibility [14]. Not only can DERs provide the grid needed flexibility, they can also improve operating efficiencies and provide economic opportunities for consumers [15]. However, there still remain a number of reliability and resiliency challenges with DERs.

1.1.1 Reliability

According to the National Renewable Energy Laboratory (NREL), "reliability is the ability to maintain power delivery to customers in the face of routine uncertainty in operating conditions, as in cases of fluctuating load and generation, fuel availability, and outage of assets under normal operating conditions" [16]. DERs are extremely relevant when discussing grid reliability because they can degrade power quality in distribution networks if they are not properly managed. High penetration levels of DERs can lead to overloaded equipment, over- and under-voltages, voltage imbalances, and harmonics [17, 18]. However, DERs can also be used to improve grid reliability. By controlling their active and reactive power setpoints, DERs can provide local voltage regulation and other services [15, 19, 20].

Beyond local, distribution level reliability, DERs can support transmission level reliability by providing ancillary services. DERs like batteries and thermostatically-controlled loads (TCLs) can provide peak shaving and load following [21, 22]. As reliance on intermittent renewable generation like large-scale wind and solar becomes greater, continuously matching demand and supply will become a greater challenge. The need for reserves and frequency regulation will increase [23]. In addition to providing valuable energy shifting, battery energy

storage can respond to signals faster than traditional generators. This makes them well suited to provide reserves and regulation ancillary services [24]. Improvements in advanced control strategies are also enabling flexible loads, like TCLs, to provide these services [25,26]. While providing transmission-level services, DERs are still operating within the distribution network and so it is still imperative to ensure their operation does not cause the issues highlighted in the previous paragraph.

In this dissertation, we explore how DERs can improve system reliability through the provision of ancillary services. Additionally, we explore frameworks for ensuring the DER operation does not cause unsafe operation in distribution networks. Further details can be found in Section 1.5.

1.1.2 Resiliency

In contrast to reliability, resiliency represents the ability to absorb, adapt to, and recover from low probability, high-consequence disruptions [16]. Resilience events tend to cause longer outages and impact larger geographic areas. DERs play a role in improving grid resiliency by serving load during outages. The existence of DERs also enables the existence of microgrids. Microgrids, which the U.S. Department of Energy (DOE) defines as "a group of interconnected loads and distributed energy resources within clearly defined electrical boundaries" [27], have been identified as key building blocks for future grids [28].

Microgrids, during normal conditions, can support the bulk power system by acting as points of aggregation in control systems. Additionally, microgrids, and networks of microgrids, can support the critical end-use loads when the bulk power system is not available [27, 29, 30]. There are still a number of challenges preventing the wide-scale use of microgrids and networked microgrids [31]. One challenge is dealing with uncertainty. In a distribution network, there is uncertainty in power demand, and in the presence of DERs like PV, there is uncertainty in power generation [32,33]. This dissertation explores the relevance of accounting for uncertainty when operating DERs and networked microgrids. More details are given in Section 1.5.

1.2 Electricity Market and Policy Implications

Electricity market structures and regulations need to adapt in order for new technologies to provide their full potential. Energy resources, new and old, have their own strengths and weaknesses which should be considered in regulations. Batteries, for example, have very fast ramping rates compared to traditional regulation-providing resources, making them excellent

candidates for providing frequency regulation. Despite their superior response times, battery resources were being valued by the markets at the same rate as slower resources until 2011 when Federal Energy Regulatory Commission (FERC) Order No. 755 required the markets to compensate for faster-ramping frequency regulation [34, 35]. In response to FERC order 755, PJM split its frequency regulation market into a faster-ramping and slower-ramping service, and the fast-ramping service was designed to be energy neutral for the "energy limited resources" [36]. Since the introduction of this new regulation service, energy storage capacity has grown rapidly in the PJM service territory [34], exemplifying the impacts that electricity policies and regulations can have.

Recently, there have been more regulatory changes that aim to break down barriers for new technologies and DERs. In 2018, FERC Order No. 841 required system operators to make participation in capacity, energy, and ancillary service markets easier for storage resources by incorporating the physical and operational characteristics of energy storage in the market rules [37]. In 2020, FERC Order No. 2222 made similar requirements for participation of DER aggregations in capacity, energy, and ancillary service markets [13]. However, there still remain open questions about the roles of DER aggregations in electricity markets, specifically, how to ensure the aggregator's market participation will not cause distribution network reliability and safety issues [38]. In this dissertation, we examine the impacts that market structures and regulations can have on the utility that newer energy resources, like batteries and DERs, can provide to the grid. More details will be provided in Section 1.5.

1.3 Considering Energy Justice

According to the Initiative for Energy Justice, "Energy justice refers to the goal of achieving equity in both the social and economic participation in the energy system, while also remediating social, economic, and health burdens on those historically harmed by the energy system ('frontline communities'). Energy justice explicitly centers the concerns of marginalized communities and aims to make energy more accessible, affordable, and clean and democratically managed for all communities" [39]. While many may argue that dealing with injustice in energy is a social science or policy problem, recent literature has shown that there is a place in power systems research for energy justice.

There have been large disparities by race and class in the adoption rates of DERs like rooftop PV and EVs in the U.S. [40–42]. While public policy, rather than power systems research, is a more relevant tool for dealing with inequity caused by socioeconomic factors, power systems researchers should be concerned about how grid limits within and across

utility territories may impact future DER deployment, and the potential implications for equity and access to DERs. The analysis in [43] shows that hosting capacity for DERs decreases for households in increasingly Black-identifying and disadvantaged communities. This work highlights the need to analyze the equity of electrical capacity for DER adoption so that the grid does limit equitable DER uptake in the future.

Research described in the previous paragraph shows how energy justice can play a role in power systems and grid planning. There are also many grid operation and control contexts where energy justice can have a significant impact. Consider the operation of an aggregation of batteries and TCLs providing ancillary services. The lifespan of both types of resource is impacted by the frequency or number of switching operations [44, 45]. In [44], we develop an approach to capture the uncertainty in the degradation of batteries used for energy arbitrage and for providing frequency regulation, though we did not connect this work to equity or fairness. Equity or fairness metrics could be used to ensure some subset of the total population does not degrade faster than the total population. In [46], social vulnerability to power outages is incorporated into an optimization problem for configuring networked microgrids to manage wildfire risk while minimizing the impacts on particularly vulnerable populations. Methods for pricing electricity in a grid-aware, equitable fashion for EV charging stations are presented and evaluated in [47]. In this dissertation, we aim to utilize energy justice principals to ensure equitable access to electricity market participation for DERs and DER aggregations. More details are given in Section 1.5.

1.4 Contributions of Dissertation

The key contributions of this dissertation are novel frameworks for power systems analysis, original optimization problem formulations, and new algorithms for solving those formulations.

Specifically, this dissertation presents novel analysis frameworks in the contexts of (i) managing the energy constraints of energy storage providing frequency regulation, (ii) network-safe DER coordination, and (iii) the effectiveness of convex relaxations for computing network-safe constraints.

This dissertation also presents original optimization problem formulations to (i) find the configuration of networked microgrids that will minimize load shedding during a contingency while considering load uncertainty and to (ii) compute network-safe constraints considering dynamic fairness. Key to the networked microgrids formulation are new constraints for modeling the need for a voltage source connected to each phase of each energized portion of the network.

Finally, this dissertation presents new algorithms for solving (i) the robust networked microgrid reconfiguration problem formulation and (ii) an optimal power flow problem for operating distributed generation within networked microgrids without a network model. Specifically, a cutting-plane algorithm is proposed to solve (i) and a model-free, primal-dual algorithm is proposed to solve (ii).

1.5 Organization of Dissertation

This dissertation is composed of eight main chapters which cover three projects. Chapter 2 covers the first project, which focuses on existing market structures around battery energy storage systems providing frequency regulation in the United States. The second project, which focuses on the use of dynamic networked microgrids for improving grid resilience, is covered in Chapters 3 and 4. The third project is covered in Chapters 5-8. In these chapters, we investigate an existing method for managing DERs and DER aggregations: dynamic operating envelopes. Dynamic operating envelopes, or simply operating envelopes, represent node-specific dynamic net export limits set by the system operator to ensure network reliability. In the first part of this project, we analyze market and social implications, comparing operating envelopes to another proposed DER aggregation management method. Next, we examine and address technical challenges in operating envelope implementation. Finally, we propose a more equitable implementation. A brief summary of the work presented in each chapter is described below.

Chapter 2 presents a comparison of strategies used by two U.S. Independent System Operators (ISOs), PJM and CAISO, for managing the energy constraints of energy storage providing frequency regulation. We quantitatively compare the two strategies in terms of regulation-signal following performance and additional system control effort. In this work, we model the controllers used by both ISOs for producing their frequency regulation signals and develop an approach to simulate the key aspects of both strategies. A case study on the PJM 5-bus network leveraging real area control error (ACE) data is presented. We also present a qualitative comparison of the two approaches by discussing how the ISOs level of responsibility varies between the two approaches, how the approach impacts system resource needs, and how market regulations impact the utility of the approaches.

Chapter 3 presents a robust optimization problem for reconfiguring a distribution network composed of networked microgrids in order to minimize load shedding and generator

costs during a contingency while considering load uncertainty. We model loads as uncertainty sets and use a robust formulation to ensure the partitioned power network's operation is feasible for all load realizations within the specified uncertainty set. In this chapter, we formulate a two-stage model. The first stage is a mixed-integer quadratic program (MIQP) that optimizes network partitioning decisions while minimizing total unsatisfied loads and generation costs for the nominal load realization. Subsequently, after the load uncertainty is revealed, the second-stage (recourse) problem adjusts generation set-points subject to three-phase, unbalanced power flow constraints. We present a number of simplifications and a reformulation of this infinite-dimensional optimization problem for tractability. We then develop a cutting-plane algorithm to efficiently solve the problem. Finally, we present a detailed numerical study analyzing the sensitivity of planning and operation to uncertainty set parameters, and illustrate the potential benefits of networked microgrids for maximizing load delivery. Additionally, we demonstrate the feasibility of solutions obtained from the two-stage simplified and reformulated problem against AC three-phase power flow through a sampling approach.

Chapter 4 presents improvements to the robust partitioning problem formulation presented in Chapter 3. Specifically, we modify the problem formulation for faster solve time and better scalability. We also refine the process for selecting inverter control modes by introducing new constraints to the formulation. In addition to the improved reconfiguration problem, we introduce a model-free, real-time optimal power flow algorithm for operating the dynamic networked microgrids as loads change between network reconfigurations. We then illustrate the scalability of both algorithms on a realistic distribution network.

Chapter 5 presents a comparison between the use of network-wide and nodal constraints for ensuring network-safe operation of a distribution network in the presence of a DER aggregator. We investigate their respective strengths and limitations by considering information and communication requirements. For the nodal approach, we use an operating envelope framework with two different objective functions. One objective function maximizes the sum of the envelopes across the network to get the greatest aggregate flexibility. The second objective function maximizes the smallest operating envelope in the network to get a fair allocation of flexibility across the nodes in the network. For the network-wide approach, we compute a constraint on the input of the aggregator's controller which will ensure voltage limits are obeyed. A case study is used to illustrate how the different approaches, and the consideration of fairness,

impact the aggregate flexibility from the resources.

Chapter 6 presents a case for why a second-order cone (SOC) relaxation should not be used to compute operating envelopes. Operating envelopes, which represent dynamic net export limits set by the system operator at every node in the network, are commonly computed using an optimal power flow problem. For computational tractability, linearizations or relaxations of the nonlinear power flow equations are typically used. In this chapter, two case studies and some numerical analysis are presented to explain why using a second-order cone (SOC) relaxation for constructing operating envelopes is ill considered. Additionally, we propose an objective function modification to improve the tightness of the SOC relaxation. The efficacy of this modification is illustrated by a case study.

Chapter 7 builds on the work presented in Chapter 6. In this chapter, we return to the objective function modification proposed in Chapter 6 and discuss further limitations. Additionally, we investigate the conditions under which a SOC relaxation is and is not exact for the operating envelope problem. We prove mathematically that for a purely resistive, radial network, the SOC operating envelope problem will generally be inexact. We also prove that for a purely reactive, radial network, the SOC operating envelope problem will generally be exact. The case for realistic networks, which are both resistive and reactive, is more complex. Work in this chapter further justifies our earlier statement that a SOC relaxation should not be used to construct operating envelopes.

Chapter 8 explores fairness metrics from machine learning and identifies metrics that could be incorporated into DER coordination problems. A summary of fairness metrics that have previously been used in the power systems literature within the context of the DER coordination problem is also presented. We identify that most existing fairness metrics are static – ensuring fairness at a point in time - even for inherently dynamic problems. For example, in DER coordination problems, we often care about fairness over an entire time horizon, rather than at each time step. Yet, existing literature on fair DER coordination applies fairness at each time step. The machine learning literature offers some insights on the concept of fairness over time and, more generally, how to incorporate fairness into dynamic power systems problems. We use a specific DER coordination problem – the problem of computing dynamic operating envelopes– to demonstrate how incorporation of a fair-over-time metric changes DER coordination solutions, and highlight the trade-offs that arise.

Chapter 9 concludes the dissertation and discusses directions of future work.

Note that each chapter is self-contained; notation is defined in each chapter and applies only within that chapter.

CHAPTER 2

A Comparison of Strategies for Managing Energy Constraints of Energy Storage Providing Frequency Regulation

In this chapter we present a comparison of the strategies used by two U.S. independent system operators (ISOs) for managing the energy constraints of battery energy storage providing frequency regulation. CAISO and PJM operate the majority of grid-connected batteries in the U.S. The two markets manage the energy constraints of batteries providing frequency regulation differently. PJM, which has a fast (RegD) and a slow (RegA) regulation signal, uses RegA to conditionally maintain energy neutrality of the RegD signal over short durations. CAISO offsets net energy produced/consumed for frequency regulation with energy from the real-time energy market. This chapter assesses the advantages and disadvantages of each approach. Specifically, we compare the approaches in terms of regulation signal-following performance and additional system control effort. Case study results suggest that both strategies can reliably keep a battery away from its state of charge limits but that PJM's strategy requires larger energy deviation from base operations. The work in this chapter is based on our published work [48].

2.1 Chapter Introduction

Growing reliance on intermittent and uncertain renewable energy generation has led to increase in demand for energy storage, a trend which is expected to continue [34]. Energy storage, specifically battery energy storage systems (henceforth simply batteries), can provide many services to the grid including but not limited to arbitrage, peak shaving, and frequency regulation [49]. Federal Energy Regulatory Commission (FERC) orders in the last 11 years have led to increased participation of batteries in energy markets. Most notably are FERC Order 755 (issued in 2011), which requires markets to compensate for resources

that can provide faster-ramping frequency regulation, and FERC order 841 (issued in 2018), which requires system operators to remove barriers for batteries and similar resources to participate in the capacity, energy, and ancillary services markets [34].

In response to FERC Order 755, the PJM Interconnection (PJM) split its frequency regulation service into a faster-ramping service (RegD), well-suited to batteries, and a slower-ramping service (RegA). Within a few years, more than 180 MW of large-scale battery power capacity had been installed in PJM [34], far outpacing the installation rate in other U.S. markets. The California Independent System Operator (CAISO) also experienced a large influx of battery power capacity after the California Public Utility Commission passed an energy storage mandate in 2013 requiring investor-owned utilities to procure 1,325 MW of energy storage by 2020 [34]. By the end of 2020, California had 520 MW of large-scale batteries in operation, making CAISO the U.S. electricity market with the largest battery power capacity [34].

Batteries can respond faster than conventional power plants that traditionally provide frequency regulation, making them desirable for providing frequency regulation [50, 51]. However, a key challenge to using energy storage for frequency regulation is the need to manage its energy constraints [52]. Conventional power plants have power and ramping constraints, but can generally provide frequency regulation continuously over long periods so long as they are dispatched within (i.e., not at the edges of) their operational range and the offered frequency regulation capacity respects their ramping constraints. In contrast, energy storage is energy-limited meaning that it can not continuously discharge without charging, and vice versa. This means that a consistently-biased regulation signal will cause the the storage to fill or empty, making it unable to provide frequency regulation. If the regulation signal is approximately energy neutral, i.e., the energy embodied within up regulation matches the energy embodied within down regulation, over short durations then energy storage can continually provide frequency regulation. Some independent system operators (ISOs) have developed mechanisms to achieve energy neutrality in batteries providing frequency regulation; however, they all do this differently.

The objective of this chapter is to compare the strategies used by PJM and CAISO for managing the energy constraints of batteries providing frequency regulation in order to assess the advantages and disadvantages of each approach. PJM employs a conditional neutrality controller, where energy used to provide fast frequency regulation by RegD resources (i.e., fast-ramping resources like batteries) is compensated by RegA resources (i.e., traditional, slow-ramping resources like conventional power plants) when there is sufficient capacity to do so [53]. Both signals capture up and down regulation. In CAISO, batteries are categorized as non-generator resources (NGRs), meaning they have the capability to serve

as both generation and load but are constrained by energy limits [54]. NGRs providing frequency regulation that wish to increase their regulation capacity can opt into regulation energy management (REM). In REM, the system operator is responsible for maintaining a preferred state of charge (SoC) by offsetting net energy produced/consumed by the resource for frequency regulation with energy from the real-time market [55]. CAISO uses one signal for up regulation and one signal for down regulation.

Different frequency regulation implementations and strategies for managing the energy constraints of batteries can lead to different operational outcomes. For example, PJM re-designed their regulation controller in 2016 because their old controller often caused batteries to move in the opposite direction to that needed to regulate frequency [53]. This resulted in the need to compensate the batteries' actions through more frequency regulation control effort and more frequency regulation capacity. Overall, the design of the regulation controller should balance performance and control effort, both of which impact the required frequency regulation capacity. Improving performance can improve frequency quality and decrease the system regulation requirement [56]. Achieving better frequency quality with less regulation capacity will be increasingly important as renewable generation increases [57]. Frequency regulation implementations and strategies for managing the energy constraints of batteries can also affect other reliability and cost metrics. Understanding these trade-offs will allow ISOs to make better decisions.

The main contribution of this chapter is a comparison of the strategies used by PJM and CAISO for managing the energy constraints of batteries providing frequency regulation. We quantitatively compare the strategies in terms of regulation signal-following performance and additional system control effort. To do this, we implement both regulation controllers and develop an approach to simulate the key aspects of both strategies on the PJM 5-bus system leveraging a real area control error (ACE) data. Note, this chapter does not attempt to model all details of the PJM and CAISO markets, but rather we model their strategies for managing the energy constraints of batteries providing frequency regulation.

Section 2.2 presents mathematical descriptions of the regulation controllers. Section 2.3 develops the simulation method used to compute the comparison metrics. Section 2.4 presents our case study. Conclusions are given in Section 2.5.

2.2 Regulation Controllers

This section presents the controllers used to generate the PJM and CAISO regulation signals and, for CAISO, the method of calculating the energy offset needed for REM.

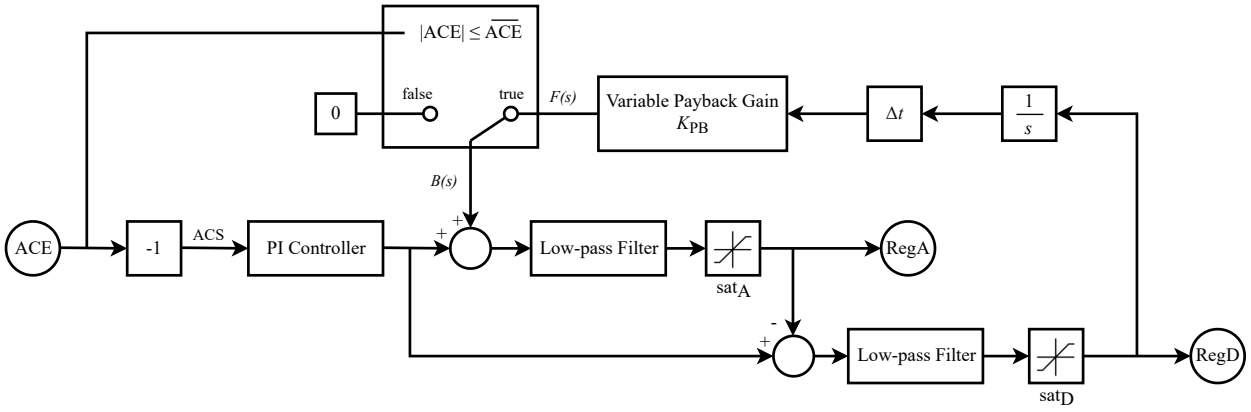


Figure 2.1: Block diagram for PJM conditional neutrality controller.

2.2.1 PJM Conditional Neutrality Controller

Here we present a mathematical representation of the PJM conditional neutrality controller and briefly summarize its key features, as described in [53]. PJM generates two types of regulation signals. The RegA signal is designed for slower-ramping resources, and the RegD signal is designed for faster-ramping, energy-limited resources. Both signals are bi-directional with symmetric limits; a negative signal represents down regulation and a positive one represents up regulation.

The controller, shown in Fig. 2.1, uses proportional-integral (PI) control with an internal feedback loop which controls the SoC of resources providing RegD. The input to the controller is the ACE, which is multiplied by -1 to obtain the ACE correcting signal (ACS). To create the RegA signal, the ACS is passed through the PI controller, combined with the accumulated neutrality bias $B(s)$ (described later), passed through a low-pass filter, and finally constrained to have a magnitude less than or equal to the total RegA capacity via a saturation filter sat_A. Mathematically,

$$\text{RegA}(s) = \text{sat}_\text{A}\left(\frac{-\text{ACE}(s)\left(\frac{K_\text{I}}{s} + K_\text{P}\right) + B(s)}{\tau_\text{A} s + 1}\right), \tag{2.1}$$

where $\text{ACE}(s)$ is the ACE signal, K_P and K_I are the proportional and integral control gains of the PI controller, τ_A is the time constant of the low-pass filter that reflects the ramping constraints of the generators providing RegA, and

$$\text{sat}_\text{A}(x) = \begin{cases} x, & \text{if } -\overline{\text{RegA}} \le x \le \overline{\text{RegA}}, \\ \overline{\text{RegA}}, & \text{otherwise}, \end{cases} \tag{2.2}$$

where $\overline{\text{RegA}}$ is the capacity for RegA.

The residual between the output of the PI controller and the RegA signal is passed through another low-pass filter and constrained to have a magnitude less than or equal to the total RegD capacity via a saturation filter sat_D, resulting in the RegD signal

$$\text{RegD}(s) = \text{sat}_\text{D}\left(\frac{-\text{ACE}(s)\left(\frac{K_\text{I}}{s} + K_\text{P}\right) - \text{RegA}(s)}{\tau_\text{D} s + 1}\right), \tag{2.3}$$

where τ_D is the time constant of the low-pass filter that reflects the faster but still limited ramping constraints of the resources providing RegD and

$$\text{sat}_\text{D}(x) = \begin{cases} x, & \text{if } -\overline{\text{RegD}} \leq x \leq \overline{\text{RegD}}, \\ \overline{\text{RegD}}, & \text{otherwise}, \end{cases} \tag{2.4}$$

where $\overline{\text{RegD}}$ is the capacity for RegD.

To determine the accumulated neutrality bias, the RegD signal is first integrated to capture the net injection or withdrawal of energy over time and multiplied by a variable payback gain K_PB (described later), i.e.,

$$F(s) = \frac{K_\text{PB} \cdot \text{RegD}(s)}{s}. \tag{2.5}$$

Then, the accumulated neutrality bias is set to $F(s)$ when the magnitude of the ACE signal at or below a designated threshold $\overline{\text{ACE}}$, i.e.,

$$B(s) = \begin{cases} F(s), & \text{if } |\text{ACE}(s)| \leq \overline{\text{ACE}}, \\ 0, & \text{otherwise}. \end{cases} \tag{2.6}$$

When the ACE is above $\overline{\text{ACE}}$, neutrality feedback is suspended. Note that both signals are unaffected by neutrality feedback when the RegA signal is at either of its limits.

Consider a single battery providing frequency regulation. The variable payback gain increases as the battery SoC deviates from 50%. In other words, the closer the battery gets to its energy limits, the further the RegA signal is pushed from the ideal control point, allowing the RegD signal to move in the direction that corrects SoC. The payback gain is calculated as

$$K_\text{PB} = \begin{cases} \frac{E_\text{B}}{2}, & \text{if } 37.5\% \leq \text{SoC} \leq 62.5\%, \\ 10E_\text{B}, & \text{if } \text{SoC} \leq 25\% \vee \text{SoC} \geq 75\%, \\ \frac{60E_\text{B}}{28}, & \text{otherwise}, \end{cases} \tag{2.7}$$

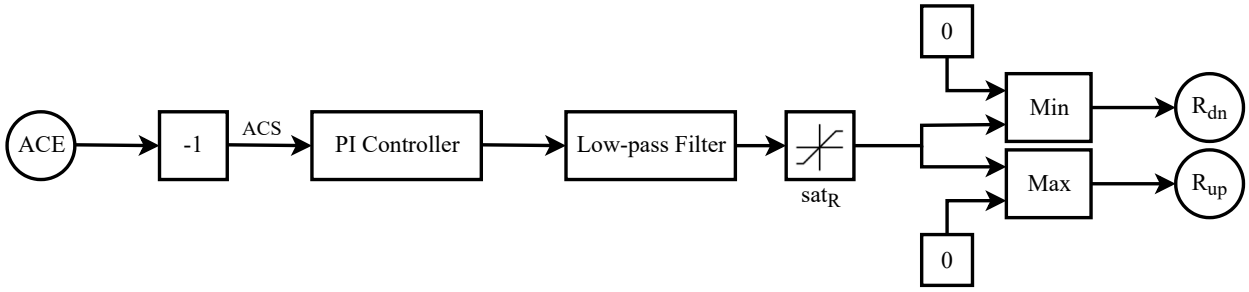


Figure 2.2: Block diagram of controller to generate CAISO regulation up and down signals.

where E_{B} is the energy capacity of the battery in MWh. The payback gain is set to restore the SoC back to 50% within 15 min if the first condition holds, 3 min if the second holds, and 7 min if the third holds. The battery SoC is estimated using the integral of the RegD signal [58].

2.2.2 CAISO Regulation Signals and REM

Here we present a mathematical representation of CAISO's regulation signal generator and REM strategy. A block diagram of the controller is given in Fig. 2.2. Like PJM, CAISO uses PI control, low pass filtering, and generates two regulation signals [59]. However, CAISO splits its regulation signal into an up and a down regulation signal, not a fast and slow regulation signal like PJM. The up regulation signal is positive and tells participating resources to increase their power output, or to produce power in the case of a battery. The down regulation signal is negative and tells participating resources to decrease their power output, or to consume power in the case of a battery. The up and down regulation signals are given by

$$\mathrm{R_{up}}(s) = \max\left(0, \mathrm{sat_R}\left(\frac{-\mathrm{ACE}(s)\left(\frac{K_\mathrm{I}}{s} + K_\mathrm{P}\right)}{\tau s + 1}\right)\right) \tag{2.8}$$

$$\mathrm{R_{dn}}(s) = \min\left(0, \mathrm{sat_R}\left(\frac{-\mathrm{ACE}(s)\left(\frac{K_\mathrm{I}}{s} + K_\mathrm{P}\right)}{\tau s + 1}\right)\right) \tag{2.9}$$

where τ is the time constant of the low-pass filter and the saturation function $\mathrm{sat_R}$ is

$$\mathrm{sat_R}(x) = \begin{cases} x, & \text{if } -\overline{\mathrm{R_{dn}}} \le x \le \overline{\mathrm{R_{up}}}, \\ -\overline{\mathrm{R_{dn}}}, & \text{if } x < -\overline{\mathrm{R_{dn}}}, \\ \overline{\mathrm{R_{up}}}, & \text{if } x > \overline{\mathrm{R_{up}}}, \end{cases} \tag{2.10}$$

where $\overline{\mathrm{R_{up}}}$ and $\overline{\mathrm{R_{dn}}}$ are the total up and down regulation capacities, respectively.

To manage the energy constraints of batteries providing frequency regulation, CAISO uses the battery's current energy level and previous REM energy offsets to decides the REM energy offset for the next real-time market period [55]. CAISO's real-time market operates every 5 min.

First, the net energy produced/consumed for frequency regulation by battery i is

$$E_{\mathrm{NET},i}(s) = \frac{\left(\eta_i \cdot \gamma_{\mathrm{dn},i} \cdot \mathrm{R_{dn}}(s) - \gamma_{\mathrm{up},i} \cdot \frac{\mathrm{R_{up}}(s)}{\eta_i}\right)}{s} \tag{2.11}$$

where η_i is the efficiency of the battery i, and $\gamma_{\mathrm{up},i}$ and $\gamma_{\mathrm{dn},i}$ are battery i's portion of the total up and down regulation capacities. Note that resources providing frequency regulation, including batteries participating in REM, are not required to bid or provide symmetric up and down regulation capacities [55]. Then, the energy level of battery i is

$$E_i(s) = \mathrm{sat_B}(E_{0,i} + E_{\mathrm{NET},i}(s) + E_{\mathrm{REM},i}(s)) \tag{2.12}$$

where $E_{0,i}$ is the initial energy level of battery i at the start of regulation provision, $E_{\mathrm{REM},i}(s)$ is the energy offset, and

$$\mathrm{sat_B}(x) = \begin{cases} 0, & \text{if } x < 0, \\ x, & \text{if } 0 \le x \le E_{\mathrm{B},i}, \\ E_{\mathrm{B},i}, & \text{if } x > E_{\mathrm{B},i}. \end{cases} \tag{2.13}$$

where $E_{\mathrm{B},i}$ is the energy capacity of battery i.

The energy offset is delivered at a constant power over each real-time market period of duration 5 min. To calculate the energy offset for each 5-min period t, we first estimate battery i's energy level at the beginning of the period using the estimated energy level 7.5 min prior to the start of the current 5-min period $e_{0,i}(t)$ and the energy offsets scheduled for those 7.5 min, i.e., the offsets in the two periods before the period of interest. Specifically,

$$e_i(t) = e_{0,i}(t) + 0.5 \cdot e_{\mathrm{REM},i}(t-2) + e_{\mathrm{REM},i}(t-1), \tag{2.14}$$

where we multiply the second term by 0.5 since we only need to consider the energy offset associated with the second 2.5 min of that period. Then, the energy offset is computed as the difference between this estimate and the preferred energy level $e_{\mathrm{pref},i}$, i.e.,

$$e_{\mathrm{REM},i}(t) = e_{\mathrm{pref},i} - e_i(t). \tag{2.15}$$

2.3 Simulation Approach and Metrics

We next describe the simulation approach we developed to compute the metrics used to compare the PJM and CAISO strategies. The overall approach is to determine the battery and generator actions at every frequency regulation time step over 24 hours. With this, we can compute the regulation-signal following performance and the additional system control effort.

The first step to determine the battery and generator actions is to compute the system dispatch by solving the AC optimal power flow (OPF) problem co-optimizing energy and frequency regulation capacity every 5 min. We do not model the day-ahead market or other reserve markets. We assume that the battery under the CAISO strategy only provides frequency regulation, as resources participating in REM are not eligible to participate in the energy market. In PJM, RegD-providing resources are not barred from also participating in the energy market. PJM's controller integrates the RegD signal to calculate the accumulated neutrality bias, but the impacts of battery round-trip efficiency are not captured and so the battery loses charge over time. We assume that the battery under the PJM strategy can participate in the real-time energy market, but for simplicity, we assume that it only does so to manage its SoC. This is a reasonable assumption, as frequency regulation is the primary use for most large-scale batteries [60]. We model the battery under the PJM strategy as a "fixed gen" resource, meaning that it self-schedules in real-time as a price taker [61]. The battery will self-dispatch when the $e_{0,i}(t)$ is below $0.2E_B$ or above $0.8E_B$. The dispatch is calculated according to 2.14 and 2.15, but in this case, the energy offset $e_{\mathrm{REM},i}(t)$ is replaced by $e_{\mathrm{PJM},i}(t)$, which represents the energy transacted in the PJM real-time energy market by the battery in time step t.

We also assume the cost of frequency regulation provision by batteries is less than the cost of frequency regulation provision by generators, and so batteries are dispatched at full capacity and do not need to be explicitly included in the OPF formulation. We use the MATPOWER function `runopf_w_res()` [2] which solves

$$\min_{\theta,\mathbf{V},\mathbf{P}_\mathrm{g},\mathbf{Q}_\mathrm{g},\mathbf{R}} \sum_{i\in\mathcal{G}} C_{\mathrm{E},i}(P_{\mathrm{g},i}) + C_{\mathrm{R},i}(R_i) \tag{2.16}$$

$$\text{s.t. } \mathbf{P}_\mathrm{bus}(\theta,\mathbf{V}) + \mathbf{P}_\mathrm{d} - C_\mathrm{g}\mathbf{P}_\mathrm{g} = 0, \tag{2.17}$$

$$\mathbf{Q}_\mathrm{bus}(\theta,\mathbf{V}) + \mathbf{Q}_\mathrm{d} - C_\mathrm{g}\mathbf{Q}_\mathrm{g} = 0 \tag{2.18}$$

$$|S_{\mathrm{f},i}(\theta,\mathbf{V})| \le S_i^{\max}, \quad \forall\ i \in \mathcal{L}. \tag{2.19}$$

$$|S_{\mathrm{t},i}(\theta,\mathbf{V})| \le S_i^{\max}, \quad \forall\ i \in \mathcal{L} \tag{2.20}$$

$$V_i^{\min} \leq V_i \leq V_i^{\max}, \quad \forall\, i \in \mathcal{B}. \tag{2.21}$$

$$P_{\mathrm{g},i}^{\min} + R_i \leq P_{\mathrm{g},i} \leq P_{\mathrm{g},i}^{\max} - R_i, \quad \forall\, i \in \mathcal{G}, \tag{2.22}$$

$$Q_{\mathrm{g},i}^{\min} \leq Q_{\mathrm{g},i} \leq Q_{\mathrm{g},i}^{\max}, \quad \forall\, i \in \mathcal{G} \tag{2.23}$$

$$\sum_i R_i \geq R^{\mathrm{req}} \tag{2.24}$$

$$0 \leq R_i, \quad \forall\, i \in \mathcal{G} \tag{2.25}$$

where θ is a vector of bus voltage angles, $\mathbf{V}$ is a vector of bus voltage magnitudes, $\mathbf{P}_{\mathrm{g}}$ and $\mathbf{Q}_{\mathrm{g}}$ are vectors of generator real and reactive power production, $\mathbf{R}$ is a vector of generator frequency regulation capacities, $\mathcal{G}$ is the set of all generators, $C_{\mathrm{E},i}(P_{\mathrm{g},i})$ is the energy cost function of generator i which depends on generator i's real power output $P_{\mathrm{g},i}$, and $C_{\mathrm{R},i}(R_i)$ is the frequency regulation cost function of generator i which depends on generator i's frequency regulation capacity R_i. Constraints (2.17) and (2.18) are nonlinear real and reactive power balance equations, where $\mathbf{P}_{\mathrm{bus}}(\theta, \mathbf{V})$ and $\mathbf{Q}_{\mathrm{bus}}(\theta, \mathbf{V})$ are vectors of real and reactive power injections at each bus, $\mathbf{P}_{\mathrm{d}}$ and $\mathbf{Q}_{\mathrm{d}}$ are vectors of the real and reactive power demand at each bus, and C_{g} is a matrix to map generators to their bus location. Constraints (2.19) and (2.20) are line flow limits, one for the *from* end and one for the *to* end of each line, where $S_{\mathrm{f},i}(\theta, \mathbf{V})$ and $S_{\mathrm{t},i}(\theta, \mathbf{V})$ represent the complex power flowing through line i, $S_i^{\max}$ represents the limit in MVA of line i, and $\mathcal{L}$ is the set of all lines. Constraint (2.21) limits the voltage V_i of bus i, where $V_i^{\min}$ and $V_i^{\max}$ are the voltage limits of bus i and $\mathcal{B}$ is the set of all buses. Constraints (2.22) and (2.23) enforce real and reactive power limits of each generator, where $P_{\mathrm{g},i}^{\min}, P_{\mathrm{g},i}^{\max}$ are the real power limits and $Q_{\mathrm{g},i}^{\min}, Q_{\mathrm{g},i}^{\max}$ are the reactive power limits of generator i. Constraint (2.24) requires the sum of the generators' frequency regulation capacities to meet the generator frequency regulation requirement R^{req}, defined as the system frequency regulation requirement minus the total frequency regulation capacity provided by batteries. Note that frequency regulation capacity is only included in the generator real power limits (2.22), meaning changes in power flows and voltages caused by actuation of frequency regulation are not constrained by system limits. However, reserve flows usually change voltages and line flows by only small amounts.

The second step to determine the battery and generator actions is to superimpose the frequency regulation actuations onto the dispatch results. For simplicity, we assume that the underlying load is fixed throughout the day, but the system load changes as the battery's load changes according to self-dispatch in PJM and energy offset in CAISO. Specifically, the battery's load is included in the real power demand at the bus where the battery is connected. The battery's load is modeled as a positive demand when the battery is charging

and a negative demand when it is discharging. This interaction between the regulation actuation and the real-time energy dispatch requires that the battery's load be updated and the AC-OPF problem be re-solved for every 5-min dispatch period. This results in a real-time energy dispatch that changes every 5 min and regulation actuations that change within that 5-min period.

2.3.1 Regulation signal-following performance

Using the battery actions, we can calculate the regulation signal-following performance by comparing the actions to the frequency regulation signal(s). In practice, PJM and CAISO define their performance scores for frequency regulation differently. CAISO, like many other ISOs, captures a unit's accuracy in signal following by integrating absolute error, as discussed in [62]. PJM incorporates delay, correlation, and accuracy to develop a more complex measure of performance [63]. For simplicity, we use the integration of absolute error between the signal and battery actuation at each time step (i.e., CAISO's approach). We assume that the controls and power electronics of batteries enable them to perfectly follow the signal unless a battery's energy constraints are active.

2.3.2 Additional system control effort

We use two measures of additional system control effort (ASCE) to quantify how the non-energy constrained resources modify their outputs to manage the energy constraints of the batteries. The first measure of additional system control effort, referred to as ASCE1, is the absolute change in energy produced by the non-energy constrained resources as a result of the energy constraint management strategy.

For the PJM strategy, ASCE1 is the integral of the absolute difference between the RegA signal and what the signal would have been if there were no conditional neutrality feedback

$$\Delta E^{\mathrm{R}}(t) = \int \left| \widetilde{\mathrm{RegA}}(t) - \mathrm{RegA}(t) \right| dt, \tag{2.26}$$

added to the difference between the total generator dispatch and what the total generator dispatch would have been without the battery's energy market participation

$$\Delta E^{\mathrm{G}}(t) = \Delta t \sum_{t} \sum_{i} |\widetilde{P_{\mathrm{g},i}}(t) - P_{\mathrm{g},i}(t)|, \tag{2.27}$$

where $\widetilde{\cdot}$ denotes a value if there were no conditional neutrality feedback and Δt is the duration of the real-time energy market dispatch interval in seconds.

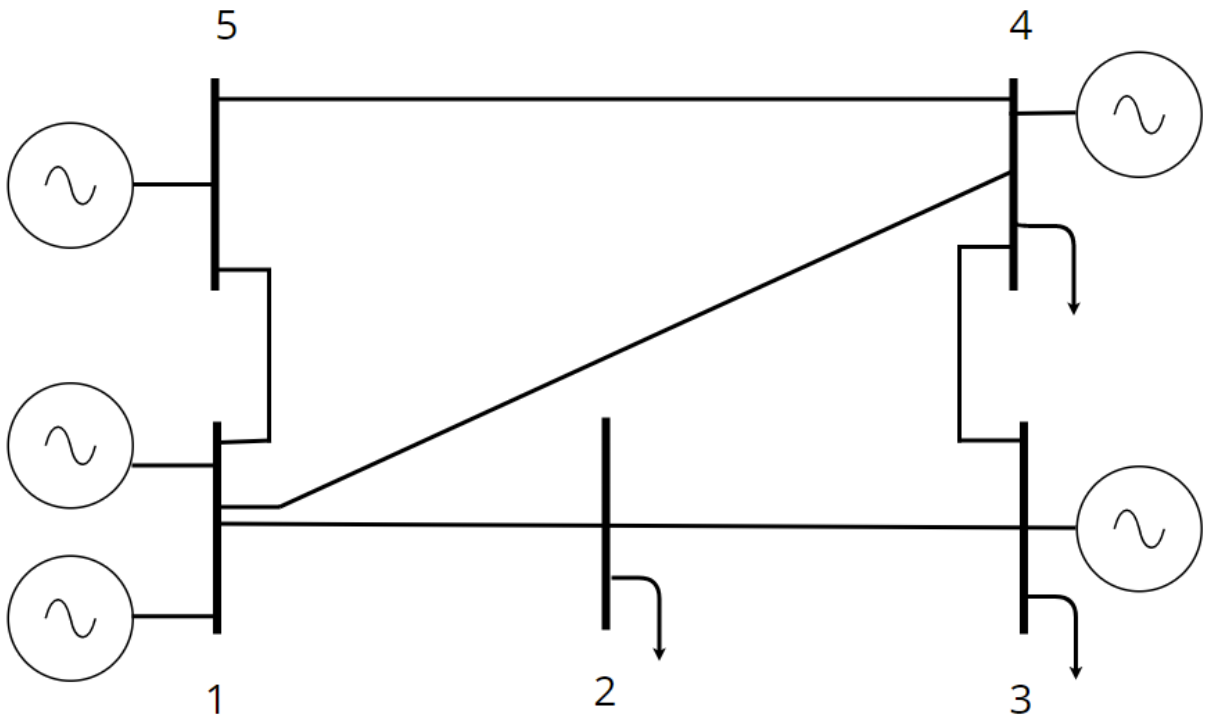


Figure 2.3: One-line diagram of the PJM 5-bus system without battery.

For the CAISO strategy, ASCE1 is the absolute value of the difference between the total generator dispatch and what the total generator dispatch would have been without REM, i.e., the energy needed for REM plus battery losses. Therefore, it is equal to (2.27), where $\widetilde{\cdot}$ now denotes the value if there were no REM.

The second measure of additional system control effort, ASCE2, is the net change in energy produced by the non-energy constrained resources as a result of the energy constraint management strategies. Therefore, to compute ASCE2, we use the same process we used for ASCE1 except we remove the absolute values from (2.26) and (2.27).

2.4 Case Study

We next describe our case study setup and results detailing our comparison on the PJM and CAISO approaches.

Table 2.1: Case Study Parameters

Parameter	Symbol	Value
Proportional Gain	K_{P}	1 (-)
Integral Gain	K_{I}	0.001 (-)
RegA Time Constant	τ_{A}	150 (s)
RegD Time Constant	τ_{D}	10 (s)
CAISO Time Constant	τ	10 (s)
Battery Energy Capacity	E_{B}	1.89 (MWh)
Battery Power Capacity	P_{B}	3 (MW)
Regulation Requirement	R^{req}	5 (MW)
ACE Limit	$\overline{\mathrm{ACE}}$	4 (MW)
Preferred Energy Level	e_{pref}	0.94 (MWh)
Battery Efficiency	η	90 (%)
Time Step	Δt	300 (s)

2.4.1 Setup

This section presents a case study in which both strategies are implemented on the PJM 5-bus system (case 5 in MATPOWER [2]) shown in Fig. 2.3. The case study parameters are given in Table 2.1. The regulation capacity requirement is typically 0.6-0.9% of the total load [64, 65]. The total load in the MATPOWER case 5 system is 1000 MW. Therefore, the total regulation capacity (i.e., both RegA and RegD in PJM) was chosen to be 8 MW or 0.8% of the total load. For PJM we assume only batteries provide RegD and only generators provide RegA. As no more than 40% of regulation can be provided by RegD in PJM [66], in both PJM and CAISO we set the amount of regulation provided by the generators in the system to 5 MW and the amount of regulation provided by batteries to 3 MW. A single battery, with specifications representing the average battery serving PJM in 2019 [34] scaled such that the power limit is 3 MW, was included in the system. The battery was placed at Bus 2, though the location was varied to check the sensitivity of the results to the connection point.

The case 5 data was edited to include the 5 MW regulation requirement and enable regulation provision by generators 3 and 5. The other generators were not considered for frequency regulation as they are either dispatched close to their full capacity or not dispatched in the base case. The cost of supplying frequency regulation was set to 1 \$/MWh for all participating generators. We assume there is no cost to the battery for providing regulation capacity. We assume that all resources providing regulation offer symmetric capacity.

All modeling and simulation was done in MATLAB and Simulink. The regulation signals for the entire 24 hour period were generated using real ACE data from PJM [67] scaled to

Table 2.2: Average Performance Metrics (and Standard Deviations)

	PJM	CAISO
Performance Score (%)	100.0 (0)	100.0 (0)
ASCE1 (MWh)	5.238 (0.566)	0.941 (0.187)
ASCE2 (MWh)	-3.236 (0.914)	-0.940 (0.189)

fit the 5-bus system. The same ACE data was used for both controllers.

Initial simulations showed windup in the PI controller used by both the PJM and CAISO controllers. We were unable to find information in ISO publications on whether this occurs in real operation and if so, how the ISOs manage it. However, literature suggests that windup is a common issue in the generation of regulation signals [68, 69]. To manage windup in our simulations, we implemented the clamping anti-windup mechanism built into Simulink's PID controller. We tuned the mechanism to find the largest output saturation limit that removed the windup, resulting in limits of [-6,6].

2.4.2 Results

ACE signal data from [67] corresponding to 14 different 24-hour periods was used to simulate both energy management strategies. The average performance metrics and their standard deviations for each strategy are shown in Table 2.2. The results suggest that both strategies were able to prevent the battery from reaching its energy constraints. However, the PJM strategy relied on the battery's participation in the real-time energy market in order to be effective over multiple consecutive hours.

In every tested case, the PJM strategy resulted in ASCE metrics with magnitudes significantly larger than those resulting from the CAISO strategy. This indicates that the overall system's energy output deviates further from what it would have been has there been no energy constraints to manage. The net change in energy, corresponding to ASCE2, resulting from both strategies was negative. This means that the non-energy constrained generators decreased their overall energy production in order to manage the energy constraints of the battery. This makes sense, as regulation signals are generally biased in the "lower" direction [66]. Under a "lower" or negative regulation signal, a battery is charging, and so it will subsequently need to be discharged to maintain energy neutrality. Resources that need not operate under energy neutrality, i.e., non-energy constrained resources, must then lower their power output at that later time in order for the net power injection into the system to remain the same.

Under the PJM strategy, the accumulated neutrality bias, $B(s)$ in Fig. 2.1, is feedback

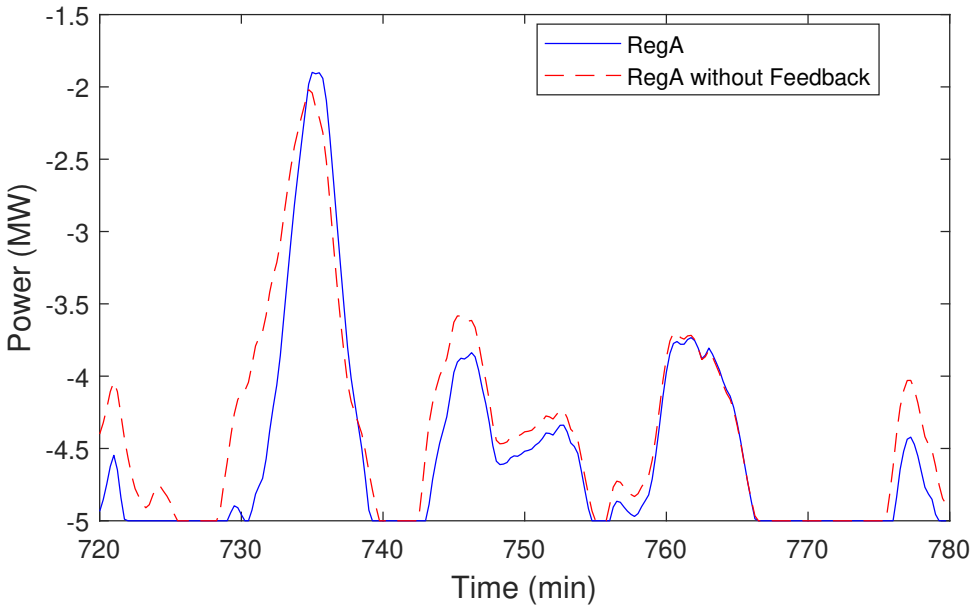
that adjusts the RegA signal at a later time so that the RegD signal can move towards energy neutrality. If the RegD signal has been biased in the negative direction over time, the feedback will lower the RegA signal such that the RegD signal can move in the opposite direction without decreasing the overall effectiveness of the regulation. An example of this is shown in Fig. 2.4a and Fig. 2.4b. Under the CAISO strategy, any accumulation or removal of energy in the battery is managed through REM in the energy market. In the case that regulation has been biased in the down direction over time, the battery will have accumulated energy and will need to export it into the energy market. In order for this to happen without changing the net power into the market, the total power output by the other power sources in the system must decrease their output accordingly. Figure 2.5 shows the power, assumed fixed over each 5-min period, transacted by the battery in the energy market under both the PJM and CAISO strategies. From the figure it can be seen that generally the CAISO battery is injecting power into the energy market to offset energy it has accumulated through regulation provision. It can also be seen that the battery under the PJM strategy purchases power every few hours to recover energy lost due to inefficiency.

It is important to note that while both strategies resulted in a decrease in produced energy, the decrease was significantly larger under the PJM strategy. The experienced decrease in produced power could be a benefit or a detriment, depending on certain factors. For example, if the non-energy constrained generators are polluting fossil fuel generators, then decreasing their power output could decrease pollution. However, the decrease in produced power could also push those generators into less efficient operating ranges, negating the positive environmental impacts of power production reduction and reducing the profitability of providing regulation. More analysis is necessary to establish the effects of the reduction in power production.

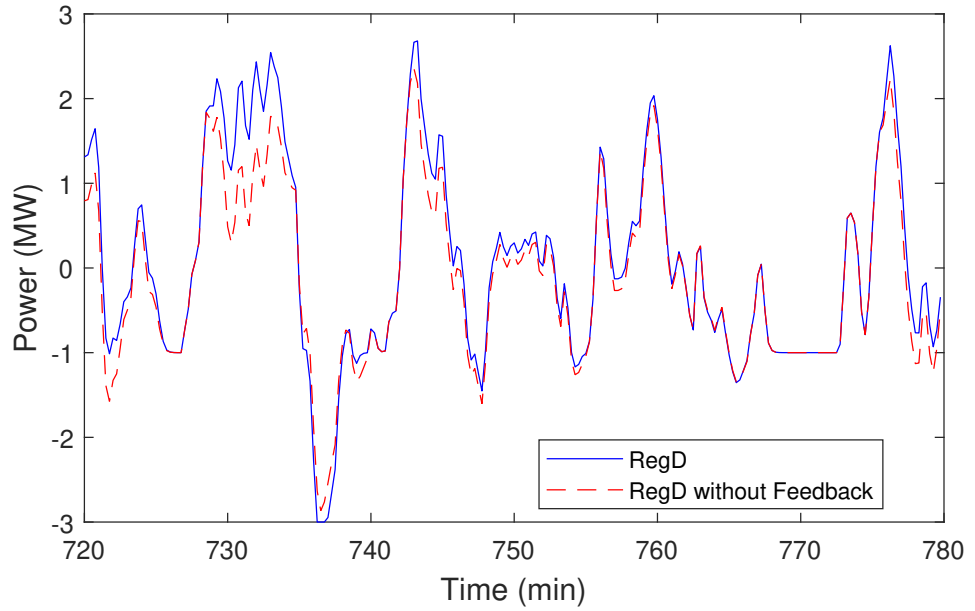
To assess whether the battery's location within the system impacts the metrics, the battery was separately modeled at each bus and simulated using the same ACE data. For both the strategies, the metrics changed only a small amount as we varied battery location, indicating that battery location is insignificant in the comparison of the two strategies.

2.5 Chapter Conclusions

This chapter presented a comparison of the strategies used by PJM and CAISO for managing the energy constraints of a battery providing frequency regulation. The case study results suggest that both strategies are sufficient to manage the energy constraints of a battery, but that the PJM strategy requires the battery operator to help manage the battery's SoC by offsetting energy lost due to inefficiency with energy purchased in the real-time energy



(a)



(b)

Figure 2.4: Comparison of the PJM regulation signals with and without feedback. 2.4a shows a comparison between the RegA signal generated by the PJM controller and what the RegA signal would have been if there were no feedback. 2.4b shows the same comparison in terms of RegD. Both figures represents 1 hour of the signal taken from one of the simulated cases.

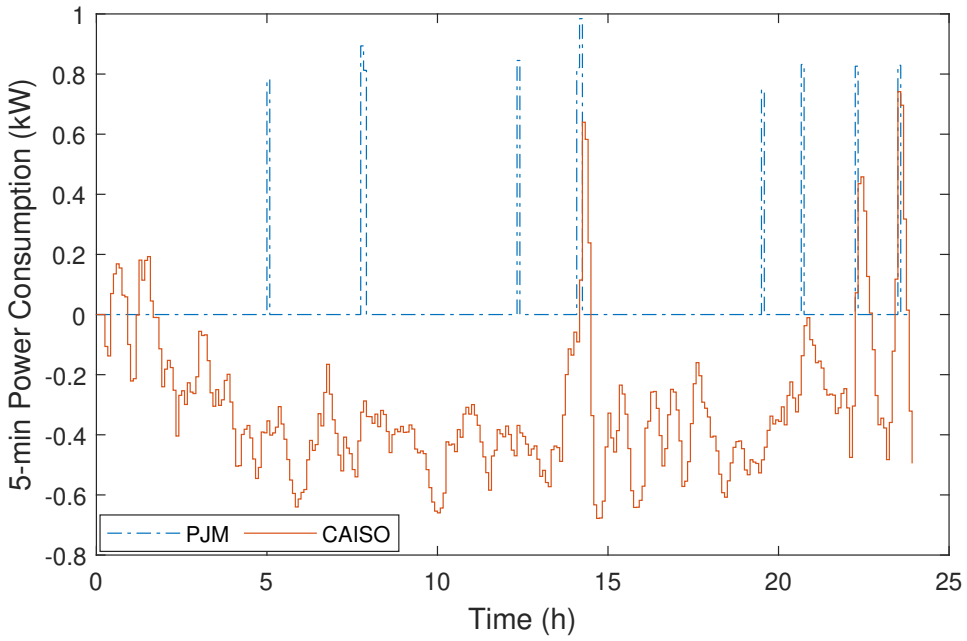


Figure 2.5: A plot of the fixed power transactions made by the battery in each 5-min real-time market period. A positive value represents power purchased from the market (charging) and a negative value represents power sold to the market (discharging).

market. Additionally, the PJM strategy resulted in a larger deviation in total energy production by the non-energy constrained resources when compared to how the system would have operated without any energy constraints to manage. Both strategies resulted in a net power production reduction by non-energy constrained generators, with a larger reduction under the PJM strategy. More analysis is needed to understand whether this reduction is beneficial or detrimental to the system.

A key difference in the structures of the two strategies is the level of responsibility that falls on the ISO. Under the CAISO strategy, the ISO is entirely responsible for managing the SoC of a resource under REM. This requires that CAISO must obtain information regarding SoC, efficiency, and/or other pertinent information on a regular basis for every resource participating in REM. PJM, on the other hand, leaves some of the responsibility up to the energy constrained resource operator. Under regular operation, PJM's conditional neutrality controller can be run autonomously and only requires information internal to the ISO. Managing energy constraints in PJM relies partially on the battery operator, but the operator is incentivized to manage SoC through performance dependent regulation payment. ISOs should consider the trade-off between the level of effort/communication required on their part when making design decisions regarding market mechanisms for managing energy-constrained resources.

Another consideration to make when evaluating the advantages and disadvantages of these two strategies are their implications for overall system resource mix needs. For example, the PJM strategy requires resources which are capable of following the RegA signal, a signal which is generally not energy neutral. This indicates that in its current implementation, there are limitations on how much of the regulation service can be provided by energy-limited resources. Currently, PJM limits procurement of the RegD service to 40% of its regulation needs [66]. Under the CAISO strategy, all regulation services could potentially be provided by batteries or other energy-limited resources.

When comparing the two strategies discussed in this chapter, it is important to note that the REM strategy used by CAISO is optional. Energy storage resources can participate is CAISO's regulation market without participating in REM. Opting into the REM participation model allows a resource owner to bid up to four times more capacity for frequency regulation compared to a non-REM NGR. However, it also means forfeiting the ability to participate in the energy market or other ancillary service markets and potentially losing potential profit streams. The REM mechanism will not provide the intended benefits to the system if it goes unused. The PJM strategy places no such participation limitations on energy storage resources following its RegD signal.

There were a number of assumptions made during the controller design and implementation process that may not accurately represent the ISOs' implementations. These assumptions were made to fill in gaps in the documentation of these approaches. For example, little information on how CAISO derives regulation signals from ACE could be found, so it was assumed that the time constant of the low-pass filter was the same as the time constant in the low-pass filter for the RegD signal. In the PJM controller, it was assumed that the ACE magnitude at which conditional neutrality would be suspended was 4 MW, which is approximately the 90-percentile of the scaled ACE data used. Without adequate knowledge of the true implementations, sensitivity analysis should be done to assess the importance of these design parameters.

Another limitation of this work is that only a small test system was used. Implementation on the MATPOWER case 9 system, a 9-bus system, gave similar results. In future work, more realistic system sizes and topologies should be tested to assess their effects on the results.

Additional future work on this topic will be to investigate the merits and drawbacks of the two outlined strategies for managing battery energy constraints from the perspective of the battery owner. The owner of a battery providing frequency regulation would want to know which strategy would result in the greatest profit and/or the smallest level of degradation.

CHAPTER 3

Robust Partitioning and Operation for Maximal Uncertain-Load Delivery in Distribution Networks

In this chapter, we present a two-stage mixed-integer robust optimization problem for reconfiguring networked microgrids. The solution to our optimization problem is *guaranteed to be robust and feasible* to all realizations of loads within a specified uncertainty set, while maximizing load delivery. To solve this problem, we propose a cutting-plane algorithm, with convergence guarantees, which approximates a convex recourse function with sub-gradient cuts. Finally, we provide a detailed case study on the IEEE 37-bus test system to demonstrate the benefits of networking microgrids to maximize uncertain-load delivery. The work in this chapter is based on our published work [70].

3.1 Chapter Introduction

Recently there has been increased interest in how networked microgrids can improve the resiliency and economics of operation of modern distribution grids, particularly during extreme weather events and contingencies [71–73]. Under such events, it can be desirable to isolate impacted areas from the rest of the system [74]. In the distribution network, which is typically radial, this can lead to widespread power outages. The ability to partition the network into multiple self-sufficient sub-networks, or microgrids, could alleviate this issue. Ideally, this partitioning should minimize load shedding, or in other words, maximize load delivery.

Maximizing delivery of *uncertain* load within the distribution network while minimizing generation costs is challenging. Unlike transmission networks, distribution networks are typically unbalanced. Additionally, if load must be shed, switches are typically used to shed

entire sub-networks, not just the fraction of load that cannot be met [75]. This further complicates balancing power supply and demand.

The introduction of distributed energy resources (DERs) has created additional challenges, as well as opportunities, for distribution network resiliency [75, 76]. Ref. [76] presents a mixed-integer linear program (MILP) with chance constraints to find a network configuration that minimizes switching costs and expected costs of up-stream power supply while accounting for uncertainty in distributed generation. However, [76] does not consider load uncertainty, which is inherent in distribution networks. Some works do consider load uncertainty. A two-stage robust formulation for distribution network reconfiguration with uncertain loads is presented in [77] and a two-stage robust formulation for scheduling DERs to hedge against load shedding in the case that the distribution network is disconnected from the upstream grid is presented in [78]. While [77] considers network reconfiguration under load uncertainty and [78] considers load shedding under load uncertainty, these papers do not consider network reconfiguration to minimize load shedding in unbalanced networks with load uncertainty.

To deal with this planning problem under uncertain loads, we propose to use a robust optimization approach by modeling loads as uncertainty sets. This approach is guaranteed to provide a robust partitioning strategy such that the partitioned power network's operation is feasible for all realizations of load within the specified uncertainty set. In this chapter, we formulate a two-stage robust optimization model where the first stage is a mixed-integer quadratic program (MIQP) that optimizes the network partitioning decisions while minimizing the total unsatisfied loads and generation costs for the nominal load realization. After the uncertainty of the load is revealed, the second-stage (recourse) problem performs corrective operations in generation set-points subject to three-phase, unbalanced power flow constraints. This two-stage problem of minimizing the worst-case cost of operation and unsatisfied loads is an infinite-dimensional mixed-integer optimization problem, which is usually not tractable without reformulation.

To address this challenging problem and make it tractable, we propose following solution strategies: (a) To handle the complexity of radial topology requirements (in the first-stage), we utilize a flow-based model to ensure all sub-networks are radial and any islanded sub-network contains an independent voltage/power source. (b) To make the recourse problem tractable, we use linearized "LinDist3Flow" constraints which are known to perform well on distribution networks. (c) To solve the two-stage robust optimization model, we generalize the cutting-plane algorithm in [32] by decomposing the problem into a mixed-integer master and infinitely-many convex sub-problems. Since handling the latter is intractable, we instead find the most violated inequality across all elements of the uncertainty set, by solving a

max − min problem. Further, to solve this max − min problem to optimality, we use the property of convex recourse over a polyhedral set to restrict the search to the extreme points of the uncertainty set.

Finally, we present a detailed numerical study analyzing the sensitivity of planning and operation to uncertainty set parameters, and illustrate how networked microgrids may be beneficial for maximizing load delivery.

3.2 Problem Formulation

In this section, we present necessary notation, the network configuration constraints, and the single-stage robust optimization problem formulation.

3.2.1 Notation and Preliminaries

Bold typeface represents vector notation and blackboard bold typeface represents matrix notation. The $|\cdot|$ operation represents the cardinality when the input is a set, the absolute value when the input is a real number, and magnitude when the input is a complex number.

Consider a distribution network with a set of nodes $\mathcal{N}$, a set of lines $\mathcal{L}$, and a set of phases Φ. There is also a set of transformers $\mathcal{E}^x$ which can be sub-divided into a set of wye-connected transformers $\mathcal{E}^{x,Y}$, and a set of delta-connected transformers $\mathcal{E}^{x,\Delta}$, such that $\mathcal{E}^x = \mathcal{E}^{x,Y} \cup \mathcal{E}^{x,\Delta}$. The network has a meshed structure, but we assume that it can only be operated in radial configurations, as is typical for protection coordination [77]. Within the network, there is a set $\mathcal{G}$ of controllable distributed generators (DGs) g. The complex power injected into the grid by generator g on phase ϕ is given by s_g^ϕ.

There is also a set of uncontrollable loads $\mathcal{D}$. The complex power demanded by load d on phase ϕ is given by $s_d^\phi = s_d^{0,\phi} + u_d^\phi$, where $s_d^{0,\phi}$ is the nominal load power and u_d^ϕ represents the load uncertainty defined by the set

$$\mathcal{U} = \left\{ u_d^\phi \in \mathbb{R}^{|\mathcal{D}\times\Phi|} \;\middle|\; \underline{s}_d^\phi - s_d^{0,\phi} \leqslant u_d^\phi \;\leqslant\; \overline{s}_d^\phi - s_d^{0,\phi} \;\forall \phi \in \Phi, \forall d \in \mathcal{D} \right\}. \tag{3.1}$$

where $\overline{s}_d^\phi$ and $\underline{s}_d^\phi$ represent the upper and lower bounds of uncertain load d on phase ϕ.

To capture unbalanced, three-phase power flow typical of distribution grids, the formulation presented in this chapter uses the LinDist3Flow model to approximate the AC power flow equations [79, 80]. Let v_i^ϕ represent the voltage magnitude on phase ϕ at node i and let $w_i^\phi = (v_i^\phi)^2$. Let $z_{ij}^{\phi\psi} = r_{ij}^{\phi\psi} + jx_{ij}^{\phi\psi}$ represent the self and mutual impedances on the line connecting nodes i and j between phases ϕ and ψ. The power flowing on the line between

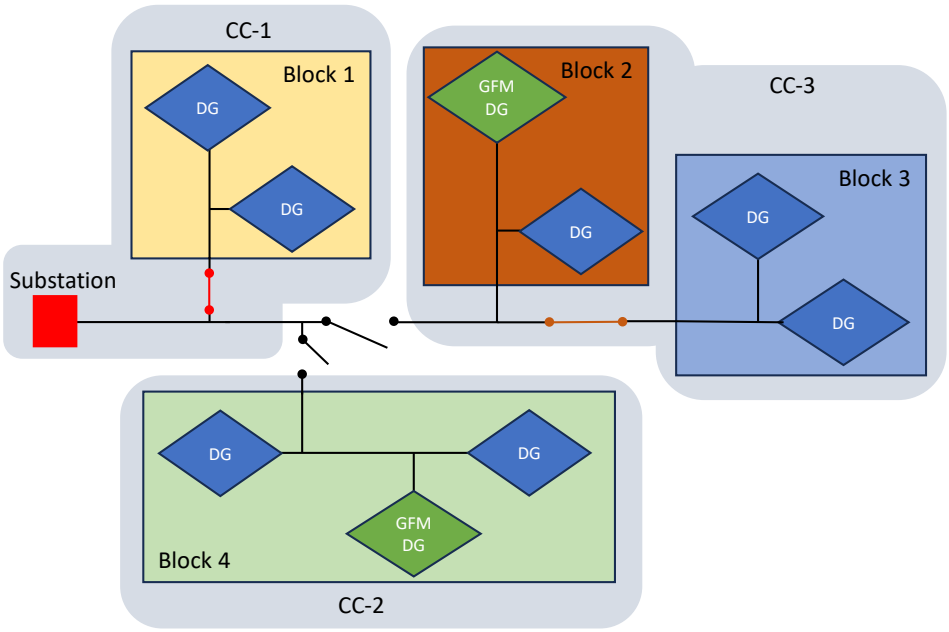


Figure 3.1: Illustration of a dynamic partition of networked microgrids using switches. Here, load blocks are interconnected by switches to form connected components (CCs) that act as independent microgrids. Each CC contains uncertain loads and a set of DGs, with one acting as a Grid-Forming DG (GFM-DG) if that particular CC is energized.

nodes i and j on phase ϕ is given by $s_{ij}^{\phi} = p_{ij}^{\phi} + jq_{ij}^{\phi}$.

Within the network, there is a set of switches $\mathcal{E}^{\text{sw}}$ that can be opened or closed to reconfigure the network. A connected component (CC) is a group of two or more connected nodes [81]. A microgrid is a CC containing at least one load and at least one generator. Let $\mathcal{B}$ be the set of CCs that exist when every switch in the network is open. The CCs within this set will be referred to as blocks. When a switch between two blocks is closed, the two blocks form one CC. This implies that the number of blocks in the network is static but the number of CCs changes as the switch configurations change. The relationship between blocks, switches, and CCs is illustrated in Fig. 3.1.

3.2.2 Network Configuration Constraints

There are two general requirements for network configuration. The first is that any energized CC cannot contain any loops, i.e., each CC must be a spanning tree. The second is that any energized CC must contain at least one grid-forming DG (GFM-DG).

3.2.2.1 Radiality Constraints

To enforce a radial topology in every component in the network, we use the directed multi-commodity flow-based model of the spanning tree constraints in the case with islands given by [81]. For brevity, we omit the formulation of the constraints in this chapter and refer the reader to [81] for details. For the remainder of this chapter, we will reference this model as the radiality constraints.

3.2.2.2 Grid-Forming Generator Constraints

In order to be energized, a CC must contain a generator capable of serving load within that CC. Generators in the distribution network are typically inverter-based resources, which can either be grid-forming or grid-following. A grid-forming generator controls the AC-side voltage, acting as a voltage source for the network. A grid-following generator controls the AC-side current and follows the phase angle of the existing grid voltage [82]. When two generators in the same small network are operating as grid-forming, they can independently try to control voltage and frequency, leading to instability [83]. To avoid this, we require that every energized CC in the network have exactly one GFM-DG and all other generators in the CC must be grid-following.

To determine whether there is a GFM-DG within a CC, we use a coloring scheme. A CC, specifically its connected switches, is colored by the internal block containing the GFM-DG. We define y_{ij}^{l} as a binary variable which denotes whether switch ij is colored by block l, z_l^{bl} as a binary variable which denotes whether block l is energized, and z_g^{inv} as a binary variable which denotes whether generator g is grid-forming. When switch ij has been colored by block l, y_{ij}^{l} takes a value of 1, and it takes a value of 0 otherwise. When a block is energized, z^{bl} takes the value of 1, and 0 otherwise. Similarly, when a generator is grid-forming, z^{inv} takes a value of 1, and 0 otherwise.

Let $\mathcal{G}_l$ and $\mathcal{E}_l^{\text{sw}}$ be the set of generators and switches, respectively, connected to block l. The relationship between the block states z_l^{bl} and the generator states z_g^{inv} is defined by

$$|z_i^{\text{bl}} - z_j^{\text{bl}}| \leq (1 - z_{ij}^{\text{sw}}), \qquad \forall ij \in \mathcal{E}^{\text{sw}} \tag{3.2}$$

$$z_l^{\text{bl}} \underline{s_g} \leq s_g \leq z_l^{\text{bl}} \overline{s_g}, \qquad \forall g \in \mathcal{G}_l, \forall l \in \mathcal{B} \tag{3.3}$$

$$z_l^{\text{bl}} - \sum_{ij \in \mathcal{E}_l^{\text{sw}}} z_{ij}^{\text{sw}} \leq \sum_{i \in \mathcal{G}_l} z_i^{\text{inv}} \leq z_l^{\text{bl}}, \qquad \forall l \in \mathcal{B} \tag{3.4}$$

where (3.2) states that if switch ij is closed, then the blocks it connects are either both energized or both de-energized; (3.3) enforces generator power limits for generators within an energized block and states that generators within a de-energized block cannot produce

power; and (3.4) states that, if a block is energized and not connected to another block, then it must contain a GFM-DG.

The coloring scheme used to determine whether a GFM-DG exists within a CC is described by

$$\sum_{l\in\mathcal{B}} y_{ij}^{l} \leqslant z_{ij}^{\mathrm{sw}}, \quad \forall ij \in \mathcal{E}^{\mathrm{sw}} \tag{3.5}$$

$$y_{ij}^{l} - (1 - z_{ij}^{\mathrm{sw}}) \leq \sum_{i\in\mathcal{G}_l} z_{i}^{\mathrm{inv}} \leq y_{ij}^{l} + (1 - z_{ij}^{\mathrm{sw}}),\ \forall l \in \mathcal{B}, \forall ij \in \mathcal{E}^{\mathrm{sw}} \tag{3.6}$$

$$\begin{aligned} y_{dc}^{l'} - (1 - z_{dc}^{\mathrm{sw}}) - (1 - z_{ab}^{\mathrm{sw}}) \leq y_{ab}^{l'} \leq y_{dc}^{l'} + (1 - z_{dc}^{\mathrm{sw}}) + (1 - z_{ab}^{\mathrm{sw}}), \\ \forall l, l' \in \mathcal{B}, \forall ab \in \mathcal{E}^{\mathrm{sw}}, \forall dc \in \mathcal{E}^{\mathrm{sw}} \setminus ab \end{aligned} \tag{3.7}$$

$$y_{ij}^{l} \leq \sum_{i\in\mathcal{G}_l} z_{i}^{\mathrm{inv}}, \quad \forall l \in \mathcal{B}, \forall ij \in \mathcal{E}^{\mathrm{sw}} \tag{3.8}$$

$$z_{l}^{\mathrm{bl}} \leq \sum_{i\in\mathcal{G}_l} z_{i}^{\mathrm{inv}} + \sum_{ij\in\mathcal{E}_l^{\mathrm{sw}}} \sum_{l\in\mathcal{B}} y_{ij}^{l}, \quad \forall l \in \mathcal{B} \tag{3.9}$$

where (3.5) states that a closed switch has at most one color and an open switch has no color; (3.6) states that if switch ij is closed and colored by block l, then switch ij is in the same CC as block l and block l contains a GFM-DG; (3.7) ensures that if two switches are closed and connected to the same block, then they must have the same color; (3.8) enforces that a switch cannot have color l unless block l contains a GFM-DG; and (3.9) enforces that a block cannot be energized unless it contains a GFM-DG or it is connected to at least one closed switch.

Let $\mathcal{E}_l^v$ be a set of virtual edges between block l and all other blocks l', oriented from l to l' (there are $|\mathcal{B}| - 1$ of these edges for each l). Let ξ_{ij}^{l} represent a unit of flow of commodity l across the virtual edge from i to j. For each $ij \in \mathcal{E}_l^{\mathrm{sw}}$, there is an arbitrary orientation (e.g., either $i = l$ or $j = l$). Then the following set of constraints can be used to determine if there is a connection between a GFM-DG and a CC.

$$-z_{ij}^{\mathrm{sw}}(|\mathcal{E}^{\mathrm{sw}}|) \leq \eta_{ij}^{l} \leq z_{ij}^{\mathrm{sw}}(|\mathcal{E}^{\mathrm{sw}}|), \quad \forall ij \in \mathcal{E}_l^{\mathrm{sw}},\ \forall l \in \mathcal{B} \tag{3.10}$$

$$0 \leq \xi_{ij}^{l} \leq 1, \quad \forall ij \in \mathcal{E}_l^{v}, \forall l \in \mathcal{B} \tag{3.11}$$

$$\sum_{ij\in\mathcal{E}_l^{\mathrm{sw}}:i=l} \eta_{ij}^{l} - \sum_{ij\in\mathcal{E}_l^{\mathrm{sw}}:j=l} \eta_{ij}^{l} + \sum_{ij\in\mathcal{E}_l^{v}} \xi_{ij}^{l} = |\mathcal{B}| - 1,\ \forall l \in \mathcal{B} \tag{3.12}$$

$$\sum_{ij\in\mathcal{E}_l^{\mathrm{sw}}:i=l'} \eta_{ij}^{l} - \sum_{ij\in\mathcal{E}_l^{\mathrm{sw}}:j=l'} \eta_{ij}^{l} - \xi_{ll'}^{l} = -1,\ \forall l' \neq l, \forall l \in \mathcal{B} \tag{3.13}$$

$$y_{ij}^{l} \leq 1 - \xi_{ll'}^{l}, \quad \forall l' \neq l, ij \in \mathcal{E}_{l'}^{\mathrm{sw}}, \forall l \in \mathcal{B} \tag{3.14}$$

$$z^{\text{bl}}, z^{\text{sw}}, z^{\text{inv}}, y^l \in \{0,1\} \tag{3.15}$$

Constraint (3.10) states that, for a closed switch ij, the magnitude of flow from block l across switch ij, η_{ij}^l, is bounded by the number of switches in the network; (3.11) states that at most one unit of flow can flow across each virtual edge; (3.12) (together with (3.10) and (3.11)) states that every block l must send out enough units of flow such that every other block l' gets one unit; (3.13) requires that every block l' consumes one unit of flow from block l; (3.14) states that if there is flow on the virtual line between l and l', then $y_{ij}^l = 0$ for every $ij \in \mathcal{E}_{l'}^{\text{sw}}$; and (3.15) defines $z^{\text{bl}}, z^{\text{sw}}, z^{\text{inv}}, y_{ij}^l$ as binary variables.

3.2.3 Single-Stage Robust Partitioning and Operation Problem

We now define the single-stage Robust Partitioning and Operation Problem (RPOP) for distribution grids. The RPOP's optimal solution is a set of network partitions and generator set-points that minimize the load shed and operational cost, and is guaranteed to be feasible and robust against all realizations of uncertain loads. The formulation is

$$\min \sum_{l \in \mathcal{B}} \alpha_l (1 - z_l^{\text{bl}}) + \sum_{g \in G} c_{1,g} s_g^p + c_{0,g} \tag{3.16a}$$

$$\text{s.t. Radiality Constraints (Sec. 3.2.2.1), } (3.2) - (3.15) \tag{3.16b}$$

$$z_l^{\text{bl}} \underline{v_i}^2 \leq w_{i,\phi} \leq z_l^{\text{bl}} \overline{v_i}^2, \ \forall \phi \in \Phi, \forall i \in \mathcal{N}_l, \forall l \in \mathcal{B} \tag{3.16c}$$

$$\mathbf{w}_i = \mathbf{w}_j - \mathbb{M}_{ij}^p \mathbf{p}_{ij} - \mathbb{M}_{ij}^q \mathbf{q}_{ij}, \ \forall i,j \in \mathcal{N}, \ \forall ij \in \mathcal{L} \tag{3.16d}$$

$$|s_{ij}^\phi| \leq \overline{s_{ij}}, \quad \forall \phi \in \Phi_{ij}, \forall ij \in \mathcal{L} \tag{3.16e}$$

$$|s_{ij}^\phi| \leq z_{ij}^{\text{sw}} \overline{s_{ij}}, \quad \forall \phi \in \Phi_{ij}, \forall ij \in \mathcal{E}^{\text{sw}} \tag{3.16f}$$

$$w_i^\phi = n_{ij}^2 w_j^\phi, \quad \forall \phi \in \Phi_{ij}, \forall ij \in \mathcal{E}^{x,Y} \tag{3.16g}$$

$$s_{ij}^\phi = s_{ji}^\phi, \quad \forall \phi \in \Phi_{ij}, \forall ij \in \mathcal{E}^{x,Y} \tag{3.16h}$$

$$3(w_{i,\phi} + w_{i,\psi}) = 2(n_{ij})^2 w_{j,\phi}, \ \forall (\phi,\psi) \in \{(a,b),(b,c),(c,a)\}, \ \forall ij \in \mathcal{E}^{x,\Delta} \tag{3.16i}$$

$$\begin{aligned} 2p_{ij,\phi} = &-(p_{ji,\phi} + p_{ji,\psi}) + (q_{ji,\psi} - q_{ji,\phi})/\sqrt{3}, \\ &\forall (\phi,\psi) \in \{(a,c),(b,a),(c,b)\}, \ \forall ij \in \mathcal{E}^{x,\Delta} \end{aligned} \tag{3.16j}$$

$$\begin{aligned} 2q_{ij,\phi} = &(p_{ji,\phi} - p_{ji,\psi})/\sqrt{3} - (q_{ji,\psi} + q_{ji,\phi}), \\ &\forall (\phi,\psi) \in \{(a,c),(b,a),(c,b)\}, \ \forall ij \in \mathcal{E}^{x,\Delta} \end{aligned} \tag{3.16k}$$

$$|s_{ij}^\phi| \leq \overline{s_{ij}^\phi}, \quad \forall \phi \in \Phi_{ij}, \forall ij \in \mathcal{E}^x \tag{3.16l}$$

$$\sum_{ij \in \mathcal{E}_i} s_{ij}^\phi = \sum_{g \in i} s_g^\phi - z_k^{\text{bl}} \sum_{d \in \mathcal{D}_i} \mathbf{s}_d^\phi - \sum_{c \in \Phi_i} y_c^\phi w_i^\phi, \ \forall \phi \in \Phi_i, \forall i \in l, \ \forall l \in \mathcal{B} \tag{3.16m}$$

where $\mathcal{E} = \mathcal{L} \cup \mathcal{E}^{\text{sw}} \cup \mathcal{E}^{x}$ is the set of all lines, switches, and transformers. The objective function minimizes the number of de-energized blocks and the generation cost, where α_l is a weighting parameter for block l used to designate block priority, and $c_{1,g}, c_{0,g}$ are the parameters of the linear cost function of generator g. The voltage limits at each bus are enforced by (3.16c) and the voltage drop between bus j and downstream bus i is computed in (3.16d), where [79]

$$\mathbb{M}^{p}_{ij} = \begin{bmatrix} -2r_{aa} & r_{ab} - \sqrt{3}x_{ab} & r_{ac} + \sqrt{3}x_{ac} \\ r_{ba} + \sqrt{3}x_{ba} & -2r_{bb} & r_{bc} - \sqrt{3}x_{bc} \\ r_{ca} - \sqrt{3}x_{ca} & r_{cb} + \sqrt{3}x_{cb} & -2r_{cc} \end{bmatrix}_{ij},$$

$$\mathbb{M}^{q}_{ij} = \begin{bmatrix} -2x_{aa} & x_{ab} + \sqrt{3}r_{ab} & x_{ac} - \sqrt{3}r_{ac} \\ x_{ba} - \sqrt{3}r_{ba} & -2x_{bb} & x_{bc} + \sqrt{3}r_{bc} \\ x_{ca} + \sqrt{3}r_{ca} & x_{cb} - \sqrt{3}r_{cb} & -2x_{cc} \end{bmatrix}_{ij}.$$

Constraints (3.16e), (3.16f), and (3.16l) define the power flow limits for each line, switch, and transformer, respectively. Constraints (3.16g) and (3.16i) define the voltage transformations across each wye-connected and delta-connected transformer, where n_{ij} is the tap ratio of transformer ij. Constraints (3.16h), (3.16j) and (3.16k) define the relationship between the directions of power flow on each wye-connected and delta-connected transformer. Finally, (3.16m) is the linearized power balance equation [79].

3.3 A Cutting-Plane Algorithm to solve the RPOP

Since it is intractable to solve the RPOP as given in Section 3.2.3 using any off-the-shelf solvers, we propose a two-stage version of the RPOP, which can be solved effectively to global optimality using an iterative cutting-plane algorithm.

3.3.1 Two-stage Robust Partitioning and Operation Problem

The RPOP in (3.16) can be exactly reformulated as a master problem and a set of subproblems [84]. The master, or first-stage, decision variables are the controllable power injections, $\mathbf{s}^{\phi}_{g}\ \forall \phi \in \Phi,\ \forall g \in \mathcal{G}$, the switch configurations $z^{\text{sw}}_{ij},\ \forall ij \in \mathcal{E}^{\text{sw}}$, the operating state of each generator $z^{\text{inv}}_{g},\ \forall g \in \mathcal{G}$ as either grid-forming or grid-following, the energized state of each block $z^{\text{bl}}_{l},\ \forall l \in \mathcal{B}$, and the additional variables defined in the network configuration constraints. Let $\mathbf{x}$ be a vector of variables $\mathbf{s}^{\phi}_{g}, z^{\text{sw}}_{ij}, z^{\text{inv}}_{g}, z^{\text{bl}}_{l}$ for every generator, switch, and block in the network. Let $\mathbf{s}^{*}_{d}$ be the worst-case uncertain load realization. The master problem,

which relaxes the single-stage problem by ignoring the power flow constraints, is

$$\min \sum_{l\in\mathcal{B}} \alpha_l(1-z_l^{\text{bl}}) + \sum_{g\in G} c_{1,g}s_g^p + c_{0,g} + \theta \tag{M}$$

$$\text{s.t. Radiality Constraints (Sec. 3.2.2.1), } (3.2)-(3.15) \tag{3.17a}$$

$$V_2(\mathbf{x}_k^*, \mathbf{s}_{d,k}^*) + \pi_k^{\intercal} A(\mathbf{x}-\mathbf{x}_k^*) \leq \theta, \forall k = 1,2,... \tag{3.17b}$$

where a subscript k denotes the value at the k^{th} iteration, $\mathbf{x}_k^*$ denotes the optimal solution of (M) at the k^{th} iteration, $V_2(\mathbf{x}_k^*, \mathbf{s}_{d,k}^*)$ is the objective value of the k^{th} subproblem, π is a vector of dual variables corresponding to equations in (S_1) containing $\mathbf{x}$, and A is the coefficient on $\mathbf{x}$ in those equations.

The second stage of the problem, or the subproblem, is solved after the uncertainty has been revealed. In the second stage, small adjustments to the controllable power injections are allowed, given by variables o^+, o^-. These variables are bounded by generator ramping capabilities and capacity constraints. In addition to these variables, the squared bus voltages $w_i^\phi\ \forall\phi\in\Phi_i, \forall i\in\mathcal{N}$, and power flows $s_{ij}^\phi\ \forall\phi\in\Phi_{ij}, \forall ij\in\mathcal{E}$ are determined by the power flow equations in this stage. The subproblem formulation is

$$\min\ \omega\left(\sum_{i\in\mathcal{N}}\sum_{\phi\in\Phi_i}\left(h_i^{+,\phi}+h_i^{-,\phi}\right)\right) + \sum_{g\in G}\sum_{\phi\in\Phi_g} c_{1,g}o_g^\phi \tag{S_1}$$

$$s.t.\ (3.16c)-(3.16l),$$

$$\sum_{ij\in\mathcal{E}_i} s_{ij}^\phi = \sum_{g\in i}\left(s_g^{\phi *} + o_g^{+,\phi} - o_g^{-,\phi}\right) - z_k^{\text{bl}*}\sum_{d\in\mathcal{D}_i} s_d^\phi - \sum_{c\in\Phi_i} y_c^\phi w_i^\phi,\ \forall i\in k,\ \forall k\in\mathcal{B}, \tag{3.18a}$$

$$o_g^{+,\phi} \leq z_i^{\text{bl}*}\overline{s_g^\phi} - s_g^{\phi *},\ \forall\phi\in\Phi_g, \forall g\in i, \forall i\in\mathcal{B}, \tag{3.18b}$$

$$o_g^{-,\phi} \leq s_g^{\phi *} - z_i^{\text{bl}*}\underline{s_g^\phi},\ \forall\phi\in\Phi_g,\ \forall g\in i,\ \forall i\in\mathcal{B}, \tag{3.18c}$$

$$o_g^{+,\phi} \leq \overline{o_g^\phi},\ \forall\phi\in\Phi_g,\ \forall g\in i,\ \forall i\in\mathcal{B}, \tag{3.18d}$$

$$o_g^{-,\phi} \leq \overline{o_g^\phi},\ \forall\phi\in\Phi_g,\ \forall g\in i,\ \forall i\in\mathcal{B}, \tag{3.18e}$$

$$o_g^{+,\phi}, o_g^{-,\phi} \geq 0,\ \forall\phi\in\Phi_g,\ \forall g\in i,\ \forall i\in\mathcal{B}, \tag{3.18f}$$

$$h_i^{+,\phi}, h_i^{-,\phi}, \geq 0,\ \forall\phi\in\Phi_i,\ \forall i\in\mathcal{N}, \tag{3.18g}$$

where ω is a weighting parameter, and $h_i^{+,\phi}, h_i^{-,\phi}$ are slack variables to represent a violation of the power balance on phase ϕ at node i. If any of these slack variables are non-zero at optimality, then for the candidate solution $\mathbf{x}^*$ and uncertain load realization $\mathbf{s}_d$, there are no feasible o^+, o^- that satisfy the power flow equations. With this, a feasibility cut (3.17b) is generated to ensure that the candidate solution $\mathbf{x}^*$ cannot be chosen again in subsequent

iterations of the master problem. Constraints (3.18b)-(3.18f) define the limits on generator set-point modifications based on ramping and capacity limits.

The decomposition algorithm is not directly implementable because there are infinitely many subproblems. Instead, it is desirable to find and solve only the subproblem with the most violated power balance equation across all elements of the uncertainty set. To find this most violated subproblem, we must solve a max-min problem of the form:

$$\begin{aligned} &\max_{\mathcal{U}} \ \min \ \omega \left(\sum_{i \in \mathcal{N}} \sum_{\phi \in \Phi_i} \left(h_i^{+,\phi} + h_i^{-,\phi} \right) \right) + \sum_{g \in G} \sum_{\phi \in \Phi_g} c_{1,g} o_g^{\phi} \qquad (S_2) \\ &s.t. \quad (3.16c) - (3.16l), (3.18b) - (3.18g) \end{aligned}$$

However, solving the bilevel problem (S_2) is intractable because there are infinitely many uncertain load realizations. Convex optimization theory guarantees that the largest optimal objective, i.e., the solution to the max-min problem, will occur at one of the extreme points of the uncertainty set since the inner minimization problem is a convex function of the uncertain load parameters [85]. Using this result, we can replace $\mathcal{U}$ in (S_2) with a finite-dimensional uncertainty set

$$\widehat{\mathcal{U}} = \Bigg\{ u_d^{\phi} \in \mathbb{R}^{|\mathcal{D} \times \Phi|} \ \Bigg| \ u_d^{\phi} = \zeta_d^{+}(\overline{s}_d^{\phi}) + \zeta_d^{-}(\underline{s}_d^{\phi}) - s_d^{0,\phi}, \\ \zeta_d^{+} + \zeta_d^{-} = 1, \ \zeta_d^{+}, \zeta_d^{-} \in \{0,1\}, \ \forall \phi \in \Phi, \forall d \in \mathcal{D} \Bigg\}.$$

To further reduce the complexity of uncertainty modeling, we assume that the load variation for multi-phase loads at a bus is uni-directional, meaning ζ_d^{+}, ζ_d^{-} are indexed by loads but not by phases. Thus, the reduced finite-dimensional (S_2) problem can be replaced by solving the modified subproblem for every possible combination of ζ_d^{+}, ζ_d^{-} and take the solution which gives the largest objective, i.e.,

$$\begin{aligned} &\min \ \omega \left(\sum_{i \in \mathcal{N}} \sum_{\phi \in \Phi_i} \left(h_i^{+,\phi} + h_i^{-,\phi} \right) \right) + \sum_{g \in G} \sum_{\phi \in \Phi_g} c_{1,g} o_g^{\phi} \qquad (E) \\ &s.t. \ (3.16c) - (3.16l), (3.18b) - (3.18g), \\ &\quad \sum_{ij \in \mathcal{E}_i} s_{ij}^{\phi} = \sum_{g \in i} \left(s_g^{\phi *} + o_g^{+,\phi} - o_g^{-,\phi} \right) - z_k^{\mathrm{bl}*} \sum_{d \in \mathcal{D}_i} \left(s_d^{0,\phi} + \zeta_d^{+} \overline{s}_d^{\phi} - \zeta_d^{-} \underline{s}_d^{\phi} \right) - \sum_{c \in \Phi_i} y_c^{\phi} w_i^{\phi}, \\ &\qquad \forall i \in k, \ \forall k \in \mathcal{B}, \\ &\quad \zeta_d^{+} + \zeta_d^{-} = z_i^{\mathrm{bl}*}, \ \ \zeta_d^{+}, \zeta_d^{-} \in \{0,1\}, \ \forall d \in \mathcal{D}_i, \ \forall i \in \mathcal{B}. \end{aligned}$$

This approach still requires solving $2^{|\mathcal{D}|}$ number of (E) problems, and may not scale well as the number of uncertain loads increases.

3.3.2 A Cutting-plane Algorithm

We propose Algorithm 1 to solve the two-stage RPOP. In summary, the master problem (M) is solved for the network configuration and generator set-points (master solution) in Step 4. Given this master solution, (S_2) is solved for every scenario in $\widehat{\mathcal{U}}$ to get the worst-case load realization in Step 5. Finally, the subproblem (S_1) is solved in Step 6 to check if the chosen master solution is feasible for the worst-case load realization. If they are feasible, the algorithm terminates with an optimal solution to the RPOP. If not feasible, i.e., there is non-zero slack $h^{+,\phi}, h^{-,\phi}$, then a sub-gradient cut is added to (M) in Step 3 and the process is repeated.

Convergence guarantee: Algorithm 1 is guaranteed to converge in a finite number of iterations because there is always a finite number of load blocks, and in the worst-case, the sub-gradient cuts will lead to every block in the network being de-energized in order to satisfy the termination criterion, as shown in step (2) of Algorithm 1.

Algorithm 1 : Cutting-plane algorithm for two-stage RPOP

1: Initialize: $k \leftarrow 1$, $h_i^{+,\phi} \leftarrow \infty$, $h_i^{-,\phi} \leftarrow \infty \ \forall i \in \mathcal{N}$, $\epsilon > 0$, $V_2(\mathbf{x}_1^*, \mathbf{s}_{d,1}^*) \leftarrow 0$, and $\pi_1 \leftarrow 0$
2: **while** $\sum_{i\in\mathcal{N}} \sum_{\phi\in\Phi_i} \left(h_i^{+,\phi} + h_i^{-,\phi}\right) > \epsilon$ **do**
3: Append $V_2(\mathbf{x}_k^*, \mathbf{s}_{d,k}^*) + \pi_k^\intercal A(\mathbf{x} - \mathbf{x}_k^*) \leq \theta$ to (M)
4: Solve master problem (M) for $\mathbf{x}_k^*$
5: Given $\mathbf{x}_k^*$, find the worst-case uncertainty realization $s_{d,k}^*$ by solving (E) for every scenario in $\hat{\mathcal{U}}$
6: Given $\mathbf{x}_k^*$ and $s_{d,k}^*$, solve Subproblem (S_1) for $h^{+,\phi}, h^{-,\phi}, o^{+,\phi}, o^{-,\phi}$
7: Set $k \leftarrow k + 1$
8: **end while**
9: Output: $\mathbf{x}_{k-1}^*, o^{+,\phi}, o^{-,\phi}$

3.4 Numerical Results

We now present results illustrating how robust partitioning and operation using Algorithm 1 can maximize load delivery.

3.4.1 Implementation details

The proposed optimization formulations and Algorithm 1 were implemented using JuMP v1.13.0 [86] in Julia v1.9.2 programming language. PowerModelsONM.jl [75] was used as the basis for all implementations. All computational results were computed with Gurobi 9.1.2 [87] as an MICP solver on a 1.3 GHz 4-Core Intel Core i7 processor with 16GB memory.

3.4.2 Test case: IEEE 37-bus test system

To illustrate the benefits of network partitioning that is robust against load uncertainty, we present a case study using a modified version of the unbalanced, three-phase, *IEEE 37-bus test network* [88], whose single-line simplified diagram is shown in Fig. 3.2. The network was modified to include 10 controllable switches and 7 controllable DGs. Three of the controllable switches are part of three redundant lines (dashed) with sufficient capacity to transport the necessary power between networked microgrids. The controllable switches allow the network to be partitioned into up to 7 blocks. We consider the case where a disruptive event is upstream of the substation, requiring that the network be isolated from the main grid. The switch between the substation and node 701 is opened to perform this isolation.

The network contains 30 loads, unevenly distributed across the nodes and the three phases, making the network very unbalanced [88]. The total nominal load in the network is 2542 kW. Six of the 30 loads, distributed across the network, are modeled with uncertainty The remaining 24 loads are fixed at their nominal values. We consider using this reduced set of uncertain loads reasonable, owing to the computational burden of solving the exponential number of (E) problems for every iteration of the algorithm.

The total generation capacity of the DGs in the network is 2180 kW, distributed unevenly between the 7 DGs. The ramping limit $\overline{o}_g$ in (3.18) for each generator was taken as 30% of its capacity $\overline{s}_g$. The block weighting parameters α_l in (M) were given by $10 + 0.01(|\mathcal{D}_l|)\ \forall l \in \mathcal{B}$, where $\mathcal{D}_l$ is the set of loads in block l. The weighting parameter ω in (E) was set to 705, a value determined empirically to aid in convergence.

3.4.3 RPOP's performance for varying levels of load uncertainty

The results in this section represent the solutions found using Algorithm 1 to solve the 2-stage RPOP, under varying levels of load uncertainty. For this study, we consider uncertainty levels of 0% (nominal case), 10%, 15%, and 25%. The costs of generation and load shedding, the number of energized blocks and closed switches, as well as Algorithm 1 run times, are given in Table 3.1. We find that the total cost (generation + load shed given in (M)) increases

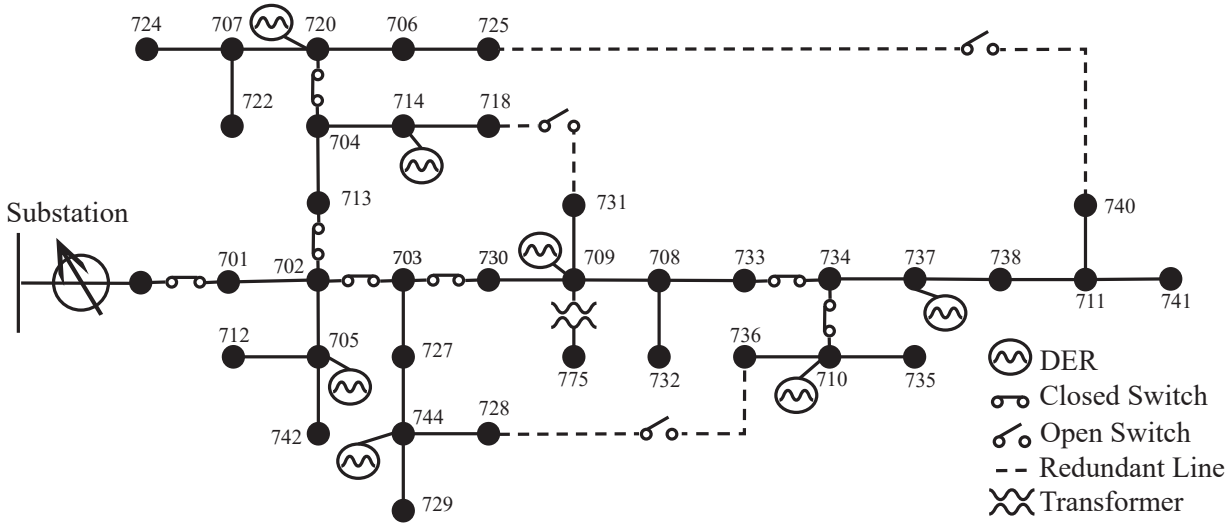


Figure 3.2: Single-line diagram of the 37-bus network without loads shown.

Table 3.1: Sensitivity of Operating Costs and Algorithm Run Times to Load Uncertainty Percentage

Uncertain Load (%)	Gen Cost ($)	Load Shed Cost ($)	# of Energized Blocks	# of Closed Switches	Run Time (sec.)	Run Time for best IFS (sec.)
0	15,399	21,100	5	4	100.8	45.67
10	12,295	31,140	4	3	1952.6	1708.2
15	12,299	31,140	4	3	2500.4	2359.8
25	9,317	41,160	3	2	4599.9	4572.5

monotonically with increases in load uncertainty. At higher levels of uncertainty, decreases in the number of energized blocks lead to lower generation costs and higher load shedding costs.

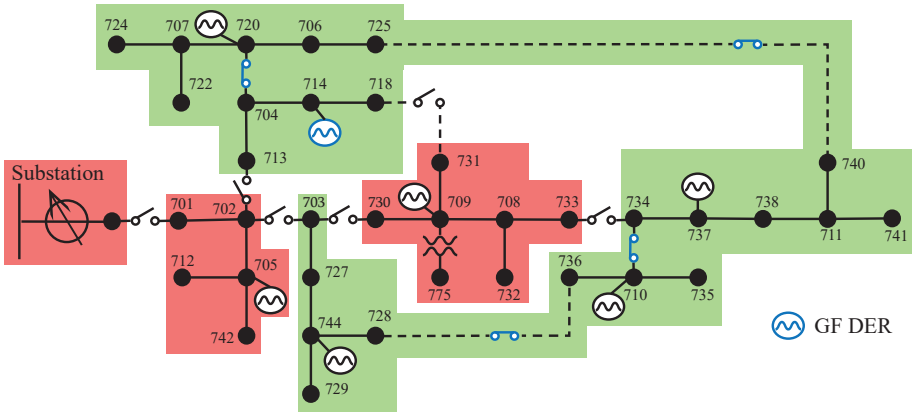
In Table 3.1, as expected, there is a significant increase in the run times for cases with load uncertainty compared to the nominal case. This is primarily because, for every iteration of Algorithm 1, obtaining the worst-case uncertainty realization requires solving $2^{|\mathcal{D}|}$ quadratically-constrained convex programs (E). Moreover, run times increase for higher levels of uncertainty because more iterations/cuts in Algorithm 1 are necessary to approximate the second-stage cost function and remain robust against the larger uncertainty sets. The last column of Table 3.1 gives the run times at which Algorithm 1 reaches the best integer feasible solution (IFS), i.e., the optimal integer solution for the 2-stage RPOP, under each uncertainty level. It is interesting to note that the best IFS is found within 70% of total run time, on average.

Optimal network configurations and block states for 0% (nominal case), 10%, 15% and 25% uncertainty levels are shown in Fig. 3.3. In Fig. 3.3(a), a single inter-connected microgrid is formed using two redundant lines to maximize load delivery. Note that even without uncertainty, the DGs are incapable of satisfying every load. As load uncertainty increases beyond 10%, it is not possible to guarantee that all loads within the energized CC of the nominal case can be met by the DGs. In order to remain robust to the worst-case realization of uncertain load, more blocks must be de-energized, as shown in Fig. 3.3(b) and Fig. 3.3(c).

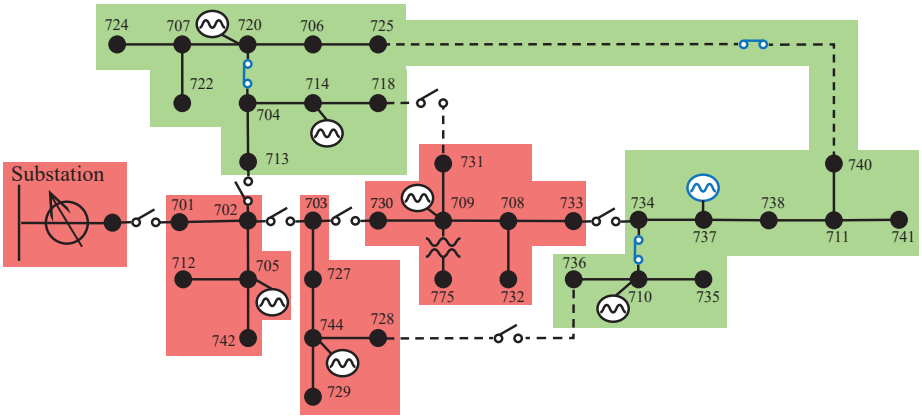
If network partitioning were not possible (i.e., the network was fixed to Fig. 3.2), for all levels of uncertainty, the optimal solution is to de-energize all load. This is primarily due to the modeling assumption that it is not possible to shed individual loads in the distribution network, an assumption practiced by most electric utilities. In contrast, the ability to partition the network and form *networked microgrids can significantly increase the amount of load served in the network*. For example, under the nominal loading conditions and with 10% uncertainty, the optimal partitioning solution of the 2-stage RPOP increases the served load to 1190 kW, meaning 53.2% of total load is served.

3.4.4 RPOP's performance against deterministic counterparts

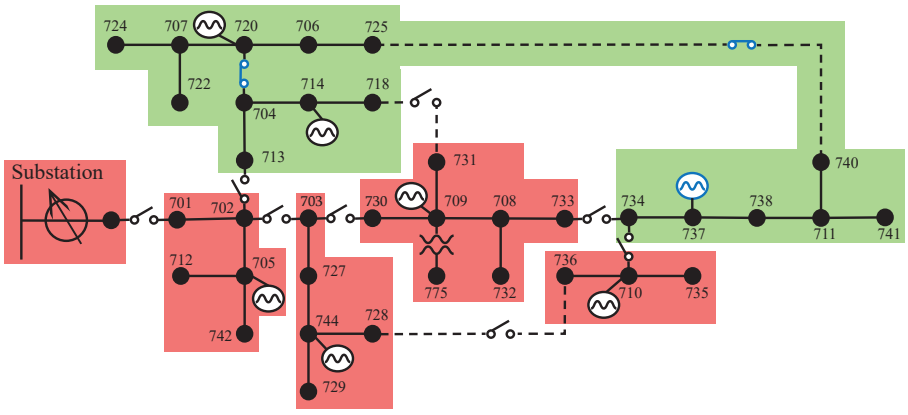
We now consider the case when the network is partitioned without accounting for load uncertainty. For this analysis, we fix the switch and load block states to the optimal solution of the nominal load case (as shown in Fig. 3.3(a), and set the DG limits to $\pm 30\%$ of their capacity around the set-points found for the nominal case. We assume that this limit is reasonable for fast ramping DGs typically found in distribution grids. Then, we determine



(a) 0% (nominal) and 10% load uncertainty. Served load = 1190 kW.



(b) 15% load uncertainty. Served load = 938 kW.



(c) 25% load uncertainty. Served load = 811 kW.

Figure 3.3: Optimal robust partitioning of the 37-bus network with varying levels of uncertain loads. We assume the substation is out-of-service. Energized and de-energized CCs are colored in green and red, respectively. The GFM-DG and the closed switches are highlighted in blue.

operational feasibility for varying levels of load uncertainty via out-of-sample feasibility tests. For each level of uncertainty, we generate 10,000 random load samples from the uncertainty set and for each sample, we compute LinDist3Flow power flow to test for feasibility. We label a sample as feasible only if all engineering limits are satisfied.

The percentage of out-of-sample loads that were found feasible for 10%, 15% and 20% level of load uncertainty were 94.37%, 86.63% and 78.37%, respectively. As expected, the percent of feasible load samples decreases with increases in uncertainty. For 10% uncertainty, 5.63% of load samples were infeasible although the optimal network configuration for this level of uncertainty was identical to that of the 0% (nominal) load uncertainty case (see Fig. 3.3(a)). This is explained by the difference in optimal DG set-points found in the RPOP for these two cases and the above-mentioned DG ramping limits. This demonstrates the importance of accounting for operational decisions and limits when making robust planning decisions. *In summary*, this analysis suggests that at lower levels of uncertainty and with fast ramping DGs to handle real-time load fluctuations, configuring the network based on deterministic planning can almost always satisfy engineering limits. In contrast, at higher levels of uncertainty, *network partitioning and operation without considering uncertainty can make the grid less resilient and more vulnerable to disruptive events*, like extreme weather.

3.5 Chapter Conclusions

In this chapter, we presented a mixed-integer robust partitioning and operation problem (RPOP) to find a network configuration and generator set-points that minimize generation costs and the amount of undelivered uncertain-load. To make this problem tractable, we proposed a novel two-stage RPOP reformulation where the first-stage problem optimizes network partitioning decisions to maximize the load delivery, using a mixed-integer program, and given these decisions, the second-stage problem verifies the robustness and feasibility of linearized three-phase unbalanced power flow to all uncertain load realizations. We also presented a cutting-plane algorithm to solve this two-stage RPOP efficiently. To illustrate algorithm's efficacy during a disruptive event that separates the distribution grid from the main grid, a case study using a modified IEEE 37-bus test system was presented. The results clearly indicate that partitioning a distribution grid by forming networked microgrids can significantly reduce load shedding. Moreover, the optimal network configuration and an operating point corresponding to nominal loading conditions can be infeasible to the power flow under the worst-case load uncertainty, even at levels of uncertainty as low as 10%. This highlights the need to consider a robust formulation.

Future work includes scaling these approaches to larger, more realistic distribution grids

by developing load-clustering-based heuristics to accelerate solving the max-min problems. We also plan to consider less-conservative uncertainty sets and include battery storage devices and renewable sources. Finally, to ensure practicality, we will also provide guarantees on non-convex three-phase AC power flow feasibility while ensuring tractability and robustness based on simplified power flow models.

CHAPTER 4

Reconfiguration and Real-Time Operation of Networked Microgrids Under Load Uncertainty

This chapter builds upon the work in Chapter 3 on the two-stage mixed-integer robust optimization problem for configuring dynamic networked microgrids (DNMGs), improving the solve time and scalability. Furthermore, we introduce a model-free, real-time optimal power flow algorithm to manage DNMG operations in the time between reconfigurations. A case study on a realistic network based on part of the San Francisco Bay Area demonstrates the scalability of both approaches. The case study also illustrates the ability to maintain power flow feasibility as loads vary and operating conditions change when the methods are used in tandem. The work in this chapter is based on our published work [89].

4.1 Chapter Introduction

More than a decade ago, the U.S. Department of Energy identified microgrids as a key building block in grids of the future [27]. Recent research has shown that microgrids can improve the resiliency and economic efficiency of distribution grids, especially during extreme weather events and unforeseen contingencies [71–73]. Real-world implementations have shown that microgrids improve resilience during natural disasters, like Superstorm Sandy and Hurricane Maria [90, 91].

Beyond stand-alone microgrids, recent research has focused on what are known as nested microgrids, collaborative microgrids, or dynamic networked microgrids (DNMGs) [92–94]. DNMGs are individual microgrids which can be connected to each other in order to facilitate resource sharing and form new microgrids with dynamic boundaries [95]. Compared to more traditional microgrids, DNMGs offer superior adaptability to volatile loading and uncertain generation availability [96]. Their ability to reconfigure in response to contingencies, isolating

impacted areas while maintaining operation in other parts of the network, can improve system resilience. Moreover, the ability to optimize over both connectivity and utilization of distributed generators (DGs) within DNMGs can reduce power losses and costs [97].

Despite the attention that DNMGs, or microgrids more generally, have received, there are still a number of open questions as to how to operate them [75,76]. The literature is missing a unified approach for addressing load uncertainty, contingency management, phase unbalance, network reconfiguration, inverter control modes, and real-time operation of DNMGs. Ref. [76] presents a chance-constrained distribution network reconfiguration problem that accounts for generation uncertainty, but does not consider load uncertainty, which is inherent in distribution networks. Some studies do consider load uncertainty. For instance, [77] proposes a two-stage robust formulation and [98] presents a single-stage mixed-integer conic formulation for distribution network reconfiguration in the presence of load uncertainty. However, contingencies wherein load shedding may be necessary are not considered. With the exception of [76], these papers and many others on distribution network reconfiguration [99–101] consider only balanced networks despite the unbalanced nature of distribution networks. In [70], we addressed the problem of reconfiguration of DNMGs to maximize uncertain-load delivery in unbalanced multi-phase networks during a contingency using robust optimization and a cutting-plane method. A similar problem was approached using stochastic optimization, where load and solar generation scenarios represent uncertainty, in [102]. However, [102] assumes that individual loads can be shed and does not address the role of grid-forming/grid-following inverter control modes.

Deciding network topology is only the first step in DNMG operation. Once the topology is chosen, i.e., where the microgrid boundaries lay is decided, operational decisions like power injections must be made. Existing literature on real-time operation of microgrids does not consider the complex reconfiguration enabled by DNMGs. For example, managing the energy exchanged between fixed-boundary microgrids with load uncertainty [103] or both load and generation uncertainty [104,105] given full network information has been considered. In [78], a two-stage robust formulation for scheduling DGs to mitigate load shedding during an islanding event is proposed. In [106], a decentralized droop control scheme which relies on an augmented Newton-type power flow formulation is presented. These existing works assume a complete model of the distribution network, which may be unrealistic for a network composed of DNMGs with changing boundaries.

In this chapter, we build on the work in [70] to improve the inverter control mode criteria, solve time, and scalability. We also incorporate a model-free, real-time optimal power flow (MFRT-OPF) algorithm that uses voltage measurements and measured changes in slack bus power injections to respond to load changes and manage voltage deviations via decentralized

control actions that can be leveraged to operate the network between reconfigurations.

This chapter contributes to the literature by (i) improving the solve time and scalability of the work in [70] (ii) integrating a model-free control method to manage real-time load changes and voltage deviations within DNMGs that ensures network feasibility between reconfigurations given load uncertainty, and (iii) presenting a detailed case study on a realistic distribution network, demonstrating the scalability of the proposed algorithms as well as the reliability and resiliency improvements they enable.

This chapter is organized as follows: Section 4.2 introduces the robust partitioning problem, with notation, network configuration constraints, and the single-stage formulation in Subsections 4.2.1, 4.2.2, and 4.2.3, respectively. Section 4.3 details the cutting-plane algorithm for solving the robust partitioning problem. The MFRT-OPF algorithm is described in Section 4.4. Section 4.5 presents a case study using the two algorithms, and Section 4.6 provides the conclusions.

4.2 Robust Partitioning Problem Formulation

In this section, we present notation, the network configuration constraints which include the new GFM-DG constraints, and a modified version of the single-stage robust optimization problem formulation presented in our prior work [70].

4.2.1 Notation and Preliminaries

In this chapter, vectors are indicated by bold typeface and matrices are indicated by blackboard bold typeface. The $|\cdot|$ operation represents cardinality when the input is a set, absolute value when the input is a number, and magnitude when the input is a complex number.

Consider a distribution network with a set of buses $\mathcal{N}$, a set of lines $\mathcal{L}$, a set of phases Φ, and a set of switches $\mathcal{E}^{\text{sw}}$. The network can be reconfigured by opening or closing switches. For generality, we assume the network has a meshed structure when all switches are closed. To align with typical protection coordination schemes [77], we assume that the network can only be operated in radial configurations. Within the network, there is a set of transformers $\mathcal{E}^{x}$ composed of a set of wye-connected transformers $\mathcal{E}^{x,Y}$ and a set of delta-connected transformers $\mathcal{E}^{x,\Delta}$, such that $\mathcal{E}^{x} = \mathcal{E}^{x,Y} \cup \mathcal{E}^{x,\Delta}$. Within the network, there is a set $\mathcal{G}$ of controllable DGs g. The apparent power injected into the grid by generator g on phase ϕ is given by s_g^{ϕ}.

Additionally, there is a set of uncontrollable and uncertain loads $\mathcal{D}$. The apparent power demanded by load d on phase ϕ is given by $s_d^{\phi} = s_d^{0,\phi} + u_d^{\phi}$, where $s_d^{0,\phi}$ is the nominal load power and u_d^{ϕ} is the load uncertainty defined by the set

$$\mathcal{U} = \left\{ u_d^\phi \in \mathbb{R}^{|\mathcal{D}\times\Phi|} \;\middle|\; \underline{s}_d^\phi - s_d^{0,\phi} \leqslant u_d^\phi \leqslant \overline{s}_d^\phi - s_d^{0,\phi},\ \forall\phi \in \Phi, \forall d \in \mathcal{D} \right\}, \quad (4.1)$$

where $\overline{s}_d^\phi$ and $\underline{s}_d^\phi$ represent the upper and lower bounds of uncertain load d on phase ϕ.

The formulation presented in this chapter uses the LinDist3Flow model to approximate the AC power flow equations while capturing the unbalanced, three-phase power flow typical of distribution grids [79, 80]. In the LinDist3Flow model, the equations are written in terms of squared voltage and current magnitudes. Let w_i^ϕ represent the squared magnitude of the voltage on phase ϕ at bus i and let l_{ij}^ϕ represent the squared magnitude of the current flowing on phase ϕ of the line connecting buses i and j. Let $z_{ij}^{\phi\psi} = r_{ij}^{\phi\psi} + jx_{ij}^{\phi\psi}$ represent the self and mutual impedances on the line connecting buses i and j between phases ϕ and ψ. When $\phi = \psi$, z represents self impedance, otherwise it represents mutual impedance. The complex power flowing on the line between buses i and j on phase ϕ is given by $s_{ij}^\phi = p_{ij}^\phi + jq_{ij}^\phi$, where p and q represent active and reactive power, respectively.

A connected component (CC) is a set of buses that are electrically connected, including single isolated buses [81]. We consider a microgrid as a CC containing at least one load and at least one voltage source. We define $\mathcal{B}$ as the set of CCs that exist when every switch in the network is open. The CCs within this set will be referred to as blocks. When a switch between two blocks is closed, the two blocks form one CC, as shown in Fig. 4.1. Thus, the set of blocks in the network remains static, while the CCs change as switches open or close.

4.2.2 Network Configuration Constraints

Two general requirements govern network configuration: First, every energized CC must be a spanning tree, devoid of loops to satisfy typical protection schemes. Second, each energized CC must contain at least one voltage source.

4.2.2.1 Radiality Constraints

A radial topology is enforced in each CC using the directed multi-commodity flow-based model of spanning tree constraints given in [81]. For brevity, we omit the constraints here and refer the reader to [81] for details. In the remainder of this chapter, this model will be referred to as the radiality constraints.

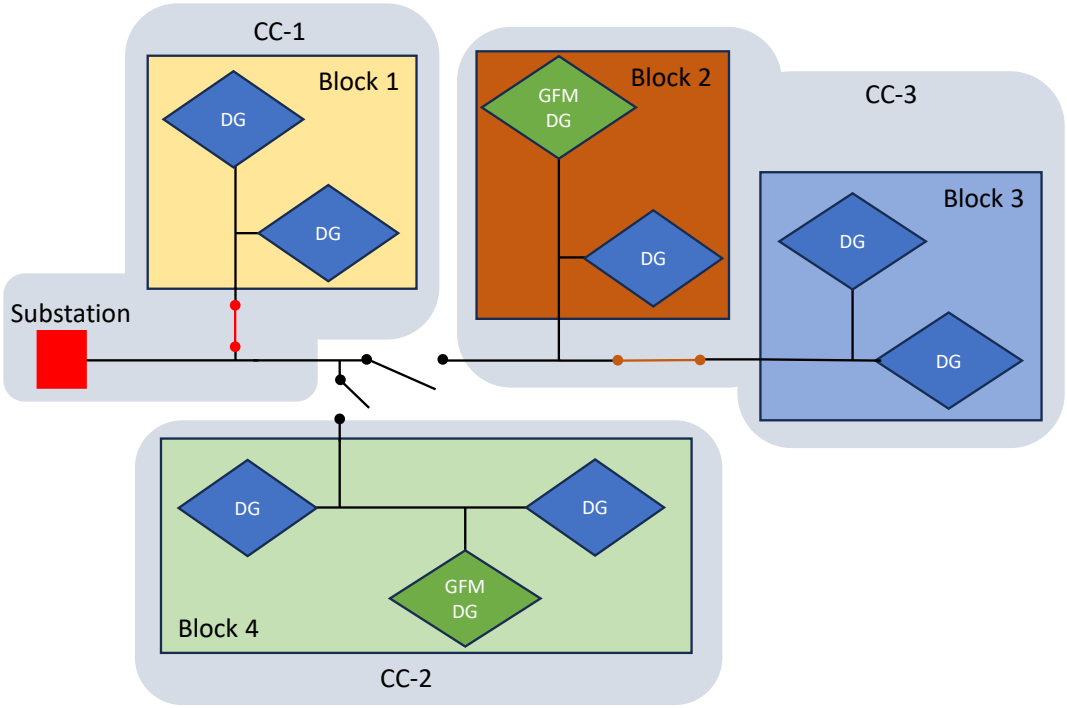


Figure 4.1: Dynamic reconfiguration of networked microgrids via switches. Blocks are connected by switches to form connected components (CCs). Each energized CC, which functions as an independent microgrid, contains uncertain loads and DGs, with at least one DG serving as a voltage source.

4.2.2.2 Grid-Forming DG Constraints

An energized CC must contain a voltage source that is connected to each active phase. Distribution network DGs are typically inverter-based resources, which can operate as either grid-forming or grid-following. A grid-forming DG (GFM-DG) controls the AC-side voltage, acting as a voltage source for the network, while a grid-following DG controls the AC-side current and "follows the phase angle of the existing grid voltage" [82]. Uncoordinated operation of two or more GFM-DGs in close proximity can lead to independent control of voltage and frequency, potentially leading to instability [83]. Control strategies exist for facilitating multiple GFM-DGs in a microgrid [107,108], but may be incompatible with older, existing equipment [109]. To remain generalizable, the following constraints ensure that each CC contains at least one GFM-DG and no more than k^{DG} GFM-DG, where $k^{\mathrm{DG}} \geqslant 1$ is a design parameter representing the maximum number of DGs that can simultaneously operate as grid-forming within a CC. Choice of k^{DG} should be consistent with equipment limitations and the selected control strategy.

Let z_l^{bl}, z_{ij}^{sw}, and z_g^{inv} indicate whether block l is energized, the switch between blocks i and j is closed, and DG g is grid-forming, respectively. Each variable equals 1 if active (energized block, closed switch, or grid-forming DG) and 0 otherwise. Let $\mathcal{G}_l$ and $\mathcal{E}_l^{\mathrm{sw}}$ be the set of DGs and switches, respectively, connected to block l. The relationship between the block states z_l^{bl} and the DG states z_g^{inv} is defined by

$$|z_i^{\mathrm{bl}} - z_j^{\mathrm{bl}}| \leqslant (1 - z_{ij}^{\mathrm{sw}}), \qquad \forall ij \in \mathcal{E}^{\mathrm{sw}} \tag{4.2}$$

$$z_l^{\mathrm{bl}} \underline{s_g} \leqslant s_g^{\phi} \leqslant z_l^{\mathrm{bl}} \overline{s_g}, \qquad \forall g \in \mathcal{G}_l, \forall l \in \mathcal{B} \tag{4.3}$$

$$z_l^{\mathrm{bl}} - \sum_{ij \in \mathcal{E}_l^{\mathrm{sw}}} z_{ij}^{\mathrm{sw}} \leqslant \sum_{i \in \mathcal{G}_l} z_i^{\mathrm{inv}} \leqslant k^{\mathrm{DG}} z_l^{\mathrm{bl}}, \qquad \forall l \in \mathcal{B} \tag{4.4}$$

where (4.2) enforces that blocks connected by a closed switch must be either both energized or both de-energized; (4.3) enforces generation power limits for DGs within an energized block and prevents a DG within a de-energized block from producing power; and (4.4) states that a block must contain at least one and no more than k^{DG} GFM-DG if it is energized and not connected to another block.

Coloring Scheme To ensure consistency across networked blocks, i.e., all blocks within a CC share the same grid-forming inverter(s), we apply a coloring scheme based on the PowerModelsONM.jl implementation [75]. Closed switches are colored, or labeled, with the block in their CC that contains a GFM-DG. We define binary variables y_{ij}^l to indicate whether switch ij is colored by block l, where $y_{ij}^l = 1$ if true, and 0 otherwise. Note that a

single switch can be colored by up to k^{DG} blocks. The coloring scheme is described by:

$$\sum_{l\in\mathcal{B}} y_{ij}^{l} \leqslant k^{\mathrm{DG}} z_{ij}^{\mathrm{sw}}, \quad \forall ij \in \mathcal{E}^{\mathrm{sw}} \tag{4.5}$$

$$y_{ij}^{l} - (1 - z_{ij}^{\mathrm{sw}}) \leqslant \sum_{i\in\mathcal{G}_l} z_{i}^{\mathrm{inv}} \leqslant k^{\mathrm{DG}} \left(y_{ij}^{l} + (1 - z_{ij}^{\mathrm{sw}})\right), \forall l \in \mathcal{B}, \forall ij \in \mathcal{E}^{\mathrm{sw}} \tag{4.6}$$

$$y_{dc}^{l'} - (1 - z_{dc}^{\mathrm{sw}}) - (1 - z_{ab}^{\mathrm{sw}}) \leqslant y_{ab}^{l'} \leqslant y_{dc}^{l'} + (1 - z_{dc}^{\mathrm{sw}}) + (1 - z_{ab}^{\mathrm{sw}}), \quad \forall ab \neq dc \in \mathcal{E}_{l}^{\mathrm{sw}}, \forall l, l' \in \mathcal{B} \tag{4.7}$$

$$y_{ij}^{l} \leqslant \sum_{i\in\mathcal{G}_l} z_{i}^{\mathrm{inv}}, \quad \forall l \in \mathcal{B}, \forall ij \in \mathcal{E}^{\mathrm{sw}} \tag{4.8}$$

$$z_{l}^{\mathrm{bl}} \leqslant \sum_{i\in\mathcal{G}_l} z_{i}^{\mathrm{inv}} + \sum_{ij\in\mathcal{E}_{l}^{\mathrm{sw}}} \sum_{l\in\mathcal{B}} y_{ij}^{l}, \quad \forall l \in \mathcal{B} \tag{4.9}$$

$$z^{\mathrm{bl}}, z^{\mathrm{sw}}, z^{\mathrm{inv}}, y^{l} \in \{0, 1\} \tag{4.10}$$

where (4.5) restricts an open switch to be colorless and a closed switch to have at most k^{DG} colors. Constraint (4.6) necessitates that if switch ij is closed and colored by block l, then it is in the same CC as block l, which contains at least one GFM-DG. Constraint (4.7) enforces that two closed switches connected to the same block must have the same color. Constraint (4.8) states that unless block l contains at least one GFM-DG, a switch cannot have color l. Constraint (4.9) states that a block can only be energized if it contains at least one GFM-DG or it is connected to at least one closed switch. Lastly, (4.10) defines $z^{\mathrm{bl}}, z^{\mathrm{sw}}, z^{\mathrm{inv}}$ and y^{l} as binary variables.

Commodity Flow In conjunction with the coloring scheme, we use a multi-commodity flow model similar to the one in [81] to ensure that a GFM-DG is present within a CC. Let $\mathcal{E}_{l}^{v}$ be a set of virtual edges between block l and all other blocks l', oriented from l to l' (there are $|\mathcal{B}| - 1$ of these edges for each l). Let μ_{ij}^{l} represent a unit of flow of commodity l across the virtual edge from i to j. For each $ij \in \mathcal{E}_{l}^{\mathrm{sw}}$, there is an arbitrary orientation (e.g., either $i = l$ or $j = l$). Then the following set of constraints can be used to determine whether a GFM-DG is connected to a CC.

$$-z_{ij}^{\mathrm{sw}}(|\mathcal{E}^{\mathrm{sw}}|) \leqslant \eta_{ij}^{l} \leqslant z_{ij}^{\mathrm{sw}}(|\mathcal{E}^{\mathrm{sw}}|), \quad \forall ij \in \mathcal{E}_{l}^{\mathrm{sw}}, \ \forall l \in \mathcal{B} \tag{4.11}$$

$$0 \leqslant \mu_{ij}^{l} \leqslant 1, \quad \forall ij \in \mathcal{E}_{l}^{v}, \forall l \in \mathcal{B} \tag{4.12}$$

$$\sum_{ij\in\mathcal{E}_{l}^{\mathrm{sw}}:i=l} \eta_{ij}^{l} - \sum_{ij\in\mathcal{E}_{l}^{\mathrm{sw}}:j=l} \eta_{ij}^{l} + \sum_{ij\in\mathcal{E}_{l}^{v}} \mu_{ij}^{l} = |\mathcal{B}| - 1, \forall l \in \mathcal{B} \tag{4.13}$$

$$\sum_{ij\in\mathcal{E}_{l}^{\mathrm{sw}}:i=l'} \eta_{ij}^{l} - \sum_{ij\in\mathcal{E}_{l}^{\mathrm{sw}}:j=l'} \eta_{ij}^{l} - \mu_{ll'}^{l} = -1, \forall l' \neq l, \forall l \in \mathcal{B} \tag{4.14}$$

$$y_{ij}^{l} \leqslant 1 - \mu_{ll'}^{l}, \quad \forall l' \neq l, ij \in \mathcal{E}_{l'}^{\text{sw}}, \forall l \in \mathcal{B} \tag{4.15}$$

Constraint (4.11) limits the flow magnitude η_{ij}^{l} across a closed switch ij from block l by the number of switches in the network. Constraint (4.12) restricts flow across each virtual edge to one unit or less. Constraints (4.13) and (4.14) collectively ensure flow balance among blocks l and l'. Constraint (4.15) ensures $y_{ij}^{l} = 0$ for every $ij \in \mathcal{E}_{l'}^{\text{sw}}$ if there is flow on the virtual line between l and l'.

Maximum Phase Connections If the network contains blocks with different phase configurations, i.e., some are 3-phase while others are 2- or single-phase, additional constraints are needed to ensure that the DG selected as GFM is connected to every active phase in the CC. Each block $l \in \mathcal{B}$ is assigned a maximum phase parameter $\Phi_l^{\max} \in \{1, 2, 3\}$, representing the highest number of phases among all buses in block l. Formally,

$$\Phi_l^{\max} = \max_{i \in \mathcal{N}_l} |\Phi_i|, \quad \forall l \in \mathcal{B}$$

where $|\Phi_i|$ indicates the number of phases present at bus i. The following constraint ensures that a DG can only be selected as GFM if it is connected to every phase that is present in the block where it is located:

$$z_g^{\text{inv}} = 0, \quad \forall g \notin \mathcal{G}_l^{\Phi_l^{\max}}, \forall l \in \mathcal{B} \tag{4.16}$$

where $\mathcal{G}_l^{\Phi_l^{\max}}$ represents the set of DGs in block l that are connected to $\Phi_l^{\max}$ number of phases. Because CCs can contain multiple blocks connected by switches, it must also be checked that any GFM-DG is connected to the maximum number of phases active within the blocks it is connected to. Consider the following "one-hop" and "two-hop" constraints

$$z_g^{\text{inv}} \leqslant 1 - z_{lj}^{\text{sw}}, \quad \forall g \in \mathcal{D}_l, \forall lj \in \mathcal{E}_l^{\text{sw},\underline{\Phi}}, \forall l \in \mathcal{B} \tag{4.17}$$

$$z_g^{\text{inv}} \leqslant 2 - z_{lj}^{\text{sw}} - z_{jk}^{\text{sw}}, \quad \forall g \in \mathcal{D}_l, \forall lj \in \mathcal{E}_l^{\text{sw}} \setminus \mathcal{E}_l^{\text{sw},\underline{\Phi}}, jk \in \mathcal{E}_j^{\text{sw},\underline{\Phi}}, \forall l \in \mathcal{B} \tag{4.18}$$

where $\mathcal{E}_l^{\text{sw},\underline{\Phi}}$ represents the set of switches that connect block l to a neighboring block j such that $\Phi_l^{\max} < \Phi_j^{\max}$. If a network contains a sequence of more than two neighboring blocks where all have $\Phi_l^{\max} < 3$, the above constraints would be necessary but may not be sufficient. The addition of constraints (4.16)-(4.18) generalize the formulation in [70] to be compatible with realistic multi-phase networks.

4.2.3 Single-Stage Robust Partitioning and Operation Problem

This section details the single-stage Robust Partitioning and Operation Problem (RPOP) for distribution grids composed of DNMGs. Its optimal solution comprises network partitions and generator set-points that minimize the costs of load shed and power generation while ensuring feasibility and robustness against all realizations of uncertain loads. The formulation is

$$\min \sum_{l\in\mathcal{B}} \beta_l^{\mathrm{B}}(1-z_l^{\mathrm{bl}}) + \sum_{g\in G}\sum_{\phi\in\Phi_g} c_{1,g}s_g^{\phi} + c_{0,g}z_g^{\mathrm{bl}} \tag{4.19a}$$

$$\text{s.t. Radiality Constraints (Sec. 4.2.2.1), (4.2)} - \text{(4.18)} \tag{4.19b}$$

$$z_l^{\mathrm{bl}}\underline{v_i}^2 \leqslant w_{i,\phi} \leqslant z_l^{\mathrm{bl}}\overline{v_i}^2,\ \forall\phi\in\Phi_i, \forall i\in\mathcal{N}_l, \forall l\in\mathcal{B} \tag{4.19c}$$

$$\mathbf{w}_i = \mathbf{w}_j - \mathbb{M}_{ij}^{p}\mathbf{p}_{ij} - \mathbb{M}_{ij}^{q}\mathbf{q}_{ij}, \forall i,j\in\mathcal{N},\ \forall ij\in\mathcal{L} \tag{4.19d}$$

$$|s_{ij}^{\phi}| \leqslant \overline{s_{ij}^{\phi}}, \quad \forall\phi\in\Phi_{ij}, \forall ij\in\mathcal{L}\cup\mathcal{E}^{x} \tag{4.19e}$$

$$|s_{ij}^{\phi}| \leqslant z_{ij}^{\mathrm{sw}}\overline{s_{ij}^{\phi}}, \quad \forall\phi\in\Phi_{ij}, \forall ij\in\mathcal{E}^{\mathrm{sw}} \tag{4.19f}$$

$$w_i^{\phi} = n_{ij}^2 w_j^{\phi}, \quad \forall\phi\in\Phi_{ij}, \forall ij\in\mathcal{E}^{x,Y} \tag{4.19g}$$

$$3(w_{i,\phi}+w_{i,\psi}) = 2(n_{ij})^2 w_{j,\phi}, \quad \forall(\phi,\psi)\in\{(a,b),(b,c),(c,a)\},\ \forall ij\in\mathcal{E}^{x,\Delta} \tag{4.19h}$$

$$s_{ij}^{\phi} = s_{ji}^{\phi}, \quad \forall\phi\in\Phi_{ij}, \forall ij\in\mathcal{E}^{x,Y} \tag{4.19i}$$

$$2p_{ij,\phi} = -(p_{ji,\phi}+p_{ji,\psi}) + (q_{ji,\psi}-q_{ji,\phi})/\sqrt{3}, \quad \forall(\phi,\psi)\in\{(a,c),(b,a),(c,b)\},\ \forall ij\in\mathcal{E}^{x,\Delta} \tag{4.19j}$$

$$2q_{ij,\phi} = (p_{ji,\phi}-p_{ji,\psi})/\sqrt{3} - (q_{ji,\psi}+q_{ji,\phi}), \quad \forall(\phi,\psi)\in\{(a,c),(b,a),(c,b)\},\ \forall ij\in\mathcal{E}^{x,\Delta} \tag{4.19k}$$

$$z_i^{\mathrm{bl}}\underline{s_g^{\phi}} \leqslant s_g^{\phi} \leqslant z_i^{\mathrm{bl}}\overline{s_g^{\phi}},\ \forall\phi\in\Phi_g, \forall g\in i, \forall i\in\mathcal{B} \tag{4.19l}$$

$$\sum_{ij\in\mathcal{E}_i} s_{ij}^{\phi} = \sum_{g\in i} s_g^{\phi} - z_k^{\mathrm{bl}}\sum_{d\in\mathcal{D}_i} s_d^{\phi} - \sum_{c\in\Phi_i} y_c^{\phi}w_i^{\phi},\ \forall\phi\in\Phi_i, \forall i\in l,\ \forall l\in\mathcal{B} \tag{4.19m}$$

where z_g^{bl} represents the block state of the block containing generator g, and $\mathcal{E}=\mathcal{L}\cup\mathcal{E}^{\mathrm{sw}}\cup\mathcal{E}^{x}$ is the set of all lines, switches, and transformers. The objective function minimizes the cost of de-energizing blocks and generation, where β_l^{B} is a weighting parameter for block l indicating priority, and $c_{1,g}, c_{0,g}$ are parameters of the linear cost function of generator g. The voltage limits at each bus are enforced by (4.19c) and the linearized voltage drop between bus j and downstream bus i is computed in (4.19d), where variables represented with bold typeface

are 3-phase vectors, and

$$\mathbb{M}_{ij}^{p} = \begin{bmatrix} -2r_{aa} & r_{ab} - \sqrt{3}x_{ab} & r_{ac} + \sqrt{3}x_{ac} \\ r_{ba} + \sqrt{3}x_{ba} & -2r_{bb} & r_{bc} - \sqrt{3}x_{bc} \\ r_{ca} - \sqrt{3}x_{ca} & r_{cb} + \sqrt{3}x_{cb} & -2r_{cc} \end{bmatrix}_{ij},$$

$$\mathbb{M}_{ij}^{q} = \begin{bmatrix} -2x_{aa} & x_{ab} + \sqrt{3}r_{ab} & x_{ac} - \sqrt{3}r_{ac} \\ x_{ba} - \sqrt{3}r_{ba} & -2x_{bb} & x_{bc} + \sqrt{3}r_{bc} \\ x_{ca} + \sqrt{3}r_{ca} & x_{cb} - \sqrt{3}r_{cb} & -2x_{cc} \end{bmatrix}_{ij}.$$

Constraints (4.19e) and (4.19f) define the power flow limits for each line, transformer, and switch. Constraints (4.19g) and (4.19h) define the voltage transformations across each wye-connected and delta-connected transformer, where n_{ij} is the tap ratio of transformer ij. Constraints (4.19i), (4.19j) and (4.19k) define the relationship between the directions of power flow on each wye-connected and delta-connected transformer. Lastly, (4.19m) represents linearized power balance.

4.3 A Cutting-Plane Algorithm to solve the RPOP

It is intractable to solve the RPOP as given in Section 4.2.3 using off-the-shelf solvers. We now present a two-stage version of the RPOP, which can be solved to global optimality using an iterative cutting-plane algorithm.

4.3.1 Two-stage Robust Partitioning and Operation Problem

The RPOP in (4.19) has an equivalent two-stage formulation composed of a master problem and a set of subproblems [84]. The master (first-stage) decision variables include power injections, $\mathbf{s}_g^{\phi}\ \forall \phi \in \Phi,\ \forall g \in \mathcal{G}$, switch configurations $z_{ij}^{\text{sw}}\ \forall ij \in \mathcal{E}^{\text{sw}}$, generator operating states $z_g^{\text{inv}}\ \forall g \in \mathcal{G}$ as either grid-forming or grid-following, block states $z_l^{\text{bl}}\ \forall l \in \mathcal{B}$, and additional configuration and power flow variables.

Let $\mathbf{x}$ represent a vector of variables $\mathbf{s}_g^{\phi}, z_{ij}^{\text{sw}}, z_g^{\text{inv}}, z_l^{\text{bl}}$ including every generator, switch, and block in the network. Let $\mathbf{s}_d^*$ be the worst-case uncertain load realization. The master problem, which relaxes the single-stage problem by ignoring load uncertainty, is

$$\min \sum_{l \in \mathcal{B}} \beta_l^{\text{B}}(1 - z_l^{\text{bl}}) + \sum_{g \in G} \sum_{\phi \in \Phi_g} c_{1,g} s_g^{\phi} + c_{0,g} z_g^{\text{bl}} + \theta \qquad (M)$$

$$\text{s.t. Radiality Constraints (Sec. 4.2.2.1), } (4.2) - (4.10),$$

$$(4.19c) - (4.19m),$$
$$V_2(\mathbf{x}_k^*, \mathbf{s}_{d,k}^*) + \pi_k^\intercal A(\mathbf{x} - \mathbf{x}_k^*) \leqslant \theta, \forall k = 1, 2, ... \tag{4.20a}$$

where subscript k denotes the k^{th} iteration; $\mathbf{x}_k^*$ is the optimal solution of (M); $V_2(\mathbf{x}_k^*, \mathbf{s}_{d,k}^*)$ is the subproblem objective at iteration k; $\boldsymbol{\pi}$ is the vector of dual variables for the subproblem constraints involving master variables; and A is coefficient matrix from (S_1) corresponding to the master variables. Our previous work's master problem omitted constraints (4.19c)–(4.19m). To improve the initial master solution and reduce convergence time, we now include the LinDist3Flow equations for a single load scenario.

In the subproblem (second-stage), the integer variables and generation power set-points from the master problem are fixed. After the uncertainty is realized, adjustments to the generation power set-points, o^+ and o^-, are permitted but bounded by generator ramping capabilities and capacity constraints. The subproblem formulation is

$$\min \ \beta^{\text{S}} \left(\sum_{i \in \mathcal{N}} \sum_{\phi \in \Phi_i} \left(h_i^{+,\phi} + h_i^{-,\phi} \right) \right) + \sum_{g \in G} \sum_{\phi \in \Phi_g} c_{1,g} o_g^\phi \tag{S_1}$$
$$\text{s.t.} \quad (4.19c) - (4.19k),$$
$$\begin{aligned} \sum_{ij \in \mathcal{E}_i} s_{ij}^\phi + h_i^{+,\phi} - h_i^{-,\phi} = \sum_{g \in i} \left(s_g^{\phi *} + o_g^{+,\phi} - o_g^{-,\phi} \right) \\ - z_k^{\text{bl}*} \sum_{d \in \mathcal{D}_i} s_d^\phi - \sum_{c \in \Phi_i} y_c^\phi w_i^\phi, \ \forall i \in k, \ \forall k \in \mathcal{B}, \end{aligned} \tag{4.21a}$$
$$o_g^{+,\phi} \leqslant z_i^{\text{bl}*} \overline{s_g^\phi} - s_g^{\phi *}, \ \forall \phi \in \Phi_g, \forall g \in i, \forall i \in \mathcal{B}, \tag{4.21b}$$
$$o_g^{-,\phi} \leqslant s_g^{\phi *} - z_i^{\text{bl}*} \underline{s_g^\phi}, \ \forall \phi \in \Phi_g, \ \forall g \in i, \ \forall i \in \mathcal{B}, \tag{4.21c}$$
$$0 \leqslant \ o_g^{+,\phi}, \ o_g^{-,\phi} \ \leqslant \overline{o_g^\phi}, \ \forall \phi \in \Phi_g, \ \forall g \in i, \ \forall i \in \mathcal{B}, \tag{4.21d}$$
$$h_i^{+,\phi}, h_i^{-,\phi} \geqslant 0, \ \forall \phi \in \Phi_i, \ \forall i \in \mathcal{N}. \tag{4.21e}$$

where β^{S} is a weighting parameter and $h_i^{+,\phi}, h_i^{-,\phi}$ are slack variables indicating a power balance violation on phase ϕ at bus i. The realized load and injection adjustments are incorporated into (4.21a). If any slack variables are non-zero at optimality, there exists no feasible o^+, o^- that satisfy the power flow equations for the candidate solution $\mathbf{x}^*$ and uncertain load realization $\mathbf{s}_d$. In such cases, a feasibility cut (4.20a) is generated to remove $\mathbf{x}^*$ from the feasible region of subsequent iterations of the master problem. Constraints (4.21b)-(4.21d) set limits on generator set-point modifications based on ramping and capacity limits.

A decomposition algorithm cannot be directly implemented due to infinitely many subproblems arising from uncertain load realizations. Instead, we identify and solve only the

subproblem with the most violated power balance constraints within the given uncertainty set. This entails solving a bilevel max − min problem of the form

$$\max_{\mathcal{U}} \ \min \ \beta^{\mathrm{S}} \left(\sum_{i \in \mathcal{N}} \sum_{\phi \in \Phi_i} \left(h_i^{+,\phi} + h_i^{-,\phi} \right) \right) + \sum_{g \in G} \sum_{\phi \in \Phi_g} c_{1,g} o_g^{\phi} \tag{S_2}$$
$$\text{s.t.} \quad (4.19\text{c}) - (4.19\text{k}), (4.21\text{a}) - (4.21\text{e})$$

We know from convex optimization theory that the optimal solution to the max − min problem (S_2) lies at one of the extreme points (minimum or maximum values) of the uncertainty set, since the inner minimization is a convex function of the uncertain load [85]. To improve the computational tractability of our prior work [70], we adopt a simplified uncertainty model by assuming that loads vary uniformly within predefined "clusters"–i.e., all loads in a cluster simultaneously take on either their minimum or maximum values. This assumption is reasonable, as it captures correlated load behavior often observed in practice, such as geographically grouped loads responding similarly to weather, pricing signals, or time-of-use effects. By limiting the uncertainty set to a smaller set of scenarios, defined by the extreme points of these clusters, we reduce its dimensionality and significantly lower the number of subproblem evaluations required in the cutting-plane algorithm 2. Leveraging this, we replace $\mathcal{U}$ in (S_2) with a finite-dimensional uncertainty set

$$\widehat{\mathcal{U}} = \Bigg\{ u_d^{\phi} \in \mathbb{R}^{|\mathcal{D} \times \Phi|} \ \Bigg| \ u_d^{\phi} = \zeta_{\gamma}^{+} (\overline{s}_d^{\phi}) + \zeta_{\gamma}^{-} (\underline{s}_d^{\phi}) - s_d^{0,\phi}, \ \zeta_{\gamma}^{+} + \zeta_{\gamma}^{-} = 1, \ \zeta_{\gamma}^{+}, \zeta_{\gamma}^{-} \in \{0,1\}, \\ \forall \phi \in \Phi, \forall d \in \mathcal{D}_{\gamma}, \forall \gamma \in \Gamma \Bigg\}. \tag{4.23}$$

where Γ is a set of load clusters. Thus, the reduced finite-dimensional (S_2) problem can be replaced by solving the modified subproblem for every possible combination of ζ_d^{+}, ζ_d^{-}, selecting the solution that yields the largest objective, i.e.,

$$\min \ \beta^{\mathrm{S}} \left(\sum_{i \in \mathcal{N}} \sum_{\phi \in \Phi_i} \left(h_i^{+,\phi} + h_i^{-,\phi} \right) \right) + \sum_{g \in G} \sum_{\phi \in \Phi_g} c_{1,g} o_g^{\phi} \tag{E}$$
$$\text{s.t.} \quad (4.19\text{c}) - (4.19\text{k}), (4.21\text{b}) - (4.21\text{e}),$$
$$\sum_{ij \in \mathcal{E}_i} s_{ij}^{\phi} + h_i^{+,\phi} - h_i^{-,\phi} = \sum_{g \in i} \left(s_g^{\phi *} + o_g^{+,\phi} - o_g^{-,\phi} \right) - z_k^{\mathrm{bl}*} \sum_{d \in \mathcal{D}_i} \left(s_d^{0,\phi} + \zeta_{\gamma}^{+} \overline{s}_d^{\phi} - \zeta_{\gamma}^{-} \underline{s}_d^{\phi} \right) \\ - \sum_{c \in \Phi_i} y_c^{\phi} w_i^{\phi}, \ \forall i \in k, \ \forall k \in \mathcal{B}_{\gamma}, \forall \gamma \in \Gamma,$$
$$\zeta_{\gamma}^{+}, \zeta_{\gamma}^{-} \in \{0,1\}, \forall \gamma \in \Gamma.$$

Note that for simplicity we assume that all loads in a block are in the same load cluster. This approach still requires solving $2^{|\Gamma|}$ number of quadratically-constrained convex programs (E), and may not scale efficiently as the number of uncertain load clusters increases.

4.3.2 A Cutting-plane Algorithm

We propose a cutting-plane algorithm, outlined in Algorithm 2, to solve the two-stage RPOP. After initialization, the master problem (M) is solved for the network configuration and generator set-points (master solution, $\mathbf{x}^*$) in Step 4 of Algorithm 2. Given $\mathbf{x}^*$, (S_2) is solved for every scenario in $\widehat{\mathcal{U}}$ to obtain the worst-case load realization in Step 5. Finally, the subproblem (S_1) is solved in Step 6 to check the feasibility of the master solution given the worst-case load realization. If $\mathbf{x}^*$ is feasible, then it is an optimal solution to the RPOP and the algorithm terminates. Otherwise, if there is non-zero slack $h^{+,\phi}, h^{-,\phi}$, a sub-gradient cut is added to (M) in Step 3 and the process is repeated.

Algorithm 2 : Cutting-plane algorithm for two-stage RPOP

1: Initialize: $k \leftarrow 1$, $h_i^{+,\phi} \leftarrow \infty$, $h_i^{-,\phi} \leftarrow \infty \ \forall i \in \mathcal{N}$, $\epsilon > 0$, $V_2(\mathbf{x}_1^*, \mathbf{s}_{d,1}^*) \leftarrow 0$, and $\pi_1 \leftarrow 0$
2: **while** $\sum_{i\in\mathcal{N}} \sum_{\phi\in\Phi_i} \left(h_i^{+,\phi} + h_i^{-,\phi}\right) > \epsilon$ **do**
3: Append $V_2(\mathbf{x}_k^*, \mathbf{s}_{d,k}^*) + \pi_k^\intercal A(\mathbf{x} - \mathbf{x}_k^*) \leqslant \theta$ to (M)
4: Solve master problem (M) for $\mathbf{x}_k^*$
5: Given $\mathbf{x}_k^*$, find the worst-case uncertainty realization $s_{d,k}^*$ by solving (E) for every scenario in $\hat{\mathcal{U}}$
6: Given $\mathbf{x}_k^*$ and $s_{d,k}^*$, solve Subproblem (S_1) for $h^{+,\phi}, h^{-,\phi}, o^{+,\phi}, o^{-,\phi}$
7: Set $k \leftarrow k + 1$
8: **end while**
9: Output: $\mathbf{x}_{k-1}^*,\ o^{+,\phi},\ o^{-,\phi}$

Convergence guarantee: The finite number of blocks in a distribution network guarantees that Algorithm 2 will converge within a finite number of iterations. In extreme cases, sub-gradient cuts will be added until every block is de-energized to meet the termination criterion, as indicated in Step (2).

4.4 Model-free Real-Time Optimal Power Flow

In this section, we consider real-time optimization of the power injections of DGs within the DNMGs. The goal is to drive the slack bus power injections to follow an active power reference signal $P_0^\bullet$ while keeping voltages within safe bounds as loads change. This is achieved by formulating an OPF problem and using the model-free primal-dual method

presented in [110], modified for use on DNMGs, to solve it. This approach assumes that generation at any slack bus and all bus voltages can be measured.

Consider a distribution network composed of a set of CCs $\mathcal{E}^{\mathrm{CC}}$, which represent DNMGs. CC m contains a set Φ_m of phases and a set $\mathcal{G}_m$ of controllable DGs. Let $\mathbf{s}_m$ be a vector of all decision variables corresponding to CC m, where each controllable DG $g \in \mathcal{G}_m$ has active and reactive power $s_g = \{p_g, q_g\}$. Let $\boldsymbol{\ell}_m$ be a vector of the uncontrollable active and reactive power loads in CC m. Let $v_m(\mathbf{s}_m, \boldsymbol{\ell}_m)$ be a vector of the voltage magnitudes at every PQ node in CC m. Let $P_m^{\mathrm{sl}}(\mathbf{s}_m, \boldsymbol{\ell}_m)$ be the power injection at the slack bus in CC m. This work assumes that each CC has one slack bus—either the substation or the bus connected to a GFM-DG—while all other buses remain PQ buses.

The OPF problem we aim to solve is

$$\min \sum_{m \in \mathcal{E}^{\mathrm{CC}}} \sum_{\phi \in \Phi_m} \left(P_m^{sl,\phi}(\mathbf{s}_m, \boldsymbol{\ell}_m) - P_m^{sl,\bullet,\phi} \right)^2 \tag{4.25}$$

$$\text{s.t. } \underline{v_i} \leqslant v_i^{\phi}(\mathbf{s}, \boldsymbol{\ell}) \leqslant \overline{v_i}, \quad \forall \phi \in \Phi_i, \forall i \in \mathcal{N}_m, \forall m \in \mathcal{E}^{\mathrm{CC}} \tag{4.26}$$

$$0 \leqslant p_g^{\phi} \leqslant \overline{P}_g^{\mathrm{DG}}, \quad \forall \phi \in \Phi_g, \forall g \in \mathcal{G}_m, \forall m \in \mathcal{E}^{\mathrm{CC}} \tag{4.27}$$

$$0 \leqslant q_g^{\phi} \leqslant \overline{Q}_g^{\mathrm{DG}}, \quad \forall \phi \in \Phi_g, \forall g \in \mathcal{G}_m, \forall m \in \mathcal{E}^{\mathrm{CC}} \tag{4.28}$$

where $P_m^{sl,\bullet,\phi}$ is an active-power reference signal for slack bus injections in CC m on phase ϕ; $\underline{v_i}$ and $\overline{v_i}$ are upper and lower voltage limits, respectively; $\mathcal{N}_m$ is the set of buses in CC m; Φ_i is the set of phases at bus i; Φ_g is the set of phases that generator g is connected to; $\overline{P}_g^{\mathrm{DG}}$ and $\overline{Q}_g^{\mathrm{DG}}$ are active and reactive power limits for DG g.

We use the term node to refer to a single phase at a single bus, e.g., a three-phase bus is comprised of three nodes. Define N_m^{ϕ} as the total number of nodes present in CC m, i.e., $N_m^{\phi} := \sum_{i \in \mathcal{N}_m} |\Phi_i|$. Let $\xi^{(\mathbf{k})} \in \mathbb{R}^{N_m^{\phi} \times 1}$ be a vector of deterministic exploration signals obtained by sampling

$$\xi_g^{\phi}(t) = \epsilon \cos(\omega_g^{\phi} t), \quad \forall g \in \mathcal{G} \tag{4.29}$$

where $\epsilon > 0$ is some small value, and ω_g^{ϕ} is a unique frequency for each generator g and generator phase ϕ such that $\omega_i^{\phi} \neq \omega_i^{\psi} \neq \omega_j^{\phi} \; \forall \; \phi \neq \psi \in \Phi_i, \forall i \neq j \in \mathcal{G}$. Define $f_m^{(k)} = \sum_{\phi \in \Phi_m} \left(P_m^{sl,\phi}(\mathbf{s}_m^{(k)}, \boldsymbol{\ell}_m^{(k)}) - P_m^{sl,\bullet,\phi} \right)^2$ for each $m \in \mathcal{E}^{\mathrm{CC}}$ and let

$$\mathbf{g}^{(k)} = \begin{bmatrix} \mathbf{v}(\mathbf{x}^{(k)}, \boldsymbol{\ell}^{(k)}) - \overline{\mathbf{v}} \\ \underline{\mathbf{v}} - \mathbf{v}(\mathbf{x}^{(k)}, \boldsymbol{\ell}^{(k)}) \end{bmatrix}. \tag{4.30}$$

We introduce a vector ν of size $2N_m^{\phi}$ for each CC. Each element in ν is either one or zero. A value of one indicates the node where the associated voltage in $\mathbf{g}$ is measured is in that

CC, while a value of zero indicates the node belongs to a different CC. This vector can be constructed using the switch states and a simple connectivity test. Let $\rho, \delta > 0$ represent the small regularization parameters of the regularized Lagrangian function, and let $\alpha > 0$ be a constant step size. Then (4.25) can be solved using Algorithm 3, a modified version of the primal-dual algorithm presented in [110]. Figure 4.2 illustrates the incorporation of the MFRT-OPF with the RPOP.

Algorithm 3 : Model-Free Primal-Dual Algorithm

1: Initialize $\lambda_m^{(1)} = \mathbf{0} \in \mathbb{R}^{2N_m^{\phi} \times 1}$ for each CC m and at each time step k, perform the following steps:

2: **Forward Exploration:** Apply $\mathbf{s}_+^{(k)} := \mathbf{s}^{(k)} + \xi^{(k)}$ to the system, and collect measurement $\hat{\mathbf{y}}_+^{(k)}$ of output $\mathbf{y}^{(k)}(\mathbf{s}_+^{(k)})$.

3: **Backward Exploration:** Apply $\mathbf{s}_-^{(k)} := \mathbf{s}^{(k)} - \xi^{(k)}$ to the system, and collect measurement $\hat{\mathbf{y}}_-^{(k)}$ of output $\mathbf{y}^{(k)}(\mathbf{s}_-^{(k)})$.

4: **Approximate Gradient:** Compute the approximate gradient for the primal step

$$\begin{aligned}\hat{\nabla}\mathcal{L}_m^{(k)} :=& \nabla_{\mathbf{s}} \mathbf{f}_m^{(k)}(\mathbf{s}^{(k)}) + \frac{1}{2\epsilon}\xi^{(k)}\left[\mathbf{f}_m^{(k)}(\hat{\mathbf{y}}_+^{(k)}) - \mathbf{f}_m^{(k)}(\hat{\mathbf{y}}_-^{(k)})\right] \\ &+ \frac{1}{2\epsilon}\xi^{(k)}(\lambda_m^{(k)})^{\top}\left[\nu_m \odot \left(\mathbf{g}^{(k)}(\hat{\mathbf{y}}_+^{(k)}) - \mathbf{g}^{(k)}(\hat{\mathbf{y}}_-^{(k)})\right)\right]\end{aligned} \tag{4.31}$$

where subscript m denotes values corresponding to CC m, $\mathbf{f}_m^{(k)}(\hat{\mathbf{y}}^{(k)}) \in \mathbb{R}^{N^{\phi_m} \times 1}$ represents a vector where element j corresponds to $f_m^{(k)}$ evaluated at element j of $\hat{\mathbf{y}}^{(k)}$, and $\odot$ represents the Hadamard product.

5: **Approximate Primal Step:** Compute

$$\mathbf{s}^{(k+1)} = Proj_{\chi^{(k)}}\{(1 - \alpha\rho)\mathbf{s}^{(k)} - \alpha \sum_{m \in \mathcal{E}^{\mathrm{CC}}} \hat{\nabla}\mathcal{L}_m^{(k)}\} \tag{4.32}$$

where χ is a convex set representing operational constraints, and $Proj_{\chi}\{\mathbf{z}\} := \arg\min_{\mathbf{s} \in \chi} \|\mathbf{z} - \mathbf{s}\|$ denotes projection.

6: **Dual Step:** Compute

$$\lambda_m^{(k+1)} = Proj_{\mathcal{D}^{(k)}}\left\{(1 - \alpha\delta)\lambda_m^{(k)} - \alpha\left(\nu_m \odot \mathbf{g}^{(k)}\left(\frac{1}{2}(\hat{\mathbf{y}}_+^{(k)} + \hat{\mathbf{y}}_-^{(k)})\right)\right)\right\} \tag{4.33}$$

4.5 Case Study: SMART-DS

This section presents a case study on a realistic distribution network to demonstrate the effectiveness of both algorithms.

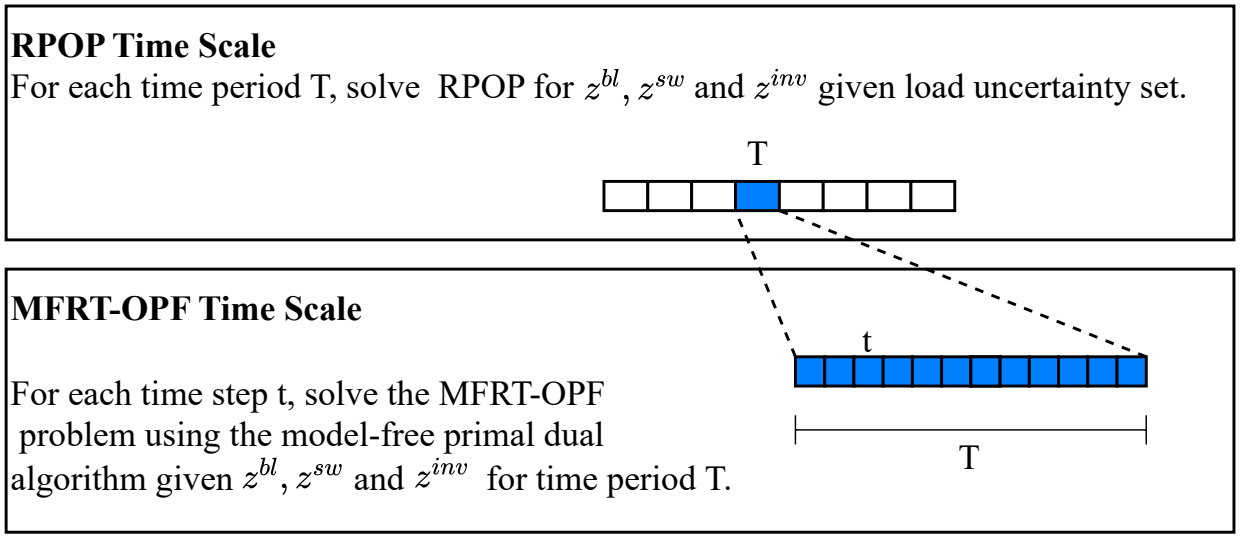


Figure 4.2: Diagram illustrating the integration of the faster time scale MFRT-OPF algorithm with the RPOP.

4.5.1 Network Details

The case study uses a synthetic distribution network based on part of the San Francisco Bay Area from the SMART-DS Synthetic Electrical Network Data OpenDSS models [111]. The network includes 714 multi-phase buses (1,565 total nodes), 652 lines, and 29 controllable switches, two of which are redundant lines added to create potential loops. With all controllable switches open, the network forms 28 blocks, ranging in size from a single single-phase bus to 69 buses spanning 1 to 3 phases. Figure 4.3 shows the block connections. In Fig. 4.3, blocks are grouped into clusters based on geographic spacing where the total magnitude of active power load is approximately balanced across clusters. When solving the RPOP, it is assumed that loads within each cluster vary together, as described in Section 4.3.1. For example, if a load in Block 6 is at its maximum, then all loads in Blocks 6, 13, and 27 are also at their maximum.

The network includes 123 DGs of varying sizes, all assumed to have power injection capabilities like solar photovoltaics. Five DGs are 3-phase, located in Blocks 6, 17, 21, 23, and 25, while the rest are single-phase. Blocks 1, 2, 3, 8, 13, 19, 20, 26, and 28 consist only of single-phase buses ($\Phi_l^{\max} = 1$), while all other blocks contain at least one 3-phase bus ($\Phi_l^{\max} = 3$).

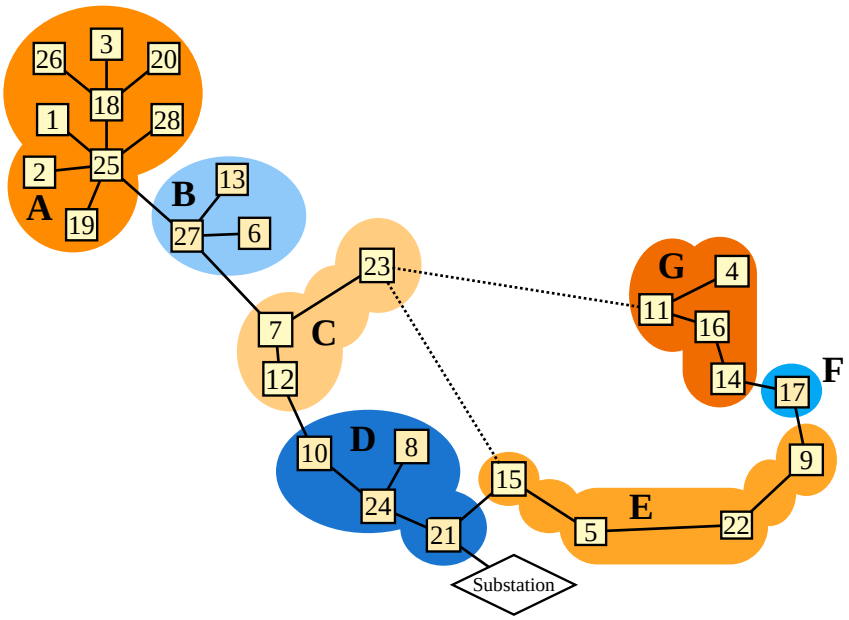


Figure 4.3: Illustration of the load blocks and the switches that connect them. Load clusters A-G are indicated by the blue and orange backgrounds grouping blocks together.

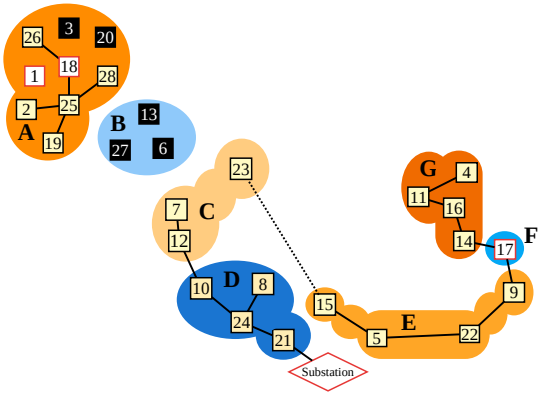
4.5.2 Implementation Details

Algorithms 2 and 3 were implemented using JuMP v1.23.2 in Julia language v1.10.5, with PowerModelsONM.jl v3.3.0 [75] as the foundational framework. Optimization tasks were solved using Gurobi 11.0.2 for mixed-integer convex problems or IPOPT 3.14.4 for nonlinear local optimization on a 1.3 GHz 4-core Intel Core i7 processor with 16GB memory.

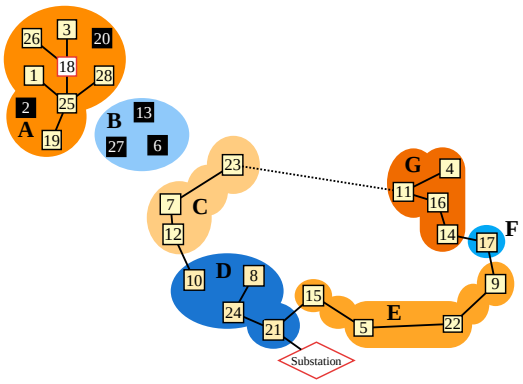
For the case study, $k^{\text{DG}} = 1$, meaning only one GFM-DG or voltage source can exist within an energized CC. In (4.19c)-(4.19m), $\overline{s}_d^{\phi}$, the maximum possible load scenario, is used as the load realization. While any load realization could be applied, using the maximum often led to faster convergence times.

4.5.3 RPOP Results

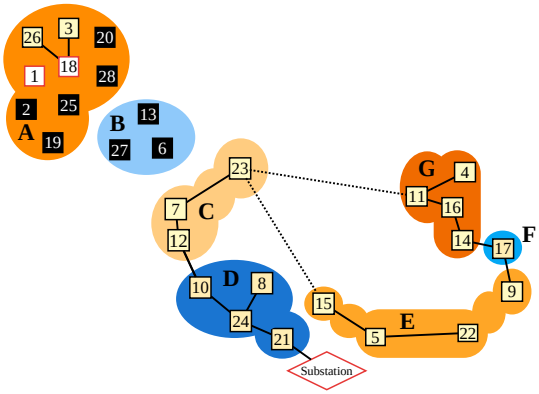
The results presented here are for a scenario in which a contingency in Block 27 requires it to be isolated and disabled. All loads are at their nominal values as published in the SMART-DS dataset. Figure 4.4a shows the optimal network partitioning without considering load uncertainty. For 5%, 10%, and 20% load uncertainty, the optimal partitioning under this contingency is shown in Figs. 4.4b, 4.4c, and 4.4d, respectively. As load uncertainty increases, islanded blocks must be connected to other CCs, and additional blocks may need



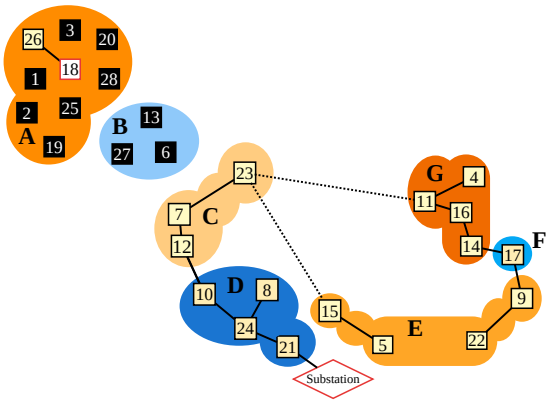
(a) 0% load uncertainty (nominal)



(b) 5% load uncertainty



(c) 10% load uncertainty



(d) 20% load uncertainty

Figure 4.4: Optimal partitioning of the SMART-DS network under varying uncertain loads. Black blocks indicate de-energized blocks, yellow blocks without outlines indicate the presence of a GFM-DG or substation voltage source, and black lines represent closed switches. Load clusters A-G are indicated by the blue and orange backgrounds grouping blocks together.

Table 4.1: RPOP run times and feasibility

Load Uncertainty (%)	Run Time (s)	Sampled Load Uncertainty (%)	Feasible Samples			
			Non-clustered		Clustered	
			Lin (%)	Full (%)	Lin (%)	Full (%)
0	57.98	5	100	100	99.8	100
		10	100	100	91.8	96.9
		20	90.8	90.8	63.8	66.2
5	60.19	5	100	100	100	100
10	21.59	10	100	100	100	100
20	99.65	20	100	100	100	100

Lin = LinDist3Flow, Full = AC-PF

to be disabled. Run times for the RPOP under each uncertainty level are provided in Table 4.1, showing significant reductions compared to [70]. This improvement stems from incorporating LinDist3Flow equations with a representative load scenario in the master problem and clustering load uncertainty, reducing the number of cuts (and iterations) needed to approximate the subproblem.

We empirically assess the robustness of the two-stage RPOP solutions, constrained by linearized LinDist3Flow, against both LinDist3Flow and non-convex AC Power Flow (AC-PF) constraints, while also analyzing the impact of ignoring uncertainty during partitioning. Table 4.1 shows the percentage of random load samples from $\mathcal{U}$ that were feasible under LinDist3Flow and AC-PF constraints for different partitioning solutions. These percentages were obtained by solving the RPOP for the assumed load uncertainty level in the first column, fixing the network configuration (switch, inverter, and load block states), and generating $1,000$ random load samples from $\mathcal{U}$ for the uncertainty level in the third column. Each load realization was tested for feasibility with LinDist3Flow and AC-PF equations. Both non-clustered and clustered load uncertainty were sampled, as shown in the $4-5$th and $6-7$th columns, respectively. Samples were generated by randomly selecting values from $[-x, x]$, where x represents the percent uncertainty (e.g., $x = 0.2$ for 20% uncertainty). For non-clustered samples, this was applied to each individual load as $s_d = s_d^0(1+x)$. For clustered samples, the same approach was used, but x was generated per cluster, assigning the same x to all loads in that cluster. Network configuration decisions always assume clustered load uncertainty. The AC-PF feasibility values in Table 4.1 represent an approximate lower bound, as the solver only detects local infeasibility and each sample

was tested with only a single warm-start value.

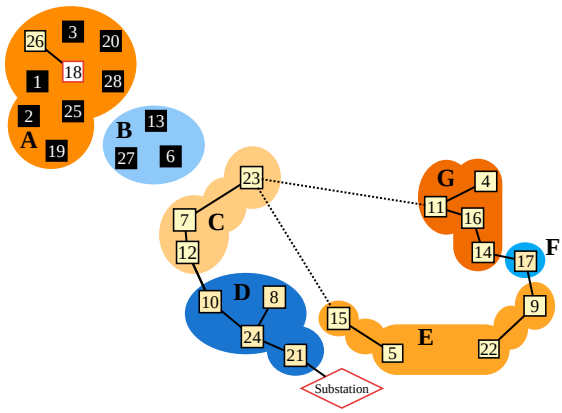
The top three rows in Table 4.1, corresponding to 0% load uncertainty during partitioning, show the optimal configuration obtained from the non-robust (deterministic) version of the partitioning problem. These results suggest that accounting for load uncertainty is critical when uncertainty is high but offers limited benefit below 10%, especially when loads tend to vary in the same direction, as captured by uncertainty clustering. The bottom three rows, corresponding to partitioning solutions based on the uncertainty levels in the first column, confirm the robustness of the RPOP solution. They also demonstrate that the LinDist3Flow formulation effectively approximates the nonconvex power flow equations.

4.5.4 Real-time Control Results

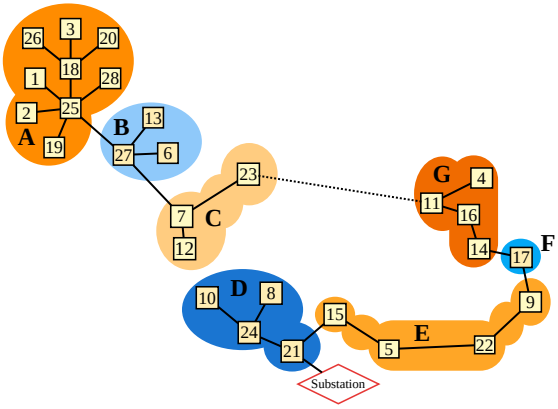
The results in this section are based on the MFRT-OPF algorithm from Section 4.4, using the optimal partition from the RPOP under 20% load uncertainty across three contingency scenarios. In the first 60 time steps ($T = 1$), Block 27 is de-energized due to an internal contingency (as in Section 4.5.3), and all loads start at their nominal values as published in the SMART-DS dataset. From time steps 61–120 ($T = 2$), there are no contingencies, and loads start at 90% of their nominal values. Finally, from time steps 121–180 ($T = 3$), the substation is disconnected, and loads start at 120% of their nominal values. The corresponding network partitions for these three scenarios are shown in Figs. 4.5a, 4.5b, and 4.5c.

The reference signal for each slack generator, $P_{sl}^{\bullet}$, is to maintain its initial set-point for each time period. When the network load changes, the slack generator in each CC responds immediately but returns to its original set-point as other controllable generators adjust to address slack injections or voltage violations.

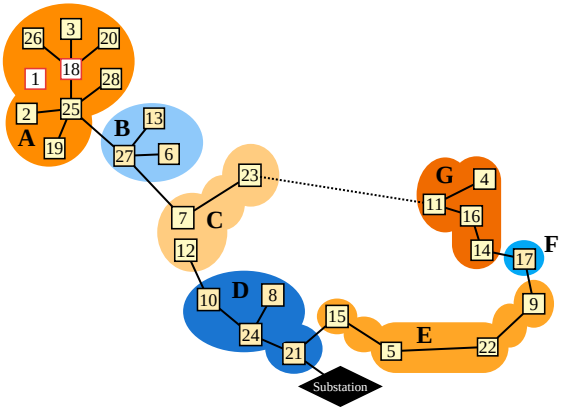
Figure 4.6a shows the total active power demand in each CC over time. CCs are named after the block hosting the voltage source (e.g., CC-18 refers to the CC containing Block 18 when it includes a GFM-DG, as in $T = 1$ and $T = 3$). At time step 7, all enabled loads increase by 15% from their nominal values. At time step 40, loads in CC-18 decrease by 3%, while those in CC-S remain unchanged. Additional step changes for enabled loads follow: a 2% decrease at time 80, then 6% and 5% increases at times 136 and 157, respectively. Figure 4.6b shows the slack generators' responses to load variations. Both generators compensate for the 15% increase at time 7, then return to their nominal set-points. However, when the loads in CC-18 are reduced at time step 40, only the slack generator in Block 18 responds. Similar response patterns are observed for later load steps under different configurations.



(a) Topology for t = 1 to t = 60

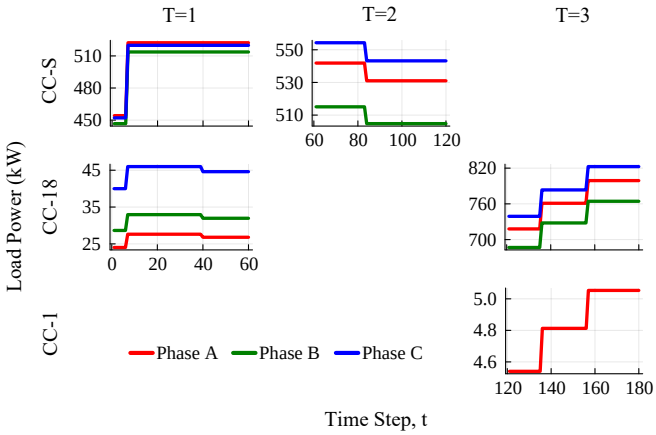


(b) Topology for t = 61 to t = 120

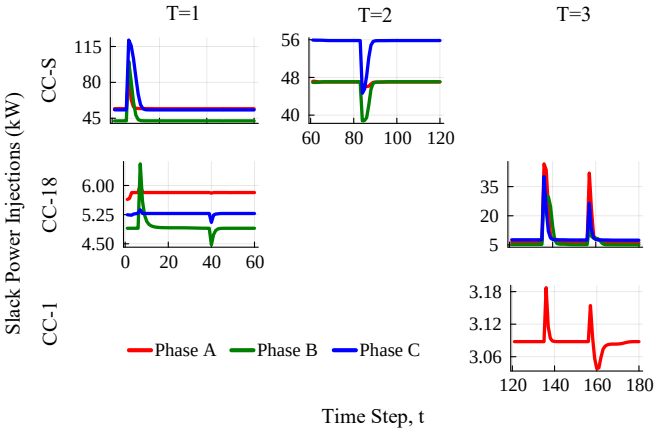


(c) Topology for t = 121 to t = 180

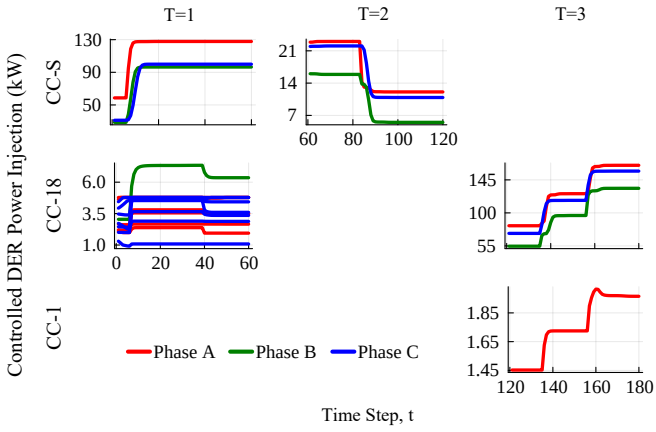
Figure 4.5: Optimal partitioning of the SMART-DS network assuming 20% load uncertainty. Black blocks indicate de-energized blocks, yellow blocks without outlines indicate the presence of a GFM-DG or substation voltage source, and black lines represent closed switches. Load clusters A-G are indicated by the blue and orange backgrounds grouping blocks together.



(a) Total load over time in each CC



(b) Slack generator power injections over time as network configuration changes



(c) Controlled DG active power injections over time as network configuration changes

Figure 4.6: MFRT-OPF results.

Figure 4.6c illustrates the controlled responses of the DGs to changes in slack generator power injections. The set of responsive DGs varies with the network configuration, as the number, size, and load of each CC influence the required capacity across phases. For instance, in $T = 1$, most DGs in CC-18, excluding the GFM-DG, are single-phase and relatively small. To manage potential 20% load changes, multiple controllable DGs are needed to restore the GFM-DG to its original set-point.

4.6 Chapter Conclusions

In this chapter, we presented an improved version of the RPOP algorithm presented in [70]. The main improvements were (1) the additional GFM-DG constraints ((4.16)-(4.18)), (2) the inclusion in the master problem of the LinDist3Flow equations for a single load scenario, and (3) the spatial clustering of load uncertainty. Improvement (1) enables the RPOP algorithm to more intelligently select which DG in each CC should be GFM, ensuring that each present phase is connected to a voltage source. Improvements (2) and (3) led to significant improvements in solve time and the ability to use the algorithm on a large, realistic distribution network.

In addition to the improvements presented for the RPOP, we also presented a MFRT-OPF algorithm. This algorithm enables quick responses to changes in load between reconfigurations. Additionally, the model-free method is well suited for the DNMG setting, where the network structure is frequently changing and may have unknown or uncertain parameters.

In future work, we aim to incorporate storage units, offering valuable flexibility, into both the RPOP and MFRT-OPF algorithms. For the RPOP, this will require carefully modeling the non-convex complementarity constraints to prevent simultaneous charging and discharging, while ensuring feasible operations for all uncertainty realizations. For both RPOP and MFRT-OPF, the time-coupled nature of state-of-charge will be a key consideration.

CHAPTER 5

Nodal Operating Envelopes vs. Network-wide Constraints: What is better for network-safe coordination of DERs? [1]

This chapter presents a comparative analysis of two distinct approaches that leverage a constraint set for network-safe coordination: nodal operating envelopes versus network-wide constraints on the action of a DER aggregator. We investigate their respective strengths and limitations by considering information and communication requirements and trade-offs in terms of flexibility and fairness. The availability of potentially private information to the aggregator or to the distribution system operator determines which of the approaches is feasible. Case study results suggest that if the goal is to maximize DER flexibility, a nodal constraint approach should be used. However, if the aggregator does not have information on how the constraints map to its DERs and/or does not have the ability to send out node-specific control inputs, the nodal constraint approach is not feasible, and a network-wide constraint approach is needed. The results also show that a network-wide constraint approach constraining the aggregator's control input provides a good balance between flexibility and fairness. The work in this chapter is based on our published work [112].

5.1 Chapter Introduction

As distributed energy resources (DERs), like roof-top solar, energy storage, and thermostatically controlled loads (TCLs) become more prevalent, interest in actively managing DERs within the distribution network to provide grid services and participate in electricity markets increases. Active participation of DERs can improve reliability, decrease operating costs, and lower the environmental impacts of power system operations [113]. Compared

[1] The work presented in this chapter reflects equal contributions of myself, Hannah Moring, and Dr. Sunho Jang, who also included this work in his dissertation.

to traditional transmission-level generation, most individual DERs are too small to provide significant benefit to the system. But coordinated together they can have a much bigger impact. However, if not properly managed, DERs and DER aggregations can lead to unsafe distribution network operation, for example, over- and under-voltages, over-current violations, and transformer overheating [17]. This has led to calls for increased coordination, for example, between transmission system operators (TSOs) and distribution system operators (DSOs) [114, 115].

DER aggregations can be operated by either the DSO or by a third-party aggregator. In the case that the DSO is coordinating DERs to provide grid services, it could explicitly manage network constraints through a centralized algorithm, e.g., the framework proposed in [116, 117]. However, in competitive electricity markets, DSOs usually cannot participate in wholesale electricity markets (and utility companies that have both distribution and generation businesses must follow strict rules ensuring key information that could affect market competitiveness, e.g., the DSO's network models, cannot flow from one business to the other). Therefore, in the United States, Australia, and parts of Europe it is likely that third-party aggregators will coordinate DERs to provide market-based services [118]. For security and privacy reasons, third-party aggregators cannot have access to detailed distribution network information needed to assess the network impacts of their control strategies. This means that some level of communication between the aggregator and DSO (and/or between the DSO and market operator) is required to ensure network safety. The structure that this communication should take is still an open question [13, 119]. Distribution network and operational data could be leveraged by the aggregator to improve the performance of its DER coordination strategy. However, the DSO is reluctant to share, or in many cases prohibited from sharing, its network details. This implies a trade-off between the performance of grid services through network-safe DER coordination and the DSO's need for privacy. Therefore, it is crucial to understand the data requirements of different approaches for ensuring network-safe DER coordination.

In this work, we consider two approaches for network-safe DER coordination: calculating net power injection limits at every node in the network or leveraging a network-wide constraint for an aggregator's control action. Net power injection limits, which are specified for each node in the network and updated as system conditions change, have gained attention in recent years, particularly in Australia where they are known as dynamic operating envelopes, or just operating envelopes [120, 121]. In other places, this is called dynamic hosting capacity [122]. These limits can be obtained by solving a modified version of the optimal power flow (OPF) problem, where the objective is to maximize a function of the net power injections at every node without violating any network constraints [120–123]. The form of

the objective, and whether or not equity/fairness is considered can significantly impact the bounds at each node [121,124]. In [120], a linearized, three-phase optimal power flow (OPF) problem incorporating tap-changing transformers is used to calculate power export and import limits at every node, and then the effectiveness of those limits are assessed using a probabilistic approach. A convex inner approximation of the feasible operating region of the nodal power injections is presented in [122], where an approximation of power flow's nonlinearities is used to ensure feasibility for the worst-case current. A market-based mechanism to allocate portions of operating envelopes to each aggregator is proposed in [125]. These approaches require the DSO, who has necessary network information, to calculate the nodal limits and share them with individual resources or aggregators, such that the limits can be incorporated into control strategies.

Alternatively, the DSO can impose network-level constraints on either the behavior of the resource aggregation (i.e., aggregate power) or the action taken by the aggregator to ensure safe network operation. Ref. [126] introduces a method to quantify the network-safe aggregate power flexibility at a substation in an unbalanced distribution network. A methodology for calculating network-safe aggregate power flexibility that takes into account temporal coupling constraints is proposed in [127]. Ref. [128, 129] introduced a control algorithm for aggregate TCLs that limit the number of TCLs turned ON or OFF, thereby constraining their collective power consumption and [130] proposed a method to compute network-safe bounds on the norm of power deviation across all nodes of the network. The approach in [131,132] employs Monte Carlo simulation and the bisection method to compute a constraint set on the aggregator's broadcast control input to DERs. Under any input in this constraint set, a chance constraint on network safety is guaranteed.

Given the existing literature on nodal and network-wide constraints, it is unclear whether one method or the other is generally better or if certain scenarios are more suited for each method. A deeper understanding of the strengths, weaknesses, and trade-offs of these two approaches is needed. Motivated by this, this chapter conducts a comprehensive comparison of the performance of nodal versus network-wide constraints for the safe operation of DERs in distribution networks.

We note that there are a variety of alternative approaches to DSO-aggregator coordination as well. For example, [133] proposes an iterative approach based on distribution locational marginal prices, wherein aggregator power schedules are updated until they converge. Ref. [134] proposes a market-based approach for a DSO to procure flexibility from aggregators. Both of these approaches assume the existence of DSO markets, which are unlikely to emerge in the United States and therefore not considered in this chapter. Another type of non-market based approach is DSO-centric as opposed to aggregator-centric [135] in

that, instead of the DSO sending constraints, the aggregator sends its desired actions/constraints and the DSO must determine if they are feasible. For example, [136] proposed a blocking strategy used by the DSO to block aggregator control inputs that would cause network constraint violations. Ref. [137] proposes an iterative approach wherein the aggregator shares its desired operating envelope with the DSO, who determines whether network violations would occur. Then, the DSO calculates a penalty for operating envelopes that would violate network constraints and the aggregator updates its operating envelopes to avoid the penalty. While these approaches are valid and interesting, we limit our analysis in this work to aggregator-centric approaches.

The contributions of this chapter are as follows. We provide a qualitative discussion of nodal versus network-wide constraints for maintaining safe operations in active distribution networks. We then provide an analytical analysis using case studies to compare the two approaches. Specifically, we begin by discussing the differences between these approaches in terms of the information required by each entity and further assumptions made in each approach. We then detail each approach mathematically. Subsequently, we present numerical simulations to evaluate the level of flexibility provided to the network by the resources under each approach. For the case study, we utilize methods based on [138] and [131], for nodal and network-wide constraints, respectively.

The structure of this chapter is as follows. Section 5.2 provides a qualitative discussion of the two approaches. In Sections 5.3 and 5.4, we will briefly describe the details of the methods used to determine the nodal and network-wide constraints used in the case studies. In Section 5.5, we will present three case studies to highlight how the two approaches compare in practice. The network details will be given in 5.5.1. The results are presented in 5.5.2. Lastly, Section 5.6 will present our conclusions.

5.2 Discussion of Approaches

In this section, we provide a general discussion on nodal constraints and network-wide constraints for maintaining safe operations within active distribution networks. We then describe the specific frameworks for DER coordination, the nodal constraint approach, and the network-wide constraint approach that are used to draw a more detailed comparison in the remainder of this chapter. We discuss the differences in the type of constraints computed, communication requirements, and assumptions for each of the approaches.

5.2.1 General Discussion

Generally, safe operation in power systems means that bus voltages and line currents are within some bounds defined by equipment limitations. Network safety could be ensured by directly constraining bus voltages and line currents or by indirectly constraining these quantities by constraining net power injections. Based on the information available to the DSO and aggregator, power injections can be managed either at a nodal or network-wide level. Bounding power injections at a nodal level means defining individual limits at every node in the network in such a way that if every node is operating within its limits, then the voltage at every bus and the current on every line in the network should be within safe limits. This approach can be used when DERs at every node are acting independently or DERs across the network are being coordinated.

Alternatively, constraints on network-wide power injections, or by proxy an aggregator's control input, could be used for network-safe DER coordination. This type of constraint is appropriate when the aggregator cannot directly control nodal power injections, i.e., the aggregator does not know which DERs are connected to which nodes. When the DSO computes this type of constraint, it must consider the worst-case permitted by the network-wide constraint, e.g., assuming the aggregator leverages the full capacity of the constraint using only the DERs connected at the farthest node from the substation. This makes the network-wide constraint approach more conservative than the nodal power constraint in general.

However, additional information can be used to reduce the conservativism of the network-wide approach, and equity considerations can make the nodal approach more conservative [134, 139]. It is unclear whether the nodal approach would always outperform the network-wide approach, or what trade-offs may exist. In order to shed some light on this, we consider the network-wide approach proposed in [131], which relies on an understanding of how an aggregator's control policy will directly impact DER behavior, and we consider a nodal approach with and without equity considerations [138, 140]. While the nodal constraint approach assumes that the aggregator utilizes DERs' private information (e.g., each DER's node in the network), the network-wide approach assumes that the DSO leverages the aggregator's private information (e.g., aggregator's DER control policy). Thus, comparing these two approaches is expected to reveal a trade-off between DER flexibility and the privacy of each entity.

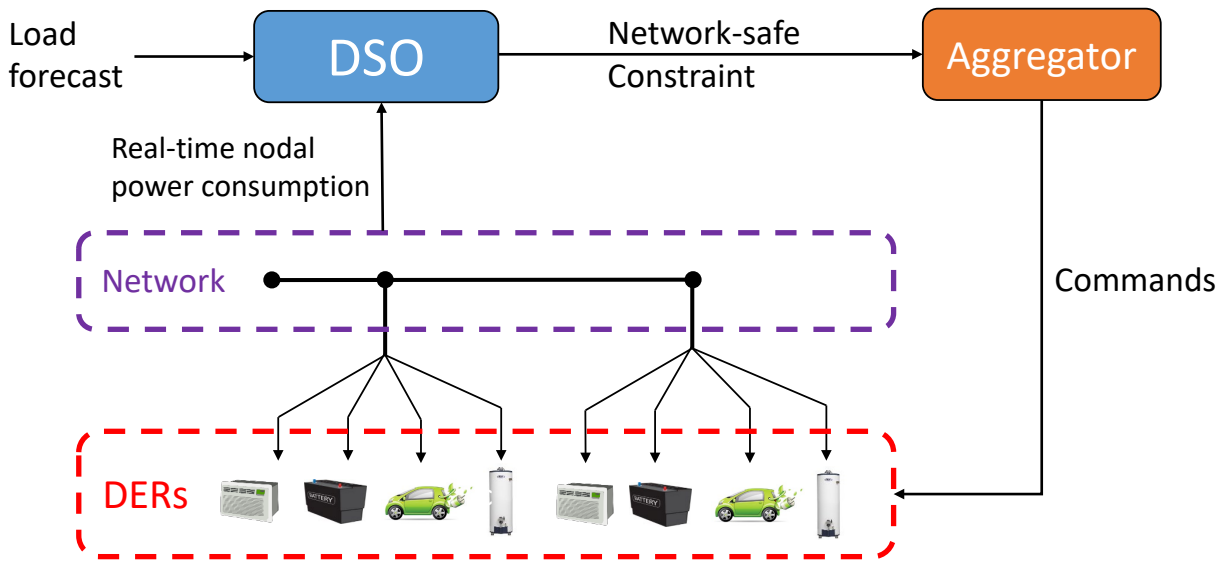


Figure 5.1: Communications between the DSO, aggregator, network, and DERs.

5.2.2 Considered Framework

We consider a framework in which there is a single aggregator coordinating all of the DERs in a distribution network. The DSO and the aggregator communicate with each other for network-safe DER coordination, as illustrated in Fig. 5.1. Here, the DSO sends some form of network-safety constraints to the aggregator and then the aggregator coordinates the DERs to provide grid-services while satisfying those constraints. This architecture is consistent with aggregator-centric network-safe DER coordination as defined in [135].

We assume that the DSO has detailed information needed for power flow calculations, such as the network topology, line parameters, and DER locations. Using this information, the DSO computes network-safe constraints; the type of the constraints depends on the approach used. Then, the DSO sends the obtained network-safe constraints to the aggregator. While the aggregator coordinates the participating DERs, it must satisfy the received constraints.

5.2.3 Discussion of Specific Approaches

Under the nodal constraint approach, $2|\mathcal{N}|$ constraints are constructed and updated as the network state changes, where $\mathcal{N}$ is the set of nodes in the network and $|\cdot|$ denotes cardinality. At each node i, the DSO computes the DER power consumption lower bound $\underline{p}_i$ and upper bound $\overline{p}_i$. Then, the nodal constraints ensuring network safety are given by

$$\underline{p}_i \leq \sum_{k \in \mathcal{I}_i} p_k^{\mathrm{D}} \leq \overline{p}_i, \quad \forall i \in \mathcal{N}. \tag{5.1}$$

Table 5.1: Comparing the Assumptions for Nodal vs. Network-wide Constraint Approaches

	Nodal Constraints on Power	Network-Wide Constraints on Control Input
DSO has detailed network info like topology, line impedances, and DER locations	yes	yes
DSO has accurate uncontrollable load forecasts	yes*	yes*
DSO knows DER capacities	yes*	yes
DSO knows how control input affects DER power consumption	no	yes
Aggregator knows which DERs correspond to each constraint	yes	no
All DERs in the network are operated by one aggregator	no	yes*
All DERs at a single node are operated by the aggregator	yes*	yes*
The relationship between voltage and power consumption of the DERs is monotonic	yes	yes

*Assumption can be relaxed but could result in more conservative operational constraints

where p_k^{D} is the power consumption of DER k, and $\mathcal{I}_i$ is the set of the indices of the DERs at node i. This approach assumes that the aggregator knows $\mathcal{I}_i$ for every node i and the corresponding $(\underline{p}_i, \overline{p}_i)$ in order to satisfy (5.1). Assuming the DSO knows $\mathcal{I}_i$ for every node i, it may be unwilling or unable to provide the aggregator with that information due to privacy concerns. Without that information, the aggregator cannot directly control the nodal DER power consumption $\sum_{k\in\mathcal{I}_i} p_k^{\mathrm{D}}$, leaving the nodal power bounds $(\underline{p}_i, \overline{p}_i)$ useless to the aggregator.

The network-wide constraint approach considers a scenario in which the aggregator cannot directly control the nodal DER power consumption. It is assumed that the aggregator sends a scalar input, denoted by u, to the DERs throughout the network. Upon receipt of the input u, the DERs adjust their power consumption in response to u. We assume that the power consumption of the DERs is monotonic with respect to u, enabling the aggregator to steer the direction of changes to the aggregate power consumption. Such a framework is considered in [131] wherein the input u signals the probability that TCLs should switch ON or OFF. As a result, the number of TCLs turned ON or OFF is likely proportional to the aggregator's input. The DSO leverages its knowledge of the impact of u on DERs' power consumption to compute network-safe input bounds $(\underline{u}, \overline{u})$ and sends them to the aggregator. After receiving these bounds, the aggregator must choose an input u such that $\underline{u} \leq u \leq \overline{u}$ holds, ensuring safe operation of the network.

The remaining assumptions made by the two approaches used in the case studies are summarized in Table 5.1. One of the common assumptions is that the DSO has accurate forecasts for uncontrollable loads, i.e., the loads in the network that are not controlled by the aggregator. We note that this condition can be relaxed to account for uncertainty as long as the DSO can quantify the load uncertainty. Under the nodal constraint approach, it is not strictly necessary that the DSO knows the DER capacities. However, if the DSO has this information it allows them to more effectively define the constraints at each node. The assumption that only a single aggregator is controlling every DER in the network or every DER at a node could also be relaxed. However, relaxing it would require the DSO to assign bounds to each aggregator either at a network-wide or nodal level. The impacts of this require investigation in future work. One common assumption between the approaches is that the relationship between voltage and power consumption is monotonic. Specifically, the nodal constraint method assumes that if $\underline{p}_i$ and $\overline{p}_i$ define the safe power bounds according to the modified OPF, any p_i such that $\underline{p}_i \leq p_i \leq \overline{p}_i$ will result in safe voltages. The network-wide constraint method assumes that as power consumption increases at every node, network voltages will decrease. We note that this may not always hold in practice due to the nonlinearities in the power flow equations.

5.3 Constructing Nodal Constraints

As noted in Section 5.1, nodal constraints on power consumption can be obtained by solving a modified version of the OPF problem. In this section, we will provide a brief overview of the optimization problem, based on the formulation in [138], that we used to determine the nodal constraints, or operating envelopes, in the case studies. There are two similar optimization problems, one to find the upper bound and one to find the lower bound. Both problems must be re-solved at each time step to determine the appropriate power bounds as the system loading changes.

Our modified OPF problem uses the branch flow formulation [141], where voltages and current angles are omitted by writing the power flow and voltage difference equations in terms of the squared magnitudes. We denote the set of lines in the network by $\mathcal{L}$. Let $z_{ij} = r_{ij} + jx_{ij}$ represent the impedance on the line connecting nodes i and j. The uncontrollable loads' active and reactive power consumption at node i are p_i^{l} and q_i^{l}, respectively. The per unit squared voltage limits at each bus are $\underline{v}, \overline{v}$.

First, we will present the formulation for finding the upper bounds on nodal power consumption. The decision variables are the upper bound on DER power consumption $\overline{p}_i$ at each node i, p_{ij} representing the active power flowing from node i to node j; q_{ij} representing

the reactive power flowing from node i to node j; the squared voltage magnitude $v_i = |V_i|^2$ at each node i; and $l_{ij} = |I_{ij}|^2$ representing the squared current magnitude on the line connecting node i and node j. The constraints of the problem are

$$\sum_{k\in\mathcal{I}_i} p_k^{\text{Dmin}} \leq \overline{p}_i \leq \sum_{k\in\mathcal{I}_i} p_k^{\text{Dmax}}, \quad \forall i \in \mathcal{N} \tag{5.2a}$$

$$\sum_{i:i\to j} (p_{ij} - r_{ij} l_{ij}) - \overline{p}_j - p_j^{\text{l}} = \sum_{k:j\to k} p_{jk}, \; \forall j \in \mathcal{N} \tag{5.2b}$$

$$\sum_{i:i\to j} (q_{ij} - x_{ij} l_{ij}) - q_j^{\text{l}} = \sum_{k:j\to k} q_{jk}, \; \forall j \in \mathcal{N} \tag{5.2c}$$

$$v_i = v_j + 2(r_{ij} p_{ij} + x_{ij} q_{ij}) - (r_{ij}^2 + x_{ij}^2) l_{ij}, \; \forall i \in \mathcal{N} \tag{5.2d}$$

$$p_{ij}^2 + q_{ij}^2 = l_{ij} v_i, \quad \forall ij \in \mathcal{L} \tag{5.2e}$$

$$\underline{v} \leq v_i \leq \overline{v}, \quad \forall i \in \mathcal{N} \tag{5.2f}$$

Constraint (5.2a) enforces that the upper limit on total power consumption at each node is not lower than the minimum total power consumption of the DERs at that node and not greater than the maximum total power consumption of the DERs at that node, where p_k^{Dmin} and p_k^{Dmax} are the minimum and maximum power consumption of DER k, respectively. Constraints (5.2b) and (5.2c) enforce active and reactive power balance, where notation $i : i \to j$ specifies that we should sum over all lines ij injecting power into j, and $k : j \to k$ specifies that we should sum over all lines jk consuming power from j. Constraint (5.2d) defines the voltage drop between bus i and the downstream bus j. Lastly, (5.2f) enforces the voltage limits at each bus.

This approach only ensures network safety when the nodal power is precisely $\overline{p}_i$, not necessarily for all nodal powers below this bound. However, the assumption of a monotonic relationship between the nodal powers and the network voltages lends that any $\sum_{k\in\mathcal{I}_i} p_k^{\text{D}} \leq \overline{p}_i$ is safe. When using a linear approximation of the power flow equations, as is commonly done when constructing operating envelopes [120,140], this monotonic relationship can be proven. In general, monotonicity does not hold for the nonlinear power flow equations, but it often holds empirically.

As noted in Section 5.1, the form of the objective function depends on the goals of the DSO. For example, the DSO may want to maximize the total allowable power consumption by DERs across the network, which could lead to significant discrepancies in limit sizes depending on the location of each node relative to the substation. This is because the power consumption of customers farther down the feeder will generally have a larger impact on voltages due to the radial structure of distribution networks and the nonlinearities of power

flow [140]. Considering fairness would lead to different nodal constraints. To provide a more thorough comparison between nodal constraints and network-wide constraints, we will solve the modified OPF problem using two different objective functions.

The first objective function used maximizes the sum of the real power limit across every node, given by

$$\max \sum_{i \in \mathcal{N}} \overline{p}_i. \tag{5.3}$$

For the remainder of this chapter, the nodal constraint approach using this objective function will be referred to as the MaxSum operating envelope approach or *MaxSum OE approach*. This will lead to the greatest total network flexibility, but will favor nodes closer to the substation. To obtain more evenly distributed limits, the second objective maximizes the smallest nodal limit of the network. This "fair" objective is written as

$$\max \ \gamma \tag{5.4}$$

and requires the additional constraint

$$\gamma \leq \overline{p}_i, \quad \forall i \in \mathcal{N}, \tag{5.5}$$

where (5.5) transforms a max min objective into a linear objective by defining the smallest operating envelope to be maximized. For the remainder of this chapter, the nodal constraint approach using this objective function will be referred to as the Fair operating envelope approach or *Fair OE approach*.

The formulation for finding the lower bounds on nodal power consumption is the same except that the objective is minimized and $\overline{p}_i$ is replaced by $\underline{p}_i$.

5.4 Constructing Network-wide Constraints

In this section, we provide an overview of a coordination framework between an aggregator and DSO utilizing a network-wide constraint, developed in [131]. We also explain how the approach can be compared to the nodal constraint approach.

These earlier studies [131] consider a stochastic setting, wherein the uncontrollable loads are uncertain and the aggregator's input u signals the probability of TCL mode switching. They impose the chance constraint to manage under-voltages

$$\Pr\left(\min_{i \in \mathcal{N}} v_i(u) \geq \underline{v}\right) \geq 1 - \epsilon, \tag{5.6}$$

where $v_i(u)$ represents the voltage at node i under the aggregator's input u, and $1-\epsilon$ denotes the desired probability of network safety. A similar constraint could be used to manage over-voltages. Ref. [131] shows that (5.6) holds at a specified confidence level provided that the empirical safe probability, derived from a sufficiently large number of uncertainty realizations, is adequately high.

It is assumed that the DSO has knowledge of how the input u influences the power consumption of the DERs, and hence can conduct simulations of the nodal voltages within the network under any input u. Specifically, the DSO computes the nodal voltages for a large number of realizations of the uncertainties, evaluates if the number of realizations and the resulting empirical safe probability are sufficiently large, and then verifies whether or not (5.6) is satisfied for an input u at the desired confidence level. Employing the bisection method [142], the DSO iteratively updates u and computes the nodal voltages to determine the maximum upper bound $\overline{u}$ such that (5.6) is satisfied for any input at or below $\overline{u}$. Subsequently, the DSO sends the upper bound $\overline{u}$ to the aggregator, who must select an input $u \leq \overline{u}$.

For comparison with the nodal constraint approach in Section 5.3, we adapt the network-wide constraint approach to suit a deterministic scenario. In this scenario, both the uncontrollable load p_j^{l} and the power consumption of the DERs under an input u are deterministic. Thus, the voltage at each node $v_i(u)$ is a deterministic function of the input u and the DSO can compute the voltages by solving the power flow equations.

The chance constraint (5.6) is replaced by the deterministic constraint

$$\underline{v} \leq v_i(u) \leq \overline{v} \qquad \forall i \in \mathcal{N}. \tag{5.7}$$

The aggregator's input u, which must be in the range $[0, 1]$, adjusts the power consumption of DER k according to

$$p_k^{\mathrm{D}}(u) = p_k^{\mathrm{Dmin}} + u\left(p_k^{\mathrm{Dmax}} - p_k^{\mathrm{Dmin}}\right), \tag{5.8}$$

which is a linear and increasing function of the aggregator's input u. Then, DER power consumption at node i under the input u is

$$p_i(u) = \sum_{k \in \mathcal{I}_i} p_k^{\mathrm{D}}(u) = \sum_{k \in \mathcal{I}_i} p_k^{\mathrm{Dmin}} + u \sum_{k \in \mathcal{I}_i} \left(p_k^{\mathrm{Dmax}} - p_k^{\mathrm{Dmin}}\right). \tag{5.9}$$

Thus, DER power consumption at each node $p_i(u)$ is linear and monotonic with respect to the input u.

While the approach proposed in [131] leveraged a large number of uncertainty realizations in the stochastic setting, we leverage an adaptation wherein we solve an optimization problem

to obtain $\overline{u}$ that satisfies (5.7) for the deterministic setting. Since the DSO knows that the power consumption of the DERs at node i changes according to (5.9), to find $\overline{u}$, the DSO solves the following optimization problem,

$$\max_{\overline{u}} \ \overline{u} \tag{5.10a}$$

$$\text{s.t. } (5.2\text{b}) - (5.2\text{f}) \text{ with } \overline{p}_j \text{ replaced by } p_j(\overline{u}). \tag{5.10b}$$

Here, instead of solving this problem using an optimization solver, we use the bisection method as in [131].

While this approach provides less degrees of freedom in DER control, it allows the DSO to understand the type of control the aggregator uses and also the correlation between the DERs' nodal power consumptions. Consequently, this knowledge could lead to less conservative operating envelopes at certain nodes when compared to the Fair OE approach, where no correlation is known/assumed. This consequence is illustrated in the case studies in Section 5.5.

For the remainder of this chapter, the network-wide constraint approach outlined in this section will be referred to as the Input Constraint approach or the *Input Const approach*.

5.5 Case Studies

5.5.1 Setup

The network used in the case studies presented below is the 56-bus balanced distribution network introduced in [1]. It is a modified version of the IEEE 123-bus network [143]. The network is illustrated in Fig. 5.2. For simplicity, we assume there are no capacitor banks in the network and no voltage regulators except for one at the substation. The voltage at the substation is set to 1.02 pu and the bounds on the voltages are $\underline{v} = 0.95$ pu and $\overline{v} = 1.05$ pu. Any operation leading to values below or above these limits is considered unsafe. Lastly, we assume that all DERs in the network are controllable TCLs, i.e., they are only capable of consuming power. We also assume that every node has at least one TCL connected to it and that all TCLs are coordinated by a single aggregator.

We consider three scenarios to illustrate the differences in operational outcomes when using nodal versus network-wide constraints for maintaining safe operations in active distribution networks. In Scenario 1, there is an even distribution of DERs across the nodes participating in the network and the uncontrollable load at every node is the same. Specifically, we assume that the same number of DERs, each with the same p_k^{Dmax}, are at each

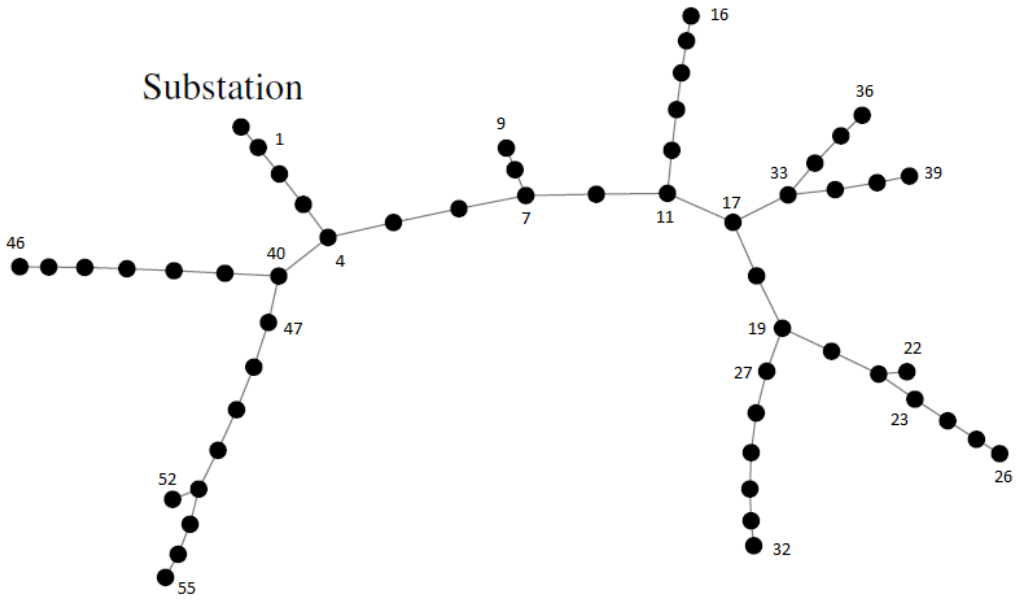


Figure 5.2: Single-line diagram of 56-bus network presented in [1].

node in the network. While this scenario is unlikely to occur in the real world, its simplicity will provide a clear picture of how each of the methods works in principle. In the second, more realistic scenario, the number of DERs at each node, the power capacity of each DER, and the uncontrollable loads at each node are varied. Scenario 3 is identical to Scenario 2 except that all DERs have been removed from nodes 20-32, the nodes farthest away from the substation. This scenario is used to highlight how the relative performance of the approaches changes with changes in the DER distribution.

For all three scenarios, nodal and network-wide constraints were constructed using the methods outlined in Sections 5.3 and 5.4 under various loading conditions. We define the nodal nominal real and reactive load $\tilde{p}_j$ and $\tilde{q}_j$ at each node j, and set the load p_j^{l} and q_j^{l} to be proportional to the nominal power as follows

$$p_j^{\mathrm{l}} = \alpha \tilde{p}_j, \quad q_j^{\mathrm{l}} = \alpha \tilde{q}_j. \tag{5.11}$$

where α is a coefficient used to adjust the level of the uncontrollable load. In the case studies, we vary the value of α to see how loading conditions impact the bounds constructed by each approach.

5.5.2 Results

In this section, we present the results of the case studies on the 56-bus network. The figures illustrate the bounds $\overline{p}_i$ for the nodal constraint approaches and $p_i(\overline{u})$ for the network-wide constraint approach using (5.9). Specifically, we interpret the maximum power consumption $p_i(\overline{u})$ as an effective nodal bound, though the aggregator does not use these bounds.

5.5.2.1 Scenario 1

First, we present the results of the evenly distributed DERs scenario, as it provides the simplest comparison. Fig. 5.3 shows that under this network setup, the allowable power consumption by the DERs at each node was the same between the Fair OE approach and the Input Constraint approach. The MaxSum OE approach led to most of the nodes having larger allowable power consumption levels but prevented some nodes farthest from the substation from having any allowable power consumption. In terms of the total allowable aggregate power consumption by DERs in the network, to be referred to as *flexibility* for the remainder of the chapter, the Fair OE and the Input Constraint approaches gave the same level of flexibility regardless of the uncontrollable loading conditions. The MaxSum OE approach provided about 20% more flexibility than the other two approaches under each of the tested loading conditions. However, this greater total flexibility came at the cost of no flexibility at certain nodes in the network.

5.5.2.2 Scenario 2

When the distribution of DERs and loads within the network is varied, a more realistic scenario, the comparison between nodal constraints and network-wide constraints is less cut and dried. Fig. 5.4 shows the real power limits at each node found by all three approaches under a single loading condition. As in the evenly distributed DER scenario, the MaxSum OE approach led to the largest power consumption limit at most nodes, but left the DERs at nodes 20-32 without the ability to consume power. The Fair OE approach led to the least variation in limit magnitudes out of the three approaches, but as shown in Fig. 5.5, it led to the lowest total power consumption across the network.

The Input Constraint approach did not achieve the same level of total network flexibility as the MaxSum OE approach (Fig. 5.5). However, it did result in similar limits at nodes away from the substation compared to the Fair OE approach while still enabling larger limits at other nodes. In that sense, the Input Constraint approach was able to achieve a good compromise between total flexibility and fairness. This ability stems from a single characteristic of the approach, which is that the power consumption of each DER is directly

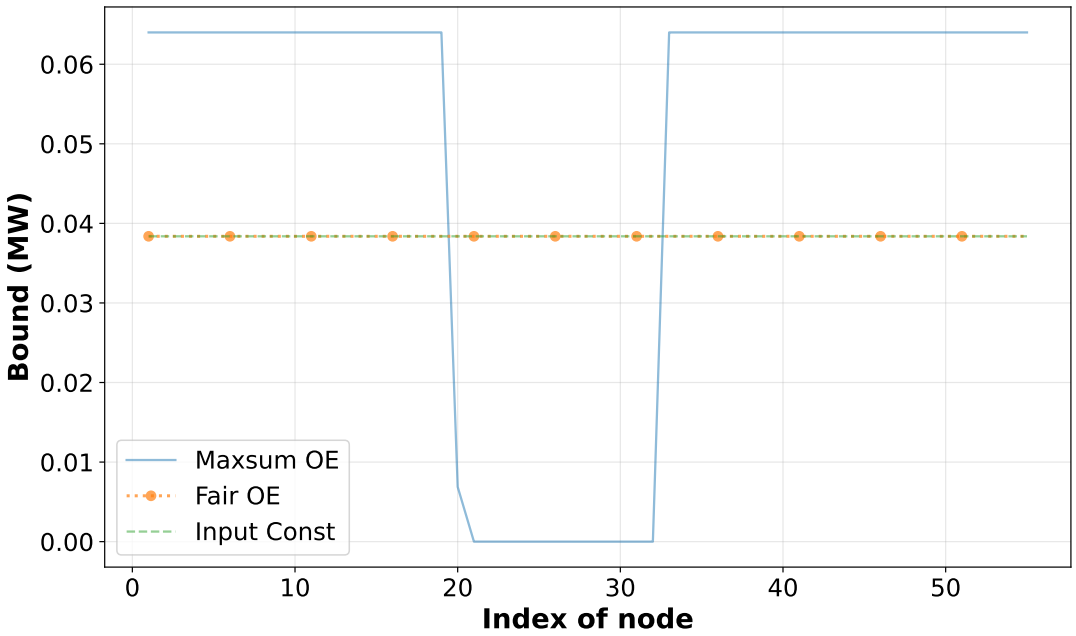


Figure 5.3: Comparison of the real power limits based on nodal constraints found using the Maxsum OE approach, the Fair OE approach, and the Input Const approach at each node for Scenario 1.

proportional to the aggregator's control input. Unlike in the nodal constraint approach, where no correlation is assumed between the nodal power consumptions, this additional knowledge of the behavior of power consumption across the nodes can be leveraged to increase the total flexibility. Fig. 5.5, which shows the total power consumption by the DERs across the network as the loads increase, suggests that the advantage of having that additional information decreases as the load in the network increases.

5.5.2.3 Scenario 3

Removing DERs from the nodes farthest from the substation (nodes 20-32), which are typically the most constrained, gives the Input Constraint method an advantage similar to the one that the MaxSum OE approach gains by disregarding fairness. However, as network loading increases, shown in Fig 5.6, the MaxSum OE approach is able to maintain a higher level of flexibility by removing flexibility at nodes 18 and 19.

5.5.2.4 Key Takeaways

The above results suggest that if the single goal of the DSO or the aggregator is to maximize the total flexibility of the DERs, the MaxSum OE approach is best. However, the MaxSum OE approach is only feasible if the aggregator has information on which operating envelopes

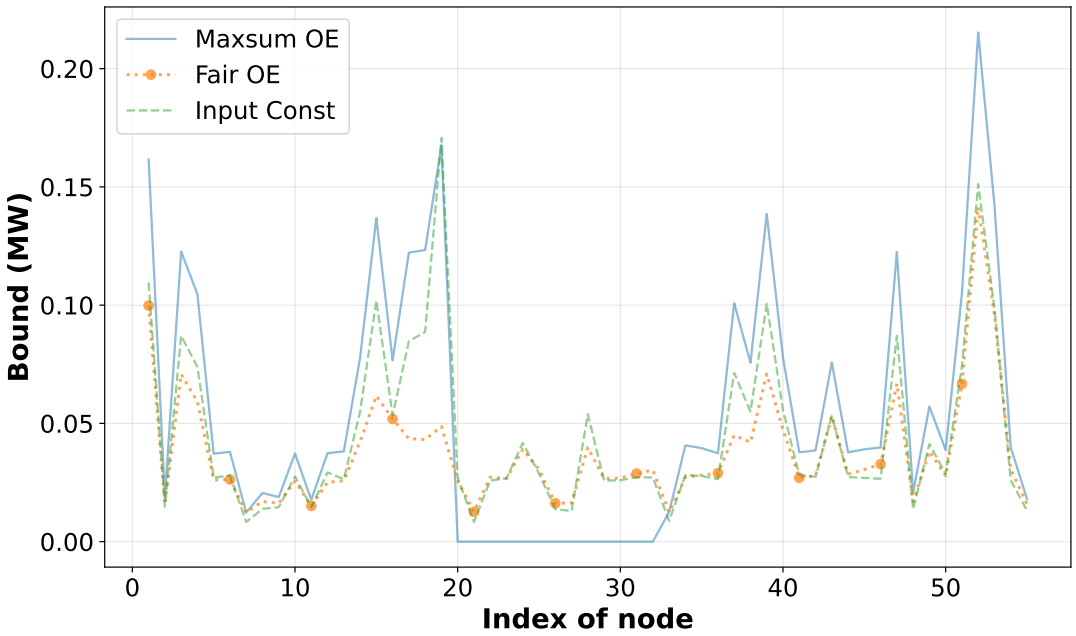


Figure 5.4: Comparison of the real power limits found using the Maxsum OE approach, the Fair OE approach, and the Input Const approach at each node.

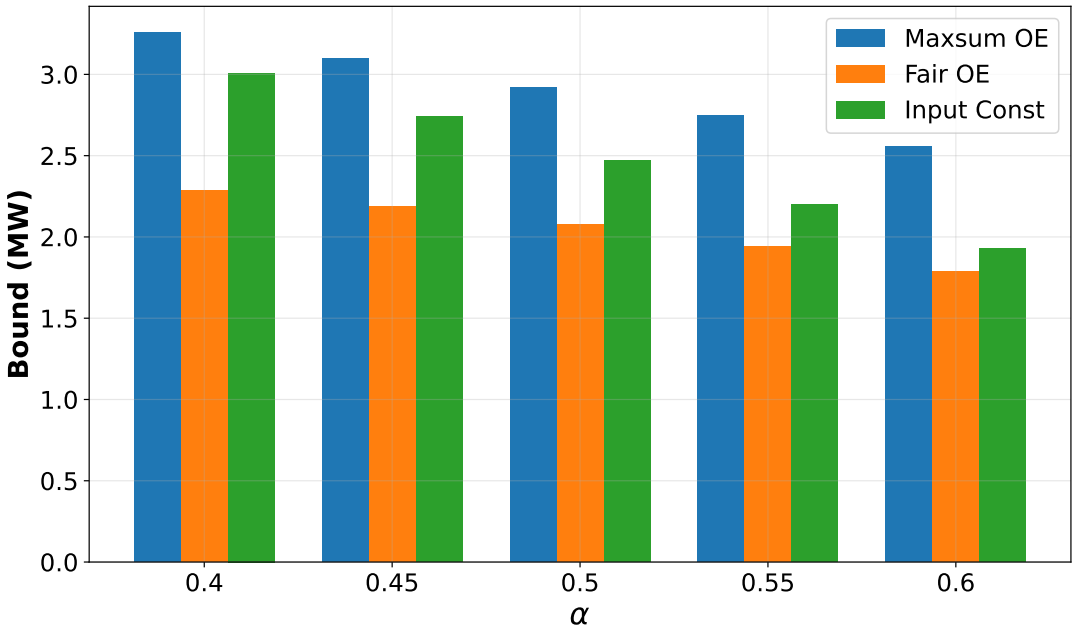


Figure 5.5: Comparison of the total network flexibility found using the Maxsum OE approach, the Fair OE approach, and the Input Const approach with respect to network loading increases for Scenario 2.

apply to which DERs and if it has the ability to send out node-specific control inputs. If fairness is a concern, the MaxSum OE approach is less appealing. In that case, the Fair OE

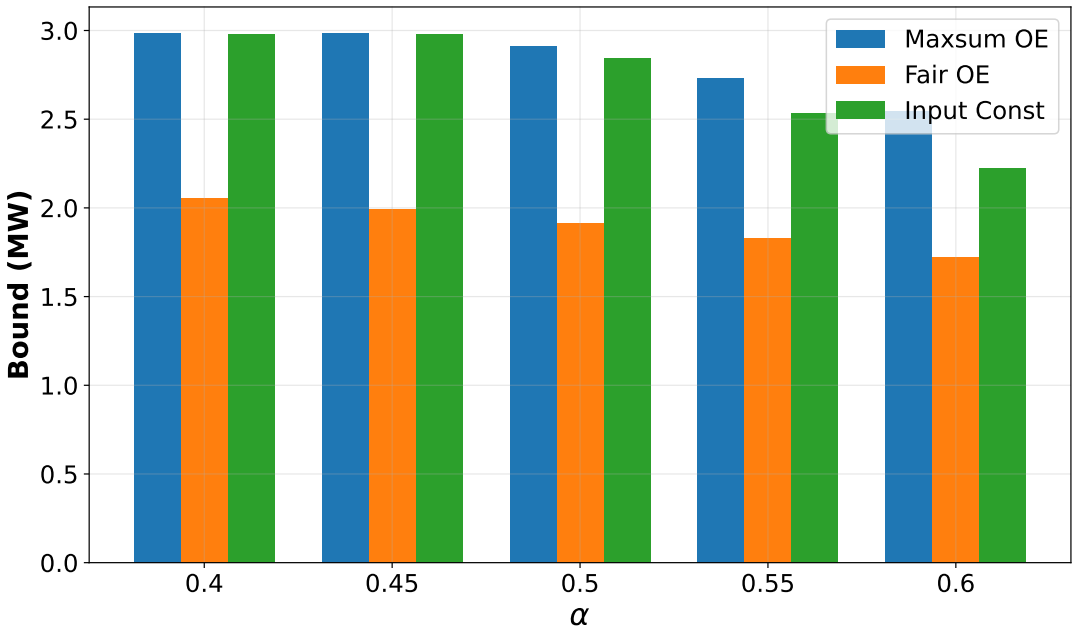


Figure 5.6: Comparison of the total network flexibility from nodal constraints (Fair OE and MaxSum OE) and network-wide constraints (Input Const) with respect to network loading increases for Scenario 3.

approach can be used if, again, the aggregator has information on which operating envelopes apply to which DERs and the ability to send out node-specific control inputs. Alternatively, if this information is not available to the aggregator, and if the aggregator provides the DSO with information needed to assess the impacts of the aggregator's control input on the DERs, the Input Constraint approach can provide a good trade-off between fairness and flexibility. This balance arises from knowing that the DERs will respond linearly to the control input. In the nodal constraint approach, no correlation is assumed between the nodal power consumptions.

5.6 Chapter Conclusions

In this chapter, we presented a qualitative and quantitative comparison of nodal and network-wide constraints for ensuring the safe operation of active distribution networks. Specifically, we discussed the assumptions and shared information requirements of each approach. Subsequently, we used three case studies to illustrate how the approaches compare under different conditions.

The discussion highlights that a key difference between the two approaches is who shares potentially private information with whom. The nodal constraint approach used in this

chapter requires that the DSO shares the set of DERs at each node with the aggregator, and the network-wide approach requires the aggregator to share information about its control policy with the DSO. The case studies highlight how considering equity increases the conservativism of the nodal constraint method, and how having additional information on how the DERs' actions are correlated can lead to the network-wide constraint method being less conservative when equity is considered. The key takeaway from this comparison is that each approach is only feasible under specific rules or market structures. One approach cannot simply be swapped for the other. Flexibility objectives should be considered when designing the market structures and regulations, as it is the structures and regulations that determine the possible approaches.

CHAPTER 6

Inexactness of Second Order Cone Relaxations for Calculating Operating Envelopes

In this chapter, we explore the efficacy of using a second-order cone relaxation of the power flow equations when calculating operating envelopes. Operating envelopes, which have gained significant attention and implementation in Australia, represent net export limits set by the system operator on every node in the distribution network that change as system conditions change. They are calculated using an optimal power flow problem, frequently using a linearization or relaxation of the nonlinear power flow equations. This chapter presents two case studies and some numerical analysis to explain why a second order cone relaxation of the power flow equations will lead to ineffective operating envelopes. A modification to the objective function which allows the second order cone relaxation to nearly recover the solution to the nonlinear formulation is also presented. The work in this chapter is based on our published work [138].

6.1 Chapter Introduction

The number of small-scale distributed energy resources (DERs), like roof-top solar photovoltaics (PV), batteries, and electric vehicles, connected to distribution networks has been growing rapidly in recent years [4]. DERs will play an important role in the decarbonization of the electricity sector, as they provide needed flexibility [144]. This flexibility refers to the capacity to adjust power production/demand to maintain safe network operations. Individually, DERs are too small to provide significant flexibility to the system, but aggregated together they can have a much bigger impact. Active participation by DERs and DER aggregations in the distribution network can lead to network violations like over- and under-voltages [17,126]. Numerous solutions have been proposed to maintain safe operations

in distribution networks under the presence of DERs and DER aggregations, including coordination strategies between aggregators and distribution system operators (DSOs) [136], constructing a constraint set on aggregator controls [132], constructing a convex inner approximation of the optimal power flow (OPF) to quantify feeder capacity [123], and constructing dynamic operating envelopes [120, 121, 124, 140].

Operating envelopes represent the import and/or export limits at each active node in the distribution network that would prevent unsafe operations [140]. An active node is defined as any node within the distribution network that has a controllable DER capable of exporting or importing power connected to it. An efficient way to do this is to solve a modified version of the OPF problem. The OPF problem is an optimization problem which was originally formulated to find the lowest cost generator dispatch that lies within network constraints [145]. Since its introduction, it has been generalized so that OPF can refer to any optimization problem subject to the power flow equations and other operational constraints [146]. The OPF problem is nonlinear and non-convex, making it difficult to solve and computationally intractable for large networks. The use of convex relaxations of the power flow equations can alleviate this issue. However, relaxations do not always give exact or feasible solutions [141]. Here we investigate how they work for operating envelope problems, which have been proposed to ensure safe operations of active distribution networks.

The objective of this chapter is to highlight issues that can arise when using a SOC relaxation of the power flow equations to calculate operating envelopes. A review of existing literature suggests that either a SOC relaxation or a linearized version of the power flow equations is typically utilized in the calculation of operating envelopes. For example, the current injection-based three-phase power flow equations are linearized about a predefined voltage point using a first-order Taylor series in [124, 139]. In [140], the three-phase branch flow power flow equations are linearized about an estimate of the real and reactive power flows. Both of these linearization techniques require an estimate or measurement of either voltage or power and may run into problems if the estimates are inaccurate or if there is a significant change in the system state. Alternatively, a second-order cone (SOC) relaxation of the power flow equations was used in [121]. A SOC relaxation provides computational tractability, but does not require estimates or measurements like linearization-based approaches. However, SOC relaxations do not always produce feasible solutions to the original nonlinear problem.

There are two main contributions of this chapter. The first is a discussion of the use of the SOC relaxation of the power flow equations to calculate operating envelopes. Specifically, this chapter outlines why the SOC relaxation of the power flow equations will not produce feasible solutions to the original nonlinear operating envelope problem and should not be used to calculate operating envelopes. Two case studies illustrate this and a discussion of

the numerical results is presented. The second contribution of the chapter is a modification to the objective function of the SOC formulation that results in a solution very close to the solution of the full nonlinear problem.

Section 6.2 presents the chapter's notation and OPF formulations for calculating operating envelopes. The modified objective function and discussion of its merits are given in Section 6.2.3. Section 6.3 presents two case studies to illustrate issues with using the SOC relaxation within the operating envelope problem. Conclusions are given in Section 6.4.

6.2 Problem Formulations

Consider a radial distribution network with a set of nodes $\mathcal{N}$ and a set of lines $\mathcal{L}$. For simplicity, we assume the network is balanced and therefore can be represented by its single-phase equivalent circuit. We will use the branch flow method for representing power flow [141], where the voltage and current angles of the system can be omitted by writing the power flow and voltage difference equations in terms of the voltage and current magnitudes squared. Let $z_{ij} = r_{ij} + jx_{ij}$ represent the impedance on the line connecting nodes i and j. The reactive power demand at node i is q_i^{d}. The complex power flow limit on the line connecting nodes i and j is $\overline{s}_{ij}$. The per unit squared voltage limits at each bus are $\underline{v}, \overline{v}$.

Equity or fairness is an important consideration when formulating an optimization problem to find operating envelopes [121, 124, 139, 140]. When a linear objective function is used to maximize the aggregated operating envelopes, nodes further down the feeder receive significantly smaller allocations [140]. This means that a customer with PV who is far from the feeder head will have less ability to sell their excess power production than would a customer who is close to the feeder head. Therefore, the operating envelope formulation in this chapter utilizes the objective function proposed in [121], which maximizes the smallest operating envelope to allocate operating envelopes fairly across active nodes. We also analyzed a version of the formulation presented in this chapter with the objective of maximizing the sum of the operating envelopes across the feeder. The results were similar in terms of inexactness and infeasibility of the solution with respect to the original nonlinear problem. Those results are not included for brevity.

6.2.1 AC-OPF Branch Flow Formulation

We first define the full nonlinear operating envelope problem, which leverages the AC power flow equations. This formulation is based on the formulation given in [121] but differs in that we do not explicitly define the operating envelopes as the difference between PV generation

and load at every node. Rather, we define the operating envelopes as the net export at every node. Additionally, we do not model an upper limit on the operating envelopes based on DER capacity.

Our decision variables are $\mathbf{p}^{\text{exp}}$, a vector with elements p_i^{exp} representing the operating envelope at each node i, i.e., the maximum net real power export at each node i; $\underline{p}^{\text{exp}}$, the smallest magnitude operating envelope in the network; $\mathbf{P}$, a matrix of active branch power flows with elements p_{ij} representing the active power flowing from node i to node j; $\mathbf{Q}$, a matrix of reactive branch power flows with elements q_{ij} representing the reactive power flowing from node i to node j; $\mathbf{v}$, a vector with elements representing the squared voltage magnitude $v_i = |V_i|^2$ at each node i; and $\mathbf{L}$, a matrix of squared current magnitudes with elements $l_{ij} = |I_{ij}|^2$ representing the squared current magnitude on the line connecting nodes i and j. Let $\mathbf{x}$ be a vector of stacked decision variables. We compute operating envelopes $\mathbf{p}^{\text{exp}}$ by solving,

$$\max_{\mathbf{x}} \ \underline{p}^{\text{exp}} \tag{6.1a}$$

$$\text{s.t. } \underline{p}^{\text{exp}} \leq p_i^{\text{exp}}, \quad \forall i \in \mathcal{N} \tag{6.1b}$$

$$\sum_{i:i\to j} (p_{ij} - r_{ij} l_{ij}) + p_j^{\text{exp}} = \sum_{k:j\to k} p_{jk}, \ \forall j \in \mathcal{N} \tag{6.1c}$$

$$\sum_{i:i\to j} (q_{ij} - x_{ij} l_{ij}) - q_j^{\text{d}} = \sum_{k:j\to k} q_{jk}, \ \forall j \in \mathcal{N} \tag{6.1d}$$

$$v_i = v_j + 2(r_{ij} p_{ij} + x_{ij} q_{ij}) - (r_{ij}^2 + x_{ij}^2) l_{ij}, \ \forall i \in \mathcal{N} \tag{6.1e}$$

$$p_{ij}^2 + q_{ij}^2 = l_{ij} v_i, \quad \forall ij \in \mathcal{L} \tag{6.1f}$$

$$p_{ij}^2 + q_{ij}^2 \leq \overline{s}_{ij}^2, \quad \forall ij \in \mathcal{L} \tag{6.1g}$$

$$\underline{v} \leq v_i \leq \overline{v}, \quad \forall i \in \mathcal{N} \tag{6.1h}$$

Constraint (6.1b) transforms a max min objective into a linear objective by defining the smallest operating envelope to be maximized. Constraints (6.1c) and (6.1d) enforce active and reactive power balance, where notation $i : i \to j$ specifies that we should sum over all lines ij injecting power into j, and $k : j \to k$ specifies that we should sum over all lines jk consuming power from j. Constraint (6.1e) defines the voltage drop between bus i and the downstream bus j. Constraint (6.1f) defines the squared complex power flowing from bus i to j and (6.1g) limits it. Finally, constraint (6.1h) enforces the voltage limits at each bus. This formulation assumes monotonicity, i.e., if p^{exp} defines a valid operating envelope, then any injection less than p^{exp} is feasible. We note that this may not always be true in practice since (6.1f) is non-convex.

With the exception of the objective and constraint (6.1b), problem (6.1) is a standard OPF formulation. Since (6.1f) is non-convex, the problem is difficult to solve and impractical to scale to large systems. For this reason, operating envelopes are generally calculated using a linearization or relaxation of the power flow equations [121, 124, 139, 140].

6.2.2 Second-Order Cone Relaxation

The SOC relaxation was first proposed for the branch flow model in [141]. The only difference from the full nonlinear formulation (6.1) is that constraint (6.1f) is replaced with the SOC constraint

$$\left\| \begin{matrix} 2p_{ij} \\ 2q_{ij} \\ l_{ij} - v_i \end{matrix} \right\|_2 \leq l_{ij} + v_i, \qquad \forall ij \in \mathcal{L}, \tag{6.2}$$

which is equivalent to $p_{ij}^2 + q_{ij}^2 \leq l_{ij} v_i$, a relaxation of (6.1f). Then, the SOC formulation is

$$\max \ \ \underline{p}^{\text{exp}} \tag{6.3a}$$

$$\text{s.t.} \ \ (6.1\text{b}) - (6.1\text{e}), (6.1\text{g}), (6.1\text{h}), (6.2). \tag{6.3b}$$

The solution given by this formulation is exact, i.e., it is the solution to the full nonlinear problem, if it is feasible in the full nonlinear problem, i.e., $p_{ij}^2 + q_{ij}^2 = l_{ij} v_i$ for every $ij \in \mathcal{L}$. For a solution of the SOC problem that is not exact, the difference between the left-hand and right-hand sides of this equation can be used to quantify the inexactness of the solution.

While this SOC relaxation has been successfully used for a variety of OPF problems, the SOC relaxation is problematic when used in operating envelope problems, as we will show in Section 6.3. We next give some intuition for why this is the case. In this SOC formulation, there is no direct calculation of squared current l_{ij}. Instead it is constrained by (6.1c)-(6.1e), (6.2), and indirectly by the remaining constraints. Some upper and lower bounds on the squared currents can be derived from these constraints. For example, (6.2) gives us a lower bound

$$l_{ij} \geq \frac{p_{ij}^2 + q_{ij}^2}{v_i}, \tag{6.4}$$

and (6.1e) together with (6.1h) give us an upper bound

$$l_{ij} \leq \frac{\underline{v} - v_j - 2(r_{ij} p_{ij} + x_{ij} q_{ij})}{(r_{ij}^2 + x_{ij}^2)}, \tag{6.5}$$

and a lower bound

$$l_{ij} \geq \frac{\overline{v} - v_j - 2(r_{ij}p_{ij} + x_{ij}q_{ij})}{(r_{ij}^2 + x_{ij}^2)}. \tag{6.6}$$

Further bounds can be derived from the other constraints. Within these bounds, the squared currents can take any value. However, only one of the possible values is a solution to the power flow equations for a given voltage, real power flow, and reactive power flow, i.e., the value that satisfies (6.1f). The SOC formulation will not find that solution because larger currents can result in calculated feasible voltages corresponding to larger operating envelopes. Specifically, the flexibility introduced by the SOC relaxation of the power flow equations allows for artificial increases in the squared current. A larger squared current in (6.1c) permits larger values of p^{exp} without significant changes to real power flow, and simultaneously, decreases the change in voltage between node j and node i in (6.1e). Hence, this flexibility will lead to operating envelopes that are too large to be effective.

Furthermore, the objective of maximizing the smallest operating envelope across the network does not meet the conditions needed to prove the exactness of a SOC relaxation of an OPF formulation utilizing the branch-flow model outlined in [141]. Namely, the cost function is not strictly decreasing in current or line losses.

6.2.3 Objective Function Modification

In this section, a possible method for improving the efficacy of operating envelopes calculated using SOC relaxations of the power flow equations is presented.

As mentioned in the previous section, the solution from the SOC formulation takes advantage of the flexibility in the squared current variables to permit larger operating envelopes, which fail to ensure safe operation of the actual (nonlinear) power network. A possible remedy for this is to penalize power losses in the objective, as they are a function of current squared. We believe that this makes the objective function strictly decreasing in both current and line losses, satisfying conditions in [141]. The simplest augmented objective function would be

$$\max_{\mathbf{x}} \ \underline{p}^{\text{exp}} - \sum_{ij \in \mathcal{L}} l_{ij} r_{ij}. \tag{6.7}$$

However, differences in magnitude between the two terms can lead to undesirable outcomes. Because the losses term is a sum over the entire network, it can have a greater magnitude than $\underline{p}^{\text{exp}}$. If so, the solution will prioritize loss minimization, and therefore power flowing through each branch, rather than maximizing operating envelopes.

In order to achieve a solution close to the full nonlinear operating envelope problem solution, we can add a weight to the losses term such that the augmented objective function

becomes

$$\max_{\mathbf{x}} \ \underline{p}^{\text{exp}} - \lambda \sum_{ij \in \mathcal{L}} l_{ij} r_{ij}, \tag{6.8}$$

where λ is a weighting parameter found heuristically.

The issue with this approach is that the solution to the full nonlinear operating envelope problem must be known in order to precisely tune the weighting parameter. However, it can be possible to approximately tune the parameter without prior knowledge of the full nonlinear solution using the inexactness as a guide, as we will show in Section 6.3. We note that the best choice of weighting parameter is dependent on the system loading conditions, meaning the parameter must be re-tuned as the system conditions change. This tuning process could be challenging in real time.

6.3 Case Study

6.3.1 Setup

In this section, two case studies will be used to highlight the implications of using the SOC relaxation of the operating envelope problem. The first case study will be on a simple 4-bus network, based on the MATPOWER "case4_dist" test case [2], where numerical results will provide clear insights on the impacts of using a SOC relaxation. Subsequently, a 56-bus network, which was modified from the IEEE 123-bus network and presented in [1], will be used to illustrate the extent of the problem in a larger, more realistic network. The 4-bus network is shown in Fig. 6.1(a) and the 56-bus network is shown in Fig. 6.1(b). Note that the substation is considered to be the last bus, or bus 4 in the 4-bus network and bus 56 in the 56-bus network. In both cases, bus 1 is the bus connected to the substation. In this study, we assume there are no capacitor banks in the network and we assume there are no voltage regulators except for one at the substation. The voltage at the substation is set to 1.0 p.u. For simplicity, we assume that there is a controllable DER at each bus. This means that power can be injected at every bus and therefore every bus needs an operating envelope. Voltages between 0.95 and 1.05 p.u. are considered safe. Any operation that leads to values below or above these limits will be considered unsafe.

To show how the SOC relaxation of the power flow equations impacts the calculation of operating envelopes, both the full nonlinear operating envelope formulation and the SOC formulation will be used to calculate operating envelopes for each node in the network. The solutions will be compared in terms of the magnitude of the obtained operating envelopes, and the exactness of the SOC relaxation will be discussed. To analyze the efficacy of the

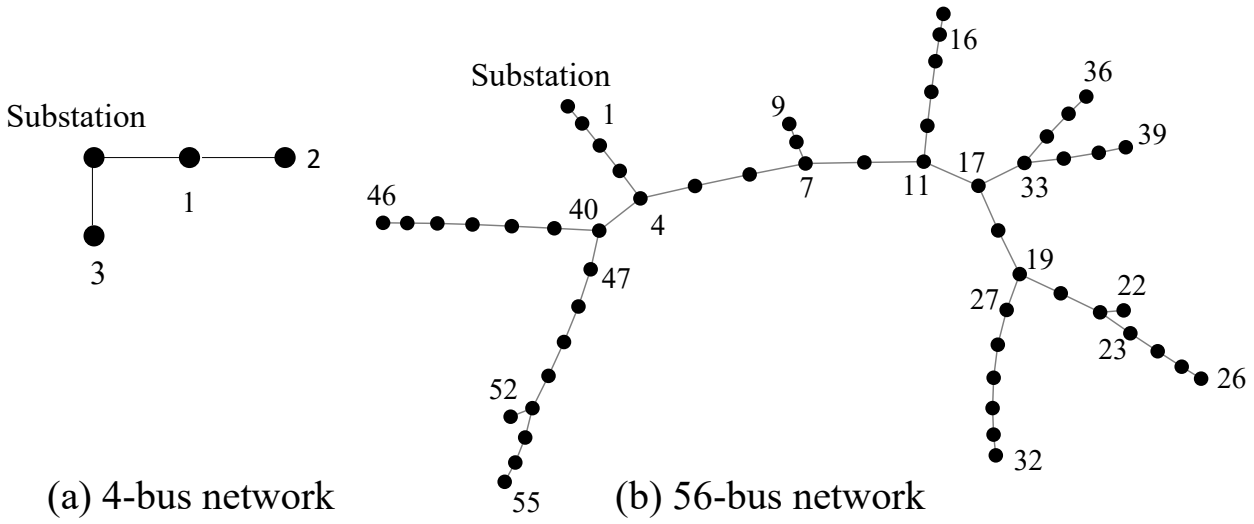


Figure 6.1: One line diagrams of the (a) 4-bus network, based on a network available from [2], and (b) 56-bus network presented in [1].

resulting operating envelopes, the nonlinear power flow equations will be solved for each formulation assuming the net power inject at each node is equal to the upper limit set by the operating envelopes.

Both the nonlinear and SOC problems were solved in Julia using the JuMP package [147]. The solvers used were IPOPT and CPLEX 12.7.1 for the nonlinear and SOC problems, respectively.

6.3.2 Results

This section presents the solutions to the full nonlinear operating envelope formulation and the SOC formulation of the operating envelope problem for both the 4-bus and the 56-bus networks. Also presented in this section are the results for solving the AC power flow equations given the net real power injections corresponding to the limits of the operating envelope at each bus in the network.

6.3.2.1 4-Bus Network

The results in this section are for the 4-bus network. Under the full nonlinear operating envelope formulation, the operating envelopes found are 6.84 MW at buses 1 and 2, and 15.89 MW at bus 3. When the active power injection into the network is equal to these operating envelopes, the voltages at each bus correspond to the values shown in Fig. 6.2. As can be seen in the figure, the voltage at every bus is within safe limits. Using the SOC

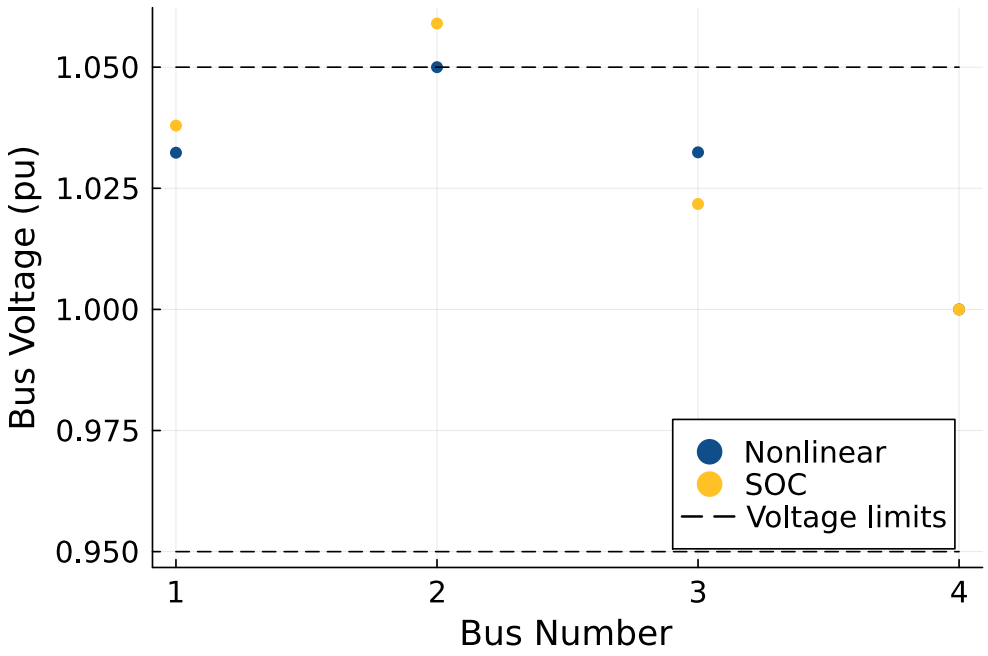


Figure 6.2: The voltage at each bus in the 4-bus network resulting from solving AC power flow with power exports at each node equal to the operating envelope limits calculated using the nonlinear and SOC operating envelope formulations.

relaxation, the operating envelopes found are 13.87 MW at buses 1 and 2, and 18.93 MW at bus 3. The bus voltages resulting from solving the AC power flow when power equal to the corresponding operating envelope is injected at buses 1-3 in the network are also shown in Fig. 6.2. The operating envelopes found by the SOC relaxation do not prevent unsafe operations.

Fig. 6.3 shows the difference between $l_{ij}v_i$ and $p_{ij}^2 + q_{ij}^2$ as a reflection of the inexactness of the relaxation. The values for each of the variables in the SOC formulation solution are given in Table 6.1 and the results from solving the AC power flow assuming the active power injections are equal to the operating envelopes found by the SOC relaxation are given in Table 6.2. The values for each of the variables in the full nonlinear operating envelope problem solution are given in Table 6.3. A comparison of the three values for each variable can be used to illustrate why the SOC relaxation is not exact, and why the resulting operating envelopes are ineffective. Compared to the SOC formulation, the AC power flow using the operating envelopes generated from the SOC formulation results in larger magnitude active power flows through the branches, smaller magnitude reactive power flows through the branches, smaller magnitudes current magnitudes through the branches, and higher voltage magnitudes at the buses. Using these trends and (6.1c), it can be deduced that the SOC relaxation is using the flexibility in the current values to increase the operating

Table 6.1: Numerical Results for SOC Formulation

Bus	1	2	3
Operating Envelope (MW)	13.87	13.87	13.93
Voltage (p.u.)	1.020	1.041	1.039
Line	4-1	1-2	4-3
Active Power (MW)	-22.36	-11.28	-15.07
Reactive Power (MW)	11.18	5.37	1.91
Current (kA)	30.57	29.37	16.90

Table 6.2: Numerical Results for AC Power Flow Using Operating Envelopes Generated from SOC Formulation

Bus	1	2	3
Operating Envelope (MW)	13.87	13.87	13.93
Voltage (p.u.)	1.056	1.091	1.040
Line	4-1	1-2	4-3
Active Power (MW)	-25.26	-13.39	-15.23
Reactive Power (MW)	5.37	1.17	1.61
Current (kA)	25.12	12.86	15.01

envelopes by increasing the line losses, which are represented by $r_{ij}l_{ij}$ in (6.1c). The total system losses in the solution to the full nonlinear operating envelope problem are 1.347 MW. In comparison, the total system losses in the solution to the SOC problem and the AC power flow using the resulting operating envelopes are 6.248 and 3.066 MW, respectively.

6.3.2.2 56-Bus Network

The following results are from the 56-bus network. Under the full nonlinear operating envelope formulation, the operating envelope at every node is equal to 209.3 kW. When every node is injecting 209.3 kW of power into the network, the voltages at each bus correspond

Table 6.3: Numerical Results for Full Nonlinear Operating Envelope Formulation

Bus	1	2	3
Operating Envelope (MW)	6.84	6.84	15.89
Voltage (p.u.)	1.032	1.050	1.040
Line	4-1	1-2	4-3
Active Power (MW)	-13.05	-6.72	-15.19
Reactive Power (MW)	1.69	0.46	1.60
Current (kA)	13.15	6.52	15.28

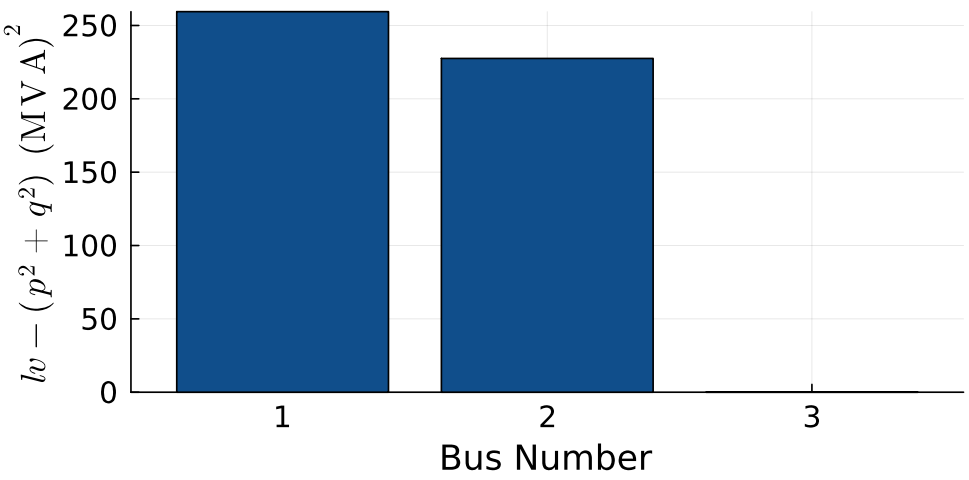


Figure 6.3: The inexactness of the SOC relaxation of the power flow equations for the 4-bus network.

to the values shown in Fig. 6.4. As can be seen in the figure, the voltage at every bus is within safe limits. A few of the buses far away from the substation are at the upper voltage limit, but this is to be expected at the edge of safe operation.

When the SOC relaxation of the power flow equations is used with the same objective function, the solution found gives an operating envelope at every node equal to 601.3 kW. This value is significantly larger than the value given by the full nonlinear operating envelope formulation. The bus voltages resulting from solving the AC power flow when power equal to the corresponding operating envelope is injected at each bus in the network are also shown in Fig. 6.4. It is clear from the figure that these operating envelopes do not prevent unsafe operation. Using the limits calculated from the SOC relaxation would likely lead to extremely high over-voltages.

These unsafe voltages calculated according to the nonlinear power flow equations do not match the voltages given as part of the solution to the SOC operating envelope problem. The difference between the voltages calculated from the SOC formulation and from the AC power flow equations arises from the dependence on current. Fig. 6.5 shows the difference between $l_{ij}v_i$ and $p_{ij}^2 + q_{ij}^2$ for each bus in the network. If the SOC relaxation were exact and the power flow equations were satisfied, the difference at each bus would be zero. As can be seen in the figure, that is not the case. Given that the calculated voltages must be between 0.95 and 1.05 p.u. to be a feasible solution to (6.3), the very large differences must arise from large current values. These large currents would lead to large real power losses. The total system losses in the solution to the full nonlinear operating envelope problem and in the solution to the SOC problem are 0.839 and 12.639 MW, respectively.

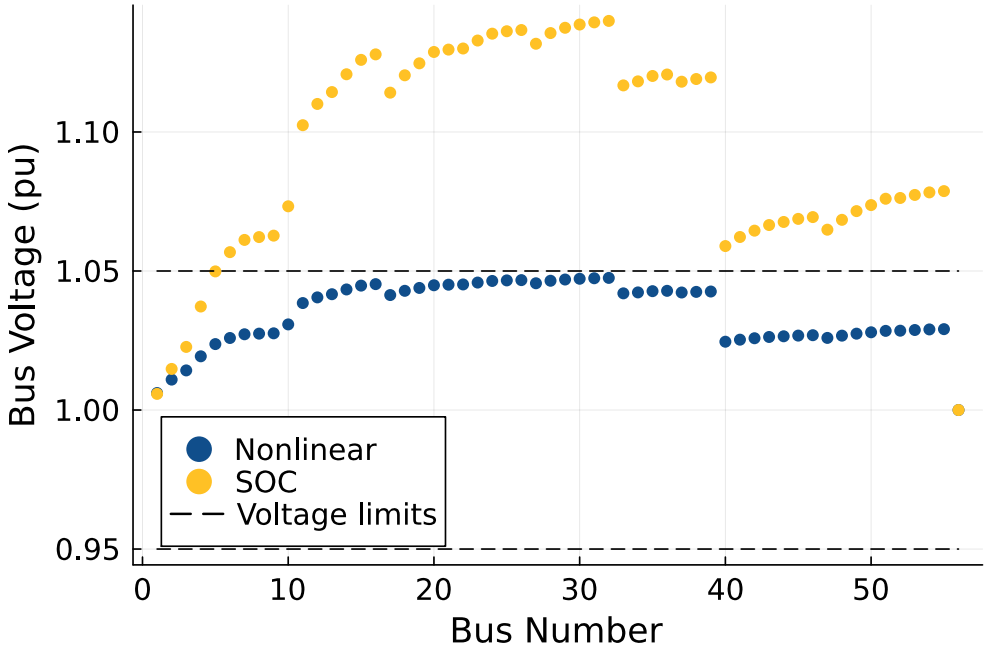


Figure 6.4: The voltage at each bus in the 56-bus network resulting from solving AC power flow with power exports at each node equal to the operating envelope limits calculated using the nonlinear and SOC operating envelope formulations.

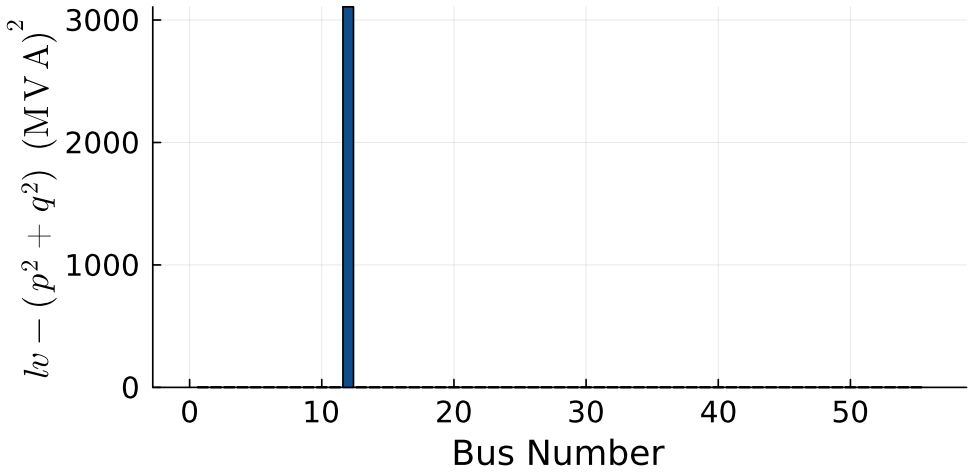


Figure 6.5: The inexactness of the SOC relaxation of the power flow equations for the 56-bus network.

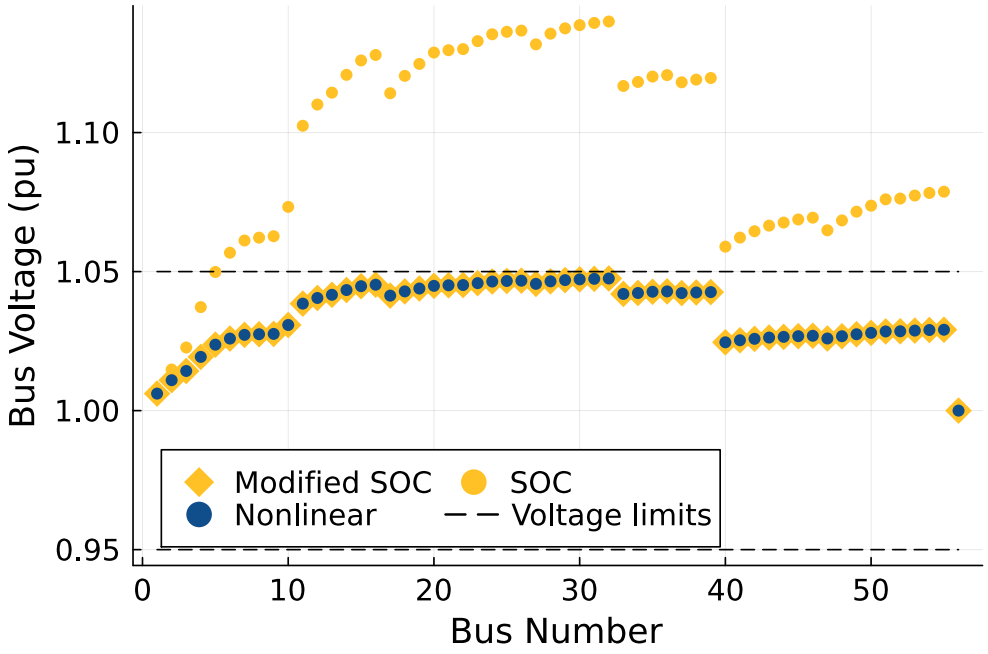


Figure 6.6: The voltage at each bus in the 56-bus network resulting from solving AC power flow with power exports at each node equal to the operating envelope limits calculated using the nonlinear, original SOC, and modified SOC operating envelope formulations.

If the objective function for the SOC formulation is modified to take the form of (6.8) with $\lambda = 0.11$, the resulting operating envelopes have maximum export limits of 209.3 kW at each bus, nearly matching the nonlinear solution. Fig. 6.6 shows the bus voltages resulting from solving the AC power flow when power equal to the corresponding operating envelope generated with the modified SOC formulation is injected at each bus in the network. Also, Fig. 6.7 shows the inexactness of the modified SOC formulation; it is very small compared to that of Fig. 6.5. Fig. 6.8 shows the sum of the inexactness as the weighting parameter is increased. It also shows the resulting operating envelope for each bus (i.e., all buses have the same operating envelope). In this case, to achieve low inexactness with relatively large operating envelopes, one should choose λ between 0.1 and 0.13. Choosing a value of λ higher will lead to overly conservative operating envelopes, but choosing a smaller λ will lead to unsafe operating envelopes.

6.4 Chapter Conclusions

This chapter presented two case studies to illustrate the issues that can arise when a SOC relaxation of the power flow equations is used to compute operating envelopes. Accompanying

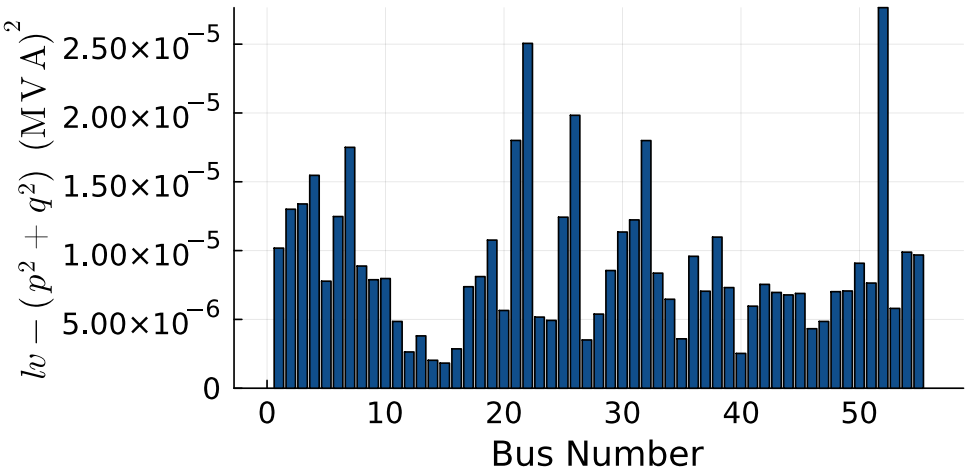


Figure 6.7: The inexactness of the modified SOC relaxation of the power flow equations for the 56-bus network. Note the different y-axis scale from Fig. 6.5.

the case studies is a numerical explanation as to why the SOC relaxation leads to ineffective operating envelopes. In brief, the SOC relaxation introduces flexibility in what values the branch currents can take. This flexibility allows for larger operating envelopes with calculated voltages within the limits. However, this flexibility does not exist in real power flow, which is governed by the nonlinear power flow equations, and so the large operating envelopes result in unsafe voltages in reality.

A potential fix to the issues discussed was also presented. By modifying the objective function to also minimize a weighted sum of the system losses, the true optimal solution can nearly be recovered. The flaw in this method is that knowing how to tune the weighting parameter relies on knowing the solution to the nonlinear problem.

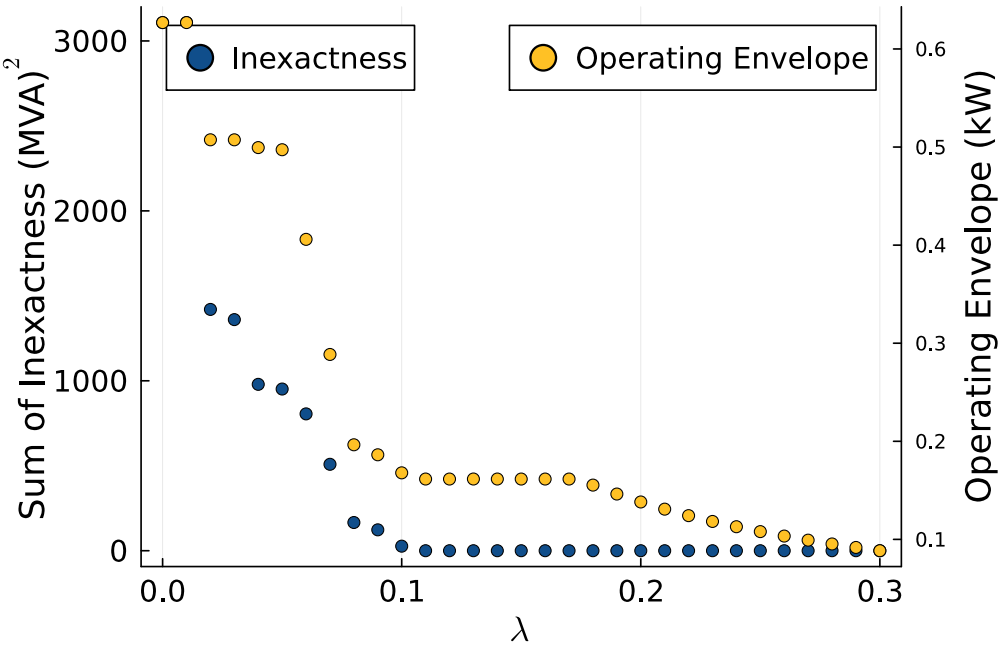


Figure 6.8: The sum of the inexactness, i.e., $lv - (p^2 + q^2)$, at every bus, and the resulting operating envelope for each bus as the weighting parameter λ is increased.

CHAPTER 7

Proof of the Inexactness of Second-Order Cone Relaxations for Operating Envelopes

In this chapter, we analyze the impacts of using convex relaxations, specifically a second-order cone relaxation, for determining operating envelopes for network-safe operation of DERs. Building on the work in the previous chapter, we illustrate the inadequacy of operating envelopes calculated using a second-order cone formulation for ensuring network safety. Then we discuss the complexity in the relationship between the relaxation, the nonlinear formulation, and the network parameters. For the case of purely resistive, radial networks and the case of purely reactive, radial networks, we prove that the second-order cone relaxation is inexact and exact, respectively. This work illustrates that while using a second-order cone relaxation to determine operating envelopes will not always result in overly large bounds, it often will and with potentially damaging consequences.

7.1 Chapter Introduction

Proliferation of small-scale distributed energy resources (DERs), such as roof-top solar photovoltaics (PV), batteries, and controllable loads, within distribution networks has become a key focus of power systems research [4, 148, 149]. Power injections or large load changes caused by DERs can lead to operational violations like over- and under-voltages, harmonics, frequency distortions, faults, and protection problems [17, 126, 150]. A wide variety of solutions have been proposed to maintain safe operations in distribution networks containing active DERs and DER aggregations, including coordination strategies between aggregators and distribution network operators [136], constructing a constraint set on aggregator controls [132], and constructing a set of nodal power injection limits, also known as operating envelopes or dynamic hosting capacity [120, 123, 124, 140, 151].

Dynamic operating envelopes, or simply operating envelopes, represent time-varying limits on power imports and/or exports at each active bus in the distribution network [140]. An

active bus is defined as any bus with a connected DER capable of generating or consuming power. To calculate operating envelopes, it is common to solve a modified version of the optimal power flow (OPF) problem. Originally formulated to find the lowest-cost generator dispatch which satisfies network constraints [145, 152], the OPF problem can refer to any optimization problem subject to the power flow equations and other operational constraints [146]. The nonlinear AC power flow equations make the OPF problem non-convex, i.e., a solution is not guaranteed to be globally optimal and can be computationally challenging for large networks. The use of convex relaxations or approximations of the power flow equations can help alleviate these issues. However, relaxations do not always give exact or feasible solutions [153].

There is extensive literature on relaxations, including second-order cone (SOC) relaxations, for the OPF problem [141, 154–159]. Existing work focuses on OPF problems with objectives such as minimizing generation costs or minimizing losses. In contrast, the operating envelope OPF problem aims to maximize the region of feasible power injections. To the best of our knowledge, there has been no prior work exploring the exactness of a SOC relaxation for a problem of this type, aside from our prior conference paper [138], which this work significantly extends, and the illustrations of SOC solutions that cannot be physically realized in [123, 160]. More discussion of existing literature on SOC relaxations and its relevance for the operating envelope problem is provided in Section 7.3.

The contribution of this chapter is an exploration of conditions for which the SOC relaxation is and is not exact for the operating envelope problem. As described above, existing studies have already shown, empirically, that the SOC relaxation is (usually) not exact for the operating envelope problem. In our prior work [138], we posited that the flexibility introduced by the SOC relaxation allows for artificial increases in the squared current. Larger squared current values create larger power losses which in turn permit artificially large operating envelope upper limits. Based on this idea, we proposed a modification to the objective function of the SOC formulation (specifically, we penalize power losses) to achieve exactness [138]. Here, we use a case study to illustrate that while this modification may lead to an exact SOC relaxation (for the penalized problem) or at least an AC power flow-feasible solution, it is not guaranteed to return the optimal solution to the original problem. Then, we analyze the unmodified SOC formulation and we show that, surprisingly, there exist conditions under which the SOC relaxation is exact for the operating envelope problem. We illustrate analytically that identifying conditions under which the relaxation is guaranteed to be exact or guaranteed to be inexact is not simple. Finally, we prove that the SOC relaxation of the operating envelope problem will not be exact for purely resistive, radial networks if at least one bus in the network is below its upper voltage limit at optimality of

the nonlinear formulation. We also prove that the SOC relaxation is exact for the operating envelope problem for purely reactive, radial networks. For realistic systems, with both positive resistance and positive reactance, we are unable to establish simple conditions on SOC relaxation exactness. For this reason, we recommend not using the SOC relaxation when computing operating envelopes.

Section 7.2 presents the chapter's notation and OPF formulations for calculating operating envelopes. The modified objective function and a case study illustrating the impacts of the SOC relaxation are discussed in Section 7.3. Section 7.4 investigates conditions for which the SOC relaxation is and is not exact for the operating envelope problem. Conclusions are given in Section 7.5.

7.2 Problem Formulations

Many different approaches and optimization formulations have been used to compute operating envelopes. One option for including the power flow equations is to use the nonlinear AC power flow; however, this requires the assumption that any power injection between the operating envelope lower (import) and upper (export) limit will not lead to operational constraint violations. Another interpretation of this assumption is that the relationship between voltage and power injections is monotonic. The authors of [161] show that this assumption does not always hold, particularly in unbalanced networks. A second option is to use a power flow linearization to improve computation time and avoid convergence issues [161], e.g., as in [120,124,162,163]. However, linearizations come with a loss of model accuracy and (most) come with no guarantees on performance/accuracy or solution feasibility. A third option is to use a convex relaxation, such as an SOC [121] or quadratically constrained [164] formulation, which can also improve computation time and convergence versus solving a nonlinear AC power flow problem. Convex relaxations have advantages over linearizations in that relaxation solutions that are feasible for the AC power flow constraints are necessarily optimal in the AC power flow problem. However, since the feasible region may extend beyond the AC power flow feasible region, relaxations may admit solutions that violate network constraints. Therefore, the remainder of this chapter will argue why relaxations should *not* be used to compute operating envelopes. A fourth option is to use a convex restriction or inner approximation of the feasible region [123,161]. In contrast to convex relaxations, the feasible region is contained within the AC power flow feasible region. However, operating envelopes are usually calculated by solving two problems, one for the lower limit and one for the upper limit. While the feasible region of each problem is convex, the union of the two feasible regions is not necessarily convex. One could either make a monotonicity assumption or find

a convex restriction of the union of the feasible regions.

In addition to the choice of power flow formulation, one also needs to choose the appropriate objection function. One choice of objective function is to maximize flexibility, e.g., the sum of the operating envelopes across the network. In addition to maximizing flexibility, it is also important to consider fairness when computing operating envelopes [121, 124, 139, 140]. When the objective is to maximize the sum of operating envelopes across the feeder, buses further down the feeder tend to receive significantly tighter limits [140]. This means that a customer with a DER who is far from the substation will have less ability to inject power and/or modify load than a customer who is close to the substation. Therefore, this chapter utilizes the objective function proposed in [121], which maximizes the smallest operating envelope. A version of the formulation presented in this chapter with the objective of maximizing the sum of the operating envelopes across the feeder was also analyzed and produced similar findings. Those results are omitted for brevity.

7.2.1 Operating Envelope AC-OPF Branch Flow Formulation

We first define the full nonlinear operating envelope problem, which incorporates the AC power flow equations. This formulation is based on [121] and used in [138]. Different from our formulation in [138], we consider a more flexible case for reactive power injections in this work, as detailed below.

Consider a radial distribution network with a set of buses $\mathcal{N}$ and a set of lines $\mathcal{L}$. Let bus 0 denote the substation. In a radial network, each bus i has exactly one parent bus, i.e., the bus immediately upstream, which we denote as i', and a set of buses immediately downstream, which we denote as $\mathcal{C}^i$. For simplicity, we assume the network is balanced and can be represented by its single-phase equivalent circuit. We use the branch flow model for representing power flow [141], where the voltage and current angles can be omitted by writing the power flow and voltage difference equations in terms of squared voltage magnitudes and squared current magnitudes. Let $z_{i'i} = r_{i'i} + jx_{i'i}$ represent the impedance of the line connecting buses i' and i. The apparent power flow limit on the line connecting buses i' and i is $\overline{s}_{i'i}$. The per unit (p.u.) squared voltage limits at each bus are $\underline{v}$ and $\overline{v}$.

We describe in detail the problem to compute export limits; import limits are computed similarly. The decision variables are p_i^{exp}, $\forall i \in \mathcal{N}$, the net active power export limits (i.e., the upper limit of the operating envelope) at all buses $i \in \mathcal{N}$; $\underline{p}^{\text{exp}}$, the smallest export limit in the network; $p_{i'i} \, \forall i'i \in \mathcal{L}$, the active power flowing from bus i' to bus i on all branches $i'i \in \mathcal{L}$; $q_{i'i} \, \forall i'i \in \mathcal{L}$, the reactive power flowing from bus i' to bus i on all branches $i'i \in \mathcal{L}$; $v_i \, \forall i \in \mathcal{N}$, the squared voltage magnitude at all buses $i \in \mathcal{N}$; and $l_{i'i} \, \forall i'i \in \mathcal{L}$, the squared

current magnitude on all lines $i'i \in \mathcal{L}$. We assume that the reactive power injections at each node, q_i^{exp}, are controllable such that the power factor at each bus is at least 0.95. Let $\mathbf{x}$ be a vector of stacked decision variables. We compute the operating envelopes by solving:

$$\max_{\mathbf{x}} \ \underline{p}^{\text{exp}} \tag{7.1a}$$

$$\text{s.t. } \underline{p}^{\text{exp}} \leq p_i^{\text{exp}}, \quad \forall i \in \mathcal{N} \tag{7.1b}$$

$$\sum_{j \in \mathcal{C}^i} p_{ij} = p_{i'i} - r_{i'i} l_{i'i} + p_i^{\text{exp}}, \ \forall i \in \mathcal{N} \tag{7.1c}$$

$$\sum_{j \in \mathcal{C}^i} q_{ij} = q_{i'i} - x_{i'i} l_{i'i} + q_i^{\text{exp}}, \ \forall i \in \mathcal{N} \tag{7.1d}$$

$$-p_i^{\text{exp}} \alpha^{\text{pf}} \leq q_i^{\text{exp}} \leq p_i^{\text{exp}} \alpha^{\text{pf}} \quad \forall i \in \mathcal{N} \tag{7.1e}$$

$$v_i = v_{i'} - 2(r_{i'i} p_{i'i} + x_{i'i} q_{i'i}) + (r_{i'i}^2 + x_{i'i}^2) l_{i'i}, \quad \forall i \in \mathcal{N} \tag{7.1f}$$

$$p_{i'i}^2 + q_{i'i}^2 = l_{i'i} v_{i'}, \quad \forall i'i \in \mathcal{L} \tag{7.1g}$$

$$p_{i'i}^2 + q_{i'i}^2 \leq \overline{s}_{i'i}^2, \quad \forall i'i \in \mathcal{L} \tag{7.1h}$$

$$\underline{v} \leq v_i \leq \overline{v}, \quad \forall i \in \mathcal{N} \tag{7.1i}$$

$$v_0 = 1, \tag{7.1j}$$

$$l_{i'i} \geq 0, \quad \forall i'i \in \mathcal{L} \tag{7.1k}$$

where $\alpha^{\text{pf}} = \tan(\cos^{-1}(0.95))$.

Constraint (7.1b) converts a max min objective into a linear one by defining the smallest export limit to be maximized. Constraints (7.1c) and (7.1d) enforce active and reactive power balance at each bus. Constraint (7.1e) ensures that the power factor at each bus is at least 0.95. Constraint (7.1f) defines the squared voltage at each bus. Constraint (7.1g) defines the squared apparent power flowing from bus i' to i and (7.1h) limits it. Constraint (7.1i) enforces the voltage limits at each bus and (7.1j) fixes the substation voltage to 1 p.u. Lastly, (7.1k) requires the squared current to be nonnegative. This formulation assumes monotonicity, i.e., if p^{exp} defines the upper bound of a valid operating envelope, then any injection less than p^{exp}, down to a similarly defined lower bound (import limit), is feasible. We note that this may not always be true in practice since (7.1g) is non-convex.

7.2.2 Second-Order Cone Relaxation

The SOC relaxation was first proposed for the branch flow model in [141] and proven in [165] to be equivalent to the SOC relaxation of the bus injection model (first proposed in [166]). The SOC formulation is obtained from the full nonlinear formulation (7.1) by relaxing the

equality in (7.1g) to $p_{i'i}^2 + q_{i'i}^2 \leq l_{i'i} v_{i'}$. This can be equivalently written in a standard SOC form as

$$\left\| \begin{array}{c} 2p_{i'i} \\ 2q_{i'i} \\ l_{i'i} - v_{i'} \end{array} \right\|_2 \leq l_{i'i} + v_{i'}, \qquad \forall i'i \in \mathcal{L}. \tag{7.2}$$

The SOC formulation of the operating envelope problem is

$$\max \underline{p}^{\text{exp}} \quad \text{s.t. (7.1b)} - \text{(7.1f)}, \ \text{(7.1h)} - \text{(7.1k)}, \ \text{(7.2)}. \tag{7.3}$$

The solution given by this formulation is *exact*, i.e., it is the solution to the nonlinear problem, if it is feasible in the nonlinear problem, i.e., if $p_{i'i}^2 + q_{i'i}^2 = l_{i'i} v_{i'}$ holds for every $i'i \in \mathcal{L}$. In the remainder of this work we use the difference between the left and right sides of this equation to quantify the solution's inexactness.

While this SOC relaxation has been successfully used for a variety of OPF problems, the SOC relaxation is problematic when used in operating envelope problems, as we will show next, and as has been shown previously in [138, 160].

7.3 SOC Inexactness

In this section, we demonstrate the issues associated with using a SOC relaxation to construct operating envelopes. First, we describe an objective function modification proposed in our prior work [138]. Then, we present a case study that demonstrates SOC inexactness within the operating envelope problem, reinforcing previous observations. The case study also reveals an issue with the objective function modification.

7.3.1 Objective Function Modification

In previous work [138], we presented a modification of the objective function for improving the efficacy of operating envelopes calculated using SOC relaxations of the power flow equations. In [138], case studies illustrated how the SOC formulation can permit larger operating envelopes, which fail to ensure acceptable voltages under the true (nonlinear) physics. In an attempt to alleviate issues believed to be caused by fictitious flexibility in current values introduced by the relaxation, we penalized power losses in the objective [138]. Specifically,

the modified objective that we presented was

$$\max_{\mathbf{x}} \ \underline{p}^{\text{exp}} - \lambda \sum_{i'i \in \mathcal{L}} l_{i'i} r_{i'i}, \tag{7.4}$$

where λ is a weighting parameter found heuristically to account for differences in magnitude between the two terms. A discussion regarding the tuning of λ is presented in [138].

In [138], we presented two case studies for which this objective function modification led to solutions that 1) closely matched the solution found using the nonlinear formulation, and 2) had negligible values for inexactness. The networks used in those two case studies were relatively small, containing only 4 and 56 buses, respectively.

7.3.2 Case Study Setup

In this section, we use a larger and more realistic network than those considered in [138] to highlight the implications of using the SOC relaxation in the operating envelope problem and also the implications of using the modified objective function. Specifically, we use the 141-bus network MATPOWER test case [2]. Note that the substation is considered to be bus 0 and bus 1 is the bus connected to the substation. For simplicity, we assume that every bus needs an operating envelope. Voltages between 0.95 and 1.05 p.u. are considered acceptable. Any operation that leads to values below or above these limits will be considered unacceptable.

To show how the SOC relaxation of the power flow equations and the objective function modification impact the calculation of operating envelopes, we compare the results from both formulations to the full nonlinear operating envelope formulation. The solutions are compared in terms of the size of the obtained operating envelopes and the efficacy of those operating envelopes, i.e., how well they maintain acceptable voltages. To analyze the efficacy of the resulting operating envelopes, the nonlinear power flow equations are solved for each formulation assuming net power injections at each bus are equal to the upper limit set by the operating envelopes. Note that because the relationship between voltage and power injections is not monotonic, or even convex, this is not guaranteed to result in the worst case voltages for any injections within the operating envelopes. However, as described in Section 7.2, it is commonly assumed that any injections within the operating envelope are permissible and will lead to acceptable voltages.

Both the nonlinear and SOC problems were solved in Julia using the JuMP package [147]. The solvers used were IPOPT 3.14.4 [167] and CPLEX 20.1.0 for the nonlinear and SOC problems, respectively.

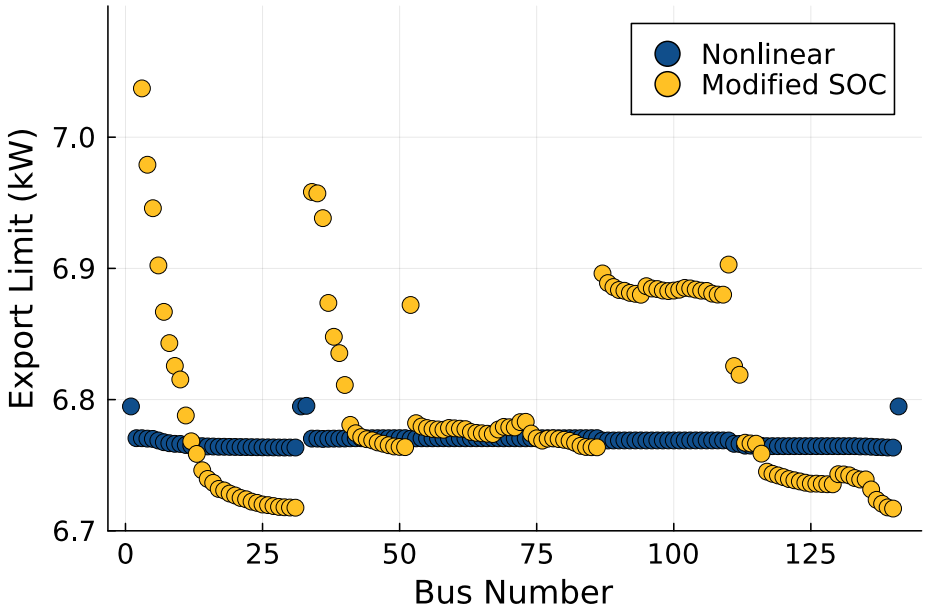
7.3.3 Case Study Results

We find that, using the full nonlinear operating envelope formulation, the operating envelope upper limits varied between 6.76 and 6.79 kW, shown as dark blue circles in Fig. 7.1a. When every bus is injecting real power equal to these limits, the voltages at each bus correspond to the values shown in dark blue in Fig. 7.1b. As can be seen in the figure, the voltage at every bus is within the voltage limits. A few of the buses far away from the substation are at the upper voltage limit, but this is to be expected at the edge of safe operation.

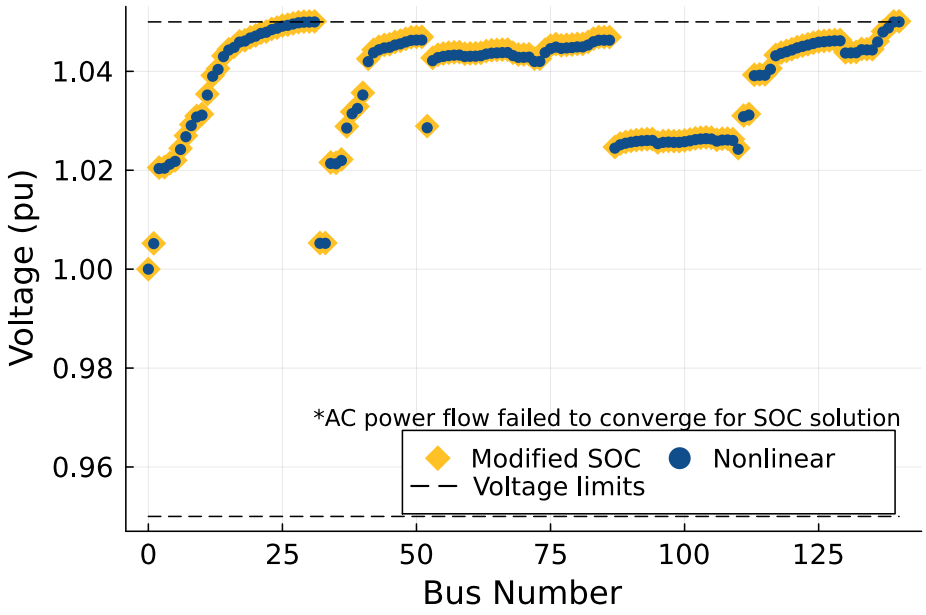
When the SOC relaxation is used with the same objective function, the solution found gives operating envelope upper limits that vary between 42.05 and 238.74 MW, shown as green stars in Fig. 7.1a. This range contains values 4 or 5 orders of magnitude larger than the range given by the nonlinear formulation. These power injection limits are so large, the AC power flow solver failed to converge when bus injections were set equal to them. The limits calculated from the SOC relaxation are so comparatively high that they are essentially equivalent to implementing no injection limits, and would likely lead to severe over-voltages, damaged equipment, and possible system instability if implemented.

When the SOC relaxation is used with the modified objective function (with $\lambda = 0.04$, where this choice will be explained below), the resulting operating envelopes have upper limits between 6.71 and 7.03 kW. While these limits are significantly closer to the limits given by the nonlinear formulation than those given by the unmodified SOC formulation, they are far from a perfect match. However, Fig. 7.1b shows that the bus voltages resulting from solving AC power flow when net power injections are equal to the operating envelopes generated via the modified SOC formulation are similar to the voltages given by the nonlinear case, and more importantly, the voltages are all safe. This means that the SOC formulation with the objective function modification can lead to safe operating envelopes. However, in more complex networks, the solution obtained will likely be different from the nonlinear solution.

Table 7.1 provides a numerical comparison between the solutions from the nonlinear formulation, the SOC formulation, and the SOC formulation using the modified objective function with $\lambda = 0.04$ (Mod SOC). Values $\underline{p}^{\text{exp}}$ represent the smallest operating envelope upper limit in the network for each case. Max Bus Inexactness values represent $\max_{i'i\in\mathcal{L}} |p_{i'i}^2 + q_{i'i}^2 - l_{i'i}v_{i'}|$ and the Total Inexactness values represent $\sum_{i'i\in\mathcal{L}} |p_{i'i}^2 + q_{i'i}^2 - l_{i'i}v_{i'}|$. The results highlight the improvements that the objective function modification have on the inexactness of the SOC formulation. However, pairing these results with the results in Fig. 7.1b tells us that even if a SOC solution does not satisfy (7.1g), i.e., the SOC is not exact, it can still result in safe voltages. This suggests that the SOC relaxation with modified objective function could be used to determine operating envelopes; however, the corresponding voltage,



(a) The operating envelopes found using the nonlinear, SOC, and modified SOC formulations with $\lambda = 0.04$.



(b) The voltage at each bus resulting from solving AC power flow with power exports at each bus set equal to the operating envelope limits calculated using the nonlinear and modified SOC formulations with $\lambda = 0.04$. Note that voltages for the SOC formulation are not shown because the AC power flow solver failed to converge.

Figure 7.1: Results for the 141-bus network using nonlinear, SOC, and modified SOC formulations.

Table 7.1: Measures of Inexactness

	Nonlinear	SOC	Mod SOC
$\underline{p}^{\text{exp}}$ (kW)	6.76	42052	6.71
Max Bus Inexactness (MVA^2)	–	44032	33.83
Total Inexactness (MVA^2)	–	152667	33.95

current, and power solution values are unreliable and likely not physically realizable.

A fundamental challenge to using the objection function modification is how to select λ, as we discussed in [138]. Figures 7.2 and 7.3 illustrate that selecting the "best" λ may not be easy, even with knowledge of the solution to the nonlinear formulation. Without the nonlinear solution, the measure of inexactness could be used to select λ. However, unlike in the small network cases in [138] where the sum of inexactness converged to zero as the operating envelope size approached the nonlinear solution, here the sum of inexactness remains significant even when the smallest operating envelope becomes smaller than the smallest operating envelope given by the nonlinear solution. In Figs. 7.1a and 7.1b and Table 7.1, we used $\lambda = 0.04$ despite the relatively high inexactness shown in Fig. 7.3 because it led to the largest operating envelopes that maintained safe voltage levels. In practice, one could select an appropriate λ by checking the voltage levels given by AC power flow with power exports at each bus set equal to the operating envelope limits.

7.4 Conditions for Inexactness

We have shown that the solutions to operating envelope problems using SOC relaxations are not always effective at maintaining acceptable voltages. Prior literature on the topic of SOC relaxations for the operating envelope problem suggests that the relaxation will never be exact [123, 138, 160]. If this can be proved mathematically, it would justify the argument that SOC relaxations should never be used for the operating envelope problem, or similar problems. Alternatively, if conditions can be found under which the relaxation is exact, then use of the SOC relaxation may be justified for those cases.

There has been significant work in the area of SOC relaxations for distribution networks, including work on distribution networks containing DERs. It is proven in [141, 168] that a SOC relaxation is exact when minimizing an objective function that is strictly increasing in line losses if over-satisfaction of load is allowed. In [169], it is shown that a SOC relaxation is exact for an OPF problem in a radial distribution network if there are no upper bounds

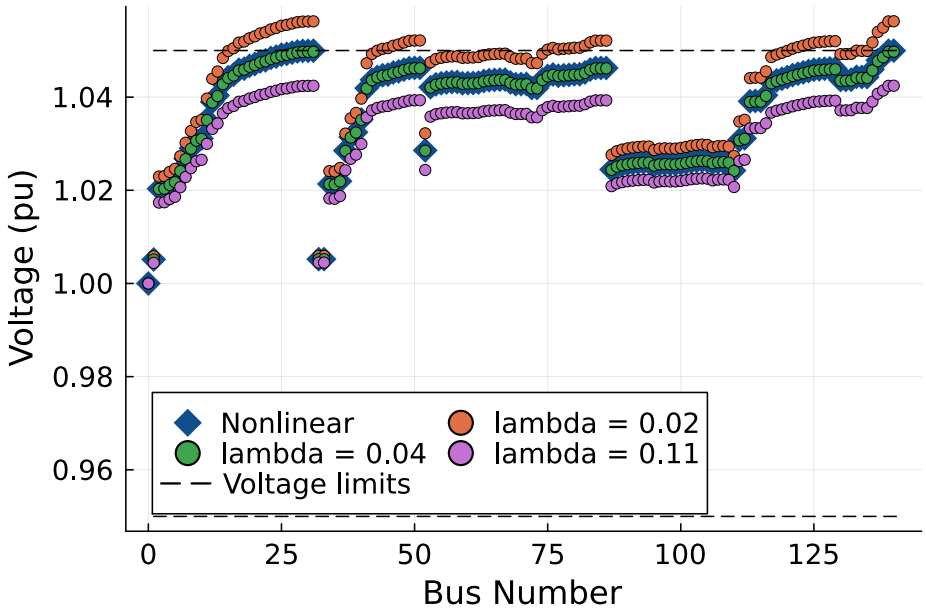


Figure 7.2: The impact of λ. Like in Fig. 7.1b, we plot the voltage at each bus in the 141-bus network resulting from solving AC power flow with power exports at each bus equal to the operating envelope limits calculated using the nonlinear and modified SOC formulations, but for three choices of λ.

on voltage, voltage magnitudes are roughly 1 p.u., $\frac{r}{x}$ is bounded, and net loads are below 1 p.u. This is shown under the condition that the objective function is strictly increasing with respect to the active power injections at the substation. In [170], it is shown that for a radial network, the SOC relaxation is exact for an objective function minimizing an increasing convex function over the power injection region. It is shown in [157] that the SOC relaxation of an OPF problem minimizing a convex objective function will be exact if no upper voltage limits are binding at optimality.

None of the above proofs apply to the operating envelope problem because, as the authors of [171] note, the sets of sufficient conditions for an exact SOC relaxation always include "a requirement on the objective to be a minimization of a function increasing with the branch flow apparent powers." Furthermore, [171] explains how these types of objective functions are at odds with what is expected of an active distribution system and provides a case study illustrating that including DER-centric objectives in the objective function can lead to an inexact SOC relaxation. They then present a cutting-plane algorithm to tighten the relaxation by iteratively decreasing losses. This approach has since been applied to the hosting capacity problem [172].

In this section, we show that there actually are cases for which the SOC relaxation is exact for the operating envelope problem. We then use numerical analysis to determine the

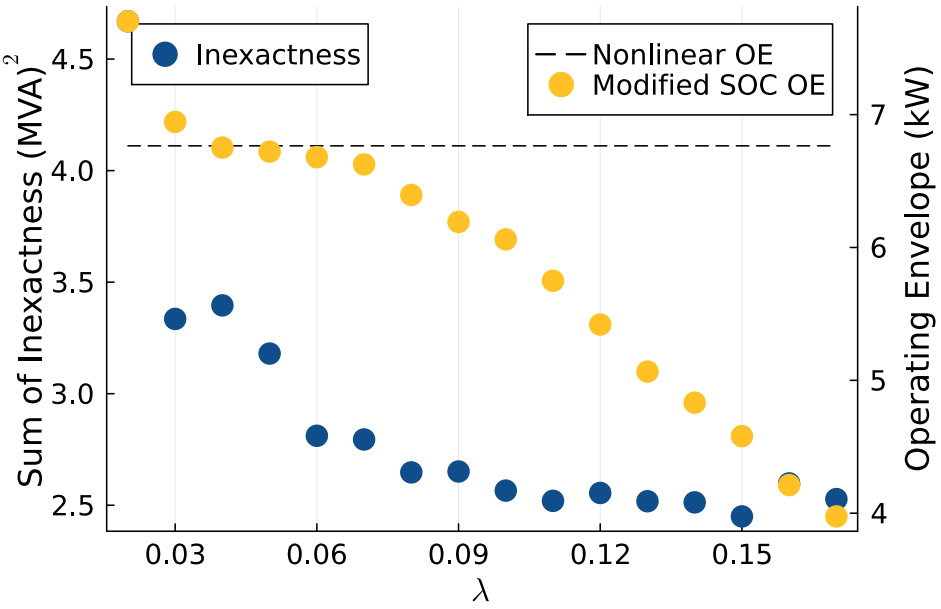


Figure 7.3: The sum of the inexactness, i.e., $lv - (p^2 + q^2)$, at every bus, and the smallest resulting operating envelope as λ is increased.

conditions under which the SOC relaxation is or is not exact. Finally, we prove mathematically that for radial networks the SOC relaxation is not exact for the operating envelope problem given a purely resistive network, and it is exact given a purely reactive network.

7.4.1 Conditions for an exact relaxation

In this subsection, we numerically analyze conditions that lead to an exact or inexact SOC relaxation of the operating envelope problem. Specifically, we explore the impacts of line parameters r and x on the optimal solution of both the nonlinear and SOC formulations. We do this by rewriting the SOC formulation in terms of the optimal solution of the nonlinear formulation and defining new variables that represent the deviations from the nonlinear variables at optimality. We then define a feasibility problem, which if feasible indicates that the SOC relaxation is not exact. We solve this feasibility problem and the rewritten SOC formulation for different r and x values and analyze the results.

For simplicity, we consider the operating envelope problem that does not consider fairness, i.e., the nonlinear form is

$$\max_{\mathbf{x}} \quad \sum_{i \in \mathcal{N}} p_i^{\text{exp}} \quad \text{s.t.} \quad (7.1c) - (7.1k), \tag{7.5}$$

and the SOC form is

$$\max_{\mathbf{x}} \quad \sum_{i\in\mathcal{N}} p_i^{\text{exp}} \quad \text{s.t.} \;\; (7.1\text{c}) - (7.1\text{f}),\; (7.1\text{h}) - (7.1\text{k}),\; (7.2). \tag{7.6}$$

Let $\mathbf{x}^* = (\mathbf{p}^{\text{exp}*}, \mathbf{q}^{\text{exp}*}, \mathbf{p}^*, \mathbf{q}^*, \mathbf{l}^*, \mathbf{v}^*)$ be the optimal solution to (7.5). Consider a candidate solution for (7.6) of the form $\hat{\mathbf{x}} = \mathbf{x}^* + \delta$ where δ represents any deviation away from the optimal solution $\mathbf{x}^*$ of (7.5). The SOC formulation can be rewritten as

$$\max_{\delta} \quad \sum_{i\in\mathcal{N}} \delta_i^{\text{p,exp}} \tag{7.7a}$$

$$\text{s.t.} \quad \sum_{j\in\mathcal{C}^i} \delta_{ij}^{\text{p}} = \delta_{i'i}^{\text{p}} - r_{i'i}\delta_{i'i}^{\text{l}} + \delta_i^{\text{p,exp}}, \forall i \in \mathcal{N} \tag{7.7b}$$

$$\sum_{j\in\mathcal{C}^i} \delta_{ij}^{\text{q}} = \delta_{i'i}^{\text{q}} - x_{i'i}\delta_{i'i}^{\text{l}} + \delta_i^{\text{q,exp}}, \forall i \in \mathcal{N} \tag{7.7c}$$

$$-(p_i^{\text{exp}} + \delta_i^{\text{p,exp}})\alpha^{\text{pf}} \le q_i^{\text{exp}} + \delta_i^{\text{q,exp}} \le \alpha^{\text{pf}}(p_i^{\text{exp}} + \delta_i^{\text{p,exp}}), \quad \forall i \in \mathcal{N} \tag{7.7d}$$

$$\delta_i^{\text{v}} = \delta_{i'}^{\text{v}} - 2(r_{i'i}\delta_{i'i}^{\text{p}} + x_{i'i}\delta_{i'i}^{\text{q}}) + (r_{i'i}^2 + x_{i'i}^2)\delta_{i'i}^{\text{l}}, \quad \forall i \in \mathcal{N} \tag{7.7e}$$

$$\left\| \begin{matrix} 2p_{i'i}^* + 2\delta_{i'i}^{\text{p}} \\ 2q_{i'i}^* + 2\delta_{i'i}^{\text{q}} \\ l_{i'i}^* + \delta_{i'i}^{\text{l}} - v_{i'}^* - \delta_{i'}^{\text{v}} \end{matrix} \right\|_2 \le l_{i'i}^* + \delta_{i'i}^{\text{l}} + v_{i'}^* + \delta_{i'}^{\text{v}}, \quad \forall i'i \in \mathcal{L} \tag{7.7f}$$

$$(p_{i'i}^* + \delta_{i'i}^{\text{p}})^2 + (q_{i'i}^* + \delta_{i'i}^{\text{q}})^2 \le \overline{s}_{i'i}^2, \quad \forall i'i \in \mathcal{L} \tag{7.7g}$$

$$\underline{v} \le v_i^* + \delta_i^{\text{v}} \le \overline{v}, \quad \forall i \in \mathcal{N} \tag{7.7h}$$

$$0 = \delta_0^{\text{v}} \tag{7.7i}$$

$$l_{i'i}^* + \delta_{i'i}^{\text{l}} \ge 0, \quad \forall i'i \in \mathcal{L} \tag{7.7j}$$

where $\delta_i^{\text{p,exp}} = \hat{p}_i^{\text{exp}} - p_i^{\text{exp}*}$, $\delta_{i'i}^{\text{p}} = \hat{p}_{i'i} - p_{i'i}^*$, etc.

If the SOC relaxation is exact, then the problem

$$\max_{\delta} \quad \sum_{i\in\mathcal{N}} \delta_i^{\text{p,exp}} \tag{7.8a}$$

$$\text{s.t.} \;\; (7.7\text{b}) - (7.7\text{j}),$$

$$\sum_{i\in\mathcal{N}\setminus 0} \delta_i^{\text{p,exp}} + \epsilon \ge 0 \tag{7.8b}$$

should not have a solution. In (7.8b), $\epsilon > 0$ represents a small positive value such that the constraint actually enforces $\sum_{i\in\mathcal{N}\setminus 0} \delta_i^{\text{exp}} > 0$.

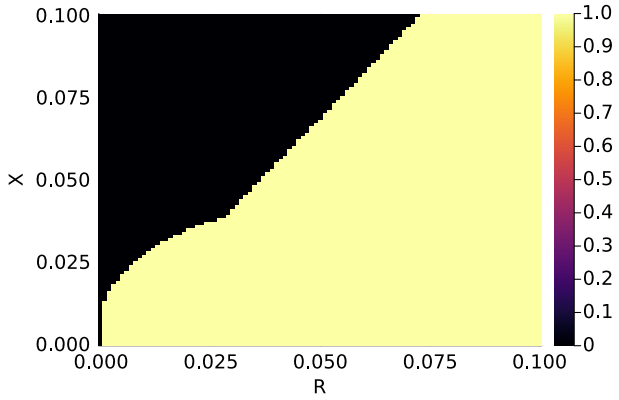
Since our formulation considers the net power injections and does not include explicit

demand parameters, the only parameters in the formulation are r, x, and the power factor considered in (7.7d). This motivated the idea that the conditions for which (7.3) is exact could be conditions on r and x. To investigate this, we solved (7.8) over a range of r and x values for a simple 2-bus example, the 56-bus example from [138], and the 141-bus example from Section 7.3.2. For the 56- and 141-bus networks, we assume all lines in the network have the same r and x values. The ranges of tested r and x values are selected to span values with similar magnitude to the r and x values given in the original network models.

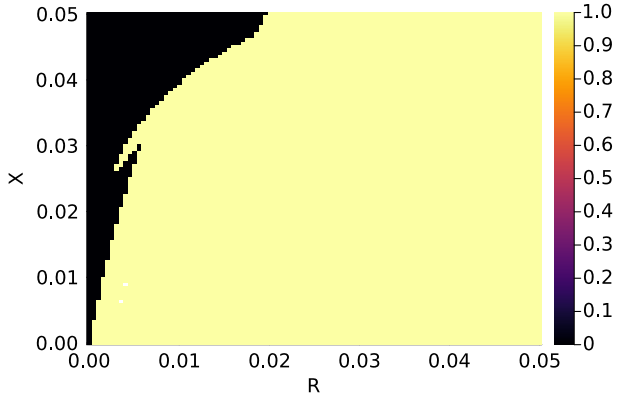
Figure 7.4 illustrates the feasibility of (7.8) for these networks over a range of r and x values. To avoid misinterpreting numerical error, we consider (7.8) infeasible and the SOC relaxation to be exact if it does not lead to at least a 0.1% improvement in the objective function, i.e., $\epsilon = 0.001 \left(\sum_{i \in \mathcal{N}} p_i^{\text{exp}*}\right)$. The black regions in Fig. 7.4 corresponds to values of r and x for which (7.8) is infeasible and therefore the SOC relaxation is exact. The yellow regions corresponds to values of r and x for which (7.8) is feasible and the SOC relaxation is not exact. The white areas in Fig. 7.4c represent values of r and x for which (7.1) was (at least locally) infeasible.

The regions in the figure suggest that whether or not the SOC relaxation is exact is dependent on r and x. However, the exact relationship is unclear. Note that there is a region of r and x values for which the SOC relaxation is exact for the operating envelope problem. This is counter to previous examples where the relaxation has always been reported to be inexact [123, 138, 160]. It is also counter to the initial intuition that because operating envelopes can increase as losses increase (assuming $r > 0$), the flexibility in current values enabled by the SOC relaxation would always lead to an inexact relaxation. Figure 7.4 does show that when $r = 0$, i.e., there are no active power losses, the relaxation is exact for each of the three tested networks. In contrast, when the network is purely resistive, i.e., $x = 0$ and $r > 0$, the relaxation is never exact. We present a mathematical proof of both of these cases in the subsequent subsections.

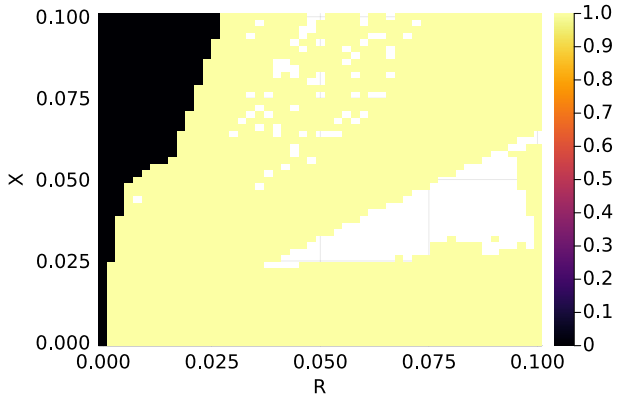
Figures 7.5a–7.5f show values of δ_{01}^{p}, δ_{01}^{q}, δ_{01}^{l}, δ_{1}^{v}, $\delta_{1}^{\text{p,exp}}$, and $\delta_{1}^{\text{q,exp}}$, i.e., the change in variable values from the optimal solution to the nonlinear formulation and the optimal solution to the SOC formulation for the 2-bus network. All six plots show three regions: i) the white region where (7.8) is infeasible, ii) the "dome-shaped" region near the bottom left corner, and iii) the region below the diagonal in the lower right corner. Except in Fig. 7.5d, the dome region and the lower diagonal region have distinct patterns with respect to r and x. This suggests that the flexibility introduced by the relaxation, which allows the SOC formulation to attain higher operating envelope values, changes not only in magnitude but also in which variables are manipulated to create this flexibility as r and x change. The squared line current value, shown in Fig. 7.5c, has the most significant change between



(a) 2-Bus network

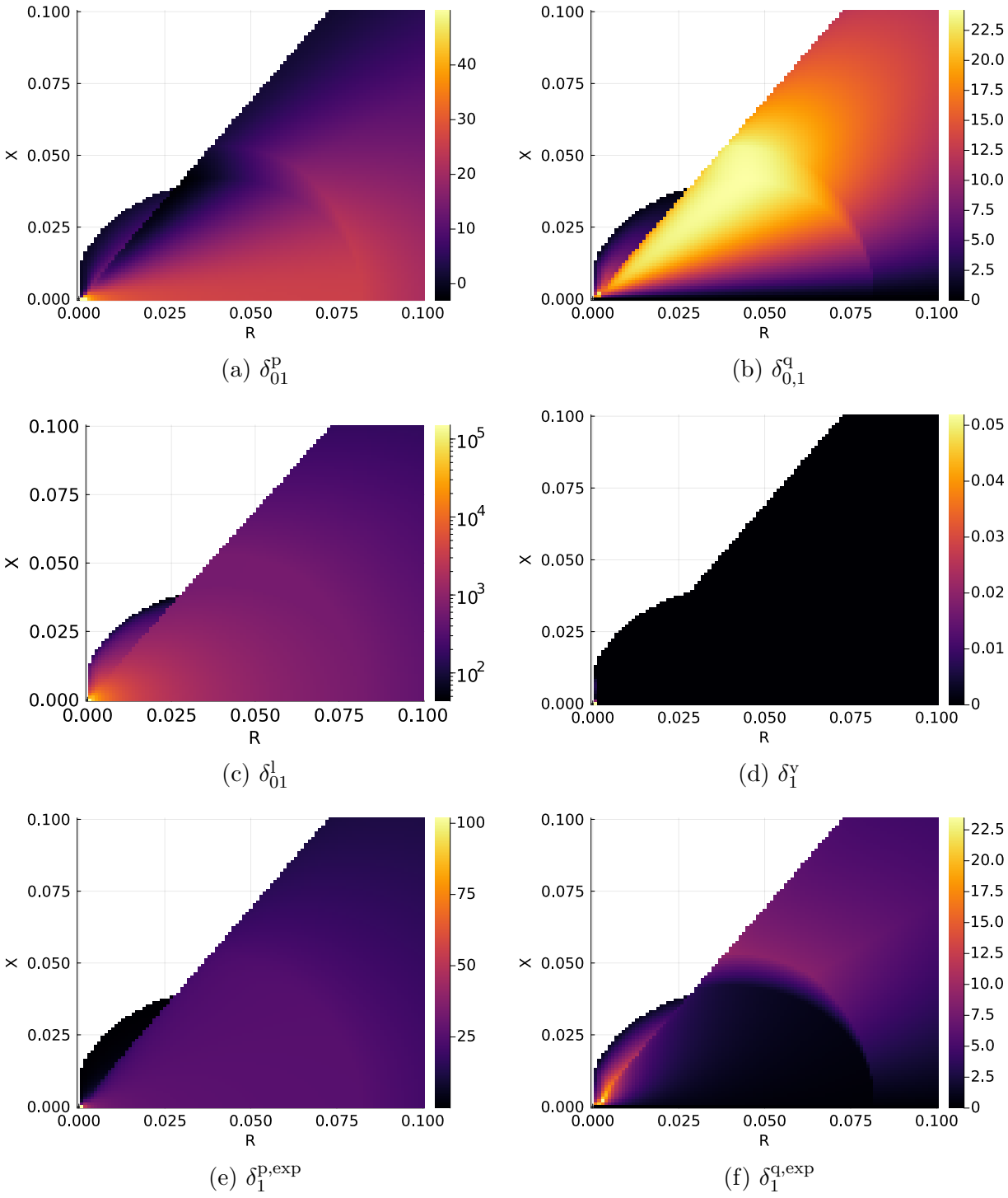


(b) 56-Bus Network



(c) 141-Bus network

Figure 7.4: Relationship between r, x and the feasibility (7.8). Black areas represent values for which (7.8) is infeasible, i.e., the SOC relaxation is exact. Yellow areas represent values for which (7.8) is feasible, i.e., the SOC relaxation is not exact. White areas represent values for which (7.1) was locally infeasible.



(a) δ_{01}^{p} (b) $\delta_{0,1}^{\mathrm{q}}$

(c) δ_{01}^{l} (d) δ_{1}^{v}

(e) $\delta_{1}^{\mathrm{p,exp}}$ (f) $\delta_{1}^{\mathrm{q,exp}}$

Figure 7.5: Deviations δ obtained by solving (7.8) for different r and x values in the 2-bus network. White space indicates values of r and x for which (7.8) is infeasible, i.e., the SOC relaxation is exact.

the nonlinear and SOC solutions, suggesting it plays a significant role in the difference in objective values. The existence of these two distinct regions and the variations within them for the simple 2-bus network suggest that there may be multiple sets of conditions under which the SOC relaxation of the operating envelope problem is not exact, and identifying precise conditions is likely difficult.

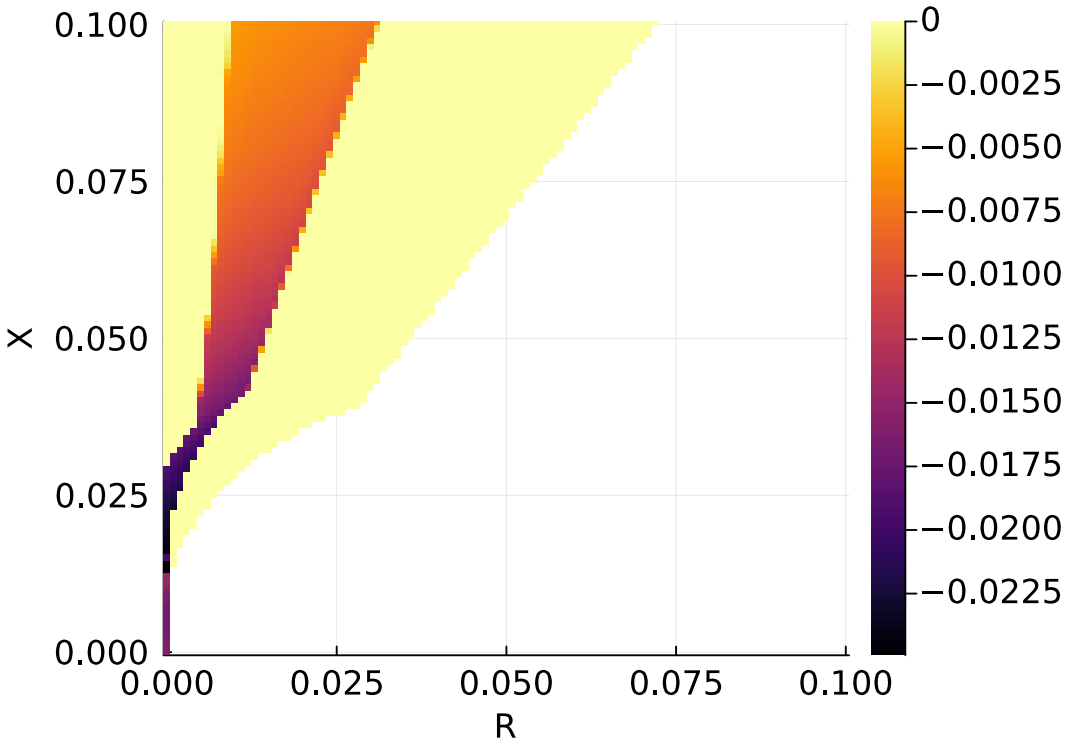
To gain insight into which constraint(s) sometimes prevent the SOC relaxation from obtaining a higher objective value than the nonlinear formulation (i.e., from being inexact), we introduce slack variables in the right side of the equality constraints of (7.8), i.e., (7.7b), (7.7c), and (7.7e). The problem with slack variables can then be solved over the r and x values for which (7.8) was infeasible and the relaxation was exact. If non-zero slack appears in only one equation or in multiple equations in such a way that it can be attributed to a single variable, and thus that variable's bounds, then identifying sufficient conditions for an exact relaxation may be straightforward.

The values of the slack variables associated with (7.7b) and (7.7e) for the 2-bus network are shown in Fig. 7.6. There are three distinct regions within the colored portion of the plots. The regions can be described as follows: 1) positive slack in the voltage drop equation and zero slack in all other equality constraints, 2) negative slack in the active power balance equation and zero slack in the voltage drop equation, and 3) negative slack in the voltage drop equation and zero slack in all other equality constraints. Similar to the argument used above, the presence of these three distinct regions for this simple 2-bus network suggests that there are multiple sets of conditions that could lead to an exact SOC relaxation.

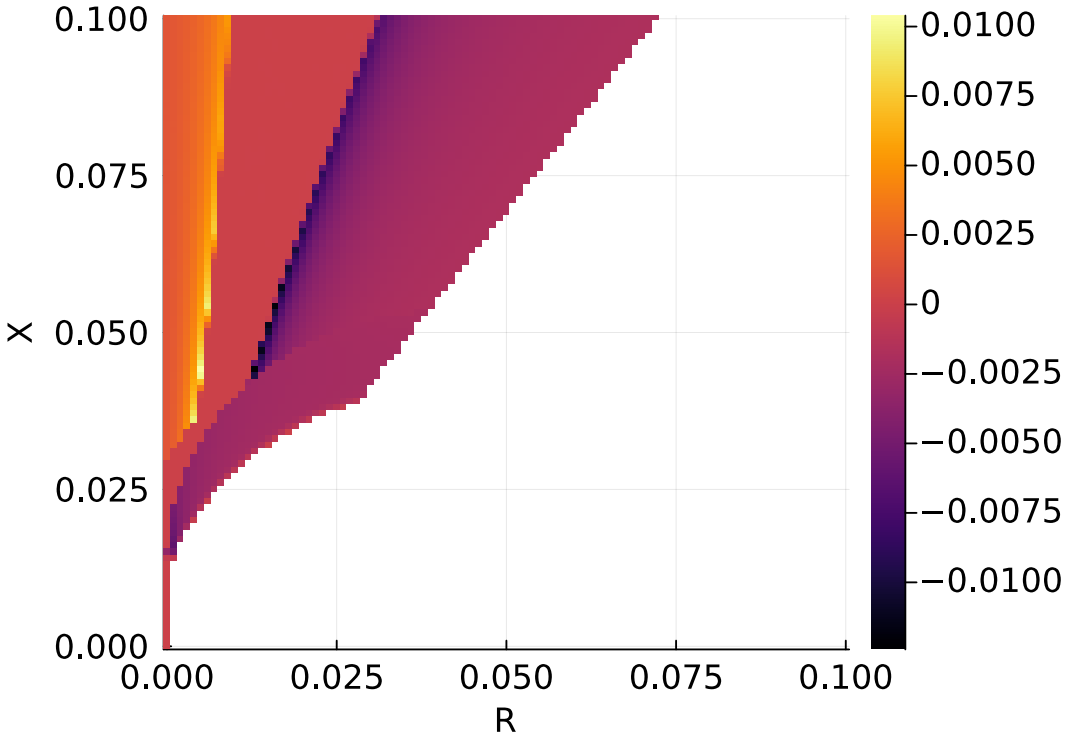
In summary, for distribution networks that contain lines with both positive resistance and positive reactance, we have shown that there are scenarios under which the SOC relaxation is exact and also scenarios under which the SOC relaxation is not exact for the operating envelope problem. Our numerical analysis, as well as our multiple failed attempts at mathematical exactness and inexactness proofs (omitted for brevity), suggests that there may not be a concise set of conditions for which the relaxation is or is not exact. Given this lack of clear and provable conditions for an exact relaxation and the undesirable consequences of an inexact relaxation in the context of the operating envelope problem, as illustrated in Section 7.3.3 and in prior work [123, 138, 160], it is ill-advised to use a SOC relaxation to calculate operating envelopes.

7.4.2 Purely Resistive Networks

Results in the previous section for the general case were complicated. However, the results did suggest that it might be possible to derive conditions for purely resistive or purely reactive



(a) Slack in active power balance (7.7b)



(b) Slack in voltage drop (7.7e)

Figure 7.6: Relationship between r, x and the slack variables in (7.8).

networks. Therefore, we now consider the case of purely resistive networks, i.e., $\forall\ i'i \in \mathcal{L}$, $r_{i'i} > 0$ and $x_{i'i} = 0$. Again, let $\mathbf{x}^* = (\mathbf{p}^{\exp*}, \mathbf{q}^{\exp*}, \mathbf{p}^*, \mathbf{q}^*, \mathbf{l}^*, \mathbf{v}^*)$ be the optimal solution to (7.5). Consider a particular bus $i \neq 0$ and assume $v_i^* < \bar{v}$. Now, consider the following candidate solution $\hat{\mathbf{x}}$ to (7.6):

$$
\begin{aligned}
&\hat{p}_i^{\exp} = p_i^{\exp*} + \frac{\varepsilon}{r_{i'i}}, && \hat{p}_k^{\exp} = p_k^{\exp*},\ \forall k \neq i \in \mathcal{N},\\
&\hat{v}_i = v_i^* + \varepsilon, && \hat{v}_k = v_k^*,\ \forall k \neq i \in \mathcal{N},\\
&\hat{l}_{i'i} = l_{i'i}^* + \frac{\varepsilon}{r_{i'i}^2}, && \hat{l}_{kn} = l_{k'k}^*,\ \forall k'k \neq i'i \in \mathcal{L},\\
&\hat{p}_{k'k} = p_{k'k}^*,\ \forall k'k \in \mathcal{L}, && \hat{q}_{k'k} = q_{k'k}^*,\ \forall k'k \in \mathcal{L},\\
&\hat{q}_k^{\exp} = q_k^{\exp*},\ \forall k \in \mathcal{N}, &&
\end{aligned}
$$

where $0 < \varepsilon \leq \bar{v} - v_i^*$ is a small perturbation. Since $\varepsilon > 0$ and $r_{i'i} > 0\ \forall\ i'i \in \mathcal{L}$, this candidate solution will have a strictly larger objective value than $\mathbf{x}^*$. We will now show that this candidate solution is feasible for (7.6) but not feasible for (7.5), i.e., the SOC relaxation is not exact. To do this, it suffices to show that (7.1c)–(7.1f) and (7.1h)–(7.1k) hold for $\hat{\mathbf{x}}$ and (7.2) holds with strict inequality for at least one line.

At bus i, plugging $\hat{\mathbf{x}}$ into (7.1c) gives

$$
\begin{aligned}
p_{i'i}^* - r_{i'i}\left(l_{i'i}^* + \frac{\varepsilon}{r_{i'i}^2}\right) + p_i^{\exp*} + \frac{\varepsilon}{r_{i'i}} &= \sum_{j \in \mathcal{C}^i} p_{ij}^*,\\
p_{i'i}^* - r_{i'i} l_{i'i}^* - \frac{\varepsilon}{r_{i'i}} + p_i^{\exp*} + \frac{\varepsilon}{r_{i'i}} &= \sum_{j \in \mathcal{C}^i} p_{ij}^*,\\
p_{i'i}^* - r_{i'i} l_{i'i}^* + p_i^{\exp*} &= \sum_{j \in \mathcal{C}^i} p_{ij}^*,
\end{aligned}
$$

which must hold if $\mathbf{x}^*$ is optimal for (7.5). For any bus $k \neq i$, plugging $\hat{\mathbf{x}}$ into (7.1c) gives $p_{k'k}^* - r_{k'k} l_{k'k}^* + p_k^{\exp*} = \sum_{n \in \mathcal{C}^k} p_{kn}^*$, which holds by the same argument. Thus, (7.1c) holds for $\hat{\mathbf{x}}$.

If $x_{k'k} = 0$, then (7.1d) at any bus k given $\hat{\mathbf{x}}$ is $q_{k'k}^* + q_k^{\exp*} = \sum_{n \in \mathcal{C}^k} q_{kn}^*$. Again, if $\mathbf{x}^*$ is optimal for (7.5), then this proves that (7.1d) holds for $\hat{\mathbf{x}}$.

Next, consider (7.1e) for $\hat{\mathbf{x}}$ at bus i,

$$
-\left(p_i^{\exp*} + \frac{\varepsilon}{r_{i'i}}\right)\alpha^{\mathrm{pf}} \leq q_i^{\exp*} \leq \left(p_i^{\exp*} + \frac{\varepsilon}{r_{i'i}}\right)\alpha^{\mathrm{pf}}.
$$

Since $\frac{\varepsilon}{r_{i'i}} > 0$, then $-\left(p_i^{\exp*} + \frac{\varepsilon}{r_{i'i}}\right)\alpha^{\mathrm{pf}} < -p_i^{\exp*}\alpha^{\mathrm{pf}}$ and $\left(p_i^{\exp*} + \frac{\varepsilon}{r_{i'i}}\right)\alpha^{\mathrm{pf}} > p_i^{\exp*}\alpha^{\mathrm{pf}}$, show-

ing that the above holds if (7.1e) holds for $\mathbf{x}^*$. At any bus $k \neq i$, $\hat{p}_k^{\text{exp}} = p_k^{\text{exp}*}$ and $\hat{q}_k^{\text{exp}} = q_k^{\text{exp}*}$ so it is trivial to show that (7.1e) holds. Thus, (7.1e) holds at all buses for $\hat{\mathbf{x}}$.

Next, consider (7.1f) for $\hat{\mathbf{x}}$ at bus i,

$$\begin{aligned} v_i^* + \varepsilon &= v_{i'}^* - 2(r_{i'i}p_{i'i}^*) + r_{i'i}^2\left(l_{i'i}^* + \frac{\varepsilon}{r_{i'i}^2}\right), \\ v_i^* + \varepsilon &= v_{i'}^* - 2(r_{i'i}p_{i'i}^*) + r_{i'i}^2 l_{i'i}^* + \varepsilon, \\ v_i^* &= v_{i'}^* - 2(r_{i'i}p_{i'i}^*) + r_{i'i}^2 l_{i'i}^*, \end{aligned}$$

which must hold if $\mathbf{x}^*$ is optimal for (7.5). For any bus $k \neq i$, $\hat{v}_k = v_k^*$, $\hat{p}_{k'k} = p_{k'k}^*$, and $\hat{l}_{k'k} = l_{k'k}^*$ so it is trivial to show that (7.1f) holds. Thus, (7.1f) holds at all buses for $\hat{\mathbf{x}}$.

For all lines $k'k \in \mathcal{L}$, $\hat{p}_{k'k} = p_{k'k}^*$ and $\hat{q}_{k'k} = q_{k'k}^*$ so it is trivial to show that (7.1h) holds for $\hat{\mathbf{x}}$.

Next, consider voltage limits (7.1i) at bus i: $\underline{v} \leq v_i^* + \varepsilon \leq \overline{v}$. The lower limit holds because $\varepsilon > 0$ and $\underline{v} \leq v_i^*$. Recall that we defined $\varepsilon \leq \overline{v} - v_i^*$, and thus the upper limits holds because $v_i^* + \varepsilon \leq \overline{v}$. For any bus $k \neq i$, $\hat{v}_k = v_k^*$ so it is trivial to show that (7.1i) holds for $\hat{\mathbf{x}}$. Similarly, since i is not the substation bus then (7.1j) holds. Since $\varepsilon > 0$, it follows that $l_{k'k}^* + \frac{\varepsilon}{r_{k'k}^2} \geq 0 \ \forall k'k \in \mathcal{L}$, if $\mathbf{x}^*$ is optimal for (7.5).

Finally, it must be shown that (7.2) holds with strict inequality on at least one line. Consider the line connecting buses i' and i, and for simplicity, consider (7.2) in its equivalent form $p_{i'i}^2 + q_{i'i}^2 \leq l_{i'i}v_{i'}$. Plugging in $\hat{\mathbf{x}}$, we get

$$\begin{aligned} (p_{i'i}^*)^2 + (q_{i'i}^*)^2 &\leq \left(l_{i'i}^* + \frac{\varepsilon}{r_{i'i}^2}\right)(v_{i'}^* + \varepsilon), \\ (p_{i'i}^*)^2 + (q_{i'i}^*)^2 &\leq l_{i'i}^* v_{i'}^* + v_{i'}^* \frac{\varepsilon}{r_{i'i}^2} + l_{i'i}^*\varepsilon + \frac{\varepsilon^2}{r_{i'i}^2}, \\ (p_{i'i}^*)^2 + (q_{i'i}^*)^2 = l_{i'i}^* v_i^* &< l_{i'i}^* v_{i'}^* + v_{i'}^* \frac{\varepsilon}{r_{i'i}^2} + l_{i'i}^*\varepsilon + \frac{\varepsilon^2}{r_{i'i}^2}. \end{aligned}$$

The last line follows from the optimality of $\mathbf{x}^*$ for (7.5) and the fact that $l_{i'i}^* \geq 0$, $v_{i'}^* \geq 0$, $\varepsilon > 0$, and $r_{i'i} > 0 \ \forall \ i'i \in \mathcal{L}$. Thus, we have proven that $\hat{\mathbf{x}}$ is feasible for (7.6), not feasible for (7.5), and leads to a higher objective value. This proves that for purely resistive, radial networks, the SOC formulation of the operating envelope problem is not exact if at least one non-substation bus has a voltage strictly lower than the upper voltage limit at optimality of the nonlinear formulation.

With the exception of the 2-bus network, all of the test cases we ran with $r > 0$ and $x = 0$ satisfied the condition that at least one non-substation bus had a voltage strictly lower than the upper voltage limit at optimality of the nonlinear formulation. In the 2-bus network, the

only non-substation bus voltage was at its upper limit over the entire range of tested $r > 0$ values, yet the relaxation was still always inexact.

To the best of our knowledge, this is the first proof that identifies conditions under which a relaxation of an OPF problem *fails* to be exact. Prior work in the area of OPF relaxations attempt to prove conditions under which the relaxation is exact. Yet, it is also of value to know under what conditions the relaxation will be sure to fail. The proof that the SOC relaxation will fail to be exact in the operating envelope problem when a network is purely resistive aligns with our initial suspicion that the SOC relaxation is able to achieve larger operating envelopes by nonphysically increasing losses.

7.4.3 Purely Reactive Networks

We now consider the case of purely reactive networks, i.e., $\forall\, i'i \in \mathcal{L}$, $r_{i'i} = 0$ and $x_{i'i} > 0$. The following proof was inspired by the proof given in [141]. For the sake of contradiction, assume that $\mathbf{x}^* = (\mathbf{p}^{\text{exp}*}, \mathbf{q}^{\text{exp}*}, \mathbf{p}^*, \mathbf{q}^*, \mathbf{l}^*, \mathbf{v}^*)$ is the optimal solution to (7.6) such that (7.2) holds with strict inequality on a particular line connecting buses i' and i, i.e., $(p^*_{i'i})^2 + (q^*_{i'i})^2 < l^*_{i'i} v^*_{i'}$ and (7.6) is not exact. Now, consider the following candidate solution $\hat{\mathbf{x}}$ to (7.6):

$$
\begin{aligned}
&\hat{p}^{\text{exp}}_i = p^{\text{exp}*}_i + \varepsilon, && \hat{p}^{\text{exp}}_k = p^{\text{exp}*}_k,\ \forall k \neq i \in \mathcal{N},\\
&\hat{p}_{i'i} = p^*_{i'i} - \varepsilon, && \hat{p}_{k'k} = p^*_{k'k},\ \forall kn \neq i'i \in \mathcal{L},\\
&\hat{q}_{k'k} = q^*_{k'k},\ \forall k'k \in \mathcal{L}, && \hat{v}_k = v^*_k,\ \forall k \in \mathcal{N},\\
&\hat{l}_{k'k} = l^*_{k'k},\ \forall k'k \in \mathcal{L}, && \hat{q}^{\text{exp}}_k = q^{\text{exp}*}_k,\ \forall k \in \mathcal{N},
\end{aligned}
$$

where $\varepsilon > 0$ is a small perturbation (not necessarily the same perturbation as in the purely resistive case). Since $\varepsilon > 0$, $\hat{\mathbf{x}}$ will have a strictly larger objective value than $\mathbf{x}^*$ if it is feasible, which would contradict the optimality of $\mathbf{x}^*$. To check feasibility, it suffices to check that there exists $\varepsilon > 0$ such that $\hat{\mathbf{x}}$ satisfies (7.1c)–(7.1f), (7.1h)–(7.1k), and (7.2). Since $\mathbf{x}^*$ is feasible, (7.1d), (7.1f), and (7.1i)–(7.1k) hold for $\hat{\mathbf{x}}$ across all buses and lines. Similarly, (7.1c), (7.1e), (7.2), and (7.1h) hold for $\hat{\mathbf{x}}$ on all lines $k'k \neq i'i$ and at all buses $k \neq i$. We will now show that (7.1c), (7.1e), (7.2), and (7.1h) hold for $\hat{\mathbf{x}}$ on line $i'i$ and at bus i. Specifically, for (7.2), we will show that improving the objective value will ultimately shape the solution such that (7.2) approaches equality.

At bus i, plugging $\hat{\mathbf{x}}$ into (7.1c) gives

$$
p^*_{i'i} - \varepsilon + p^{\text{exp}*}_i + \varepsilon = p^*_{i'i} + p^{\text{exp}*}_i = \sum_{j \in \mathcal{C}^i} p^*_{ij},
$$

which must hold if $\mathbf{x}^*$ is feasible for (7.6).

Next, consider (7.1e) for $\hat{\mathbf{x}}$ at bus i

$$-\left(p_i^{\text{exp}*}+\varepsilon\right)\alpha^{\text{pf}} \leq q_i^{\text{exp}*} \leq \left(p_i^{\text{exp}*}+\varepsilon\right)\alpha^{\text{pf}}.$$

Since $\varepsilon > 0$, then $-\left(p_i^{\text{exp}*}+\varepsilon\right)\alpha^{\text{pf}} < -p_i^{\text{exp}*}\alpha^{\text{pf}}$ and $\left(p_i^{\text{exp}*}+\varepsilon\right)\alpha^{\text{pf}} > p_i^{\text{exp}*}\alpha^{\text{pf}}$, showing that the above holds if (7.1e) holds for $\mathbf{x}^*$.

Consider (7.1h) on line $i'i$ for $\hat{\mathbf{x}}$:

$$\hat{p}_{i'i}^2 + \hat{q}_{i'i}^2 = (p_{i'i}^* - \varepsilon)^2 + (q_{i'i}^*)^2 \leq \bar{s}^2.$$

Thus (7.1h) only holds for $\hat{\mathbf{x}}$ on line $i'i$ if $(p_{i'i}^*)^2 + (q_{i'i}^*)^2 \leq \bar{s}^2 + 2\varepsilon p_{i'i}^* - \varepsilon^2$ holds.

For (7.2) on line $i'i$,

$$\begin{aligned}
0 &> (p_{i'i}^*)^2 + (q_{i'i}^*)^2 - l_{i'i}^* v_{i'}^* \\
&= (\hat{p}_{i'i} + \varepsilon)^2 + \hat{q}_{i'i}^2 - \hat{l}_{i'i}\hat{v}_{i'} \\
&= \hat{p}_{i'i}^2 + \hat{q}_{i'i}^2 - \hat{l}_{i'i}\hat{v}_{i'} + 2\varepsilon\hat{p}_{i'i} + \varepsilon^2
\end{aligned}$$

Since $r = 0$ and there are no active power losses, then $\hat{p}_{i'i} < 0$ if the sum of net export limits across the buses downstream of bus i is positive, i.e., $\sum_{k\in\mathcal{N}_i^{\text{dn}}} \hat{p}_k^{\text{exp}} > 0$, where $\mathcal{N}_i^{\text{dn}}$ denotes the set of all buses downstream of bus i. If $\hat{p}_{i'i} < 0$, then we can choose any $\varepsilon > 0$ sufficiently small such that $\hat{l}_{i'i} \geq \frac{\hat{p}_{i'i}^2 + \hat{q}_{i'i}^2}{\hat{v}_{i'}}$. This proves that the candidate solution is feasible and contradicts the optimality of $\mathbf{x}^*$. This also implies that (7.2) will hold with equality for the true optimal solution and that the relaxation is exact. We note that because the objective is to maximize $\sum_{k\in\mathcal{N}} \hat{p}_k^{\text{exp}}$, then $\hat{p}_{i'i} < 0$ typically holds. In each test case we ran, active power line flows were all negative when $r = 0$.

The proof that the SOC relaxation will be exact in the operating envelope problem when a network is purely reactive also aligns with our initial intuition. Without resistance, the SOC relaxation is unable to nonphysically increase active power losses and therefore increase the operating envelopes.

7.5 Conclusions

In this chapter we discussed the implications of using a SOC relaxation for calculating operating envelopes. Specifically, we reinforced previous concerns and observations about the inadequacy of operating envelopes calculated using a SOC relaxation in regards to network safety. We also assessed the impact of using our previously proposed objective function

modification to tighten the SOC relaxation in the operating envelope problem on a larger network. Results suggest that the modification could be used to define operating envelopes that enforce voltage limits using a SOC relaxation, but that the relaxation may not be exact.

We showed that, despite our intuition to the contrary, there are scenarios in which the SOC relaxation can be exact for the operating envelope problem. With this insight, we attempted to identify the underlying conditions that lead to an exact and an inexact relaxation. For the general and realistic case where the network contains lines with both positive resistance and positive reactance, we were unable to provide simple conditions under which the relaxation will be exact or inexact. However, our numerical analysis suggests that there may be multiple sets of conditions that lead to an exact or an inexact relaxation. For networks with purely resistive lines, we mathematically proved that if there exists at least one bus not at its maximum voltage in the optimal solution of the nonlinear formulation, then SOC relaxation will lead to a larger sum of operating envelopes than the nonlinear formulation (i.e., it will be inexact). For networks with purely reactive lines, we mathematically proved that the SOC relaxation will be exact.

The key takeaway from this work is that given a lack of straightforward conditions for an exact relaxation, it is ill-advised to use a SOC relaxation to determine operating envelopes. Nonlinear formulations, linearizations or inner-approximations are more reliable options for calculating safe operating envelopes.

CHAPTER 8

Fair-Over-Time Distributed Energy Resource Coordination

In this chapter, we explore fairness metrics and their applicability to the DER coordination problem. In particular, we investigate metrics from machine learning to identify metrics that could be incorporated into DER coordination problems and we summarize fairness metrics that have been used in the power systems literature. A key challenge is that most existing fairness metrics are static—ensuring fairness at a point in time. DER coordination problems are inherently dynamic and we often care about fairness over time, not at each time. The machine learning literature offers some ways to think about fairness over time and, more generally, how to incorporate fairness into dynamic power systems problems. We use a specific DER coordination problem—the problem of computing dynamic operating envelopes—to demonstrate how incorporation of a fair-over-time metric changes DER coordination solutions, and highlight the trade-offs that arise. The work in this chapter is based on our published work [173].

8.1 Chapter Introduction

As society has come to more fully recognize the disparate impact that electric power systems have had on different populations, the concepts of fairness, equity, and justice have emerged as key objectives in the energy transition [174]. Incorporating fairness, equity, and/or justice metrics within power system problem formulations is one way to steer towards more fair, equitable, and/or just solutions. However, defining fairness, equity, and justice such that they can be included in quantitative problem formulations is challenging. Moreover, some of these concepts, like justice, were developed in the social sciences, and trying to develop quantitative justice metrics may undermine the spirit of the concept.

Fairness is a concept that has appeared in various engineering and technical literatures such as networking, computing, and machine learning (ML) [175–177]. For example, fair-

ness has been considered in ML contexts ranging from nondiscriminatory college admissions decisions to recidivism predictions in correction processes to loan lending decisions in banking [178]. Fairness concepts from ML can be leveraged within power systems problem formulations. However, this is not usually trivial – the ML language has to be mapped to the power systems problem and often there is not a clear/clean mapping. One needs to determine what notion of fairness is appropriate, what attribute should be fair (and whether the data exists to quantify this), how to measure fairness, and how to incorporate fairness metrics into the problem formulation, e.g., an optimization or control problem.

Take, for example, the problem of coordinating distributed energy resources (DERs). DERs can provide a variety of useful services to the power grid. Further, DERs enable prosumers, consumers who also produce, to engage with the power market and reap the benefits of doing so [179]. DER coordination strategies can affect resources and participants unequally, for example, by excessively degrading or curtailing some DERs more than others, affecting energy costs/payments [180, 181]. Despite this, few DER coordination strategies explicitly account for fairness. Identifying and implementing suitable fairness approaches in these settings can be especially challenging since the problems are inherently dynamic. While the ML literature has many examples of static fairness metrics (i.e, metrics that capture fairness at a point in time), there are fewer metrics that capture dynamic fairness, time-varying fairness, or fairness-over-time.

In this chapter, we investigate fairness metrics from ML to identify metrics that could be incorporated into DER coordination problems and we summarize fairness metrics that have been used in the DER coordination literature. We find that the ML literature offers some ways to think about fairness over time and, more generally, how to incorporate fairness into dynamic DER coordination problems. We summarize the steps one should take when incorporating fairness into a power systems problem formulation. We then provide a case study that shows how to apply these steps to the dynamic operating envelope problem, which seeks to determine the range of feasible power injections from DERs at each node of the distribution network. We show how a fairness-over-time metric can be incorporated into the problem to spread curtailment across the DERs and across time, achieving a notion of fairness. We also discuss the performance-fairness trade-offs that arise when applying this metric.

Some prior power systems work has discussed fairness. For example, the literature review [182] catalogs 80 works which explore fairness within contexts ranging from demand response to shared/community energy resources, collectively referred to as local energy systems. Fairness in the operating envelope problem has been explored in [124, 139, 183–185]; however, none of these papers considered fairness over time, only fairness at each time, which

may be unnecessarily constraining.

In summary, the contributions of this chapter are fourfold. First, we compare time-varying fairness approaches from the ML literature, and then compare fairness approaches in the DER coordination literature. Second, we provide a principled method to incorporate fairness into power systems problems. Third, we apply this method to the dynamic operating envelope problem, formulate a fair-over-time dynamic operating envelop problem, and discuss the performance-fairness trade-offs that result from its use.

The rest of this chapter is organized as follows. Section 8.2 describes fairness concepts and metrics in the ML and DER coordination literatures. Section 8.3 provides an approach for how to incorporate fairness into power systems problems. Section 8.4 provides a case study on fair-over-time dynamic operating envelopes, and Section 8.5 concludes.

8.2 Fairness Concepts & Metrics

A vast body of work has come out of the ML community to address fairness. Structured approaches to fairness have arisen in the theory, vocabulary, and problem formulations of fair algorithmic decision making [177, 178, 186, 187]. For power systems problems, there is growing interest and research directed toward the incorporation of fairness. We see value in comparing the landscapes of fairness in both areas and exploring what can be gleaned from the fair-ML community. In this section, we first briefly describe common static and time-varying fairness metrics in ML, we then describe existing approaches to fairness in DER coordination, and finally we compare these landscapes of fairness.

8.2.1 Fairness in machine learning

8.2.1.1 Static metrics

Many formulations of fairness in ML have emerged to quantify and account for (un)fairness inherent to a problem setting or introduced in the algorithmic decision making process. For brevity, we will describe only three metrics used by the ML community. First, Demographic Parity (also known as Statistical Parity) desires that the outcome probability distribution for persons belonging to different groups are the same [188]. Second, Disparate Impact [189] formalizes the notion that, ideally, benefits should not disproportionately accrue among unprotected groups relative to their accrual among protected groups. The third notion of fairness is Equalized Odds/Opportunity, which formalizes the notion that the performance of a prediction model should be identical for protected groups and unprotected groups [190].

For a more descriptive discussion of these fairness metrics, see [173] and for additional static fairness metrics used in ML, see [178].

8.2.1.2 Time-varying fairness metrics

The previously mentioned fairness metrics do not explicitly account for the passage of time, which is suitable for many ML contexts characterized by batch or one-shot decision processes. However, there are settings in which decisions are coupled over time, requiring adaptations to these metrics or inviting new approaches that can measure fairness across time or update decision mechanisms in a time varying manner. Future decisions can also be coupled to past decisions through their effect on the trajectory of a dynamical system. Furthermore, metrics for fairness should be measured, optimized, or constrained over time, coupling past and future decisions.

One setting in which decisions are coupled over time is in recommender systems, like those used to suggest movies or new products to consumers based on factors like demographics and search histories. The authors of [191] consider the metric of exact-k fairness implemented using a constrained Markov decision process to limit the level of disproportionate allocation of benefits between groups. The concept of amortized fairness is introduced in [192, 193] to ensure cumulative benefits are proportional to the cumulative merit over time in the setting of recommender systems.

Gupta and Kamble [194] introduce two new dynamic fairness metrics: (i) fairness-across time and (ii) fairness-in-hindsight. A "fair across time" decision must be fair relative to both the past and the future. In other words, "similar individuals must always receive similar treatment irrespective of when they arrive" [194]. A decision is "fair in hindsight" if the current decision is fair relative to the past decisions for similar individuals.

The above mentioned dynamic fairness metrics were selected because they show potential for easy translation into dynamic power systems problems. For additional examples of dynamic fairness metrics used in the ML literature, see [173].

8.2.2 Fairness in DER coordination

The investigation and incorporation of fairness, equity, and justice in power systems problems is an emerging area of interest [174]. One way of coordinating DERs is via electricity rate design, i.e., DER reactions to time- (and spatially-) varying electricity prices can shape their actions. Some papers leverage electricity rate design to achieve more equitable or just outcomes, e.g., [195]. However, DER coordination can be achieved more directly through control- and optimization-based approaches.

For example, aggregations of DERs, such as thermostatically controlled loads (TCLs) or batteries, can be controlled to provide grid balancing services. Control commands are allocated to DERs in real-time based on system needs. This type of control can lead to unequal cycling and degradation of batteries and TCLs, which reduces their lifespan, and unequal temperature excursions (comfort impacts) for TCLs. Ensuring fair impacts is important, and fairness here is usually defined as equality of impact, i.e., the burden of participation should be equally distributed, e.g., [196]. However, mechanisms for achieving this are rarely connected to fairness. For example, in the TCL control literature it is common to assess or penalize TCL switching as a proxy for degradation, but it is uncommon to consider the disparity in the number of additional switching actions per TCL across a population of TCLs in an aggregation.

An example of an optimization-based approach to achieve DER coordination, which has seen a significant focus on fairness recently, is the dynamic operating envelopes problem. DERs have the potential to improve reliability, decrease operating costs, and lower the environmental impacts of power system operations [179, 196]. However, if not properly managed, DERs can cause over- and under-voltages, over-current violations, and transformer overheating [181, 197]. The operating envelope problem determines the net power injection limits for each node in the network and updates them as system conditions change. These limits are known colloquially as dynamic operating envelopes, simply operating envelopes, or dynamic hosting capacity [122, 197]. Such limits can be obtained by solving modified optimal power flow (OPF) problems which maximize a function of power injections/consumption at every node subject to network constraints [120, 123].

Existing literature shows that an objective function which fails to consider fairness can lead to significant discrepancies in limit sizes across the network [112, 121, 124]. This is because power consumption/injections farther from the substation will generally have a larger impact on voltages due to the radial structure of distribution networks and the nonlinearities of power flow [183].

We will now discuss how fairness has thus far been considered in the context of operating envelopes. *Weighted proportional fairness*, defined by the statement "the gain of one party should be greater than the sum of the losses of all other parties together" [139], is applied to the allocation of prosumer export power in [139]. In [183], an optimization formulation is used to maximize overall export power while penalizing deviations in the power allocations at different connection points from the mean value aggregate allocated power. In [124], an optimization formulation is used to maximize overall export power while penalizing deviations in the power allocations from the specified capacity of each prosumer with respect to installed solar PV capacity. In [185] an unbalanced three phase optimal power flow com-

putes dynamic operating envelopes that are robust to uncertainties prioritizing proportional fairness. We note that all of these papers formulate single-period optimization problems and impose fairness objectives or constraints at each time, so fairness may change in each time, but is not optimized over time.

8.2.3 Comparing fairness landscapes

In both ML and power system landscapes, notions of fairness are often characterized by the distribution of benefits and/or burdens. Considering the dimension of time can present new conceptualizations of fairness. The ML time-varying fairness concepts can provide insight on how to extend notions of fairness in DER coordination problems to address their dynamic nature. For example, some notions of fairness include a cumulative component that can address the effects of decisions over time [192,193] and others introduce a notional of fairness that current decisions should be fair relative to past decisions [194].

8.3 Incorporating fairness

We aim to assist researchers in integrating fairness into power systems research by offering a straight-forward way to approach fairness and communicate how fairness is considered in one's work. In Section 8.4, we show the usefulness of this approach through a case study. We note that [182] has also contributed to the structuring of this emerging space by introducing four dimensions – *context*, *scope*, *interpretation of fairness* and *approach* – for characterizing existing approaches to fairness used in the local energy systems literature. In contrast, our work aims to provide a prescriptive approach to the incorporation of fairness into future problem formulations.

Assuming a strong understanding of the problem setting is established, we first recommend a researcher start by identifying qualitative concepts of fairness relevant to one's problem setting. For example, [198] introduces the notion of individual fairness which requires "mapping similar individuals similarly."

Secondly, the notion must be formalized mathematically. A good starting point is to identify a measurable quantity relevant the chosen notion of fairness and then define a condition (i.e., a metric) under which the state is (un)fair with respect to that quantity. The broader energy justice community has directed much effort toward generating, identifying, cataloging, and evaluating quantities that capture the role of energy in inequity or injustice [199–202]. The power systems community has adopted some of these concepts, for example, [203] uses the distribution of cumulative load shed during public safety power shutoffs used to prevent

wildfires and [46] considers its geographic overlap with vulnerable populations, as defined by the social vulnerability index. Other quantities include energy burden (energy expenditures divided by household income) and the energy equity gap [204].

Thirdly, approaches to fairness must identify a fair-decision-making mechanism suitable for the problem. Commonly used mechanisms are an algorithm, control design, or an optimization problem. Communicating each of these steps and the reason for one's choices enables readers to understand and compare approaches across different works.

8.4 Case study

8.4.1 Incorporating fairness: the operating envelope problem

We next describe how to leverage the approach in Section 8.3 to incorporate fairness into the operating envelope problem described in Section 8.2.2.

8.4.1.1 Notions of fairness

As described earlier, the first step in addressing fairness is to identify what could be considered fair. We will now do this for the operating envelope problem. One notion of fairness is that decisions should aim "to be fair in terms of the intended operation" of each DER [124]. In other words, each DER should be free to exploit their full realizable injection capability, if desired. However, binding network constraints necessitate curtailment of injections to ensure safe operation of the network. Another commonly used notion of fairness is maximizing the minimum benefit received by any user [205–207], also known as α-fairness [175] with $\alpha = \infty$. In the context of operating envelopes, this means maximizing the minimum operating envelope that any node receives. There are certainly other notions of fairness that can be applied to the operating envelope problem, but these are the notions we will consider in this chapter.

8.4.1.2 Mathematically formalizing fairness

Both of the above notions of fairness have drawbacks in the context of operating envelopes. The first notion, fairness in terms of intended operation, will maximize the total network flexibility and minimize individual curtailment. This motivates minimizing the sum of the squared curtailment at each node in the network. Squaring the curtailment will prioritize allocation of injection limits such that the distance from the limit to the full potential of the DER(s) at each node is similar across the nodes. However, minimizing the sum of the squared curtailment will bias the allocation to nodes with larger capacities. The second

notion of fairness, maximizing the minimum, ensures that the base injection limit that every node is allocated is as large as it can be. However, it does not maximize the limits at less constrained nodes, resulting in a missed opportunity for a greater total network flexibility. For these reasons, we will use a linear combination to minimize the squared curtailment at each node and maximize the smallest operating envelope in the network.

8.4.1.3 Identifying the fair decision-making mechanism

Neither of the two notions of fairness considered here are new in the context of operating envelopes. The contribution of this chapter is to bring the notion of fairness over time into the context of the operating envelope problem, and the DER coordination problem more generally.

The fair decision-making mechanism best suited for operating envelopes is optimization, where fairness is softly enforced in the objective function. In the literature, operating envelopes are calculated by solving an optimization problem for each time period. In this manner, operating envelope allocations from previous time periods have no impact on the current allocation decisions and fairness is enforced at each time period. Inspired by methods in ML literature, we propose two methods for enforcing fairness over time. The first method is to calculate all operating envelope allocations across a time horizon by solving a single, multi-period optimization problem where allocation decisions in one time period are coupled to decisions of the other time periods through fairness. The second method, inspired by amortized fairness, is to keep track of unfairness incurred from previous allocations and use this history of unfairness to influence current decisions. In the next section, we will detail the mathematical models for these methods in the operating envelope context.

8.4.2 Problem formulation

In this section, we detail the formulations of the operating envelope problem used in our case study. We use a nonlinear OPF formulation for calculating operating envelopes, which represent upper limits on the net export at every node. For brevity, we do not consider lower limits. The decision variables are p_i^{OE}, the operating envelope at each node i; p_{ij}, the active power flowing on the line from node i to node j; q_{ij}, the reactive power flowing on the line from node i to node j; $v_i = |V_i|^2$, the squared voltage magnitude at each node i; and $l_{ij} = |I_{ij}|^2$, the squared current magnitude on the line connecting nodes i and j. Operating envelopes p^{OE} can be found without considering fairness by solving

$$\max \sum_{i \in \mathcal{N}} p_i^{\mathrm{OE}} \tag{8.1a}$$

$$\text{s.t. } 0 \leq p_i^{\text{OE}} \leq p_i^f \quad \forall i \in \mathcal{N} \tag{8.1b}$$

$$\sum_{i:i\to j}(p_{ij} - r_{ij}l_{ij}) + p_j^{\text{OE}} = \sum_{k:j\to k} p_{jk},\ \forall j \in \mathcal{N} \tag{8.1c}$$

$$\sum_{i:i\to j}(q_{ij} - x_{ij}l_{ij}) - q_j^{\text{d}} = \sum_{k:j\to k} q_{jk},\ \forall j \in \mathcal{N} \tag{8.1d}$$

$$v_i = v_j + 2(r_{ij}p_{ij} + x_{ij}q_{ij}) - (r_{ij}^2 + x_{ij}^2)l_{ij},\ \forall j \in \mathcal{N} \tag{8.1e}$$

$$p_{ij}^2 + q_{ij}^2 = l_{ij}v_i, \quad \forall ij \in \mathcal{L} \tag{8.1f}$$

$$p_{ij}^2 + q_{ij}^2 \leq \overline{s}_{ij}^2,\ \forall ij \in \mathcal{L} \tag{8.1g}$$

$$\underline{v} \leq v_i \leq \overline{v},\ \forall i \in \mathcal{N} \tag{8.1h}$$

where p_i^{f} is the forecasted power injection at node i. Constraints (8.1c) and (8.1d) enforce active and reactive power balance [141], where notation $i : i \to j$ specifies the sum over all lines ij injecting power into j, and $k : j \to k$ specifies the sum over all lines jk consuming power from j. Constraint (8.1e) defines the voltage drop between bus i and the downstream bus j. Constraint (8.1f) defines the squared apparent power flowing from bus i to j and (8.1g) limits it. Finally, constraint (8.1h) enforces the voltage limits at each bus. This formulation assumes monotonicity, i.e., if p^{OE} defines a valid operating envelope, then any injection less than p^{OE} is feasible. We note that this may not always be true in practice since (8.1f) is nonconvex.[1] To calculate the operating envelopes across a time horizon, one could solve (8.1) for each time period. The formulation given in (8.1) will be henceforth referred to as the Unfair formulation.

To incorporate fairness as it has been previously done, the objective function is changed to align with the notions of fairness introduced in the previous subsection, giving

$$\min \sum_{i\in\mathcal{N}}(1-\lambda)\left(p_i^{\text{f}} - p_i^{\text{OE}}\right)^2 - \lambda\gamma \tag{8.2a}$$

$$\text{s.t.} (8.1\text{b}) - (8.1\text{h})$$

$$\gamma \leq p_i^{\text{OE}}, \forall i \in \mathcal{N} \tag{8.2b}$$

where λ is a weighting parameter. In this formulation, the second term in the objective function, along with (8.2b), maximizes the minimum operating envelope across the nodes. Like the Unfair formulation, this formulation is a single-period problem that can be solved for each time period in a time horizon. The formulation given in (8.2) will be henceforth referred to as the Fair at Each Time (FET) formulation.

[1] Often a linear approximation of the power flow equations is used for scalability or a convex restriction is used to ensure there are no gaps in the feasible region of the operating envelopes [123]; however, linearizations are inaccurate and convex restrictions can be conservative and/or hard to find.

The first method we propose to incorporate fairness over time is to calculate all operating envelopes across a time horizon using a single, multi-period optimization problem, such as

$$\min \sum_{i \in \mathcal{N}} (1-\lambda) \left[\sum_{t \in \mathcal{T}} \left(p^{\mathrm{f}}_{i,t} - p^{\mathrm{OE}}_{i,t} \right)^2 \right] - \lambda \gamma \tag{8.3a}$$

$$\text{s.t. } 0 \leq p^{\mathrm{OE}}_{i,t} \leq p^{f}_{i,t} \quad \forall i \in \mathcal{N}, \forall t \in \mathcal{T} \tag{8.3b}$$

$$\sum_{i:i \to j} (p_{ij,t} - r_{ij} l_{ij,t}) + p^{\mathrm{OE}}_{j,t} = \sum_{k:j \to k} p_{jk,t}, \ \forall j \in \mathcal{N}, \forall t \in \mathcal{T} \tag{8.3c}$$

$$\sum_{i:i \to j} (q_{ij,t} - x_{ij} l_{ij,t}) - q^{\mathrm{d}}_{j,t} = \sum_{k:j \to k} q_{jk,t}, \ \forall j \in \mathcal{N}, \forall t \in \mathcal{T} \tag{8.3d}$$

$$v_{i,t} = v_{j,t} + 2(r_{ij} p_{ij,t} + x_{ij} q_{ij,t}) - (r^2_{ij} + x^2_{ij}) l_{ij,t}, \ \forall j \in \mathcal{N}, \forall t \in \mathcal{T} \tag{8.3e}$$

$$p^2_{ij,t} + q^2_{ij,t} = l_{ij,t} v_{i,t}, \quad \forall ij \in \mathcal{L}, \forall t \in \mathcal{T} \tag{8.3f}$$

$$p^2_{ij,t} + q^2_{ij,t} \leq \overline{s}^2_{ij}, \quad \forall ij \in \mathcal{L}, \forall t \in \mathcal{T} \tag{8.3g}$$

$$\underline{v} \leq v_{i,t} \leq \overline{v}, \quad \forall i \in \mathcal{N}, \forall t \in \mathcal{T} \tag{8.3h}$$

$$\gamma \leq \sum_{t \in \mathcal{T}} p^{\mathrm{OE}}_{i,t}, \forall i \in \mathcal{N} \tag{8.3i}$$

where the second term in the objective function, along with (8.3i), maximizes the minimum across all nodes of the sum of OE allocations over the time horizon and the variable γ couples the allocation decisions across time periods. The formulation given in (8.3) will be henceforth referred to as the Fair Over Time (FOT) formulation. In a stochastic setting, this could be implemented with model predictive control (MPC) and/or stochastic optimization.

The second method we propose for enforcing fairness over time is to incorporate the history of unfairness. This method of incorporating fairness can be formulated as either a single-period problem to be solved once for each time period in the time horizon, as with the Unfair and FET formulations. Alternatively, it could be formulated as an MPC problem where a time horizon $1, ..., T$ is divided into smaller time periods $\tau_1, ..., \tau_2$, and a series of multi-period problems could be solved sequentially to obtain allocations for the entire horizon. In this chapter, we use the former approach for simplicity. Given a function that captures past unfairness for node i, $H^{\mathrm{OE}}_{i,\tau_1}$, the Fair using History (FUH) formulation is

$$\min \sum_{i \in \mathcal{N}} (1-\lambda) \left[\sum_{t=\tau_1}^{\tau_2} H^{\mathrm{OE}}_{i,\tau_1} \left(p^{\mathrm{f}}_{i,t} - p^{\mathrm{OE}}_{i,t} \right)^2 \right] - \lambda \gamma \tag{8.4a}$$

$$\text{s.t.} (8.3\text{b}) - (8.3\text{h}) \text{ with } \mathcal{T} \text{ replacedwith } [\tau_1, \tau_2]$$

$$\gamma \leq \sum_{t \in [\tau_1, \tau_2]} p^{\mathrm{OE}}_{i,t}, \forall i \in \mathcal{N} \tag{8.4b}$$

Here, we define H^{OE}_{i,τ_1} as the weighted moving average of the squared power injection curtailment at node i at time τ, i.e.,

$$H^{\text{OE}}_{i,\tau_1} = \frac{k\left(p^{\text{OE}}_{i,\tau_1-1} - p^{\text{r}}_{i,\tau_1-1}\right)^2 + ... + \left(p^{\text{OE}}_{i,\tau_1-k} - p^{\text{r}}_{i,\tau_1-k}\right)^2}{k + (k-1) + ... + 2 + 1} \tag{8.5}$$

where $p^{\text{r}}_{i,\tau}$ is the realizable power injection at node i at time τ. In this chapter, we assume perfect forecasting such that $p^{\text{r}}_{i,\tau} = p^{\text{f}}_{i,\tau}$, but the formulation is written in a general form.

8.4.3 Results

The network used in the case study is the 56-bus balanced distribution network introduced in [1], with no capacitor banks and only a single voltage regulator at the substation. The voltage at the substation is set to 1.02 pu and the bounds on the voltages are $\underline{v} = 0.95$ pu and $\overline{v} = 1.05$ pu. The load in the network varies over time, but every node has the same load at each time. Every node has exactly one DER but the power injection capacity varies randomly across both nodes and time. Table 8.1 shows our quantitative results across the four formulations in terms of total network flexibility (performance) and fairness in terms of the smallest operating envelope, and the variances of both the operating envelope allocations and total curtailment across the nodes. For the three fair formulations, the results are given for three values of λ. Table 8.1 shows that the unfair formulation, (8.1), results in the largest total network flexibility but in the least fair allocation of operating envelopes over the time horizon based on both notions of fairness. FET results in slightly larger total flexibility than FOT, with the gap between them increasing with increasing λ. However, FOT results in the largest smallest operating envelope and the smallest variance in operating envelopes for each value of λ. The two formulations result in similar curtailment variances. For each value of λ, FUH results in the smallest network flexibility but also the smallest variance for both operating envelopes and curtailment.

Figures 8.1, 8.2, and 8.3 show the results for $\lambda = 0.5$. The total accumulated operating envelope allocation at each node is shown for each formulation in Fig. 8.1. Figure 8.1(a) shows that the Unfair formulation allocates large upper limits consistently to some nodes, and very small or even zero allocations to nodes at the feeder's ends. Figure 8.1(b) shows that FOT gives similar allocations to FET, but is able to increase the allocation of more constrained nodes without sacrificing much allocation from the other nodes. Figure 8.2 shows similar trends to the accumulated allocations, but shows the percentage of capacity curtailed at each node over the time horizon. This illustrates how the formulations compare with respect to the notion of fairness in intended operation. Under this notion, all the bars

Table 8.1: Performance vs. Fairness

λ	Formulation	Smallest Allocation	OE Variance	Curtailment Variance	Network Flexibility
	Unfair	0	17.76	14.91	276.0
0.25	FOT	2.23	3.63	2.70	253.9
	FET	1.44	3.73	2.71	254.3
	FUH	1.99	2.35	0.93	236.4
0.5	FOT	2.53	3.50	2.68	253.3
	FET	1.44	3.72	2.71	254.2
	FUH	2.03	1.74	0.94	235.7
0.75	FOT	2.93	3.23	2.72	251.9
	FET	1.44	3.73	2.71	254.2
	FUH	1.95	1.99	0.94	236.8

OE stands for Operating Envelope

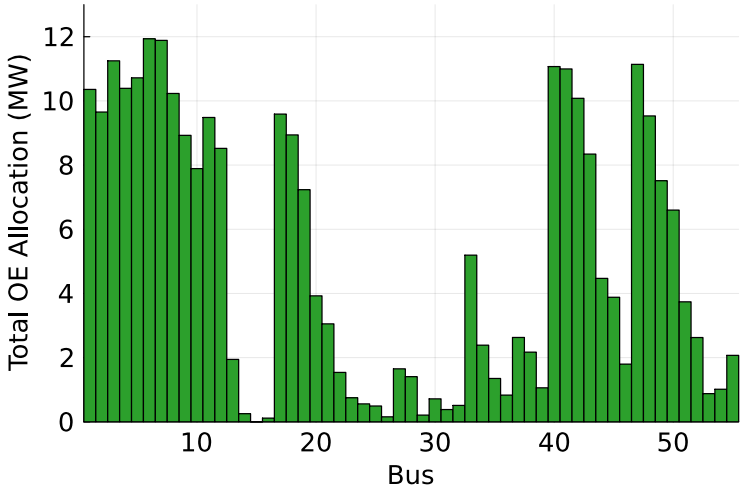
in Fig. 8.2 would be the same height for the fairest outcome.

The amount of injection capacity in the network also impacts the results. In Table 8.2, results for each formulation are shown as the DER capacities are uniformly increased. The first column in the table represents the multiplier, ω, on the nominal capacity value, where a multiplier of 1 implies capacities are at their nominal values. For these test cases, the second term in the objective function for all three fair formulations was multiplied by ω to maintain a similar weight distribution in the objectives. In the case where $\omega = 0.1$, all of the nodes can inject at their full capacities without violating network constraints, resulting in no or negligible curtailment except for under FUH. As the need for curtailment increases with increasing capacity, FOT is able to outperform FET in terms of network flexibility while maintaining better max-min fairness and comparable fairness of intended operation.

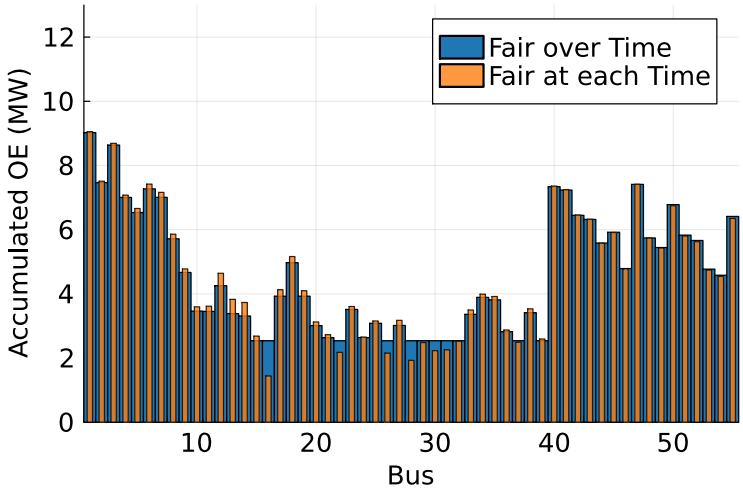
Figure 8.3 illustrates the impact of biasing the current decisions using the historical unfairness. The light blue bars represent the operating envelope allocation in the first time step and the orange bars represent the weighted moving average of historical unfairness at the end of the time horizon. The level of fairness at the end of the time horizon is significantly higher than the level of fairness at the beginning.

8.5 Chapter Conclusions

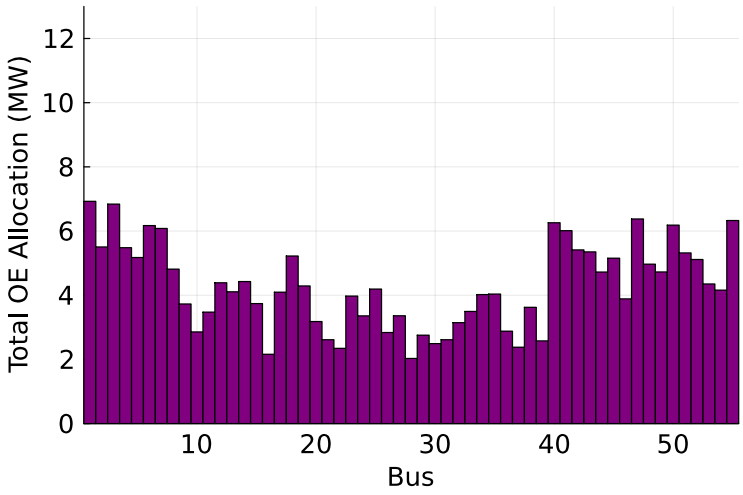
In this chapter, we discussed time-varying fairness approaches from ML literature and compared them with fairness approaches that have been previously implemented in DER coordination literature. From this analysis, we outlined a principled method for incorporating fairness into power systems problems: 1) Identify relevant notion(s) of fairness, 2) mathemat-



(a) Unfair formulation

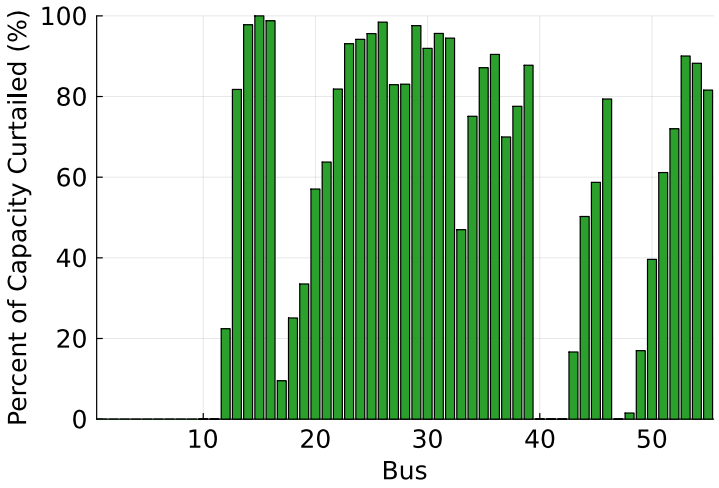


(b) Fair Over Time and Fair at Each Time formulations

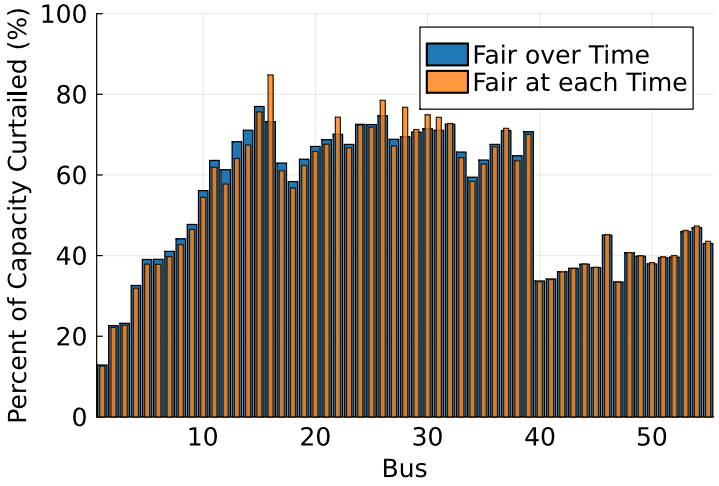


(c) Fair Using History Formulation

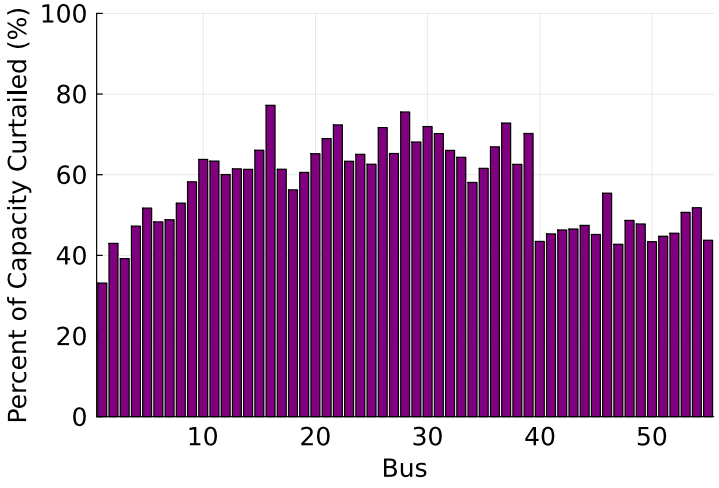
Figure 8.1: Accumulated operating envelope allocation at each node in the network



(a) Unfair formulation



(b) Fair Over Time and Fair at Each Time formulations



(c) Fair Using History Formulation

Figure 8.2: Total percentage of forecasted capacity curtailed over the time horizon, $\frac{\sum_{t\in\mathcal{T}} p^f_{i,t} - p^{\mathrm{OE}}_{i,t}}{\sum_{t\in\mathcal{T}} p^f_{i,t}}$, at each node in the network

Table 8.2: Performance vs. Fairness as DER Capacities Increase

ω	Formulation	Smallest Allocation	Variance		Network Flexibility
			OE	Curtailment	
0.1	Unfair	0.789	0.011	0	54.44
	FOT	0.789	0.011	0	54.37
	FET	0.787	0.011	0	54.38
	FUH	0.668	0.010	0	47.00
1	Unfair	0	17.76	14.91	276.0
	FOT	2.53	3.50	2.68	253.4
	FET	1.44	3.72	2.71	254.3
	FUH	2.03	1.99	0.94	235.7
3	Unfair	0	108.11	93.96	331.14
	FOT	1.74	20.48	19.38	287.68
	FET	0.74	20.76	19.36	287.03
	FUH	0.72	9.13	7.10	264.26

ω is the DER capacity multiplier, OE stands for Operating Envelope

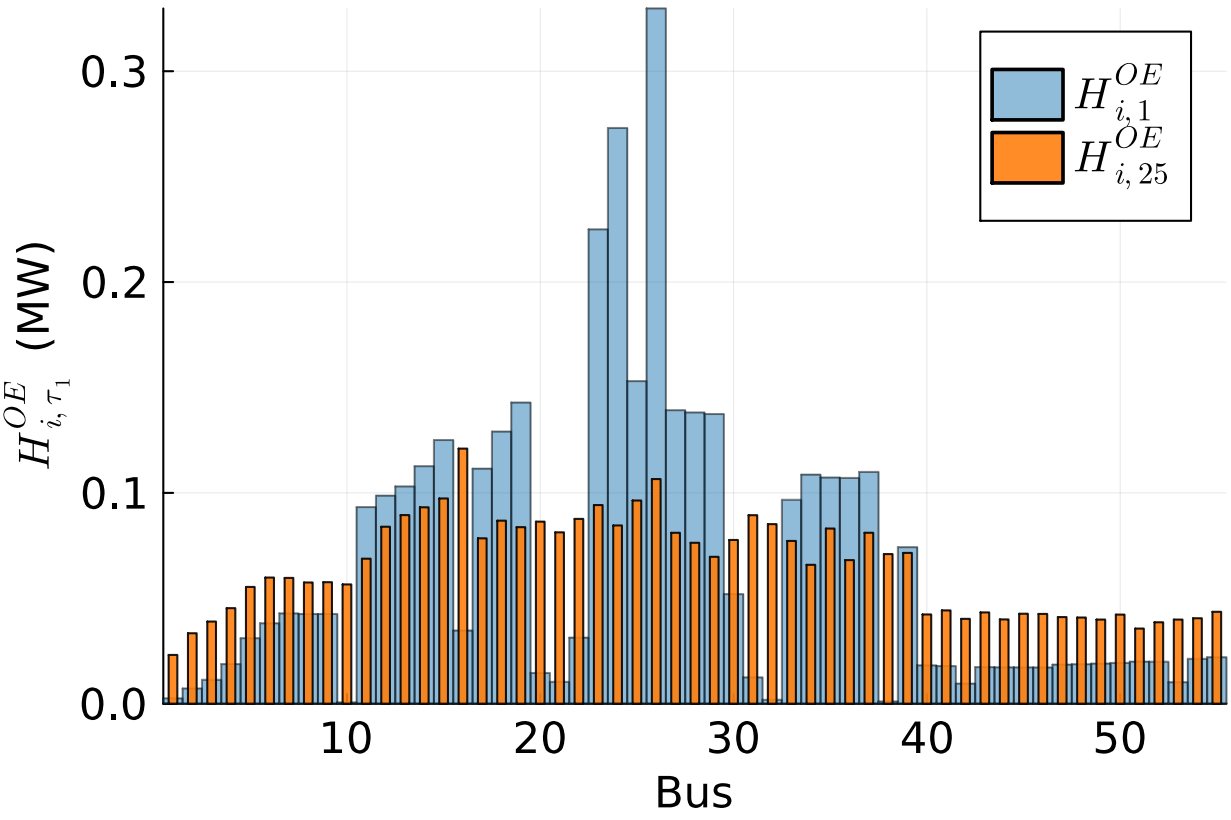


Figure 8.3: Comparison between the operating envelope allocation in the first time step, $H^{\text{OE}}_{i,1}$, and the weighted average of historical unfairness at the end of the time horizon, $H^{\text{OE}}_{i,25}$.

ically formalize the notion(s) of fairness, and 3) identify the fair-decision-making mechanism. By following these steps, authors can help other researchers efficiently assess relevance, compare approaches, and integrate key fairness methods into their own work.

Inspired by time-varying fairness approaches from the ML literature, we proposed incorporating fairness over time and illustrated the concept using the operating envelope problem. Results from the case study suggest that enforcing fairness over time rather than at every time step can lead to fairer outcomes without sacrificing total network flexibility, as compared to existing fair operating envelope implementations.

In future work, we aim to extend the notion of fairness over time to other DER coordination problems, and to explicitly consider fairness with respect to monetary costs/benefits.

CHAPTER 9

Conclusions and Directions of Future Work

Distributed energy resources (DERs) represent a potential tool in the progress towards a sustainable, reliable, resilient, and just power system, but they also have the potential to introduce new problems and exacerbate existing ones. This thesis analyzed existing strategies, proposed improvements to existing strategies, and presented new strategies for managing the operation of DERs.

9.1 Summary of Key Results

In Chapter 2 we compared the strategies employed by two U.S. Independent System Operators (ISOs) to manage the energy constraints of energy storage systems providing frequency regulation. We modeled the controllers used by the ISOs and simulated the strategies with real-world data, comparing them in terms of performance and system impact. We also discussed impacts on system resource requirements, and the impact of market regulations on practicality. Our analysis showed that while both strategies work, the CAISO strategy has a smaller system impact and places no limits on the amount of regulation that storage can provide. However, corresponding market rules within CAISO make the strategy underutilized while the PJM strategy has had such successful utilization that participation must be limited.

In Chapter 3 we formulated a robust optimization problem for partitioning distribution networks into microgrids to minimize load shedding and generator costs during contingencies, accounting for load uncertainty. We modeled loads as uncertain sets and use a robust formulation to ensure operational feasibility for all potential loads. We formulated a two-stage infinite-dimensional mixed-integer nonlinear optimization problem and then reformulated it for computational tractability. The first stage of the reformulated problem is a mixed-integer quadratic program that optimizes network partitioning decisions to minimize load shedding and generator costs given nominal loads. After the load uncertainty is revealed, generator

set-points are adjusted subject to linearized three-phase, unbalanced power flow in the second stage. To solve the problem, we developed a novel cutting-plane algorithm. A detailed numerical study highlighted the benefits of networked microgrids and the significance of considering load uncertainty during reconfiguration. We also demonstrated the feasibility of solutions obtained from the reformulated problem against nonlinear power flow through a sampling approach.

In Chapter 4 we improved upon the robust partitioning problem and cutting-plane algorithm developed in Chapter 3. We added a few additional constraints to the problem formulation to enhance the selection of grid-forming DERs (GFM-DERs). In addition, we added the LinDist3Flow equations for a single load scenario to the Master problem and simplified the uncertainty modeling using clusters. Both of these changes together led to significantly faster convergence of the cutting-plane algorithm and the ability to scale the algorithm to large, realistic networks. We also presented a model-free, real-time optimal power flow (OPF) algorithm for operating the dynamic networked microgrids (DNMGs) between reconfigurations. Lastly, we presented both algorithms in tandem on a synthetic SMART-DS distribution network composed of DNMGs. The case study results illustrated the improvements in solve time and scalability due to the modifications of the partitioning problem formulation. The case study also illustrated the ability of both algorithms, when used together, to maintain power flow feasibility despite loads variability.

In Chapter 5 we compared network-wide and nodal constraints for ensuring network-safe operation in the presence of a DER aggregation. We discussed information and communication requirements, then compared technical performance via a case study. For the nodal approach, we used an operating envelope framework with two objective functions: one maximizing the sum of the envelopes across the network and one maximizing the smallest operating envelope in the network to more equitably allocate flexibility. For the network-wide approach, we used the method proposed in [208] to compute a constraint on the input of the aggregator's controller. The case study illustrated how the approaches, and the consideration of fairness, impact the aggregate flexibility. A key takeaway from this analysis is that each approach is only feasible under specific rules or market frameworks, meaning flexibility objectives should be considered when designing the market structures and regulations.

In Chapter 6 we analyzed the impact of using a second-order cone (SOC) relaxation of the power flow equations when computing operating envelopes. Specifically, we presented two case studies and brief numerical analysis illustrating the inadequacy of the SOC relaxation for constructing operating envelopes to enforce voltage limits. We then proposed an objective function modification to improve the exactness of the SOC relaxation and illustrated its efficacy.

In Chapter 7 we built on the work in Chapter 6. We first presented a larger, more realistic case study that illustrated that the problem revealed in the small case studies in Chapter 6 worsens as the network size and complexity increases. We also illustrated that while the proposed objective function modification can still be used to determine network-safe operating envelopes, the modification may not give a solution similar to the optimal solution of the original, nonlinear problem and it also may not lead to an exact relaxation. Furthermore, we explored the conditions under which the SOC relaxation is and is not exact for the operating envelope problem. Previous examples, in both our prior work and in the literature, all produced inexact solutions, suggesting that the relaxation would always be inexact. After multiple failed attempts to prove that the SOC would always be inexact, we analytically demonstrated, for the first time, that there were in fact conditions under which the relaxation was exact for the operating envelope problem. We also documented that there are likely multiple sets of conditions under which the relaxation is exact and also multiple sets of conditions under which the relaxation is not exact for the operating envelope problem. For the simplified cases of radial, purely reactive and radial, purely resistive networks, we proved that the SOC relaxation is and is not exact, respectively, for the operating envelope problem.

In Chapter 8 we explored fairness metrics from machine learning literature and investigated their applicability to the DER coordination problem. Inspired by the inherently dynamic nature of the DER coordination problem, we proposed a fair-over-time metric and demonstrated its benefits using the operating envelope problem. Our novel approach permitted the solution to be unfair at any time step but required that the solution be fair over the entire time horizon. Results in this chapter suggest that enforcing fairness over time rather than at every time step can lead to fairer outcomes without sacrificing total network flexibility, as compared to existing fair operating envelope implementations.

9.2 Future Work

The work in this dissertation has lead to many potential directions for future research. In this section, we will outline those directions, separated by project.

9.2.1 Managing the Energy Constraints of Energy Storage

- *Consider the perspective of a storage owner:* The work in Chapter 2 compared how the two ISO strategies for managing the energy constraints of battery energy storage providing frequency regulation performed from a system level. Our analysis showed

that while the CAISO strategy has less impact on the system, it is underutilized because it is not appealing to the storage owners. It would be insightful to analyze the two strategies from the point of view of a storage owner/operator.

- *Develop an improved mechanism for managing the energy constraints of energy storage providing frequency regulation:* The insights gained from our comparison, and possibly a comparison of the strategies from the storage owners' perspective, could be used to design a new mechanism that is desirable from both the perspective of the ISO and the perspective of the battery owner.

9.2.2 Dynamic Networked Microgrids

- *Incorporate energy storage:* Energy storage can provide valuable flexibility to the operation of DNMGs. We would like to incorporate energy storage into both the reconfiguration algorithm and the real-time OPF algorithm. Doing so will require careful consideration of how to model the non-convex complementarity constraints to prevent simultaneous charging and discharging. Special care will also be needed to ensure the subproblem retains full recourse. Another challenge, for both the reconfiguration algorithm and the real-time OPF algorithm, will be modeling the time-coupled nature of energy storage.

- *Reduce the conservativeness of the reconfiguration solutions:* Robust optimization is known for producing relatively conservative solutions. In Chapter 4, the case study results illustrated particularly how conservative the reconfiguration solution based on uncertain load clustering was. It is desirable to reduce the level of conservativeness and potentially further reduce the amount of load shed during a contingency. Dynamic uncertainty sets, like those presented in [209], or distributionally robust optimization [77] could be leveraged.

- *Model generation uncertainty:* In this dissertation, we considered load uncertainty but did not consider the uncertainty inherent in some distributed generation like PV. In future work, we would like to include generational uncertainty in the problem formulation.

9.2.3 Network-Safe DER Operation

- *MPC implementation of fair-over-time:* In Chapter 8, we introduced an approach for enforcing fairness over time rather than at each point in time in the context of

operating envelopes. In future work, we would like to implement this approach using model-predictive control.

- *Economically fair operating envelopes:* The work on fair operating envelopes in this dissertation and in the literature has focused on physically fair operating envelopes, i.e., the distribution of physical power injection/consumption limits should be fair according to some metric. In general, DER owners care about their ability to gain financially from power exports but not explicitly the amount of power that they export. The relationship between financial gain and actual use of resources is more complex for demand response/load flexibility, so for now, we will focus on net power exports. Typically payment is directly tied to the amount exported, but it does not necessarily have to be. Consider a scenario where a DER aggregator manages a fleet of DERs connected to various nodes across a distribution network to provide energy services in the wholesale electricity market. At any point in time, the aggregator wants to maximize the power injection (or load flexibility) capacity for providing services but because of network constraints, this may sometimes require treating the DERs unfairly, based on their location within the feeder. However, it may be in the aggregator's best interest to treat the DERs fairly in order to prevent alienating DER owners and loosing resources. This motivates the design of a fair payment system for DER flexibility.

- *Convex inner-approximation:* In Chapters 5-8, we have presented formulations for computing the upper or low limits of net power injections, i.e., operating envelopes. An underlying assumption, in both our work and similar works, is that any net injection between the lower and upper limits would yield voltages within network limits. This assumption holds when the relationship between voltage magnitudes and power injections is monotonic, but this is not always the case, as illustrated in [123]. In future work, we would like to develop a formulation for computing operating envelopes that provably guarantees that all possible power injections between the upper and low limits at every node will yield allowable voltages.

9.3 Concluding Remarks

In this dissertation, we explored the challenges and opportunities created by the operation of DERs. Generally, we learned that the success of a novel algorithm or technological innovation is dependent not only on how well it works, but also on its economic and political context. With smaller system impact and laxer requirements on resource mix needs, the CAISO strategy for managing the energy constraints of energy storage providing frequency

regulation appears to be better than the PJM strategy. However, market rules and economic incentives have made the PJM strategy far better utilized. This observation ties in with the takeaways from the nodal versus network-wide constraint comparison, namely that market regulations dictate what new technologies or control strategies are possible. Market rules and structures should carefully consider what limitations they might introduce and they should be adaptable and responsive to new technologies. Another high level takeaway from this dissertation is that as the grid becomes more distributed and more decentralized, both the technical and socioeconomic aspects of its operation will become more complex. As our energy system progresses, it will become increasingly important to consider how changes impact all participants and to design novel solutions with equity in mind.

BIBLIOGRAPHY

[1] S. Bolognani and S. Zampieri, "On the existence and linear approximation of the power flow solution in power distribution networks," *IEEE Transactions on Power Systems*, vol. 31, no. 1, pp. 163–172, 2016.

[2] R. D. Zimmerman, C. E. Murillo-Sánchez, and R. J. Thomas, "MATPOWER: Steady-state operations, planning, and analysis tools for power systems research and education," *IEEE Transactions on Power Systems*, vol. 26, no. 1, pp. 12–19, 2011.

[3] IEA, "Global energy review 2025," IEA, Tech. Rep., 2025.

[4] IEA, "Unlocking the potential of distributed energy resources," IEA, Tech. Rep., 2022.

[5] B. Brinkmann and M. Negnevisky, "A practical approach to observability analysis and state estimation in distribution networks," in *2016 IEEE Power and Energy Society General Meeting (PESGM)*, 2016, pp. 1–5.

[6] M. Singh, "Protection coordination in distribution systems with and without distributed energy resources- a review," *Protection and Control of Modern Power Systems*, vol. 2, 2017.

[7] K. Bond, S. Butler-Sloss, D. Walter, H. Benham, E. Klock-McCook, D. Mullaney, Y. Numata, L. Speelman, C. Stranger, and N. Topping, "X-change: Cars," Rocky Mountain Institute, Tech. Rep., 2023.

[8] S. Alshahrani, M. Khalid, and M. Almuhaini, "Electric vehicles beyond energy storage and modern power networks: Challenges and applications," *IEEE Access*, vol. 7, pp. 99 031–99 064, 2019.

[9] H. Shareef, M. M. Islam, and A. Mohamed, "A review of the stage-of-the-art charging technologies, placement methodologies, and impacts of electric vehicles," *Renewable and Sustainable Energy Reviews*, vol. 64, pp. 403–420, 2016.

[10] M. Yao, D. K. Molzahn, and J. L. Mathieu, "An optimal power-flow approach to improve power system voltage stability using demand response," *IEEE Transactions on Control of Network Systems*, vol. 6, no. 3, pp. 1015–1025, 2019.

[11] C. Liu, K. T. Chau, D. Wu, and S. Gao, "Opportunities and challenges of vehicle-to-home, vehicle-to-vehicle, and vehicle-to-grid technologies," *Proceedings of the IEEE*, vol. 101, no. 11, pp. 2409–2427, 2013.

[12] D. Fischer and H. Madani, "On heat pumps in smart grids: A review," *Renewable and Sustainable Energy Reviews*, vol. 70, pp. 342–357, 2017.

[13] Federal Energy Regulatory Commission, "Order No. 2222, Participation of distributed energy resource aggregations in markets operated by regional transmission organizations and independent system operators," Federal Energy Regulatory Commission, 2020.

[14] B. Kroposki, A. Bernstein, J. King, D. Vaidhynathan, X. Zhou, C.-Y. Chang, and E. Dall'Anese, "Autonomous energy grids: Controlling the future grid with large amounts of distributed energy resources," *IEEE Power and Energy Magazine*, vol. 18, no. 6, pp. 37–46, 2020.

[15] N. Efkarpidis, T. De Rybel, and J. Driesen, "Technical assessment of centralized and localized voltage control strategies in low voltage networks," *Sustainable Energy, Grids and Networks*, vol. 8, pp. 85–97, 2016.

[16] National Renewable Energy Laboratory, "Valuing resilience in electric systems," 2022.

[17] M. Ebad and W. M. Grady, "An approach for assessing high-penetration PV impact on distribution feeders," *Electric Power Systems Research*, vol. 133, pp. 347–354, 2016.

[18] N.-K. C. Nair and L. Jing, "Power quality analysis for building integrated PV and micro wind turbine in new zealand," *Energy and Buildings*, vol. 58, pp. 302–309, 2013.

[19] A. R. Di Fazio, M. Russo, and M. De Santis, "Decentralized voltage optimization based on network partitioning in distribution systems with DGs," in *2019 1st International Conference on Energy Transition in the Mediterranean Area (SyNERGY MED)*, 2019, pp. 1–6.

[20] G. Mokhtari, A. Ghosh, G. Nourbakhsh, and G. Ledwich, "Smart robust resources control in LV network to deal with voltage rise issue," *IEEE Transactions on Sustainable Energy*, vol. 4, no. 4, pp. 1043–1050, 2013.

[21] N. A. Efkarpidis, S. Imoscopi, M. Geidl, A. Cini, S. Lukovic, C. Alippi, and I. Herbst, "Peak shaving in distribution networks using stationary energy storage systems: A Swiss case study," *Sustainable Energy, Grids and Networks*, vol. 34, p. 101018, 2023.

[22] Y. Lin, P. Barooah, and J. L. Mathieu, "Ancillary services through demand scheduling and control of commercial buildings," *IEEE Transactions on Power Systems*, vol. 32, no. 1, pp. 186–197, 2017.

[23] L. Bird, M. Milligan, and D. Lew, "Integrating variable renewable energy: Challenges and solutions," 2013.

[24] P. Denholm, J. Jorgenson, M. Hummon, T. Jenkin, D. Palchak, B. Kirby, O. Ma, and M. O'Malley, "The value of energy storage for grid applications," National Renewable Energy Laboratory, Tech. Rep., 2013.

[25] I. M. Granitsas, I. A. Hiskens, and J. L. Mathieu, "Incorporating delayed temperature dynamics into residential air conditioner models for grid frequency regulation," in *2022 IEEE Conference on Control Technology and Applications (CCTA)*, 2022, pp. 439–446.

[26] S. A. Nugroho, I. M. Granitsas, J. L. Mathieu, and I. A. Hiskens, "Aggregate modeling and non-disruptive control of residential air conditioning systems with two-zone cooling capacity," in *2022 American Control Conference (ACC)*, 2022, pp. 4668–4675.

[27] D. T. Ton and M. A. Smith, "The U.S. Department of Energy's microgrid initiative," *The Electricity Journal*, 2012.

[28] V. Donde, A. Pratt, A. Bernstein, J. Flicker, A. Madduri, C. R. Ben Ollis, R. Singh, J. Tabarez, and F. Tuffner, "Microgrids as a building block for future grids – topic 4," 2022.

[29] M. Ferrari, B. Ollis, M. Starke, and A. Massol-Deya, "Why the next microgrids will be well connected," *IEEE Spectrum*, 2023.

[30] S. Bahramirad, A. Khodaei, J. Svachula, and J. R. Aguero, "Building resilient integrated grids: One neighborhood at a time," *IEEE Electrification Magazine*, vol. 3, no. 1, pp. 48–55, 2015.

[31] B. Chen, J. Wang, X. Lu, C. Chen, and S. Zhao, "Networked microgrids for grid resilience, robustness, and efficiency: A review," *IEEE Transactions on Smart Grid*, vol. 12, no. 1, pp. 18–32, 2021.

[32] H. Yang, D. P. Morton, C. Bandi, and K. Dvijotham, "Robust optimization for electricity generation," *INFORMS Journal on Computing*, vol. 33, no. 1, pp. 336–351, 2021.

[33] A. Gholami, T. Shekari, F. Aminifar, and M. Shahidehpour, "Microgrid scheduling with uncertainty: The quest for resilience," *IEEE Transactions on Smart Grid*, vol. 7, no. 6, pp. 2849–2858, 2016.

[34] U.S. Energy Information Administration, "Battery storage in the United States: An update on market trends," 2021.

[35] Federal Energy Regulatory Commission, "Order No. 755, Frequency regulation competition in organized wholesale power markets," Federal Energy Regulatory Commission, 2011.

[36] PJM, "History of regulation market reform efforts," 2022.

[37] Federal Energy Regulatory Commission, "Order No. 841, Electric storage participation in markets operated by regional transmission organizations and independent system operators," Federal Energy Regulatory Commission, 2018.

[38] M. Heidarifar, N. Singhal, E. Ela, E. Lannoye, and L. Kristov, "Distributed energy resource aggregation participation in organized markets," Electric Power Research Institute (EPRI), Tech. Rep., 2021.

[39] S. Baker, S. DeVar, and S. DeVar, "Section 1 – defining energy justice: Connections to environmental justice, climate justice, and the just transition," 2019, accessed: Feb. 29, 2024.

[40] T. G. Reames, "Distributional disparities in residential rooftop solar potential and penetration in four cities in the United States," *Energy Research & Social Science*, vol. 69, 2020.

[41] D. Sunter, S. Castellanos, and D. Kammen, "Disparities in rooftop photovoltaics deployment in the United States by race and ethnicity," *Nature Sustainability*, vol. 2, pp. 71–76, 2019.

[42] H. A. U. Khan, S. Price, C. Avraam, and Y. Dvorkin, "Inequitable access to EV charging infrastructure," *The Electricity Journal*, vol. 35, no. 3, 2022.

[43] A. Brockway, J. Conde, and D. Callaway, "Inequitable access to distributed energy resources due to grid infrastructure limits in California," *Nature Energy*, vol. 6, p. 892–903, 2021.

[44] H. Moring and J. L. Mathieu, "Scheduling battery energy storage systems under battery capacity degradation uncertainty," in *2022 American Control Conference (ACC)*, 2022, pp. 5300–5307.

[45] J. L. Mathieu, M. Kamgarpour, J. Lygeros, and D. S. Callaway, "Energy arbitrage with thermostatically controlled loads," in *2013 European Control Conference (ECC)*, 2013, pp. 2519–2526.

[46] S. Taylor, G. Setyawan, B. Cui, A. Zamzam, and L. A. Roald, "Managing wildfire risk and promoting equity through optimal configuration of networked microgrids," in *Proceedings of the 14th ACM International Conference on Future Energy Systems*, ser. e-Energy '23. New York, NY, USA: Association for Computing Machinery, 2023, p. 189–199.

[47] E. Balogun, S. Martin, A. Degleris, and R. Rajagopal, "Equitable dynamic electricity pricing via implicitly constrained dual and subgradient methods," in *2023 IEEE International Conference on Communications, Control, and Computing Technologies for Smart Grids (SmartGridComm)*, 2023, pp. 1–7.

[48] H. Moring and J. L. Mathieu, "A comparison of strategies for managing energy constraints of energy storage providing frequency regulation," in *Proceedings of the 56th Hawaii International Conference on System Sciences (HICSS)*, 2023.

[49] T. Bowen, I. Chernyakhovskiy, and P. Denholm, "Grid-scale battery storage: Frequently asked questions," 2019.

[50] A. Ingalalli, A. Luna, V. Durvasulu, T. M. Hansen, R. Tonkoski, D. A. Copp, and T. A. Nguyen, "Energy storage systems in emerging electricity markets: Frequency regulation and resiliency," in *IEEE Power Energy Society General Meeting (PESGM)*, 2019.

[51] R. Sioshansi, P. Denholm, and T. Jenkin, "Market and policy barriers to deployment of energy storage," *Economics of Energy & Environmental Policy*, vol. 1, no. 2, pp. 47–64, 2012.

[52] O. Leitermann, "Energy storage for frequency regulation on the electric grid," Ph.D. dissertation, Massachusetts Institute of Technology, 2012.

[53] PJM, "Implementation and rationale for PJM's conditional neutrality regulation signals," 2017.

[54] CAISO, "Non-generator resource (NGR) and regulation energy management (REM) overview – phase 1," 2014.

[55] ——, "Regulation energy management draft final proposal," 2011.

[56] M. Kintner-Meyer, "Regulatory policy and markets for energy storage in North America," *Proceedings of the IEEE*, vol. 102, no. 7, pp. 1065–1072, 2014.

[57] C. A. Agostini, F. A. Armijo, C. Silva, and S. Nasirov, "The role of frequency regulation remuneration schemes in an energy matrix with high penetration of renewable energy," *Renewable Energy*, vol. 171, pp. 1097–1114, 2021.

[58] L. Meng, J. Zafar, S. K. Khadem, A. Collinson, K. C. Murchie, F. Coffele, and G. M. Burt, "Fast frequency response from energy storage systems—a review of grid standards, projects and technical issues," *IEEE Transactions on Smart Grid*, vol. 11, no. 2, pp. 1566–1581, 2020.

[59] C. Loutan, V. Gevorgian, S. Chowdhury, M. Bosanac, and E. Kester, "Avangrid Renewables Tule Wind Farm: Demonstration of capability to provide essential grid services," 2020.

[60] International Renewable Energy Agency, "Electricity storage and renewables: Costs and markets to 2030," 2017.

[61] L. Walter, "PJM energy storage participation model: Energy market," 2019.

[62] B. Xu, Y. Dvorkin, D. S. Kirschen, C. A. Silva-Monroy, and J.-P. Watson, "A comparison of policies on the participation of storage in U.S. frequency regulation markets," in *IEEE Power and Energy Society General Meeting (PESGM)*, 2016.

[63] PJM, "PJM manual 12: Balancing operations," 2020.

[64] ——, "Regulation market data," 2022.

[65] ——, "Hourly load: Metered," 2022.

[66] T. Lee, "Energy storage in PJM: Exploring frequency regulation market transformation," 2017.

[67] PJM, "Area control error," 2022.

[68] W. Ma and B. Xu, "A data-driven nonlinear recharge controller for energy storage in frequency regulation," in *IEEE Power & Energy Society General Meeting*, 2021, pp. 1–5.

[69] E. N. Sofia Guzman, M. Arriaga, C. A. Cañizares, J. W. Simpson-Porco, D. Sohm, and K. Bhattacharya, "Regulation signal design and fast frequency control with energy storage systems," *IEEE Transactions on Power Systems*, vol. 37, no. 1, pp. 224–236, 2022.

[70] H. Moring, H. Nagarajan, K. Girigoudar, D. M. Fobes, and J. L. Mathieu, "Robust partitioning and operation for maximal uncertain-load delivery in distribution grids," *Electric Power Systems Research*, vol. 235, 2024.

[71] M. Hamidieh and M. Ghassemi, "Microgrids and resilience: A review," *IEEE Access*, vol. 10, pp. 106 059–106 080, 2022.

[72] Z. Li, M. Shahidehpour, F. Aminifar, A. Alabdulwahab, and Y. Al-Turki, "Networked microgrids for enhancing the power system resilience," *Proceedings of the IEEE*, vol. 105, no. 7, pp. 1289–1310, 2017.

[73] A. Barnes, H. Nagarajan, E. Yamangil, R. Bent, and S. Backhaus, "Resilient design of large-scale distribution feeders with networked microgrids," *Electric Power Sys. Research*, vol. 171, pp. 150–157, 2019.

[74] M. Golari, N. Fan, and J. Wang, "Two-stage stochastic optimal islanding operations under severe multiple contingencies in power grids," *Electr Pwr Syst Res*, vol. 114, pp. 68–77, 2014.

[75] D. M. Fobes, H. Nagarajan, and R. Bent, "Optimal microgrid networking for maximal load delivery in phase unbalanced distribution grids: A declarative modeling approach," *IEEE Transactions on Smart Grid*, vol. 14, no. 3, pp. 1682–1691, 2022.

[76] A. Zhou, H. Zhai, M. Yang, and Y. Lin, "Three-phase unbalanced distribution network dynamic reconfiguration: A distributionally robust approach," *IEEE Transactions on Smart Grid*, vol. 13, no. 3, pp. 2063–2074, 2022.

[77] C. Lee, C. Liu, S. Mehrotra, and Z. Bie, "Robust distribution network reconfiguration," *IEEE Transactions on Smart Grid*, vol. 6, no. 2, pp. 836–842, 2015.

[78] A. Gholami, T. Shekari, and S. Grijalva, "Proactive management of microgrids for resiliency enhancement: An adaptive robust approach," *IEEE Transactions on Sustainable Energy*, vol. 10, no. 1, pp. 470–480, 2019.

[79] L. Gan and S. H. Low, "Convex relaxations and linear approximation for optimal power flow in multiphase radial networks," in *Power Systems Computation Conference*, 2014, pp. 1–9.

[80] D. M. Fobes, S. Claeys, F. Geth, and C. Coffrin, "PowerModelsDistribution.jl: An open-source framework for exploring distribution power flow formulations," *Electric Power System Research*, vol. 189, 2020.

[81] S. Lei, C. Chen, Y. Song, and Y. Hou, "Radiality constraints for resilient reconfiguration of distribution systems: Formulation and application to microgrid formation," *IEEE Transactions on Smart Grid*, vol. 11, no. 5, pp. 3944–3956, 2020.

[82] Y. Li, Y. Gu, and T. C. Green, "Revisiting grid-forming and grid-following inverters: A duality theory," *IEEE Transactions on Power Systems*, vol. 37, no. 6, pp. 4541–4554, 2022.

[83] F. Sadeque, D. Sharma, and B. Mirafzal, "Multiple grid-forming inverters in black-start: The challenges," in *IEEE 22nd Workshop on Control and Modelling of Power Electronics (COMPEL)*, 2021, pp. 1–6.

[84] A. Geoffrion, "Generalized benders decomposition," *Journal of Optimization Theory and Applications*, vol. 10, no. 4, p. 237–260, 1972.

[85] D. P. Bertsekas, *Convex Optimization Theory*. Athena Scientific, 2009.

[86] I. Dunning, J. Huchette, and M. Lubin, "JuMP: A modeling language for mathematical optimization," *SIAM Review*, vol. 59, no. 2, pp. 295–320, 2017.

[87] Gurobi Optimization, LLC, "Gurobi Optimizer Reference Manual," 2022.

[88] W. H. Kersting, "Radial distribution test feeders," in *2001 IEEE Power Engineering Society Winter Meeting. Conference Proceedings (Cat. No. 01CH37194)*, vol. 2. IEEE, 2001, pp. 908–912.

[89] H. Moring, B. K. Poola, H. Nagarajan, J. L. Mathieu, A. Bernstein, and D. M. Fobes, "Reconfiguration and real-time operation of networked microgrids under load uncertainty," *arXiv preprint arXiv:2504.15084*, 2025.

[90] C. Abbey *et al.*, "Powering through the storm: Microgrids operation for more efficient disaster recovery," *IEEE Power and Energy Mag.*, vol. 12, no. 3, pp. 67–76, 2014.

[91] M. Ferrari, B. Ollis, M. Starke, and A. Massol-Deyá, "The well-connnected microgrid: A network of microgrids can withstand severestorms," *IEEE Spectrum*, vol. 60, no. 10, pp. 36–43, 2023.

[92] S. Sharma *et al.*, "Engineering microgrids amid the evolving electrical distribution system," *Energies*, vol. 17, no. 19, 2024.

[93] Y. Ma *et al.*, "Real-time control and operation for a flexible microgrid with dynamic boundary," in *2018 IEEE Energy Conversion Congress and Exposition (ECCE)*, 2018, pp. 5158–5163.

[94] M. E. Nassar and M. M. A. Salama, "Adaptive self-adequate microgrids using dynamic boundaries," *IEEE Transactions on Smart Grid*, vol. 7, no. 1, pp. 105–113, 2016.

[95] L. Zhu *et al.*, "A smart and flexible microgrid with a low-cost scalable open-source controller," *IEEE Access*, vol. 9, pp. 162 214–162 230, 2021.

[96] M. J. Bordbari and F. Nasiri, "Networked microgrids: A review on configuration, operation, and control strategies," *Energies*, vol. 17, no. 3, 2024.

[97] M. N. Alam, S. Chakrabarti, and A. Ghosh, "Networked microgrids: State-of-the-art and future perspectives," *IEEE Transactions on Industrial Informatics*, vol. 15, no. 3, pp. 1238–1250, 2019.

[98] M. Mahdavi, K. E. K. Schmitt, and F. Jurado, "Robust distribution network reconfiguration in the presence of distributed generation under uncertainty in demand and load variations," *IEEE Transactions on Power Delivery*, vol. 38, no. 5, pp. 3480–3495, 2023.

[99] S. Babaei, R. Jiang, and C. Zhao, "Distributionally robust distribution network configuration under random contingency," *IEEE Transactions on Power Systems*, vol. 35, no. 5, pp. 3332–3341, 2020.

[100] M. Barani, J. Aghaei, M. A. Akbari, T. Niknam, H. Farahmand, and M. Korpås, "Optimal partitioning of smart distribution systems into supply-sufficient microgrids," *IEEE Transactions on Smart Grid*, vol. 10, no. 3, pp. 2523–2533, 2018.

[101] S. A. Arefifar, Y. A.-R. I. Mohamed, and T. H. El-Fouly, "Supply-adequacy-based optimal construction of microgrids in smart distribution systems," *IEEE Transactions on Smart Grid*, vol. 3, no. 3, pp. 1491–1502, 2012.

[102] A. Arif and Z. Wang, "Networked microgrids for service restoration in resilient distribution systems," *IET Generation, Transmission & Distribution*, vol. 11, no. 14, pp. 3612–3619, 2017.

[103] M. Fathi and H. Bevrani, "Adaptive energy consumption scheduling for connected microgrids under demand uncertainty," *IEEE Transactions on Power Delivery*, vol. 28, no. 3, pp. 1576–1583, 2013.

[104] H. Gao, J. Liu, L. Wang, and Z. Wei, "Decentralized energy management for networked microgrids in future distribution systems," *IEEE Transactions on Power Systems*, vol. 33, no. 4, pp. 3599–3610, 2018.

[105] N. Nikmehr and S. Najafi Ravadanegh, "Optimal power dispatch of multi-microgrids at future smart distribution grids," *IEEE Transactions on Smart Grid*, vol. 6, no. 4, pp. 1648–1657, 2015.

[106] F. Feng, P. Zhang, Y. Zhou, and L. Wang, "Distributed networked microgrids power flow," *IEEE Transactions on Power Systems*, vol. 38, no. 2, pp. 1405–1419, 2023.

[107] D. Sharma, F. Sadeque, and B. Mirafzal, "Synchronization of inverters in grid forming mode," *IEEE Access*, vol. 10, pp. 41 341–41 351, 2022.

[108] J. D. Watson, Y. Ojo, K. Laib, and I. Lestas, "A scalable control design for grid-forming inverters in microgrids," *IEEE Transactions on Smart Grid*, vol. 12, no. 6, pp. 4726–4739, 2021.

[109] H. Han, X. Hou, J. Yang, J. Wu, M. Su, and J. M. Guerrero, "Review of power sharing control strategies for islanding operation of ac microgrids," *IEEE Transactions on Smart Grid*, vol. 7, no. 1, pp. 200–215, 2016.

[110] Y. Chen, A. Bernstein, A. Devraj, and S. Meyn, "Model-free primal-dual methods for network optimization with application to real-time optimal power flow," in *American Control Conference*, 2020, pp. 3140–3147.

[111] National Renewable Energy Laboratory, "SMART-DS synthetic electrical network data OpenDSS models for SFO, GSO, and AUS."

[112] H. Moring, S. Jang, N. Ozay, and J. L. Mathieu, "Nodal operating envelopes vs. network-wide constraints: What is better for network-safe coordination of DERs?" *Electric Power Systems Research*, vol. 234, p. 110702, 2024.

[113] A. Hirsch, Y. Parag, and J. Guerrero, "Microgrids: A review of technologies, key drivers, and outstanding issues," *Renewable and Sustainable Energy Reviews*, vol. 90, pp. 402–411, 2018.

[114] A. G. Givisiez, K. Petrou, and L. F. Ochoa, "A review on TSO-DSO coordination models and solution techniques," *Electric Power Systems Research*, vol. 189, p. 106659, 2020.

[115] S. I. Vagropoulos, P. N. Biskas, and A. G. Bakirtzis, "Market-based TSO-DSO coordination for enhanced flexibility services provision," *Electric Power Systems Research*, vol. 208, p. 107883, 2022.

[116] E. Dall'Anese, S. S. Guggilam, A. Simonetto, Y. C. Chen, and S. V. Dhople, "Optimal regulation of virtual power plants," *IEEE Transactions on Power Systems*, vol. 33, no. 2, pp. 1868–1881, 2018.

[117] A. Bernstein and E. Dall'Anese, "Real-time feedback-based optimization of distribution grids: A unified approach," *IEEE Transactions on Control of Network Systems*, vol. 6, no. 3, pp. 1197–1209, 2019.

[118] Council of European Energy Regulators (CEER), "The future role of DSOs," A CEER Conclusions Paper, Tech. Rep. C15-DSO-16-03, 2015.

[119] Federal Energy Regulatory Commission, "Notice inviting post-technical conference comments," "Tech. Rep. Docket No. RM18-9-000, Apr. 2018. [Online].

[120] M. Z. Liu, L. F. Ochoa, P. K. C. Wong, and J. Theunissen, "Using OPF-based operating envelopes to facilitate residential DER services," *IEEE Transactions on Smart Grid*, vol. 13, no. 6, pp. 4494–4504, 2022.

[121] Y. Yi and G. Verbič, "Fair operating envelopes under uncertainty using chance constrained optimal power flow," *Electric Power Systems Research*, vol. 213, p. 108465, 2022.

[122] N. Nazir and M. Almassalkhi, "Convex inner approximation of the feeder hosting capacity limits on dispatchable demand," in *2019 IEEE 58th Conference on Decision and Control (CDC)*, 2019, pp. 4858–4864.

[123] ——, "Grid-aware aggregation and realtime disaggregation of distributed energy resources in radial networks," *IEEE Transactions on Power Systems*, vol. 37, no. 3, pp. 1706–1717, 2022.

[124] K. Petrou, A. T. Procopiou, L. Gutierrez-Lagos, M. Z. Liu, L. F. Ochoa, T. Langstaff, and J. M. Theunissen, "Ensuring distribution network integrity using dynamic operating limits for prosumers," *IEEE Transactions on Smart Grid*, vol. 12, no. 5, pp. 3877–3888, 2021.

[125] C. Chen, S. Bose, and L. Tong, "DSO-DERA coordination for the wholesale market participation of distributed energy resources," in *2023 IEEE Power & Energy Society General Meeting (PESGM)*. IEEE, 2023, pp. 1–5.

[126] X. Chen, E. Dall'Anese, C. Zhao, and N. Li, "Aggregate power flexibility in unbalanced distribution systems," *IEEE Transactions on Smart Grid*, vol. 11, no. 1, pp. 258–269, 2020.

[127] S. Wang and W. Wu, "Aggregate flexibility of virtual power plants with temporal coupling constraints," *IEEE Transactions on Smart Grid*, vol. 12, no. 6, pp. 5043–5051, 2021.

[128] S. Jang, N. Ozay, and J. L. Mathieu, "Large-scale invariant sets for safe coordination of thermostatic loads," in *2021 American Control Conference (ACC)*. IEEE, 2021, pp. 4163–4170.

[129] ——, "An invariant set construction method, applied to safe coordination of thermostatic loads," *IEEE Transactions on Control of Network Systems*, vol. 11, no. 4, pp. 2213–2225, 2024.

[130] S. C. Ross and J. L. Mathieu, "A method for ensuring a load aggregator's power deviations are safe for distribution networks," *Electric Power Systems Research*, vol. 189, p. 106781, 2020.

[131] S. Jang, N. Ozay, and J. L. Mathieu, "Probabilistic constraint construction for network-safe load coordination," *IEEE Transactions on Power Systems*, vol. 39, no. 2, pp. 4473–4485, 2024.

[132] ——, "Data-driven estimation of probabilistic constraints for network-safe distributed energy resource control," in *58th Annual Allerton Conference on Communication, Control, and Computing (Allerton)*, 2022, pp. 1–8.

[133] R. Rezvanfar, M. Tarafdar Hagh, and K. Zare, "Power-based distribution locational marginal pricing under high-penetration of distributed energy resources," *International Journal of Electrical Power & Energy Systems*, vol. 123, p. 106303, 2020.

[134] G. Tsaousoglou, J. Giraldo, P. Pinson, and N. Paterakis, "Mechanism design for fair and efficient DSO flexibility markets," *IEEE Transactions on Smart Grid*, vol. 12, pp. 2249–2260, 2021.

[135] S. C. Ross, N. Ozay, and J. L. Mathieu, "Coordination between an aggregator and distribution operator to achieve network-aware load control," in *2019 IEEE Milan PowerTech*. IEEE, 2019, pp. 1–6.

[136] S. Ross and J. Mathieu, "Strategies for network-safe load control with a third-party aggregator and a distribution operator," *IEEE Transactions on Power Systems*, vol. 36, no. 4, pp. 3329–3339, 2021.

[137] J. Iria, P. Scott, A. Attarha, D. Gordon, and E. Franklin, "MV-LV network-secure bidding optimisation of an aggregator of prosumers in real-time energy and reserve markets," *Energy*, vol. 242, p. 122962, 2022.

[138] H. Moring and J. L. Mathieu, "Inexactness of second order cone relaxations for calculating operating envelopes," in *2023 IEEE International Conference on Communications, Control, and Computing Technologies for Smart Grids (SmartGridComm)*, 2023.

[139] K. Petrou, M. Z. Liu, A. T. Procopiou, L. F. Ochoa, J. Theunissen, and J. Harding, "Operating envelopes for prosumers in LV networks: A weighted proportional fairness approach," in *2020 IEEE PES Innovative Smart Grid Technologies Europe (ISGT-Europe)*, 2020, pp. 579–583.

[140] M. Z. Liu, L. N. Ochoa, S. Riaz, P. Mancarella, T. Ting, J. San, and J. Theunissen, "Grid and market services from the edge: Using operating envelopes to unlock network-aware bottom-up flexibility," *IEEE Power and Energy Magazine*, vol. 19, no. 4, pp. 52–62, 2021.

[141] M. Farivar and S. H. Low, "Branch flow model: Relaxations and convexification—part I," *IEEE Trans. on Power Systems*, vol. 28, no. 3, pp. 2554–2564, 2013.

[142] R. L. Burden, J. D. Faires, and A. M. Burden, *Numerical analysis*. Cengage Learning, 2015.

[143] W. H. Kersting, "Radial distribution test feeders," *IEEE Transactions on Power Systems*, vol. 6, no. 3, pp. 975–985, 1991.

[144] P. D. Lund, J. Lindgren, J. Mikkola, and J. Salpakari, "Review of energy system flexibility measures to enable high levels of variable renewable electricity," *Renewable and Sustainable Energy Reviews*, vol. 45, pp. 785–807, 2015.

[145] J. Carpentier, "Optimal power flows," *International Journal of Electrical Power and Energy Systems*, vol. 1, no. 1, pp. 3–15, 1979.

[146] S. Frank, I. Steponavice, and S. Rebennack, "Optimal power flow: a bibliographic survey I," *Energy Systems*, vol. 3, p. 221–258, 2012.

[147] M. Lubin, O. Dowson, J. D. Garcia, J. Huchette, B. Legat, and J. P. Vielma, "JuMP 1.0: Recent improvements to a modeling language for mathematical optimization," *Mathematical Programming Computation*, 2023, in press.

[148] T. Wang, D. O'Neill, and H. Kamath, "Dynamic control and optimization of distributed energy resources in a microgrid," *IEEE Transactions on Smart Grid*, vol. 6, no. 6, pp. 2884–2894, 2015.

[149] L. Strezoski, H. Padullaparti, F. Ding, and M. Baggu, "Integration of utility distributed energy resource management system and aggregators for evolving distribution system operators," *Journal of Modern Power Systems and Clean Energy*, vol. 10, no. 2, pp. 277–285, 2022.

[150] B. Uzum, A. Onen, H. M. Hasanien, and S. M. Muyeen, "Rooftop solar pv penetration impacts on distribution network and further growth factors—a comprehensive review," *Electronics*, vol. 10, no. 1, 2021.

[151] Y. Yi and G. Verbic, "Operating envelopes under probabilistic electricity demand and solar generation forecasts," *arXiv e-prints*, pp. arXiv–2207, 2022.

[152] J. Carpentier, "Contribution to the economic dispatch problem," *Bulletin of the Society of French Electricians*, vol. 8, no. 3, pp. 431–447, 1962.

[153] B. C. Lesieutre, D. K. Molzahn, A. R. Borden, and C. L. DeMarco, "Examining the limits of the application of semidefinite programming to power flow problems," in *2011 49th Annual Allerton Conference on Communication, Control, and Computing (Allerton)*, 2011, pp. 1492–1499.

[154] S. Huang, Q. Wu, J. Wang, and H. Zhao, "A sufficient condition on convex relaxation of ac optimal power flow in distribution networks," *IEEE Transactions on Power Systems*, vol. 32, no. 2, pp. 1359–1368, 2017.

[155] J. Lavaei and S. H. Low, "Zero duality gap in optimal power flow problem," *IEEE Transactions on Power Systems*, vol. 27, no. 1, pp. 92–107, 2012.

[156] D. K. Molzahn, B. C. Lesieutre, and C. L. DeMarco, "Investigation of non-zero duality gap solutions to a semidefinite relaxation of the optimal power flow problem," in *2014 47th Hawaii International Conference on System Sciences*, 2014, pp. 2325–2334.

[157] L. Gan, N. Li, U. Topcu, and S. H. Low, "Exact convex relaxation of optimal power flow in radial networks," *IEEE Transactions on Automatic Control*, vol. 60, no. 1, pp. 72–87, 2015.

[158] X. Bai, H. Wei, K. Fujisawa, and Y. Wang, "Semidefinite programming for optimal power flow problems," *International Journal of Electrical Power & Energy Systems*, vol. 30, no. 6, pp. 383–392, 2008.

[159] D. K. Molzahn, I. A. Hiskens *et al.*, "A survey of relaxations and approximations of the power flow equations," *Foundations and Trends® in Electric Energy Systems*, vol. 4, no. 1-2, pp. 1–221, 2019.

[160] N. Nazir and M. Almassalkhi, "Market mechanism to enable grid-aware dispatch of aggregators in radial distribution networks," in *11TH Bulk Power Systems Dynamics and Control Symposium*, 2022.

[161] B. Liu and J. H. Braslavsky, "Robust dynamic operating envelopes for DER integration in unbalanced distribution networks," *IEEE Trans. Power Systems*, vol. 39, no. 2, pp. 3921–3936, 2024.

[162] J. S. Russell, P. Scott, and J. Iria, "Robust operating envelopes with phase unbalance constraints in unbalanced three-phase networks," in *2023 IEEE PES Innovative Smart Grid Technologies - Asia (ISGT Asia)*, 2023, pp. 1–5.

[163] A. Attarha, S. M. Noori R.A., M. Mahmoodi, J. Iria, and P. Scott, "Shaped operating envelopes: Distribution network capacity allocation for market services," *Electric Power Systems Research*, vol. 234, p. 110639, 2024.

[164] J. F. Franco, L. F. Ochoa, and R. Romero, "Ac opf for smart distribution networks: An efficient and robust quadratic approach," *IEEE Transactions on Smart Grid*, vol. 9, no. 5, pp. 4613–4623, 2018.

[165] B. Subhonmesh, S. H. Low, and K. M. Chandy, "Equivalence of branch flow and bus injection models," in *Allerton Conf. on Comm, Control, and Computing*, 2012, pp. 1893–1899.

[166] R. Jabr, "Radial distribution load flow using conic programming," *IEEE Trans. Power Systems*, vol. 21, no. 3, pp. 1458–1459, 2006.

[167] A. Wächter and L. T. Biegler, "On the implementation of an interior-point filter line-search algorithm for large-scale nonlinear programming," *Mathematical Programming*, vol. 106, pp. 25–57, 2006.

[168] M. Farivar, C. R. Clarke, S. H. Low, and K. M. Chandy, "Inverter var control for distribution systems with renewables," in *2011 IEEE International Conf. on Smart Grid Communications (SmartGridComm)*, 2011, pp. 457–462.

[169] N. Li, L. Chen, and S. H. Low, "Exact convex relaxation of opf for radial networks using branch flow model," in *2012 IEEE Third International Conf. on Smart Grid Communications*, 2012, pp. 7–12.

[170] B. Zhang and D. Tse, "Geometry of feasible injection region of power networks," in *2011 49th Annual Allerton Conf. on Communication, Control, and Computing*, 2011, pp. 1508–1515.

[171] S. Abdelouadoud, R. Girard, F. Neirac, and T. Guiot, "Optimal power flow of a distribution system based on increasingly tight cutting planes added to a second order cone relaxation," *International Journal of Electrical Power & Energy Systems*, vol. 69, pp. 9–17, 2015.

[172] T. Sun, Y. Song, K. Yuan, R. Hou, J. An, W. Jin, S. Zhang, and H. Cheng, "Calculation of the maximum hosting capacity of distributed photovoltaics in distribution networks considering flexible interconnections," in *2023 8th International Conf. on Power and Renewable Energy (ICPRE)*, 2023, pp. 1676–1681.

[173] H. Moring, X. Farrell, and J. L. Mathieu, "Fair-over-time distributed energy resource coordination," in *2024 60th Annual Allerton Conference on Communication, Control, and Computing*, 2024, pp. 1–8.

[174] J. Mathieu, "Algorithms for energy justice," in *Women in Power: Research and Development Advances in Electric Power Systems, Springer Women in Engineering and Science Series*, J. S. Tietjen, M. D. Ilic, L. B. Tjernberg, and N. N. Schulz, Eds. Cham, Switzerland: Springer Nature Switzerland AG, 2023.

[175] J. Mo and J. Walrand, "Fair end-to-end window-based congestion control," *IEEE/ACM Transactions on Networking*, vol. 8, no. 5, pp. 556–567, 2000.

[176] X. Xu and H. Yu, "A game theory approach to fair and efficient resource allocation in cloud computing," *Mathematical Problems in Engineering*, vol. 2014, no. 1, p. 915878, 2014.

[177] X. Zhang and M. Liu, "Fairness in learning-based sequential decision algorithms: A survey," in *Handbook of Reinforcement Learning and Control*. Springer, 2021, pp. 525–555.

[178] D. Pessach and E. Shmueli, "A review on fairness in machine learning," *ACM Computing Surveys (CSUR)*, vol. 55, no. 3, pp. 1–44, 2022.

[179] L. Bird, C. Walker, J. Womble, S. Atcitty, R. Trevizan, L. Concessao, H. Meenawat, and B. Tarekegne, "Distributed energy resources as an equity asset: Lessons learned from deployments in disadvantaged communities," *IEEE Power and Energy Magazine*, vol. 22, no. 4, pp. 64–74, 2024.

[180] M. Sufyan, N. A. Rahim, M. A. Muhammad, C. K. Tan, S. R. S. Raihan, and A. H. A. Bakar, "Charge coordination and battery lifecycle analysis of electric vehicles with V2G implementation," *Electric Power Systems Research*, vol. 184, p. 106307, 2020.

[181] S. Poudel, M. Mukherjee, R. Sadnan, and A. P. Reiman, "Fairness-aware distributed energy coordination for voltage regulation in power distribution systems," *IEEE Transactions on Sustainable Energy*, vol. 14, no. 3, pp. 1866–1880, 2023.

[182] J. Soares, F. Lezama, R. Faia, S. Limmer, M. Dietrich, T. Rodemann, S. Ramos, and Z. Vale, "Review on fairness in local energy systems," *Applied Energy*, vol. 374, p. 123933, 2024.

[183] M. R. Alam, P. T. Nguyen, L. Naranpanawe, T. K. Saha, and G. Lankeshwara, "Allocation of dynamic operating envelopes in distribution networks: Technical and equitable perspectives," *IEEE Transactions on Sustainable Energy*, vol. 15, no. 1, pp. 173–186, 2023.

[184] S. Alyami, Y. Wang, C. Wang, J. Zhao, and B. Zhao, "Adaptive real power capping method for fair overvoltage regulation of distribution networks with high penetration of PV systems," *IEEE Transactions on Smart Grid*, vol. 5, no. 6, pp. 2729–2738, 2014.

[185] B. Liu and J. H. Braslavsky, "Robust dynamic operating envelopes for DER integration in unbalanced distribution networks," *IEEE Transactions on Power Systems*, 2023.

[186] S. Caton and C. Haas, "Fairness in machine learning: A survey," *ACM Computing Surveys*, vol. 56, no. 7, pp. 1–38, 2024.

[187] Z. Tang, J. Zhang, and K. Zhang, "What-is and how-to for fairness in machine learning: A survey, reflection, and perspective," *ACM Computing Surveys*, vol. 55, no. 13s, pp. 1–37, 2023.

[188] N. Mehrabi, F. Morstatter, N. Saxena, K. Lerman, and A. Galstyan, "A survey on bias and fairness in machine learning," *ACM Computing Surveys (CSUR)*, vol. 54, no. 6, pp. 1–35, 2021.

[189] M. Feldman, S. A. Friedler, J. Moeller, C. Scheidegger, and S. Venkatasubramanian, "Certifying and removing disparate impact," in *ACM SIGKDD International Conference on Knowledge Discovery and Data Mining*, 2015, pp. 259–268.

[190] M. Hardt, E. Price, and N. Srebro, "Equality of opportunity in supervised learning," *Advances in Neural Information Processing Systems*, vol. 29, 2016.

[191] Y. Ge, S. Liu, R. Gao, Y. Xian, Y. Li, X. Zhao, C. Pei, F. Sun, J. Ge, W. Ou *et al.*, "Towards long-term fairness in recommendation," in *ACM International Conference on Web Search and Data Mining*, 2021, pp. 445–453.

[192] M. Morik, A. Singh, J. Hong, and T. Joachims, "Controlling fairness and bias in dynamic learning-to-rank," in *ACM SIGIR Conference on Research and Development in Information Retrieval*, 2020, pp. 429–438.

[193] A. J. Biega, K. P. Gummadi, and G. Weikum, "Equity of attention: Amortizing individual fairness in rankings," in *ACM SIGIR Conference on Research and Development in Information Retrieval*, 2018, p. 405–414.

[194] S. Gupta and V. Kamble, "Individual fairness in hindsight," *Journal of Machine Learning Research*, vol. 22, no. 144, pp. 1–35, 2021.

[195] H. A. U. Khan, B. Ünel, and Y. Dvorkin, "Electricity tariff design via lens of energy justice," *Omega*, vol. 117, p. 102822, 2023.

[196] L. Li, M. Dong, D. Song, J. Yang, and Q. Wang, "Distributed and real-time economic dispatch strategy for an islanded microgrid with fair participation of thermostatically controlled loads," *Energy*, vol. 261, p. 125294, 2022.

[197] J. S. Russell, P. Scott, and J. Iria, "Network-secure aggregator operating regions with flexible dispatch envelopes in unbalanced systems," *Electric Power Systems Research*, vol. 235, p. 110728, 2024.

[198] C. Dwork, M. Hardt, T. Pitassi, O. Reingold, and R. Zemel, "Fairness through awareness," in *Innovations in Theoretical Computer Science Conference*, 2012, pp. 214–226.

[199] N. L. Hanus, J. Barlow, A. Satchwell, and P. Cappers, "Assessing the current state of US energy equity regulation and legislation," Lawrence Berkeley National Laboratory. Retrieved from https://escholarship.org/uc/item/5170t55k, 2023.

[200] J. Barlow, R. Tapio, and B. Tarekegne, "Advancing the state of energy equity metrics," *The Electricity Journal*, vol. 35, no. 10, p. 107208, 2022.

[201] T. Lanckton and S. DeVar, "Justice in 100 metrics," Initiative for Energy Justice. Retrieved from https://iejusa.org/wp-content/uploads/2021/03/Justice-in-100-Metrics-2021.pdf, 2021.

[202] D. Nock, A. J. Jones, S. Bouzarovski, H. Thomson, and D. J. Bednar, "Reducing energy burden in the power sector: Metrics for assessing energy poverty," *IEEE Power and Energy Magazine*, vol. 22, no. 4, pp. 26–37, 2024.

[203] A. Kody, A. West, and D. K. Molzahn, "Sharing the load: Considering fairness in de-energization scheduling to mitigate wildfire ignition risk using rolling optimization," in *IEEE Conference on Decision and Control*, 2022, pp. 5705–5712.

[204] S. Cong, D. Nock, Y. L. Qiu, and B. Xing, "Unveiling hidden energy poverty using the energy equity gap," *Nature Communications*, vol. 13, no. 1, p. 2456, 2022.

[205] C. Zhang and J. A. Shah, "Fairness in multi-agent sequential decision-making," *Advances in Neural Information Processing Systems*, vol. 27, 2014.

[206] I. Bistritz, T. Baharav, A. Leshem, and N. Bambos, "My fair bandit: Distributed learning of max-min fairness with multi-player bandits," in *International Conference on Machine Learning*, 2020, pp. 930–940.

[207] P. Lahoti, A. Beutel, J. Chen, K. Lee, F. Prost, N. Thain, X. Wang, and E. Chi, "Fairness without demographics through adversarially reweighted learning," *Advances in Neural Information Processing Systems*, vol. 33, pp. 728–740, 2020.

[208] S. Jang, N. Ozay, and J. Mathieu, "Probabilistic constraints construction for network-safe thermostatically controlled loads control," 2022.

[209] A. Lorca and X. A. Sun, "Multistage robust unit commitment with dynamic uncertainty sets and energy storage," *IEEE Transactions on Power Systems*, vol. 32, no. 3, pp. 1678–1688, 2017.